Faculty of Science and Engineering

Department of Chemical Engineering

Corrosion and Hydrate Formation in Natural Gas Pipelines

Emmanuel Ogo-Oluwa OBANIJESU

This thesis is presented for the degree of

Doctor of Philosophy

of

Curtin University

May 2012

<u>Statement of Originality</u>

To the best of my knowledge and belief, this thesis contains no material previously published by any other person except where due acknowledgement has been made. This thesis contains no material which has been accepted for award of any other degree or diploma in any university.

I give consent to this copy of my thesis, when deposited to the University Library, to be made available for loan and photocopying subject to the provision of the Copyright Act 1968

Signature: …………………………………………….

Date: …………………………………………….

Biography of the Author

Emmanuel was born on 10th August, 1968 in Ibadan, Nigeria. He completed his B.Sc. (Chemical Engineering) degree from Obafemi Awolowo University, Nigeria in 1991 and M.Sc. (Chemical Engineering) degree at University of Lagos in 1997 with a PhD grade. He commenced his Ph.D. research at Curtin University of Technology (now Curtin University), Western Australia on 8th June 2009 under the 3-year Curtin Strategic International Research Scholarship (CSIRS) and 3-year Curtin International Postgraduate Research Scholarship (CIPRS). He also received the Australia-China Natural Gas Technology Partnership Fund Top-up Scholarship from Western Australian Energy Research Alliance (WA:ERA) in September 2010 and finally received a Departmental Top-up Scholarship from Curtin's Chemical Engineering Department in September 2011. The Ph.D. thesis was successfully completed with published two book chapters, two journal articles, four internationally peer reviewed conference papers and two seminar presentations (Australia and Malaysia).

As a Petroleum Engineer Trainee with Nigerian Petroleum Development Company Limited in 1992, Emmanuel was involved in various oilfield operations such as well drilling and completion, swabbing operation, and Bottom Hole Diagnostic Survey amongst others. He joined Josef Ross & Company Ltd, Nigeria in 1993 as a Project Engineer, where he coordinated and managed various national and international projects sponsored by Chevron (Nig) Ltd, Mobil Petroleum, World Bank, United Nations Environment Programs and Federal Government of Nigeria. Emmanuel worked as a Research Officer with Federal Institute of Industrial Research, Oshodi (FIIRO) between 1997 and 2003 before joining Ladoke Akintola University of Technology (LAUTECH), Nigeria as a Lecturer in 2004 to 2010.

Between 1997 and now, Emmanuel has been involved in pure and applied research activities that have resulted into 4 book chapters, over 20 published articles in peer-reviewed journals, 10 peer-reviewed international conference proceedings and many other technical presentations nationally and internationally. He has been teaching undergraduate and postgraduate students both in Nigeria and Australia, and also successfully supervised over 100 undergraduate and postgraduate research theses from both countries. Emmanuel was nominated for the 2010 Edition of Eni Scientific Award (Environmental Engineering Option) in Italy.

Peer Reviewed Manuscripts from this PhD Thesis

A. Published book chapters

1. Obanijesu, E.O., Akindeju, M.K., Pareek, V. and Tade, M.O. (2011), "Modeling the Natural Gas Pipeline Internal Corrosion Rate as a Result of Hydrate Formation", *In: Environmental Systems Engineering Section*, *Elsevier 21st European Symposium on Computer-Aided Process Engineering*, (Part B), E.N. Pistikopoulos, M.C. Georgiadis and A.C. Kokossis (Editors), Computer-Aided Chemical Engineering (Elsevier), Vol. 29, pp. 1160-1164.

2. Hunt, D., Akindeju, M.K., Obanijesu, E.O., Pareek, V. and Tade, M.O. (2011), "Potential Impacts and Modeling the Heat Value Loss Due to Chelation in Natural Gas Processing and Transport", *In: Energy Systems Engineering Section*, *Elsevier 21st European Symposium on Computer-Aided Process Engineering*, (Part B), E.N. Pistikopoulos, M.C. Georgiadis and A.C. Kokossis (Editors), Computer-Aided Chemical Engineering (Elsevier), Vol. 29, pp. 1648-1652.

B. Published journal articles

1. Obanijesu, E.O., Pareek, V., Gubner, R and Tade, M.O. (2011), "Hydrate Formation and its Influence on Natural Gas Pipeline Internal Corrosion Rate", *NAFTA Journal,* Year 62, No 5-6, pp 164-173.

2. Obanijesu, E.O., Pareek, V., Gubner, R and Tade, M.O. (2010), "Corrosion Education as a Tool for the Survival of Natural Gas Industry", *NAFTA Journal*, Year 61, No 12, pp 541-554.

C. Published conference proceedings

1. Obanijesu, E.O., Akindeju, M.K., Pareek, V. and Tade, M.O. (2011), "Modeling the Natural Gas Pipeline Internal Corrosion Rate as a Result of Hydrate Formation", *Elsevier 21st European Symposium on Computer-Aided Process Engineering (ESCAPE-21) Conference,* Porto Carras Resort, N. Marmaras, Chalkidiki, Greece, May 29th-June 1st

2. Hunt, D., Akindeju, M.K., Obanijesu, E.O., Pareek, V. and Tade, M.O. (2011), "Potential Impacts and Modeling the Heat Value Loss Due to Chelation in Natural Gas Processing and Transport" *Elsevier 21st European*

Symposium on Computer-Aided Process Engineering (ESCAPE-21) Conference, Porto Carras Resort, N. Marmaras, Chalkidiki, Greece, May 29th-June 1st

3. E.O. Obanijesu, V. Pareek, A. Barifcani, R. Gubner and M.O. Tade (2011), "Influence of Corrosion Inhibitors on Hydrate Formation Temperature", Presented at *3rd Regional Materials Technology Conference*, Imperial Palace Hotel, Miri, Malaysia, April 26-27.

4. Obanijesu, E.O., Pareek, V. and Tade, M.O. (2010), "Hydrate Formation and its Influence on Natural Gas Pipeline Internal Corrosion Rate", MS-128544, Presented at *Asia-Pacific Oil and Gas Conference and Exhibition*, Society of Petroleum Engineers, Mumbai, India, January 20-22.

D. *Orally presented seminars*

1. Obanijesu, E.O., Tade, M.O., Pareek, V., Gubner, R. and Barifcani, A. (2011), "Pipeline Engineering in Oil and Gas Industry: Importance and Problems", *Presented during Research & Development Seminar*, Curtin University, Miri Campus, Malaysia, April 28

2. Obanijesu, E.O., Pareek, V., Gubner, and Tade, M.O. (2010), "Corrosion Education as a Tool for the Survival of Natural Gas Industry", *Presented during Research & Development Seminar*, Curtin University, Perth, Australia, November, 2010

Dedication

To God Almighty

Who single-handedly picked me up from my rough beginning with full determination to take me to the glorious end. He has always being there for me, to HIM be the glory and honour forever more (AMEN).

To My Parents

Late Prince Akintola Adekunle and Late Madam Olusola Ajoke for taking it upon themselves to train me from their meagre resources. I appreciate you.

To my children

Oluwagbemiga, Adedamola, Adewale, Fiyinfoluwa, Aderogbayimika, Zawadi and Olusola for their understanding during the trial periods.

Acknowledgement

Knowledge is a continuous process that requires contributions in various forms and degrees from different people. Several people supported me during this research; I appreciate their valuable contributions which motivated me to the successful completion of the program.

I sincerely express my deepest gratitude to my Main Supervisor, Prof. Moses Oludayo Tade who supported me throughout my entire PhD program with his patience and knowledge. Professor Tade encouraged me to work on this challenging project and drove me hard to produce 'double thesis' through full financial support (in securing chemicals and materials) and his availability to discuss the technicality of my work (even at odd hours). I am highly honored to work with such a great man; he shared his wealth of experience with me through patience, attention, constructive criticisms, editing, direction and desire for quality. I also wish to thank my other three Supervisors in the persons of Prof. Vishnu Pareek, Prof. Rolf Gubner and Associate Prof. Ahmed Barifcani. Prof. Barifcani as an expert in hydrate formation and related problems gave me complete access to the ever precious cryogenic sapphire cell. Also, he was always available in the laboratory to discuss my experiments and results with me on many occasions; Prof. Gubner was always available to share his wealth of experience in Corrosion Science and Engineering. As a corrosion expert and Director of Western Australian Corrosion Group, he was always available to share knowledge with me; we spent qualitative time together to discuss my methodology. He also supplied all the corrosion inhibitors through his corrosion research group. Prof. Pareek supported with advice, motivation and always happy to assist with computers and accessories. I equally thank my Thesis Chairman

TABLE OF CONTENTS

LIST OF TABLES

LIST OF FIGURES

xviii

Nomenclatures

ST	=	Scaling tendency
R_{FeCO_3}	=	Precipitation rate of iron carbonate (mm/yr)
CR	=	Corrosion rate (mm/yr)
εR_j	=	The source or sink due to chemical reaction
C_j	=	The concentration of species j (kmol/m^3)
ε	=	The porosity of the film
ϕ	=	Porosity of the porous media
D_j^{eff}	=	The Effective diffusion coefficient of species j (which include both the molecular and the turbulent components, m^2/s)
R_j	=	The source or sink of species j due to all the chemical reactions in which the particular species is involved, kmolm^{-3}s^{-1})
t	=	Time, (s)
x	=	The spatial coordinate (m)
α_i	=	The specific capacity
C_{Cl}	=	The amount or concentration of chlorine ions
J_{Cl}	=	The diffusion flux of chloride ions
Q_{Cl}	=	The sink term
S	=	The Saturation
S_r	=	Salinity ratio (Actual salinity/nominal salinity)
$f(S_r)$	=	Corrosion rate correction factor for salinity (Corrosion rate at actual salinity/Corrosion rate at nominal condition)
M_{Fe}	=	The Molecular weight of iron
i_{corr}	=	Corrosion current density
Z_{Fe}	=	Number of electric charge of iron
F	=	Faraday number/constant (96487 C/e$^-$)
R_{Corr}	=	Corrosion rate
ρ_{gO_2}	=	Density of dissolved O$_2$ in pore water (kg/m^3)
ρ_{dO_2}	=	Density of gaseous O$_2$ (kg/m^3)

J_{O_2}	=	Total flux of dissolved and gaseous O_2 (kg/m^2.s)
Q_{O_2}	=	Sink term for the rate of consumption due to corrosion (kg/m^{3}s)
W_{rust}	=	Accumulated corrosion amount
W_{Crit}	=	Critical amount of corrosion products
ρ_{st}	=	Density of steel
ρ_{rust}	=	Density of rust
d_o	=	Original diameter
d_s	=	Displaced steel (i.e. diameter of displacement)
D	=	Material thickness.
γ	=	A constant introduced as a magnification factor ($\gamma \geq 0$)
δ	=	A constant introduced to adjust a truncated portion ($\delta \geq 0$)
β	=	A constant corresponding to mean value of the distribution
ε	=	A constant corresponding to the standard deviation of the distribution.
$f(T_r) =$		Corrosion rate correction factor for temperature (Corrosion rate at actual temperature/Corrosion rate at nominal temperature)
T_r	=	Temperature ratio (Actual temp/nominal temp)
c	=	Constant representing the slope of the $f(T_r) - T_r$ relationship
d	=	The constant representing the $f(T_r)$ value at zero T_r
T	=	Temperature (^{O}K)
S	=	Salinity {Part per thousand ($^0/_{oo}$)}
$f(V_r) =$		Corrosion rate correction factor for velocity
V_r	=	Velocity ratio
λ	=	Magnification factor ($\lambda \geq 0$)
v	=	Velocity
θ	=	Constant to adjust the truncated portion of the distribution ($\theta \geq 0$)
SR	=	Saturation ratio
τ_o	=	The constant controlling the slope at (t=0)
$\frac{1}{\tau_o}$	=	The slope at t=0

P_i	=	The weighting factor representing the relative duration of the ith stationary period along the lifetime of material; and $d_{c,i}$ is the short-term corrosion wastage of the ith period.
Φ	=	The Electric potential (V)
D_i	=	Diffusion coefficient (m^2s^{-1})
Z_i	=	The charge (e^-/mol)
R	=	Universal constant ($Jmol^{-1}k^{-1}$)
$S_{i,j}$	=	Stoichiometric coefficient of species i in the jth homogenous reaction
r_j	=	The Rate ($molm^{-3}s^{-1}$)
∇	=	Divergence operator written in 3-D Cartesian coordinates
Cr_t	=	Corrosion Rate at temperature T (mm/yr.)
k_t	=	Temperature constant
Z	=	Compressibility factor
k	=	Pipe roughness (m)
T_c	=	Temperature at standard condition (60ᵼF/15.55ᵼC)
S	=	Wall shear stress (Pa)
f	=	Friction factor
$f(pH)_t =$		pH factor at temp t
U_m	=	Mixed velocity (m/s)
ρ_m	=	Mixture density (Kg/m^3)
k	=	Pipe roughness (m)
D	=	Pipe diameter (mm)
μ_m	=	Mixed viscosity (Ns/m^2)
ρ_G	=	Gas density (Kg/m^3)
ρ_L	=	Liquid density (Kg/m^3)
ρ_m	=	Mixture density (Kg/m^3)
λ	=	Liquid fraction
$U_G^{\ s}$	=	Gas superficial velocity (m/s)
$U_L^{\ s}$	=	Liquid Superficial velocity (m/s)
U_m	=	Mixed velocity (m/s)

μ_G = Viscosity of gas (Ns/m^2)

μ_L = Viscosity of liquid (Ns/m^2)

μ_w = Viscosity of water (Ns/m2)

μ_m = Mixed viscosity

Q_G = Volumetric flow rate of gas (m^3/s)

Q_L = Volumetric flow rate of liquid (m^3/s)

R = Gas constant

T = Operating temperature

C_p = Heat capacity

ΔS = Entropy change,

ΔH = Enthalpy change,

Z = Compressibility factor

T_c = Temp at standard condition (60°F/15.55^{O}C)

ϕ = Fugacity coefficient (watercut)

ρ_g = Specific gravity

$U^s{}_G$ = Gas superficial velocity (m/s)

ΔG = Gibb free energy

f_i = The fluid fugacity

$\dfrac{\partial(\varepsilon C_j)}{\partial t}$ = Accumulation term

$\dfrac{\partial}{\partial x}\left(\varepsilon^{1.5} D_j{}^{eff} \dfrac{\partial C_j}{\partial x}\right)$ = The net flux

Abstract

Gas industry annually invests millions of dollars on corrosion inhibitors in order to minimize corrosion implications on flow assurance; however, attention has never been focused on possibilities of these chemicals to promote hydrate formation along deepwater pipelines, which would equally result in another flow assurance problem of high magnitude. This study investigated the possibilities of corrosion inhibitors to aid the formation of gas hydrate along offshore (or underwater) pipeline systems; developed a predictive model on corrosion rate for natural gas pipelines with gas hydrates as the corroding agent and finally investigated the ability of pure N_2 and H_2 gases to inhibit the formation of gas hydrates.

All experiments in this thesis were conducted by forming various water-gas systems in a cylindrical cryogenic sapphire cell. The first investigative work on hydrate-corrosion relationship was conducted by allowing contacts between an industrial grade natural gas (with 20% CO_2 content) and five different corrosion inhibitors that are commonly used at offshore fields. The equipment, consisting of several fittings could operate at a temperature range of $-160^{o}C - 60^{o}C$ (with accuracy of $\pm 0.10^{o}C$) and pressure range of 1bar to 500bar (with accuracy of ± 0.5bar). Using the 'Temperature Search' method, the hydrate formation temperature point for each inhibitor was located at 500ppm and 100bar and the result compared with that of control experiment. Due to observed significant influence, further investigations were conducted on Dodecylpyridinium Chloride (DPC) at various concentrations and pressures. The corrosion model was developed based on hydrate's thermodynamic properties such as the operating temperature, pressure, fluid fugacity, wall shear stress, superficial velocity, enthalpy, entropy and activity coefficient amongst others, and a Matlab computer code was written to simulate the generated solution algorithm. Finally, components interaction study was conducted on various gas mixtures inside the sapphire cell to investigate the ability of pure N_2 and H_2 gases to inhibit the formation of gas hydrates.

The obtained results established that all corrosion inhibitors aid hydrate promotion; this was attributed to their surfactant and hydrogen bonding properties which were essential for hydrate formation. The five investigated inhibitors showed different

promotional rates with DPC having the highest promotional ability. The different promotional rate is due to their different sizes and structures, active functional groups and affinity for water molecules which determine the type(s) of hydrogen bonding exhibited by each inhibitor while in solution. The significant performance of DPC compared to other inhibitors was justified by the specific available active functional group which obeys electronegativity trend of periodic table to determine whether the resulting bond type will be polar covalent, ionic or ionic with some covalent characteristic in nature. Also, DPC hydrates revealed strong influence of the chemical's surfactant properties at all pressures and concentrations while its Critical Micelle Concentration (CMC) was believed to be 5000ppm due to the various anomaly behaviors exhibited at this particular concentration.

The developed mathematical model adequately predicted corrosion rates with gas hydrate as the corroding agent and its effectiveness was confirmed by the level of agreement between its generated results and existing literatures. The resulting corrosion rate from hydrates could be as high as 174mm/yr (0.48mm/day). This is extremely alarming compared to the industry's aim to operate below 2mm/yr. At this rate, an underwater pipeline would be subjected to full bore rupture within some days if corrective measures are not quickly taken.

Furthermore, the components interaction study revealed that CH_4 played key roles on hydrate formation patterns during natural gas transportation through offshore pipeline system; the higher a natural gas CH_4 content, the higher the risk of hydrates promotion. It also showed that when alone, CO_2 does not form hydrate at low concentrations but showed a remarkable ability to aid hydrate formation when mixed with CH_4. This is not surprising since it is also a former with ability to form Type I hydrate due to its very small size. Again, the ability of pure N_2 and pure H_2 gases to inhibit the formation of gas hydrate was confirmed but with H_2 showing more significant effects. This was ascribed to their individual pressure condition to form hydrate. Though, N_2 gas with small molecules forms Type II hydrate at a relatively higher pressure above the investigated pressures, it still forms hydrate within higher operating pressures practiced at gas fields during the transportation. However, H_2 gas can never form hydrate at any natural gas transportation conditions. H_2 gas only forms hydrates at extremely high pressure of about 2000bar because its molecules

are too small and usually leaked out of hydrate cage, thus, reducing the amount that could be stored. By extension, these individual properties affect their interactions with natural gas during the hydrate formation process.

Conclusively, this study has essentially revealed a new hydrate-corrosion relationship and established the need for comprehensive investigations in this research area. At all the investigated pressures, it was realized that DPC prolonged the complete blockage of the glass orifice at 10000ppm. This special characteristic may suggest the potential in applying the chemical as an additive for natural gas transportation and storage in slurry forms. Finally, the use of pure N_2 or H_2 as hydrate inhibitor in the offshore pipeline would be very cost effective to the industry. However, extreme care should be taken during the selection process since there are needs to further investigate the safety factors, material availability, cost implication and recovery from the main gas stream in order to choose the better option.

1. Introduction

1.1 Background

Global energy demand has rapidly increased as a result of increase in population and industrialization, with oil and natural gas constituting over 65% of the primary sources. Measured in financial indicators, 90% of chemical products in industrially developed countries are from organic sources whose 98% production are based on oil and natural gas as basic organic chemical feeds (Janovic, 2005). Since petroleum as an energy source is non-renewable, the crude reserves are fast declining due to long period of utilization (Figure 1.1) while the global focus is now shifting towards natural gas as the major source of energy due to its abundance availability, economic viability and environmental friendliness.
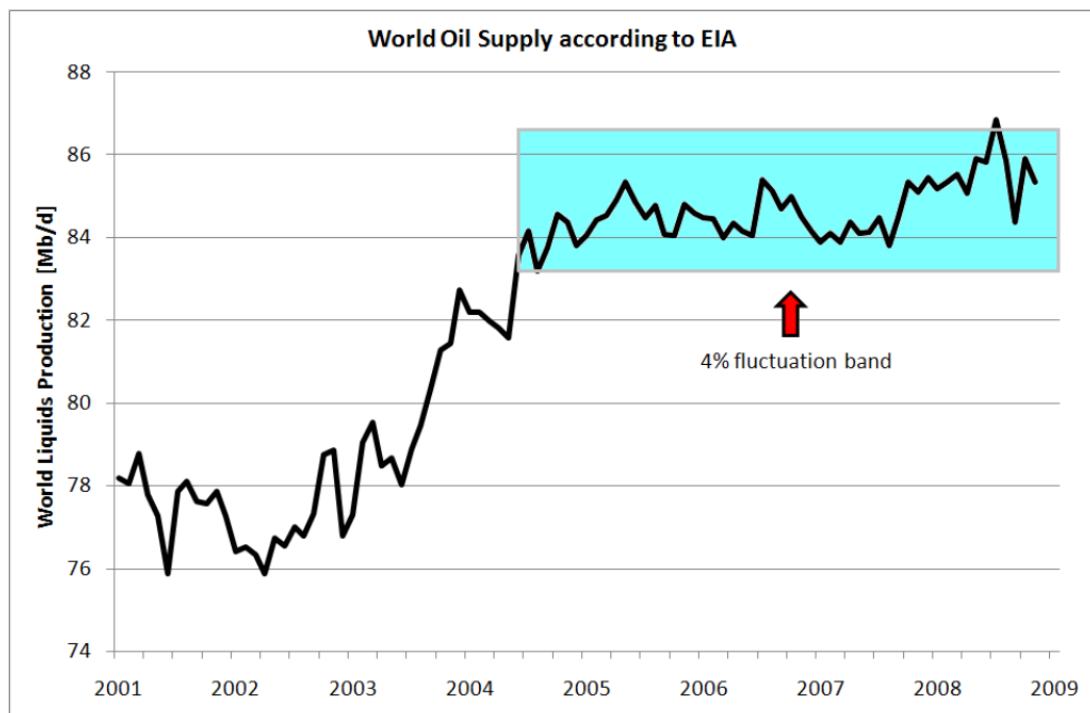
Figure 1.1: World liquid fuels production between 2001and 2008 (Hook et al, 2009)
Note: Since mid-2004, production has stayed within a 4% fluctuation band, which indicates that new production has only been able to offset the decline in existing production

The increasing use of natural gas as a primary fuel source has led to its greater production and exportation in gaseous and liquid ((Liquefied Natural Gas (LNG))

forms from many countries that hold sufficient reserves. This has equally increased the global transboundary pipeline networks with minimal considerations to the impacts its failure could have on the environment.

Natural gas is a combustible gaseous mixture of light hydrocarbon compounds and other components. Its main components are methane (CH_4) and other non-reactive hydrocarbons in gaseous state at ambient temperature and atmospheric pressure. The gas with low energy density is either found in association with crude oil (either dissolved at high temperature and pressure or as gas cap in the same reservoir) or as a non-associated gas. This origin of formation, coupled with type, location of deposit, geological structure of the region and other factors determine its composition. The gas is colorless and odorless in its pure state and when burnt, it gives off a great deal of energy with low level of pollutants compared with other fossil fuels.

As of 2007 the world natural gas reserve was estimated at 183.1 trillion cubic meters (tcm). 70% of this reserve was available in the Former Soviet Union (FSU) and the Middle East, while Oceania and Asia countries accounted for a further 8.9%. As of 2006, FSU and North American countries accounted for 53.1% of global production while the Oceania and Asian countries produced 13.1%; the African gas reserves are produced from Nigeria, Algeria, Egypt, Libya, Angola, Mozambique, Namibia, Tunisia and Tanzania (Obanijesu and Sonibare, 2005). The gas is largely consumed in North America and the FSU with United States demand for 2003 put at 786.32 bcm (Hill, 2005). Europe also has a large demand for the gas with considerable trading sourced mostly from regional supplies, Africa and the FSU. Furthermore, the Oceania and Asia countries accounted for 14.8% of total global consumption rate (Table 1.1).

After production from the reservoir, the gas distribution involves transportation through long pipeline network systems from the production platform to different terminals, treatment plants and process units under high pressure. This is followed by further transportation through another set of pipeline systems to an offtake station and onward transmission in lower pressure pipes to end-users. The pipelines may be laid over several kilometers on land or buried underground (both referred to as

onshore pipeline system) or submerged deeply inside water (offshore/deepwater pipeline system).

Table 1.1: The global natural gas reserve, production and consumption (Morikawa, 2008)

	Proven Reserve (2007)		Production (2006)		Consumption (2006)	
	(Tcm)	Share (%)	(Bcm)	Share (%)	(Bcm)	Share (%)
North America	8.0	4.4	753.2	26.1	769.9	26.7
Latin America	6.9	3.8	147.0	5.1	130.8	4.5
Europe	6.3	3.4	305.4	10.6	568.3	19.7
FSU	57.2	31.2	778.7	27.0	616.4	21.3
Africa	14.5	7.9	191.7	6.6	88.5	3.1
Middle East	73.9	40.4	334.8	11.6	287.1	9.9
Asia Oceania	16.3	8.9	377.0	13.1	426.7	14.8
Total	183.1	100.0	2887.7	100.0	2887.7	100.0

1.2 Submerged Pipelines: Failure and Consequences

Submerged gas pipelines are susceptible to failure in the form of leakage or full bore rupture (FBR) as a result of corrosion and/or hydrate formation (Huang et al, 2012; Zhang and Wu, 2012). These two flow assurance problems are caused by the flow conditions and the fluid properties that introduce thermodynamic conditions and electrochemical/chemical reactions that are conducive enough to encourage their occurrence within the pipelength. The resulting accidents always discharge the gas into the waterbody to cause hazardous impacts on the four environmental matrices (soil, vegetation, air and water). Some of the havocs are dissolution of acidic components which may cause fish scattering, abnormal behavior and reduction in production capacity; air pollution which may result into climate change; soil degradation which affects food crops; fire; explosion and human deaths. Economically, hydrate prevention costs the gas industry about US$1 million per mile (Jassim and Abdi, 2008) while corrosion loss alone on USA economy in 1995 was estimated at US$300 billion with 1% coming from pipeline industry (Battelle, 1996).

3

Several attempts have been made by the industry to prevent these two problems without success; research has shown however that the problems could only be minimized; hence the industry continues to spend heavily on inhibitors.

In the research fields, all the existing work seem to be isolating each of these two problems without consideration given to a possibility of them leading to one another; hence, the significance of this work.

This thesis investigated the feasibility of the hydrate-corrosion relationship. This was achieved by studying the possibilities of corrosion inhibitors to aid the promotion of hydrate formation along the gas pipeline and the ability of the resulting hydrate to initiate internal corrosion along the same pipelength. This study was necessitated since corrosion inhibitors have surfactant properties and structural resemblance in common with some established hydrate promoters. Five corrosion inhibitors commonly used in the gas industry were investigated while further study was carried out on the one with most significant impacts. A predictive corrosion model was also developed with gas hydrate as the corroding agent. Finally, two gases were investigated for their hydrate inhibition properties.

1.3 Aim and Objectives

The main aim of this work is to investigate the feasibility of any relationship between hydrate formation and corrosion along deepwater natural gas pipeline network systems. Consequently, the objectives of the project are:

1.   To investigate the feasibility of corrosion inhibitors to aid hydrate formation along the deepwater natural gas pipeline.

2.   To investigate if the resulting hydrates could initiate corrosion along the internal wall of the pipeline.

3.   To develop a predictive corrosion rate model as a result of the hydrate formation within the pipelength.

4.   To investigate the use of some gases to inhibit hydrate formation rate along the pipeline.

1.4 Scope of the Study

Though corrosion and hydrate formation problems are experienced in both the oil and gas pipelines, this study focused mainly on the gas pipelines. This is to prevent repitition and duplication of experiments. If the investigated problem could be established with the gas pipeline, it then extends to the oil pipelines by implications. Also, five corrosion inhibitors were investigated for the hydrate-corrosion relationship while only one was chosen for further experimentation due to its observed significant influence compared to others. For the corrosion rate modeling, gas hydrate was considered as the only corroding agent. Finally, only H_2 and N_2 gases were investigated for the inhibition behaviour.

1.5 Significance of this Study

The global increase in offshore transboundary natural gas transportation increases the risk of pipeline accidents thereby making the global environmental consequences imminent. Gas hydrates and internal corrosion have been identified as the major factors responsible for offshore pipeline failure while an accident in such environment can contaminate the aquatic environment, destroy the biological component of the ecosystem and affect human health.

Many efforts by the industry to solve one of the problems at a time always prove abortive due to the unforeseen situation that one can assist the other. It is highly likely that the existing gas hydrates within the pipelength would have initiated internal corrosions before its removal. If this happened, the corrosion would grow with time to undermine the pipe's integrity by destroying its material, hence, causing failure. Also, if hydrate is promoted due to an attempt to inhibit corrosion, a serious flow assurance problem is bound to happen. Based on this, development of adequate knowledge in hydrate-corrosion relationship would go a long way in solving many of the existing 'unsolvable' problems in the industry. An example is the application of H_2 and N_2 gases to inhibit hydrate formation along the pipeline as proposed in the closing chapter of this report.

Furthermore, many corrosion models, focusing on several corroding agents have been developed and improved upon with contingency plans put in place for such accidents; but none of such existing models have considered hydrate as a possible

cause. An important element in the existing plans is the use of mathematical models to predict the transport and fate of the fluid (Yapa and Zheng, 1998; Zheng and Yapa, 1998; Lain et al, 2002; Melchers, 2003a; Nesic et al, 2004; Obanijesu and Mosobalaje, 2008). Development of a predictive corrosion rate model on a possible hydrate-corrosion relationship will go a long way in assisting the pipe designers at the developmental stage. It will also assist the Pipeline Operator in the choice of pipe material, and to know the likely period to replace the pipes.

1.6 Contributions of This Research Work

After addressing the above objectives, significant contributions have been made in this study by establishing various relationships between hydrate formation and corrosion along natural gas pipelines. So far, there is no known literature in this research area apart from those published by the authors either through conferences or journal articles; therefore, some of the specific contributions are:

1. This thesis was able to establish that gas hydrate could initiate corrosion along the natural gas pipeline.
2. The thesis also established that corrosion inhibitors aid the hydrate formation along the deepwater gas pipeline but at different rates. It further investigated DPC at different pressures and concentrations due to its significant promotional ability which opened more knowledge to the negative and positive consequences of using the chemical.
3. Since this study appeared to be an entirely new research area, there was no known existing mathematical model to rely upon, hence, the need for an extensive literature. Finally, a functional and reliable model was developed and validated by comparing the generated results with the outputs from other related corrosion models. This model serves as another contribution to knowledge from this work.
4. This thesis established the importance of component interactions during the formation of gas hydrates and the ability of H_2 and N_2 gases to significantly inhibit this flow assurance problem.
5. Through the recommendation for further work, this thesis successfully demonstrated both the academic and commercial values of the entire study.

1.7 The Thesis Outline

The objectives of this work were achieved by following a systematic research projection based on four questions as summarized below while Figure 1.2 provides a diagrammatic representative of the thesis structure.

Step 1: Can Gas Hydrate (Clathrates) initiate Internal Corrosions along Gas Pipelines?

This question came up due to critical observations on physical shape and chemical composition of hydrates during and after formation. Both the semi and fully formed hydrates could be considered as particles, and particles are initiators of erosion-corrosion.

Thorough literature search was carried out while considering the above question. Several pipeline projects were studied with their various operating conditions. Kinetic and thermodynamic conditions aiding hydrate formation along the deepwater pipelines were studied. The clathrates flow behaviors during and after the formation were eventually used to positively fill this knowledge gap.

Step 2: Can Corrosion Inhibitors aid Hydrate Promotion along Deepwater Pipelines?

This question was necessitated due to similarities in the surfactant properties and chemical structures between corrosion inhibitors and some established hydrate promoters.

This question was answered through experimental investigations on five corrosion inhibitors commonly used at offshore regions. The considered inhibitors have different active functional groups and chemical structures. The general investigations on the inhibitors were carried out in a Cryogenic sapphire cell at 100bar and 500ppm while the particular inhibitor with the highest significant impact on hydrate formation temperature was further studied at different concentrations and pressures.

An industrially prepared natural gas composition containing 20% CO_2 was used throughout this study. A constant composition gas is needed to ascertain acceptable accuracy for this work.

Step 3: Can the Resulting Corrosion Rate be Quantified?

If hydrates actually behave like particles within the underwater pipelines to cause corrosions, the rate should be considered for quantification. This will assist in the pipeline design stage, material selection as well as in projecting the shelf-life of the pipeline.

Since this model was new, the existing corrosion models were reviewed, followed by systematic development of a functional model for the corrosion-hydrate relationship. A program, written in Matlab code was then developed to simulate the model whose validity was finally verified by comparison of the generated results with the outputs from previous corrosion models.

Step 4: Are there other possible means of inhibiting the Formation of Gas Hydrates?

Considering the cost implications of these new discoveries on the industry, there could be cheaper but still effective means of inhibiting gas hydrates along the pipeline trunk.

This part of the study was conducted by mixing the most effective hydrate formers in the gas composition (CH_4 and CO_2) at different ratios to study the impacts of component interactions on the formation properties. H_2 and N_2 were then mixed with these compositions at various ratios to study their inhibitive abilities.

Roles of Corrosion and Hydrate Formation on Natural Gas Pipeline Failures

Background → Motivations → Methodology → Contributions

Mathematical Modeling   Experimental studies

Chapter 1
Introduction

 Importance and global acceptability of natural gas (1.1)

Shortcomings on knowledge about hydrate-corrosion relationshins (1.2)

No experimental work on hydrate-corrosion relationships (1.5).

No existing corrosion rate model with gas hydrate as corroding agent (1.5)

Chapter 5

Corrosion-Hydrate model

Review of existing models (5.2)

Identified knowledge gap (5.3)

The model development (5.4)

Model simulation with required data (5.5 and appendix 1)

Model validation (5.6)

Identified the possibilities for gas hydrates to initiate internal corrosions in gas pipelines (2.6 and 7.1.1)

Documentation of case studies on pipeline failures (2.10)

Established the ability of corrosion inhibitors to promote formation of gas hydrates, chemistry and the hydrate patterns (3.4, 4.4 & 7.1.2)

Developed a corrosion rate model with gas hydrates as the corroding agent (5.4, 5.5, 5.6 and 7.1.3)

Established the ability of H_2 and N_2 gases to inhibit gas hydrates (6.4.6 and 7.1.4)

Established two potential PhD works for further studies and the Thesis commercial value (7.2)

Chapter 2
Natural Gas Pipelines: Importance and problems

Comprehensive literature review on gas pipeline history, classifications and existing projects (2.1-2.4)

Hydrate formation, types and consequences (2.5-2.7)

Natural Gas pipeline corrosion: Types, chemistry and implications on flow assurance (2.8-2.9).

Pipeline failures: Economic, safety and environmental impacts with case studies (2.10-2.11).

Chapters 3 and 4

Investigated the ability of corrosion inhibitors to promote gas hydrates

Literature review (3.2 and 4.2)
Experimental set-up (3. 3.1, 3.3.2, 3.3.3)
Preliminary investigations (3.3.4 and 4.3.2)
Experimental procedures (3.3.4, 4.3.3, 4.3.4, 4.3.5)
Results and discussions (3.4 and 4.4)

Chapter 6

Investigated the application of H_2 and N_2 gases as hydrate inhibitors

Literature review (6.2)
Preliminary studies (6.3.2)
Mixed gas preparations (6.3.3)
Experimentation (6.3.4 - 6.3.8)
Investigation on CH_4 only
Investigation on $CH_4 + H_2$
Investigation on $CO_2 + H_2$
Investigation on $CH_4 + CO_2$
Investigation on $CH_4 + CO_2 + H_2$
Investigation on $CH_4 + CO_2 + N_2$
Results and discussions (6.4)

Figure 1.2: Thesis structure.

9

2. Natural Gas Pipelines: Importance and Problems

2.1 Introduction

The global demand and utilization of natural gas and its major component (methane), compared with other fossil fuels have increased most rapidly over the past few years. The gas has been gradually accepted as a substitute to other fossil fuels since it is economically cheaper to produce; coupled with its abundance availability and environmental friendliness (Table 2.1). The gas composition varies from field to field and region to region (Table 2.2).

Table 2.1: Typical uncontrolled factors for natural gas and other stream generator fuels (Pounds per MMBtu heat input) (American Gas Association, 1986; Obanijesu and Sonibare, 2005)

	SOx	Particulate	NOx	HC	Trace Metals
Coal	5.70	2.54	0.90	0.005	0.009
Oil (Residual)	3.22	0.23	0.39	0.01	0.0002
Solid Waste	0.49	3.22	0.31	-	-
Wood	0.02	4.88	0.25	-	-
Natural Gas	0.001	0.01	0.23	0.003	0.00

Natural gas is domestically used for heating buildings and water, cooking, drying and lighting (Brkić and Tanasković, 2008; Joelsson and Gustavsson, 2009). Home appliances running on natural gas include furnaces, barbecues, fireplace logs, pool and spa heaters, and fire pits. Natural gas air conditioning also exists, though; this is not as popular as the electrical alternative.

Table 2.2: Natural gas compositions from different gas fields (Obanijesu et al, 2011)

Composition		Molar Composition (%)									
	Utorogu Nigeria	Kokori Nigeria	Burgan Kuwait	Kirkuk Iraq	Uthmaniyah S/Arabia	Hassi R'mel Algeria	Ekofisk Norway	Kapuni N/Zealand	Uch Pakistan	Lacq France	Groningen Netherland
Methane	90.19	68.42	74.3	56.9	55.5	83.7	83.3	45.6	27.3	69.0	81.3
Ethane	6.94	7.65	14.0	21.2	18.0	6.8	8.5	5.8	0.7	3.0	2.9
Propane	2.09	11.27	5.8	6.0	9.8	2.1	3.4	2.9	0.3	0.9	0.4
Butane	0.775	8.42	2.0	3.7	4.5	0.8	1.5	1.1	0.3	1.0	0.1
C_5^+	0.012	2.67	0.9	1.6	1.6	0.4	1.0	0.8	-	-	0.1
Nitrogen	-	0.16	2.9	-	0.2	5.8	0.3	-	25.2	1.5	14.31
Hydrogen sulfide	-	-	0.1	3.5	1.5	-	-	-	-	15.3	-
Carbon-dioxide	-	1.02	-	7.1	8.9	0.2	2.0	43.8	46.2	9.3	0.9

Industrially, the gas is a major source of electricity generation (Shukla et al, 2009; Tourkolias et al, 2009). As an efficient and convenient fuel, the gas is used in developed countries such as Australia, Canada and most European countries in transportation sector to run cars, trucks and heavy duty service vehicles (Kamimura, 2006; Felder and Dones, 2007), while some current researches in the aviation industry are targeted at designing aircrafts that will use natural gas as fuel (Gazzard, 2008a; Gazzard, 2008b; Greenair, 2009). Also, the gas plays a significant role in the power plant technology (Mahmut, 2005; Pilavachi et al, 2009). Natural gas is used in the making of anti-freeze and plastic. Food processing industries essentially use the gas to power up their plants while waste treatment and petroleum refining are also recognised consumers of natural gas. The gas is also useful in the production of petrochemicals.

In 2000, the total world reserve and production of the gas were 150.19 trillion cubic meters (tm^3) and $2.4223tm^3$ respectively (UNCTAD, 2009). Russia is the major producing nation (Gelb, 2006) with the global highest oil and gas reserves of 69.1 billion barrel and $48.14tm^3$ respectively (representing 38% of global natural gas reserve) while Australian conventional gas reserve as at 2006 was $2.43tm^3$ (DRET, 2009). The United States gas demand for 2003 was estimated at 786.32billion cubic meters (bm^3) (Hill, 2005) while gas demand of the EU 15 was projected to be 420–$650bm^3$ and 610-$900bm^3$ by 2010 and 2020 respectively (Table 2.3).

Table 2.3: Summary of some European gas demand scenarios (bm^3) ([a] OME,2002; [b] IEA, 2001); [c] Stern, 2001)

	1999	2010	2020
EU 15 [a]	386	500	597
EU 30 [a]	462	642	777
EU 15 [b]	386	420-650	533-650
EU 30 [c]		580-690	610-900

EU 15 = Austria, France, Belgium, Greece, Germany, Italy, Luxembourg, Netherlands, Portugal, Spain, Ireland, United Kingdom, Denmark, Sweden, Finland.

EU 30 = EU 15 + Turkey, Bulgaria, Greece, Rumania, Czech Republic, Hungary, Poland, Slovakia, Slovenia, Estonia, Latvia, Lithuania, Norway, Switzerland.

2.2 Natural Gas Production and Transportation

Natural gas exists in the reservoir as a non-associated, associated (or solution) or gas-cap gas. The non-associated gas is the one existing in a reservoir without a contact with oil, the solution gas is the one where the gas dissolves in the oil at the reservoir conditions whereas, and the gas cap is the gas overlying the oil phase in the reservoir. Of the three groups, non-associated gas represents 72% of the available global reserves while solution and gas-cap gases are 8.5% and 9.5% respectively (Valais, 1983). The gas is located thousands of meters below the earth surface with the fluid's pressure in the pores of the rocks ranging between 10MPa/km while in hydrostatic regime (only supporting the weight of the overlying fluid column) to 25MPa/km in geostatic regime (supporting all or part of the weight of the rock column) (Rojey et al, 1997). The gas molar mass and density at STP are 19.5g and 0.862Kg/m^3 respectively while (Table 2.4) shows its thermodynamic properties at NTP.

Table 2.4: Natural gas thermodynamic properties at normal temp and pressure of 293K and 1 atm (Obanijesu et al, 2010a)

MW	Density	R (Gas constant)	Cp	Cv	Cp/Cv= γ
	(kg/m^3)	kJ/(kg.K)	kJ/(kg.K)	kJ/(kg.K)	
19.5	0.8034	0.426	2.345	1.846	1.27

This compressible hydrocarbon is detected in a reservoir by sensors which are geophones for onshore reservoir or hydrophones for offshore. This is based on the analysis of the reflection of elastic waves transmitted by the seismic source, gathered on a surface marking the boundary between two layers of different acoustic impedance. For onshore reservoirs, the reflection is generated by the use of explosives to blast the reservoirs whereas; air guns are used for offshore reservoirs to discharge compressed air into the water. These will propagate pressure (P) or shear (S) waves which propagate the reflections at different velocities. The reflection of the waves on impedance discontinuities is used to obtain the structural image of the geological layer. The discovered hydrocarbon is then produced using a rotary drilling technique. The well is then completed after acquiring wireline logs to measure the

formation's characteristics and fluid in place. The casing packer and some safety devices (storm choke at downhole or surface-controlled subsurface safety valve near the surface) are then installed before installing the Christmas tree. Finally, pipelines are connected to transport the gas off the field over a long distance to a flowstation for various separation operations as required based on composition. Various products are finally transported through other set of long pipeline networks to various end users.

2.3 Natural Gas Transportation Options

Various transportation options of natural gas from off-take include long pipelines transport, methanol, Liquefied Natural Gas (LNG) and compressed natural gas (CNG) of pressure between 3000 and 3600 psi (Imperial Venture Corp, 1998). From these options, only long pipelines and LNG are in common use. The unit cost of pipeline option is clearly superior to that of LNG due to the required high cost of refrigeration and liquefaction of boiled-off liquids and the high risk of over-pressurization for LNG. Transportation by methanol and CNG demonstrate unit costs which are similar to pipelines but these are largely theoretical at present. Due to easier transportation option as the low-cost and safe mode of long distance transportation of petroleum and its products (Jacobs, 2002), the gas is conveyed from reservoir to depots, refineries, jetties and final end-users through long pipeline network systems.

2.3.1 Classification of pipelines

Pipelines are mainly divided into gas and oil pipelines depending on the nature of the cargo conveyed. Main components of a pipeline network are operational areas and the pipeline segments. Operational areas may be distribution centers, ports or refineries and are connected by pipeline segments. Gas and liquid hydrocarbon pipelines are essentially similar with the greatest operational difference resulting from the varying needs of transporting gas versus liquid. Oil pipelines require pumps to propel the liquid contents while gas lines rely on compressors to force the resource through the pipes.

Although, the fundamental design and purpose of oil and gas pipelines are similar, there are differences in their conveyance systems. Gas well flowlines connect

individual gas wells to field, gas treating and processing facilities, or to branches of a larger gathering system, processed at the treating facility to remove impurities. From field processing facilities, the dried, cleaned natural gas enters the gas transmission pipeline system, analogous to the oil trunk line system (EPA, 1997). For oil pipelines, once oil is pumped from a reservoir, it travels to a tank battery. One or more tank batteries may be installed in a single field, each serving a number of individual wells. From the tanks, oil is moved through large diameter, long-distance trunk lines to refineries or to other storage terminals.

Pipelines are usually manufactured with material of special characteristics and properties due to the nature of the conveyed cargo to be transported. Special considerations are given to factors such as tensile strength, stiffness (elastic modulus), toughness (fracture resistance), hardness (wear resistance) and fatigue resistance; the effects of high and low temperatures on the mechanical properties; corrosion resistance; thermal conductivity, electrical resistance and magnetic properties; availability in standard sizes-plates, sections and tubes; and cost. Commonly used materials are the carbon steel, stainless steel and the Monel. Stainless steel is the most frequently used corrosion resistant material in chemical industry. To impact corrosion resistance, the chromium content must be higher than 12% and the higher the chromium content, the more resistant is the alloy to corrosion in oxidizing conditions. Nickel is added to improve the corrosion resistance in non-oxidizing environments with three broad classes, which include Ferritic, Austenitic, and Martensitic depending on material compositions. The uniform structure of Austenite is the structure desired for corrosion resistance and it is widely used in the chemical industry.

Monel, the classical nickel-copper alloy with the metals in the ratio 2:1 is probably after the stainless steels. It has good mechanical properties up to 500^0C. It is more expensive than stainless steel, has good resistance to dilute mineral acids and can be used in reducing conditions where the stainless steel would be unsuitable.

The stannates, AZ91D (a Die casting magnesium alloy known as the alternative to zinc and aluminum because of its high-purity and excellent corrosion resistance) is appreciated in the industry due to its properties (Tables 2.5 and 2.6) and ability to reduce corrosion rates of a coated pipeline by behaving as a barrier to prevent the

non metallic ions' attack. Hence, it decreases the susceptibility of the alloys to corrosion; however, increasing stannate concentration was found to have an adverse effect on the corrosion resistance (Hamdy, 2008).

Table 2.5: Typical room temperature mechanical properties of AZ91 castings (Obanijesu et al, 2010b)

	AZ91A,B,D		AZ91C,E	
Property	F Temper	F Temper	T4 Temper	T6 Temper
Tensile strength , MPa (ksi)	230 (33)	165 (24)	275 (40)	275 (40)
Tensile yield strength, MPa (ksi)	150 (22)	97 (14)	90 (13)	145 (21)
Elongation in 50 mm (2in) %	3	2.5	15	6
Comprehensive yield strength at 0.2% offset, MPa (ksi)	165 (24)	97 (14)	90 (13)	130 (19)
Ultimate bearing strength, MPa (ksi)	-	415 (60)	415 (60)	515 (75)
Bearing yield strength, MPa (ksi)	-	275 (40)	305 (44)	360 (52)
Hardness, HB	63	60	55	70
Hardness, HRE	75	66	62	77
Charpy V-notch impact strength, J (ft.Ibf)	2.7 (2.0)	0.79 (0.58)	4.1 (3.0)	1.4 (1.0)

Table 2:6: Typical tensile properties of AZ91C-T6 sand castings at elevated temperatures (Obanijesu et al, 2010b)

Testing temperature		Tensile strength		Yield strength		Elongation
^{o}C	^{o}F	MPa	Ksi	MPa	Ksi	In 50mm %
150	300	185	27	97	14	40
240	400	115	27	83	12	40

2.4   Some Existing Natural Gas Pipeline Projects

Due to its rising global demand, several onshore and offshore inter-state and transboundary natural gas pipeline networks are being constructed with each transporting millions to billions cubic meters per day with construction cost running into several millions or billions of US dollar (Tables 2.7 and 2.8).

Almost 500,000 miles of oil and gas transmission pipeline criss-cross the United States (Parformak, 2004) with the Alaskan oil pipeline bringing crude oil from the Prudhoe Bay oil field on the North Slope to tanker ships docked in southern Alaska, traversing 1270 km of Alaskan wilderness (Figure 2.1). The pipeline carries up to 2 million barrels of oil per day from the Arctic coast to the Gulf of Alaska (Encarta, 2004).

Shell Transmission owns over 17 Gulf of Mexico natural gas pipelines in operation or under construction with capacity of almost 9 billion cubic feet per day (b-ft^3/d) while as at 2003, Equitable Gas Company was supplying over 250,000 customers in Southwestern Pennsylvania as well as providing natural gas distribution services to over 260,000 residential, commercial and industrial customers located mainly in the city of Pittsburgh and surrounding municipalities in Southwestern Pennsylvania.

Encarta Encyclopedia, Photo Researchers, Inc./Pat and Tom Leeson

Figure 2.1: Alaska oil pipeline - A suspended pipeline (Encarta, 2004)

Table 2.7: Various interstate pipeline projects, their diameter and length

Project name	Country	Start Point	End Point	Diameter (in)	Length (km)	Capacity	Construction Cost
	Australia	Ballera	Wallumbilla	16	293		
	Australia	Bayu Undan field	Darwin	24	187	2250 bpd	A$1.5bn
Eastern Gas Pipeline	Australia	Longford	Sydney	18	312		
	Australia	Darwin	Moomba		3500	-	
	Australia	Bunbury	Albany		320	-	
	Australia	Darwin	Dunbury		1530	-	
Natural Gas Pipeline (Offshore + onshore)	Australia	Longford, Victoria	Bell Bay,Tasmania	14	734		$350m
Gove Lateral	Australia	Moreton, Cape York	Weipa	16	670		
PNG-Qweensland Project		Torres Strait (Papua New Guinea)	Gladstone, Australia		816		
Enbridge Phase 5 (2007)	USA	Black Horse Corners Gate (North Dakota)	Route Segment E North Dakota	42	83.2	30000 bpd	US$78m
Enbridge Phase 6(2009)	USA	Western End	Minot, North Dakota	24	1050	40000 bpd	US$150m
Enbridge Phase 6 (2009)	USA	Minot	Clearbrook,			51000 bpd	

			Minnesota				
Pathfinder (Proposed)	USA	North Border Pipeline	Moyes, Minnesota and Emerson		440		
Pathfinder Natural Gas (on-going)	USA (2008-2010)	Wamsutter, Wyoming	Midwest	42	800	2.0 billion cfpd	
Bison (On-going)	USA (2008-2010)	Rookies Mountain Area	Midwest and Chicago	36	1076.8	Over 610	
Pathfinder	USA	Meeker Colorado	Wamsutter	30	225		
Escravos – Lagos Pipeline System	Nigeria	Escravos Warri	Alagbado, Lagos	24	359	2.7 billion cfpd	
WAGP	Nigeria	Alagbado, Lagos	Badagry, Lagos	30	57		
WAGP	Ghana	Takoradi	Effasu	12	80		

Table 2.8: Various global transboundary natural gas pipeline projects

Project name	From	To	Diam (in)	Length (km)	Nature	Capacity	Construction Cost
PNG-Qweensland Project	Kubutu, Papua New Guinea	Gladstone (Australia)	16	1195	Onshore/ Offshore		
Keystone XL pipeline (2008)	Alberta, Canada	Nebraska USA	36	3200	Onshore/ Offshore	1.1 million bpd	US$12 billion
WAGP, Project	Lagos, Nigeria	Takoradi, Ghana	Vary with portion	674	Offshore	11.3 billion cmpd	US$550 million
WAGP, Project	Nigeria	Cotonou, Benin	20	51	Offshore		
WAGP, 2009	Cotonou, Benin	Lome & Tema Togo	16	276	Offshore	3.39 billion cmpd	US$130 million
WAGP, 2009	Tema, Togo	Takoradi, Ghana	12	233	Offshore	1.7 billion cmpd	US$106 million
BTC Pipeline 2004	Baku, Azerbaijan	Ceyhan Turkey		1572	Offshore		US$3.6 billion
Subsea Gas Pipeline 2004	Sangachal Terminal, Azerbaijan	Central Azeri Georgia	28	186	Offshore		

Due to the mounting pressure on the gas utilization from increase in global population and industrial applications, Gas Industry is now forced to explore at deepwater regions in search for the crucial energy source; and with the successful operation of the existing pipeline networks, more countries are getting involved thereby promoting cross-border networking. Offshore gas wells run from various depths depending on the depth of the water which are generally classified as shallow or deep water. While Sangachal gas terminal pipeline, located at 55km South of Baku and covering area of 500 km^2 and known as one of the world's largest integrated oil and gas processing terminals was laid by a pipe-lay barge at 200m water depth, the depth of the six East Azeri gas well range from 4000m to 5300m; and the design depth for the Shah Deniz well is 6285m.

Saipem s.p.A constructed a $7 billion worth of natural gas export pipeline between Qatar, Oman and UAE. The two-phase project, tagged as the Dolphin Gas Project (DGC) started in March 2004 and was completed in August 2006. The project which still remains one of the largest Transboundary projects in the Middle East, involved shipping about 440,000 tons of steel pipes manufactured from Japan to the Gulf for coating and laying in a continuous process to a maximum depth of 50 meters. The first phase involved the development of two platforms in Qatar's North field, two multi-phase offshore sealines to the processing facilities and the gas treatment and compression plants at Ras Laffan. The second phase involved the construction of a 48in diameter by 364km subsea pipeline that carries gas to the UAE at a cost of $3.5bn. The pipeline, with maximum capacity of 3.2 billion cubic feet of natural gas per day (b-ft^3/d) carried its first gas in 2007 at 2b-ft^3/d with an expected life period of 25 years.

In 2004, a 1440 km long pipeline was constructed from Libya at a cost of $6.6 billion to Egypt and Tunisia for natural gas supply (Cordesman and Al-Rodhan, 2006). The Transboundary pipeline project termed "Western Libyan Gas Project" was constructed at 2km offshore Wafa Coaster Plant at the water depth of 28m. The pipeline was designed for 25 years duration at a flowrate of 5600m^3/hr.

Nigeria is presently constructing a $550 million pipeline of 617 km offshore pipeline and 57 km onshore pipe-length to transport 11.3 bm^3/d of natural gas to power generators and industrial consumers in Ghana, Benin and Togo for thermal and

industrial. The project tagged "West African Gas Pipeline (WAGP)" Project called for installation of 617 km of offshore pipeline and 57 km of onshore pipeline from an offtake at an existing natural gas system near Lagos (Amao, 2004) with a throughput capacity of 12.718 x 10^9 m^3 (450 MMscfd). The project was planned to be extended to some other West African countries with time.

Of equal importance is the on-going Gorgon project in Australia which is notably known for her significant natural gas reserves. The Gorgon Project, estimated at AUS$43 billion is designed to extract and process natural gas from eleven separate natural gas reservoirs on the North West Shelf of Western Australia. The project is set to produce up to 15 million tonnes per annum of LNG which is to be transported to China and also provide 300 tera joules (276 million ft^3) of natural gas per day to Western Australia's domestic gas pipelines. The project also incorporates a carbon dioxide (CO_2) sequestration plant that will inject up to 120 million tons of CO_2 underground within the lifetime of the plant. The processing plant for the natural gas production and CO_2 sequestration is to be built on a small section of Barrow Island, a "Class A" nature reserve. The Gorgon project involves lengthy subsea piping from the natural gas fields to the processing plant.

2.4.1 WAGP Project – Project description

WAGP project (Fig 2.2) involved transportation of 11.3 bm^3/d natural gas supplies from Nigeria to power generators and industrial consumers in Ghana, Benin and Togo for thermal and industrial uses through an additional installation of 617km of offshore pipeline and 57km of onshore pipeline from an offtake at the existing 359km Escravos-Lagos natural gas system.

The project, whose construction started in 2005 with an estimated cost of $550m and initial shelf-life of 20 years before renewal, included pipeline installation and metering, pressure regulation, gas scrubbing and compression facilities. The work was sponsored through the joint venture agreement of Nigerian National Petroleum Corporation (NNPC), ChevronTexaco West African Gas Pipeline Co. Ltd, Shell Overseas Holdings Ltd and Takoradi Power Co. Ltd and the total pipe-length is 1033km.
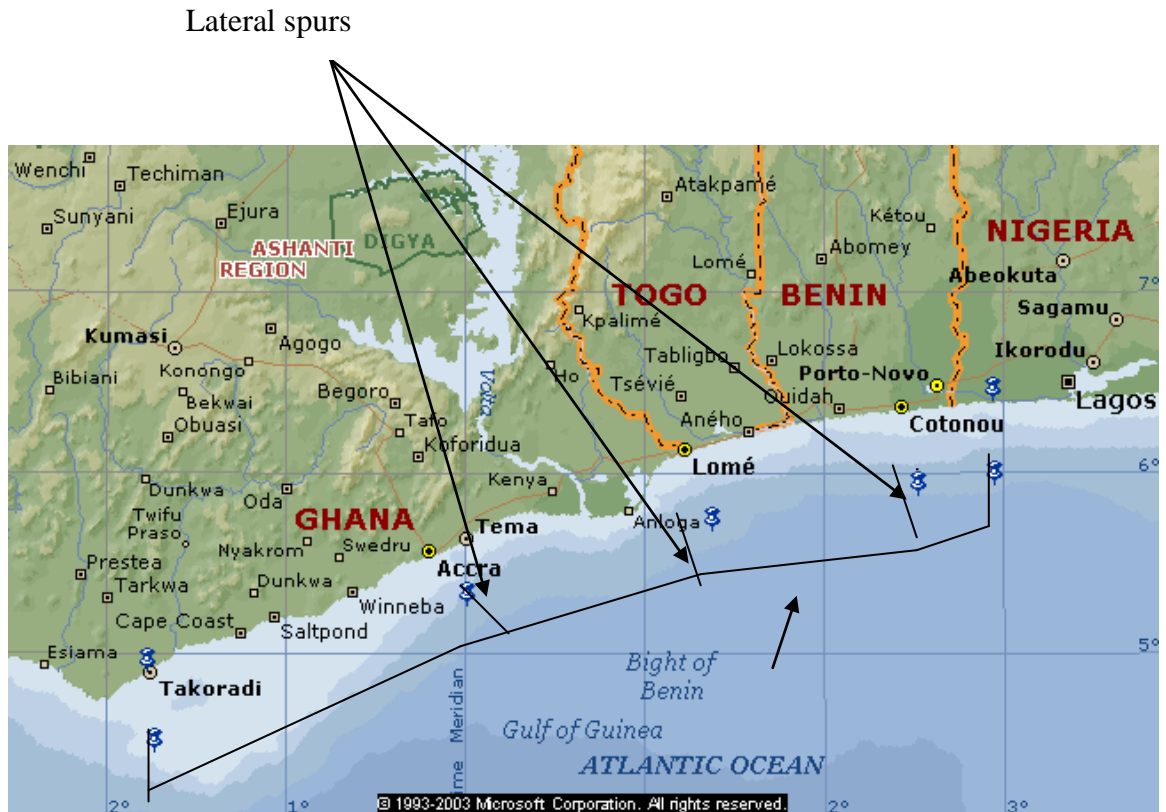
Figure 2.2: View of the WAGP project from Nigeria to Ghana with laterals at Cotonou, Lome, Tema and Takoradi (Obanijesu and Sonibare, 2005 – modified)

359km of the total 1033km pipe-length was already in place through the existing pipeline system from Escravos at Niger-Delta area of Nigeria to Alagbado in Lagos. Of the remaining 674km that was constructed, 57km of the pipe-length would transport the gas from Alagbado (Lagos) to Badagry beach in Nigeria while 617km transboundary portion ran offshore from Badagry beach (in Nigeria) through Cotonou (in Benin) and Lome (in Togo) to Takoradi Power Station (in Ghana). Another 80km offshore pipe-length was then run from Takoradi to Effasu in Ghana. Specifically, the existing Escravos-Lagos pipeline with 24in internal diameter and capacity of about 2.5b-ft^3/d (4.24 x 10^9 m^3/d) had the tie-in point to the WAGP project at Alagbado West of Lagos. The Alagbado-Badagry pipeline network had an internal diameter of 30in with length of 30km onshore and 27km offshore as an extension of the existing Escravos-Lagos Pipeline System. The onshore portion commenced at Alagbado and terminated at the Atlantic Beach in South of Ajido near Topol Badagry in Lagos state after crossing the Badagry Creek. The Badagry

23

Lagoon Creek and the Atlantic beach crossing was achieved using both the horizontal directional drilling and trenching and burial operations.

The onshore pipeline system included a mid-line relief system located off the Otta-Idi Iroko highway near Canaan Land in Ogun state. An 18000-horse power onshore compressor station was put in place at the Lagos beach from where 20in by 51km pipeline was connected and extended 15km offshore before turning west across the Nigeria-Benin border to Cotonou. While maintaining the 15km offshore extension, the internal diameter was reduced to 16in for 276km to Tema where a further size reduction to 12in for another 233km to Takoradi. Another 12in x 80km offshore pipeline was linked from Takoradi to Effasu.

Along the base route, additional lateral spurs, averaging 15km were extended from the base pipeline route to landfall regulating and metering facilities at Cotonou, Lome and Tema. The spur diameters were 8in, 10in and 18in at Cotonou, Lome and Tema respectively while a compression station operating between 40 and 150MW was installed at Cotonou. The Cotonou-Tema pipe-length with the initial cost estimate of \$130million was designed to convey 60MMscfd (1.70×10^9 m³/d) natural gas initially with the ultimate expectation of 120MMscfd (3.39×10^9 m³/d). The ultimate destination in Ghana was the Volta River Authority Plant in Takoradi. The Tema-Takoradi pipe-length with the initial cost estimate of \$106million was also designed to supply 60MMscfd (1.70×10^9 m³/d) of natural gas to Takoradi Power Plant with gas demand of 43MMscfd (1.22×10^9 m³/d) and the additional Hydro Power Plant in Effasu. In Tema, it was expected to supply VALCO power plant whose gas demand is 21MMscfd (0.60×10^9 m³/d). The specifications for each location are given in Tables 2.9 – 2.14.

Table 2.9: Benin power plant (Obanijesu and Macaulay, 2009)

Item	Comment
Operator	CEB
Capacity	40-150MW
Status	Preliminary Studies Done

Table 2.10: Segment 2 of the pipeline system (Cotonou to Tema) (Obanijesu and Macaulay, 2009)

Item	Comment
Capacity	80mmscfd (2.26 x 10^9 m^3) (initial) 120mmscfd (3.39 x 10^9 m^3) (final)
Length	276km
Diameter	16in
Cost	$130million (initial)

Table 2.11: Operating capacity of Valco power plant in Tema (Obanijesu and Macaulay, 2009)

Item	Comment
Operator	Valco
Capacity	Up to 100MW
Gas Demand	21MMSCFD (0.60 x 10^9 m^3) (Max.)
Type:	Combined Cycled Gas Turbine
Status	Under Evaluation
Remarks	Valco considering supplemental power to allow them to restart their 25% of capacity that is currently idle

Table 2.12: Segment 3 of the project (Tema to Takoradi) (Obanijesu and Macaulay, 2009)

Item	Comment
Capacity	60MMSCFD (1.70 x 10^9 m^3)
Diameter	12in
Length	233km
Cost	$106million (initial)

Table 2.13: Takoradi power plant (Obanijesu and Macaulay, 2009)

Item	Comment
Operator	Volta River Authority
Capacity	40MMSCFD (1.13 x 10^9 m^3)
Type	Combined Cycle Gas Turbine.
Type	Start-up: 2Q 1997
Status	Under construction
Initial fuel	Light crude oil
Financing	World Bank
Remarks	Two-100MW GE turbine to be installed.

Table 2.14: Tema power plant (Obanijesu and Macaulay, 2009)

Item	Comment
Operator	GNPC
Phase 1	
Capacity	131MW (simple cycle)
Expanded capacity	200MW (Combined Cycle)
Start-Up	Funding Pending
Phase2	
Capacity	120MW

2.4.2 The Australian Gorgon Project – Project Description

The Gorgon gas project, aimed at developing eleven natural gas fields (Figure 2.3) is estimated to cost about AUS$43 billion to the operators (Table 2.15).

As the biggest single investment ever made so far in Australia, the Gorgon LNG is expected to provide jobs for about 6000 people at the peak construction period, bring an export income of about $300 billion from LNG sales to customers in the Asia-Pacific over the next 20 years (Table 2.16). The project is also expected to buy about $33 billion worth of Australian good and services over the next few years and generate about $40 billion in government revenue over the next two decades.
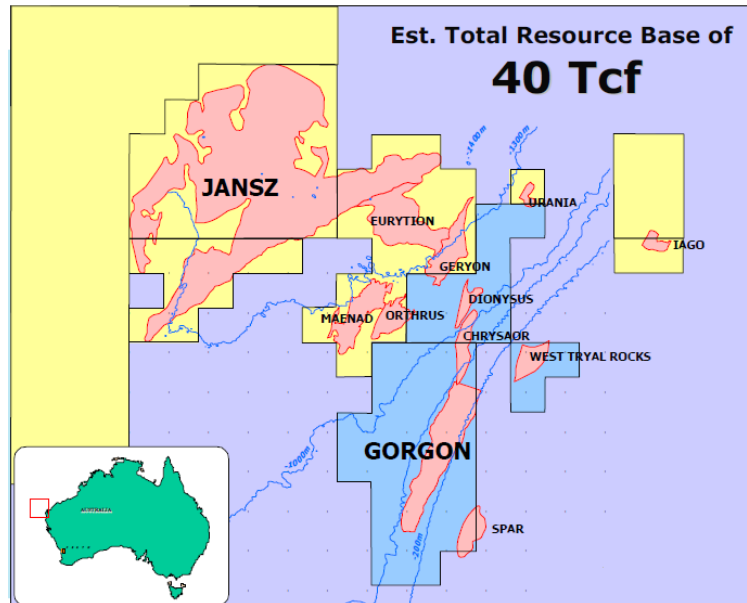
Figure 2.3: The eleven gas fields to be developed under Gorgon gas project (Thoebald, 2006).

Table 2.15: Gorgon operators by share (DSD, 2010)

Operators	Share (%)
Chevron Australia (main operator)	50
Exxon Mobil	25
Royal Dutch Shell	25

Table 2.16: Already signed sales and purchase agreements between the Gorgon Project stakeholders and Asia-Pacific establishments.

Stake holder		Quantity	Duration
Chevron Australia	Osaka Gas	1.4 Mtpa	25 years
	Tokyo Gas	1.1 Mtpa	25 years
	Chubu Electric Power	1.44 Mtpa	25 years
	GS Caltex of South Korea	0.5 Mtpa	20 years
Shell Petroleum	PetroChina		Long term
	BP		Long term
ExxonMobil	Petronet LNG (India)	1.5 Mtpa	20 year
	PetroChina (China)	2.25 Mtpa	20 year

The gas fields are located about 130 km off the north-west coast of Western Australia and collectively contain about 40 trillion cubic feet (tcf) of natural gas which is approximately 25% of Australia's known gas reservoirs with majority of the recoverable gas comings from the Jansz-lo and Gorgon fields. Gases from the fields would be channeled into Gorgon and Jansz fields depending on the nearer field and then transported through two separate subsea pipelines, one from each field (Figure 2.4) to a process plant located on Barrow Island (Figure 2.5) for separation into various components before further distribution to final destinations as Liquefied Natural Gas (LNG) or town gas (domestic gas).

Each pipeline has a different gas composition with the pipeline from Gorgon gas field consisting of high amounts of CO_2 while the pipeline from Jansz-Io predominately contains gas with very low condensate content (Table 2.17).
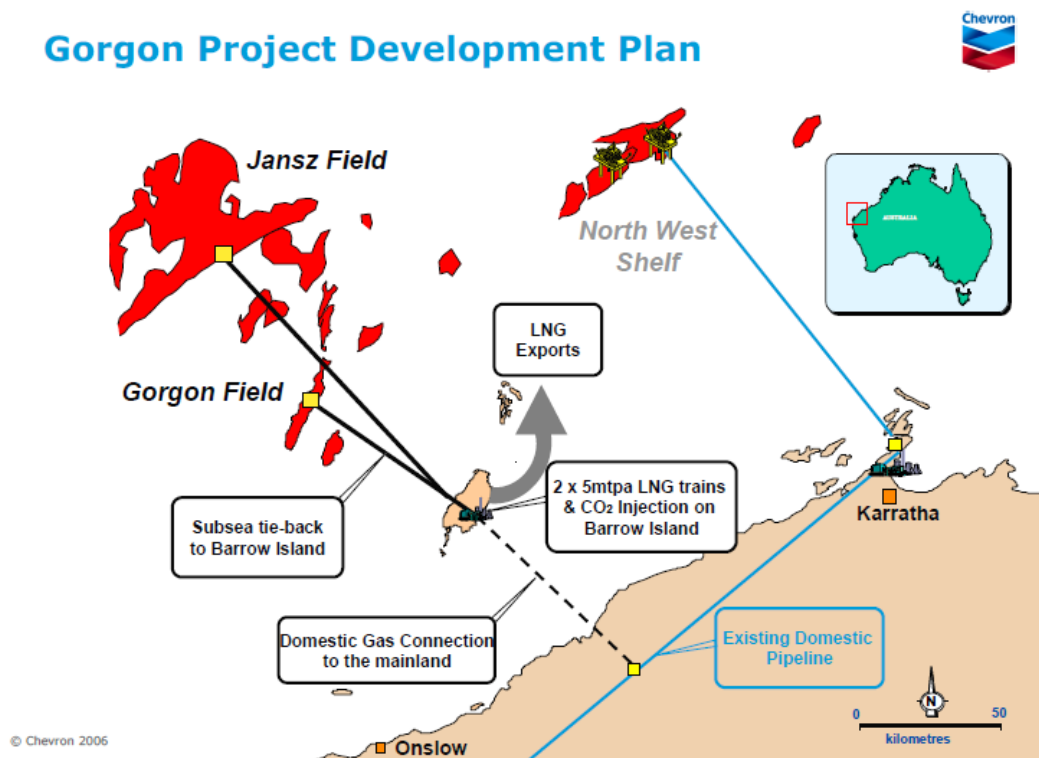
Figure 2.4: Conceptual map of Gorgon gas project showing relevant gas fields, pipelines and processing plant on Barrow Island (Theobald, 2006)
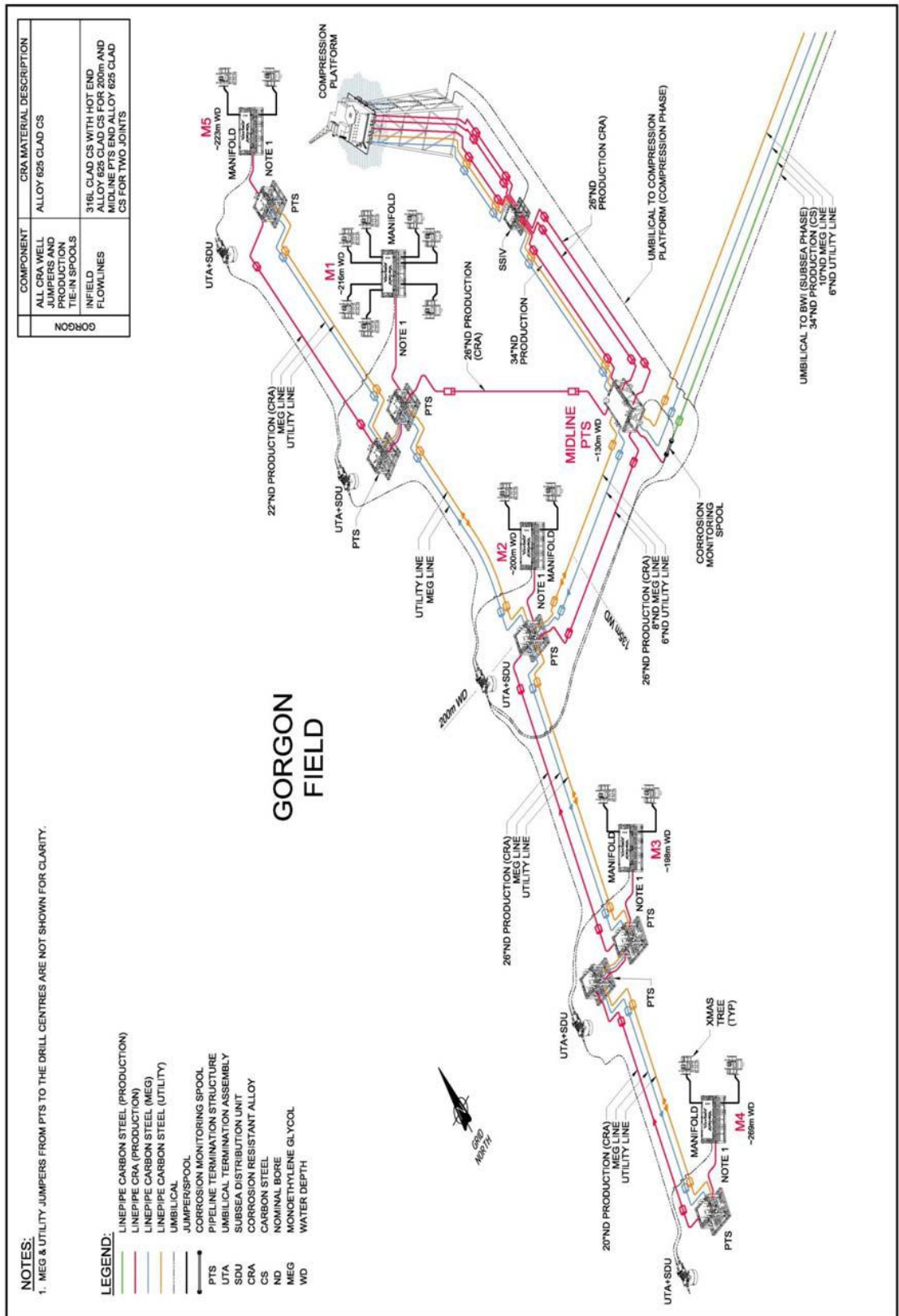
Figure 2.5: Gorgon gas project subsea well development schematic (Chevron Australia, 2011)

Table 2.17: Gorgon and Jansz fields' compositions and required specifications (Chevron Australia, 2009; Hosa et al, 2011)

Component*	Gorgon (Vol%)	Jansz (Vol%)	Typical LNG Specification (Vol%)	Current Domestic Gas Specification (Vol%)
CO_2	14-15	0.28	<100ppm	<3.6
N_2	2-3	2.35	<1	Total inert gasses <6.5
Hydrocarbons				
Methane	76.71	97.48	-	-
Ethane	3.23	3.75	-	-
Propane	0.89	1.06	-	-
Butane	0.3	0.41	-	-
Pentane and heaviers	0.13	0.63	-	-
Hydrocarbon Total	83+	97.4	99	93.5+

*Feed gas contains traces of hydrogen sulfide, mercury and aromatics from the reservoirs.

The tieback subsea pipeline from Jansz field which is 20in by 90km (Clough, 2011) is required to traverse some jagged, rocky and uneven seabed (Figure 2.6) from a depth of 1350m onto the continental shelf with substantially incline slope and cliff height of substantial maximum depth of 250m (Figure 2.7). A direct route from the Jansz field to the processing plant at Barrow Island would subject the pipeline to inclinations of up to 70 degrees, thereby passing through an area of seabed instability around the Chrysaor canyons which had recently shown some activity (Equid 2008).

The produced gas would be sent to Barrow Island where a gas treatment facility (Figure 2.8) has been installed to process 15 million tons per annum of LNG and 300 terajoules (276 million cubic feet) per day of domestic gas (Table 2.18). The treatment facility consists of three parts which are CO_2 geo-sequestration, LNG and domestic gas production facilities. The 14% CO_2 recovered from the gas stream after processing will be injected using the geo-sequestration facility into a saline aquifer approximately 2km below the production plant.

Table 2.18: Production rates of exports from Barrow Island.

Product	Production rate	Product destination
Condensate	20000 bbl/day	Japan, India and local markets
Liquefied Natural Gas	15 MTPA	Japan and India
Domestic Gas	300 terajoules/day	Perth, Western Australia

Figure 2.6: Seabed profiles at Jansz (Equid, 2008)
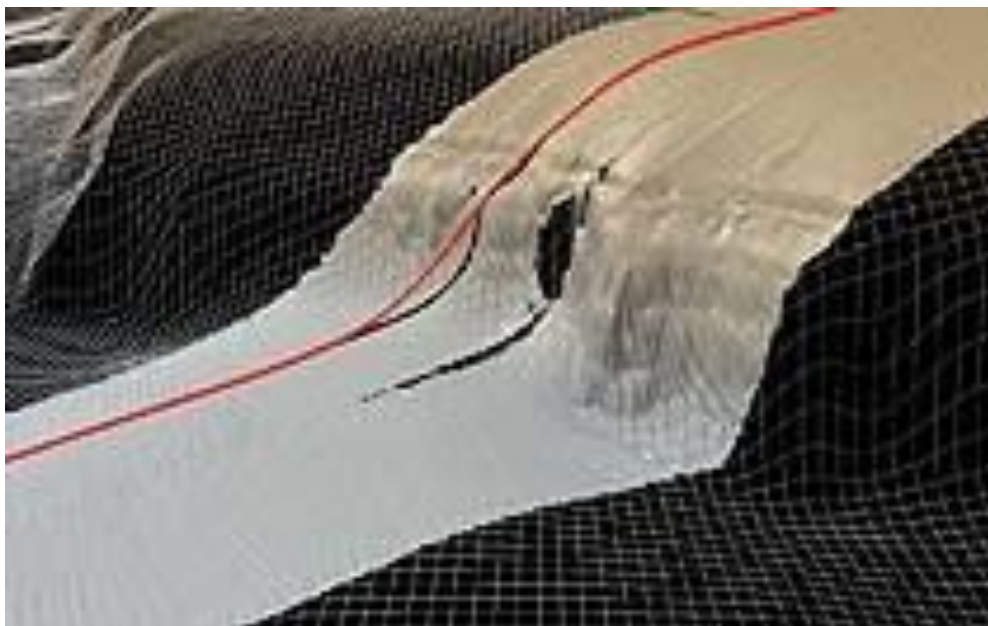
Figure 2.7: Pipe span due to cliff (RCEBC, 2009)

Figure 2.8: The gas treatment facility at Barrow Island

It is estimated that the plant will sequester a total of 120 million tons of carbon dioxide within the lifetime of the plant with a proposed maximum injection of 4.9 million tons per year through 8 wells. If these injection rates are reached, the Gorgon project is expected to reduce net global greenhouse gas emissions by approximately 45 million tons per year. Geo-sequestration injections are expected to commence in 2014 (Hosa et al. 2011).

The LNG is to be exported to China and neighboring countries whereas, the domestic gas whose main treatments involve acid gas removal, dehydration and liquefaction (Figure 2.9) is for local consumption within Western Australia.

Barrow Island (Figure 2.10) is a Class "A" nature reserve due to the presence of unique and endangered flora, fauna and surrounding waters. It is located off the Pilbara coast 85 km North-North-East of the town of Onslow and 140 km west of Karratha. The Island is approximately 25 km long and 10 km wide and covers approximately 23500 ha. It is the largest of a group of islands, including the Montebello and Lowendal Islands. The Island is home to at least 22 unique terrestrial species which include the endemic Barrow Island Euro, White winged Fairy Wren, a subterranean blink snake and a range of other cave dwelling species. The island is also a significant nesting site for marine turtles. The mean ambient wind speed

around the Island during the summer period (October to March) is 6.6 m/s and the maximum summer wind speed is 16.2 m/s. The dominant directions during summer are from the South-West and West. During winter (April to September), winds approach from the East, South and South-West and have a mean speed of 5.8 m/s and maximum speed of 19.4 m/s. Easterly gales occur between May and August with speeds in the range of 12.5–20 m/s. (MetOcean 2006).
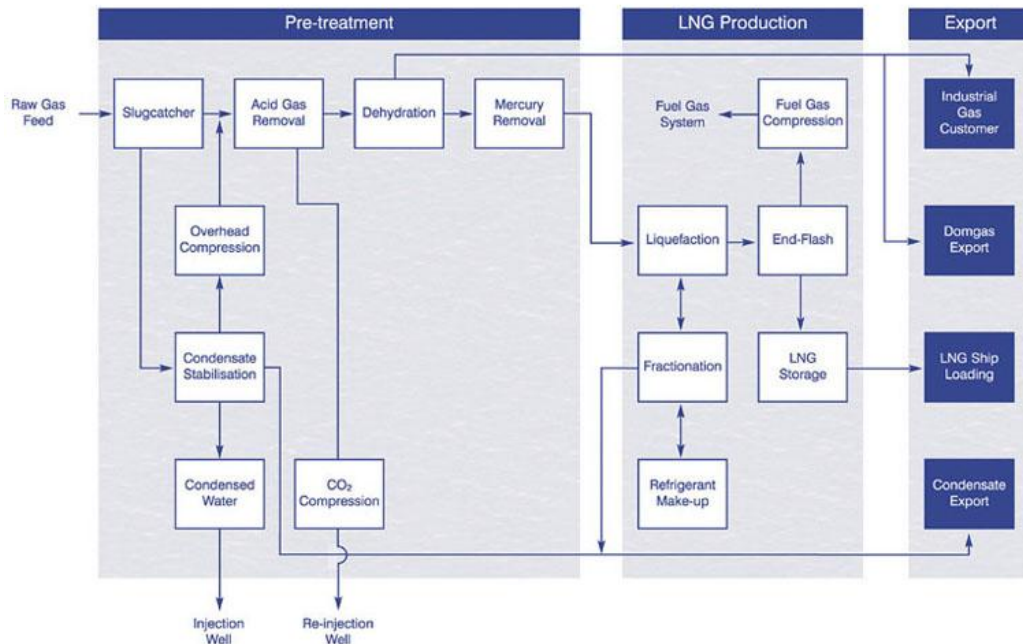
Figure 2.9: Gorgon gas processing plant (Chevron Australia, 2012)

Figure 2.10: Barrow Island and surrounding area

2.5 Hydrate Formation Problems along Offshore Gas Pipelines

2.5.1 General Description

During the offshore pipeline transportation, the low paraffinic homologous ($C_1 - C_4$) composition of natural gas usually combines with the non-hydrocarbon components of the gas (such as N_2, CO_2, H_2S) and water vapour to form gas hydrate which is one of the major flow assurance problems encountered in the production, processing and transportation of natural gas. Gas hydrates are ice-shaped, crystal lattice, solid compounds formed by the physical combination of water molecules with small hydrocarbon molecules and the non-hydrocarbon components at high pressure and low temperature due to the weak Van der Waals forces and the hydrogen bonding properties of water (Hao et al., 2006; Du et al., 2007; Liu et al. 2007). The crystalline compound is stabilized by the encapsulated smaller molecular diameters guest such as CH_4 and C_2H_6 (Sloan and Koh, 2007) which are trapped in the microcavities of a crystal lattice provided by the host water (Figure 2.11).
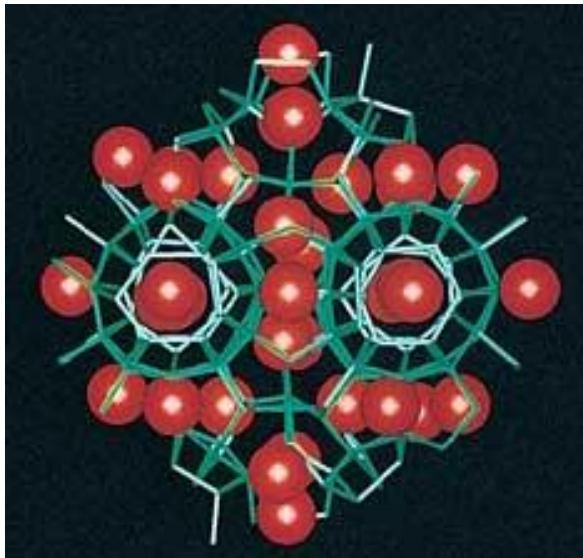
Figure 2.11: Gas hydrate when formed inside a gas pipeline (Obanijesu et al, 2011)

A typical hydrate composes of 90% H_2O while other components constitute the remaining 10% (Abdel-Aal et al, 2003). Specifically, at 1 MPa, ethane gas can form gas hydrates at temperatures below 4^OC whereas, at 3 MPa, it can easily form hydrate at temperature below 14 ^{O}C (Talaghat et al, 2009). Undersea gas transportation pipelines often have such thermodynamically suitable conditions for this formation (Palmer and King, 2008; Lorenzo, 2009) because the gas is

transported at supersonic velocity under high pressure and a very low ambient temperature.

Due to the rapid formation of gas hydrates, it is considered by far the most serious and common problem in flow assurance in the case of deep subsea transportation compared to other solid deposits (Sloan, 2005).

Hydrates have important bearing on flow assurance and safety issues in oil and gas pipelines due to their physical properties, most notably, the non-flowing crystalline solids which make them denser than typical fluid (Sloan, 2003).

2.5.2 Hydrate Formation Process

Water molecules are known to show some unusual properties through the boiling point, enthalpy of vaporization and expansion upon freezing when compared to other molecules with similar characteristics. This is explained by its possession of two unbounded pairs of electrons (from oxygen) which induce electrostatic charges on the molecules to result in hydrogen bonding. Though, hydrogen bonding is also present in alcohols and group 6A compounds with hydrogen, it is particularly stronger in water (Uno et al, 2000; Sovago et al, 2008). This enables water to form hydrates as a result of its hydrogen bonding property. This bonding causes water molecules as the host to align in regular orientation while the guest or former molecules (CH_4, C_2H_6, C_3H_8, Cl_2, H_2S, CO_2, e.t.c.) stabilize the aligned molecules through the van der Waal forces (which must be strong enough) to precipitate a solid mixture known as hydrate (Cwiklik and Devlin, 2010), however, there is no bonding between the guest and host molecules.

Solubility of the guest molecule is also of paramount importance since it must not be highly soluble in water (Martın and Peters, 2009; Jacobson and Molinero, 2010). CO_2, H_2S and SO_2 that are significantly soluble represent the upper limits while ammonia and HCl that are highly soluble in water cannot form hydrates.

Hydrate formation is enhanced by turbulence (velocity and agitation), nucleation sites and free water (Moon et al, 2003; Anderson et al, 2007; Wenji et al, 2009). Gas is normally transported at high velocity which gives rise to agitation along the pipe-length due to the flow condition. This gas will finally flow through the narrowing at the choke valves where temperature drop will be experienced due to Joule Thompson

35

effects, hence, the formation of hydrates (Harun and Watt, 2009). Presence of welded spots (elbows, tee etc), dirt, scales, slits and sands also make good nucleation sites while free-water is an enhancer since the gas-water interface is a good nucleation point.

2.5.3 Identified Types of Hydrates

Hydrates are generally grouped into Type I, Type II and Type H as defined by their structures (Hashimoto et al, 2006); however, type I and Type II are the most encountered hydrates in natural gas pipelines. Type I, with Dodecahedron (12-sided polyhedron) and Tetrakaidecahedron (14-sided polyhedron) structures is the simplest hydrate structures. It is generally formed by CH_4, C_2H_6, CO_2, and H_2S (Takeya et al, 2006; Makino et al, 2010) and consists of 14 water molecules with the theoretical formula of $X.5\frac{3}{4}H2O$ where X is the former.

Type II, with Dodecahedron and Hexakaidecahedron (16-sided polyhedron) structures and formed by N_2, C_3H_8 and $i-C_4H_{10}$ consists of 136 water molecules with $X.5\frac{2}{3}H_2O$ and $X.17H_2O$ as theoretical compositions (Das et al, 2009; Liang and Kusalik, 2010). While N_2 occupies both the small and large cages, the other two only occupy the large cages due to their sizes.

Type H can only be formed in the presence of two formers, which are of small molecule (mainly methane) and large molecules such as 2-methylbutane, 2-2 dimethyl butane, cyclohexane, etc. these large molecules are rarely found in natural gas.

Size-wise, the CH_4, H_2S, and CO_2 have the molecular size range of 4.4-5.4Å. These sizes are small enough to occupy both the small and large cages to form Type I hydrate. C_2H_6 falls within the next region of 5.6-5.8Å to occupy the large cage alone, it equally forms Type I hydrate. C_3H_8 and $i-C_4H_{10}$ with size range of 6.0-6.9Å fall within the next range to occupy only the large cages to form Type II.

2.5.4 Growth

Hydrate is ideally formed as tiny particles at the interface between the water and hydrocarbon phases. These entrained hydrate-encrusted water droplets would start to

grow if not quickly removed till it agglomerate into larger hydrates masses, leading to an increase in the slurry viscosity which finally plugs the line (Figure 2.12).
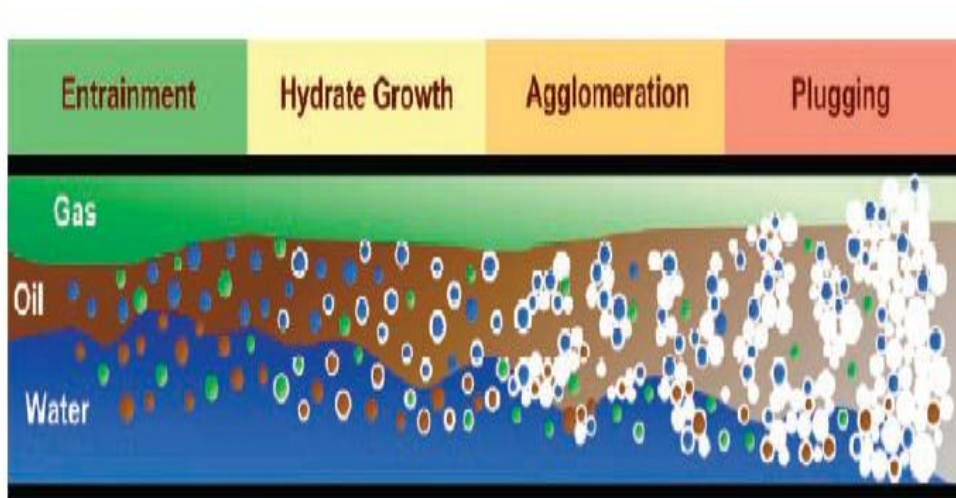
Figure 2.12: Hydrate formation model in a Gas-Oil-Water multiphase flow system

2.5.5 Hydrate Implications on Subsea Transport System

Failure to quickly remove the formed hydrate would lead to plugging of the inner orifice of the subsea transfer lines (Figure 2.13). This will lead to high pressure build-up inside the line and eventual collapse of the line to cause serious risk to the safety of operating personnel and equipment. The collapsed pipeline also releases the fluid content into the immediate environment to cause various environmental degradation problems.

Figure 2.13: Subsea gas pipeline plugged by hydrate (Lorenzo, 2009)

This problem usually costs the industry billions of dollars to mitigate annually with no permanent solution in focus. A significant operating expense equal to hundreds of millions of US dollars is annually devoted to hydrate prevention with half spent on inhibition while offshore operations additionally spends approximately US$ 1 million per mile on insulation to prevent hydrate formation along the subsea pipelines (Jassim and Abdi, 2008). Prevention of hydrate formation requires as much as 10-15% of the production cost, this is a substantial investment. Also, the continual removal of hydrate plugs from an onshore well can cost up to $1 million with an offshore pipeline costing upwards of $2-4 million (Makogon, 1997).

2.5.6 Existing Prevention/Minimization Options

Formation of hydrates require three conditions which are low temperature and high pressure with formation point values depending on the gas composition; presence of a former (or a guest) and appropriate amount of water. One of these three conditions must be eliminated in order to prevent the hydrate formation. However, apart from being desired products, the former(s) cannot be removed from the reservoir; hence, the need to work on the other two conditions.

Since hydrate formation could not be totally prevented, all efforts in the industry are directed towards inhibiting its formation and/or preventing its agglomeration by the use of chemicals generally referred to as hydrate inhibitors. These inhibitors are generally categorized into thermodynamics, kinetics and anti-coagulants (or anti-agglomeration) based on their inhibiting techniques (Frostman et al, 2003; Gao, 2009).

Thermodynamic inhibitors, which are the alcohols and glycols (both are polar solvents), and the ionic salts inhibit by depressing the freezing point. At required concentration, these chemicals effectively shift the thermodynamic equilibrium by lowering the temperature of formation point or increasing the pressure. The alcohols used in gas industry are methanol (MeOH), ethanol and glycerol while the glycols are ethylene glycol, diethylene glycol and triethylene glycol. Also, the applied ionic salts include the NaCl, $CaCl_2$, NaBr, K_2CO_3, KBr and KCl (Ostergaard et al, 2005).

According to Carroll (2009), the freezing point depression is a function of inhibitor's concentration and molar mass. This is given as

$$x_i = \frac{h_{si}\Delta T}{RT_m^2}$$

Equation 2.1

Where x_i is the mole fraction of the solute (inhibitor); ΔT is the Temprature depression (°C); R is the Universal gas constant (8.314 Jmol^{-1}k^{-1}); T_m is the Melting point of the solvent (K) and h_{si} is the Heat transfer coefficient

Conversion of the mole fraction to mass fraction followed by re-arrangement gives

$$\Delta T = \frac{M_s RT_m^2}{h_{si}} * \frac{W_i}{(100-W_i)M_i}$$

Equation 2.2

Thus

$$\Delta T = K * \frac{W_i}{(100-W_i)M_i}$$

Equation 2.3

Where

M_s is the molar mass of the solvent (the H_2O), M_i is the molar mass of the solute (the inhibitor), W_i is the weight percent of the solute (the inhibitor) and For H_2O, the K value is 1861.

While transmitting gas through pipeline, methanol is injected at low rates of 0.5 – 1.5m^3/day and high pressure of 7000Kpa (Carroll, 2009) at a typical deepwater concentration of 0.25-1.0 bbl MeOH/bbl H_2O (Frostman et al, 2003). Methyl ethylene glycol (MEG) rates are comparable to that of MeOH but very expensive cost-wise. For it to be economical, MEG is usually recovered and recycled. Though, methanol is very useful in combating hydrate formation along gas pipeline and process equipment, it however has an adverse effect by forming azeotropes with some of the gas components such as propane and butane (Hadler et al, 2009). This makes binary distillation impossible as a separation option. Also, it can easily dissolve alcohol-based corrosion inhibitors to lead to unexpected corrosion problem along the line (Carroll, 2009). Also, small quantity of air from the atmosphere usually dissolves into methanol during its storage. As this is injected into the pipeline system with methanol as inhibitor, the air accumulates within the line with time to promote corrosion.

Furthermore, based on National Fluid Power Association (NFPA) rating (Table 2.19), methanol is highly flammable compared to glycols. This makes its storage

more dangerous especially, at a confined place such as offshore rigs. Ethylene glycol is slightly toxic, though, methanol, ethanol, dietheylene glycol and triethylene glycol are non-toxic.

Table 2.19: The NFPA rating for methanol (MSDS, 2009)

Item	Rating
Health	1
Flammability	3
Instability	0

Ammonia (NH_3) could have been a better economical and operational inhibitor compared to methanol. With NH_3, lower weight percent would have been required to achieve the same result due to its lower molar mass. It can also diffuse through the gas phase to reach the hydrate plug. However, it is toxic (Megraud et al, 1992; Klerke et al, 2008; Li and Duan, 2012) and can also react with CO_2 and H_2S in aqueous phase.

Acetone is expensive, thus, making its use as an inhibitor costly. It also promotes hydrate at low concentration while acting as an inhibitor at high concentrations (Mainusch et al, 1997).

The kinetic and anti-coagulant inhibitors however require lower dosage compared to thermodynamic inhibitors (Villano et al, 2008). The Kinetic hydrate inhibitors (KHIs) inhibit by slowing down the process of crystallization. They achieve this by causing interference with the nucleation and/or the crystal growth of hydrate, thus, delaying the growth of hydrate formation and provide enough time for transportation of the gas to its destination (Al-Adel et al, 2008; Kelland et al, 2008). They are mostly polymers and significantly soluble in water. Fu et al (2001) indicated that KHIs can reduce the hydrate formation temperature by about $11^{o}C$ at 3000ppm or lower concentration. The use of KHIs is capable of saving the industry up to 40% of chemical cost compared to thermodynamic inhibitors.

Instead of preventing the formation of hydrate, anti-coagulants inhibitors allow the formation but prevent the accumulation. This allows its transport as slurry with the natural gas thus, preventing the plugging.

However, all the inhibitor types can only significantly reduce the hydrate formation temperatures; they cannot prevent its formation. Hydrate is finally formed as the temperature along the pipelength continues to drop. This is especially imminent at the cold regions and offshore pipelines where the seawater temperature ranges between $-1°C$ to $+6°C$. The formation starts in bits and agglomerates to chips that finally solidify to plug the flowlines.

2.6 Part of Present Research Contribution to Knowledge

Before this study, all the available articles on hydrate formation have been focusing mainly on its ability to plug the pipe-length without any suggestion on its ability to initiate corrosion, thus, undermining the magnitude of this problem to pipeline industry. Obanijesu et al (2010a; 2011a) bridged this knowledge gap by identifying the ability of hydrate formation to initiate corrosion along the offshore gas pipelines. They further identify the types of corrosion that could be initiated, the mechanisms of initiation, and the consequences of the resulted corrosions and finally proposed some management options. Their work opened a new area of research interest on hydrate-corrosion relationship.

According to Obanijesu et al (2010a; 2011a), gas hydrates are capable to initiate various corrosion types along the internal portion of natural gas pipelines through physical and chemical and electrochemical processes based on the hydrate formation stage, the hydrate size and the contact period with the pipe's surface. The acidic gases (H_2S, CO_2 and Cl^-) that are part of hydrate composition are eventually responsible for the corrosions (NS, 2005; Obanijesu, 2009). Available water is also a corrosion agent. At each stage of hydrate processes, interaction and reaction take place between the hydrate composition and the pipe's inner wall to initiate the internal corrosion as henceforth reported.

2.7 Corrosion Intiation by Physical and Electrochemical Processes

At different formation stages, the fluid goes from liquid to semi-solid hydrate and finally to solid hydrate. During each of these stages, a continuous interaction between the hydrate phase and the pipe wall could initiate cavitations, erosion, pitting, galvanized and stress cracking corrosions.

41

2.7.1 Cavitation corrosion through Physical Process

The first formation stage is in a semi-solid state with the hydrate blocks having liquid inside the cavities. This will readily collapse at high impact with a rigid surface like that of pipe's wall to initiate the cavitations corrosion. Cavitation corrosion (Figure 2.14) is caused by the collapse of bubbles formed at areas of low pressure in the conveyed fluid (Roberge, 2008).
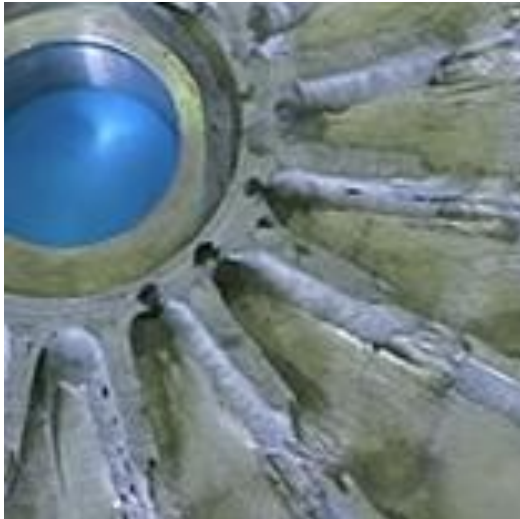
Figure 2.14: Cavitation of a nickel alloy pump impeller blade exposed to HCl acid medium (CHCMT, 2009)

The fluid, traveling at a very high speed will experience a drop in pressure at a point of discontinuity in the flow path, especially, at the joints and bends. This will lead to the formation of gas or vapor bubbles (transient voids or vacuum bubbles) in the stream which would implode upon hitting the metal surface to produce a shock wave sufficiently strong enough to remove the protective films. The cavitations corrosion is then greatly accelerated at this mechanically damaged surface by the reaction between the pipes' 'naked' surface and the acidic content of the fluid.

2.7.2 Erosion Corrosion through Physical Process

With time, the hydrates graduate from semi-solid iced-chips to solidified iced-chips. While traveling at high velocity, these chips will be bombarding the inner surface of the pipe wall to cause erosion. Erosion as the destruction of a metal by abrasion or attrition is caused by the relative motion/flow of liquid or gas (with or without suspended solids in the pipe) against the metal surface. For erosion-corrosion to

occur, there must be a constant bombardment of particles on the pipe wall surface. This gradually removes the surface protective film or the metal oxide from the metal surface, thus, exposing the surface to erosion-corrosion (Figure 2.15) from the fluid properties. Factors such as turbulence, cavitations, impingement or galvanic effects can add to the severity of erosion-corrosion attack which eventually leads to pipeline's rapid failure.

Figure 2.15: "Horseshoe" erosion-corrosion damage in a copper pipeline (Obanijesu et al, 2011d)

Likewise, the hydrate chips agglomerate with time to form bigger iced-block chips which will require more energy to transport across the surface of the pipe-wall. This movement will induce a relative motion between the pipe-wall and the hydrate block to initiate large scale of erosion-corrosion.

2.7.3 Electrolytic and Galvanic corrosions from Electrochemical Processes

The CO_2 and/or H_2S gases from the gas constituents as well as the Cl^- ions (and sometimes the acetic acid (CH_3COOH)) originating from the formation water always react with the available water during hydrate formation process. These will produce acidic solutions that dissociate with time to individually yield corrosive electrolysis products (Equation 2.4) that ultimately interact with the pipe's inner surface during the hydrate solidification process or melting (during hydrate removal).

$$H_2CO_3 \rightarrow H^+ + HCO_3^-$$
$$CH_3COOH \rightarrow H^+ + CH_3COO^-$$

Equation 2.4
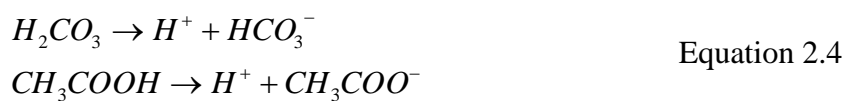
Corrosion reactions will be promoted over time from these components through electrochemical reactions to yield galvanic and electrolytic corrosions. The corrosion

43

rate will be a function of time, composition, pH and other thermodynamic properties such as temperature, pressure and gas fugacity amongst others (Obanijesu, 2009). Oxidation-reduction (or redox) reaction takes place in electrochemical corrosions with oxidation taking place at anode while reduction takes place at the cathode. However, spontaneous reactions occur in galvanic (voltaic) cells to produce galvanic corrosion attack (Figure 2.16) while non-spontaneous reactions take place in electrolytic cells.

Figure 2.16: Metals attacked by galvanic corrosion (Obanijesu et al, 2010c)

For an electrolytic cell, the anode is positive while the cathode is negative. Therefore, the anode attracts anions from the solution (Equations 2.5 and 2.6). However, the anode of a galvanic cell is negatively charged and its spontaneous oxidation is the source of the cell's electrons or negative charges while the cathode is its positive terminal.

Anode: $Fe \rightarrow Fe^{2+} + 2e^-$ Equation 2.5

Cathode: $2H^+ + 2e^- \rightarrow H_2$ Equation 2.6
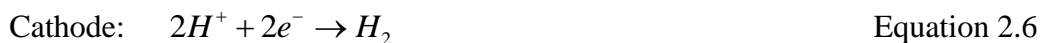
Apart from the ability of each of these corrosion types to single-handedly collapse a pipeline, they can also individually or collectively lead to pitting corrosion or Stress cracking corrosion (SCC) to partially or totally destroy the system.

2.8 Corrosion: Chemistry and Implications on Flow Assurance

Corrosion has been identified to be responsible for almost 50% of pipeline failure in the industrialized countries (Table 2.20). Corrosion is the chemical or

44

electrochemical reaction between a material, usually a metal, and its environment that produces a deterioration of the material and its properties (HGMCE, 2004).

The process involves electrolytic action whereby the substances which increase the concentration of hydrogen ions (H^+) such as acids and acid salts stimulate it while those substances that increase hydroxyl ion (OH^-) inhibit it. Pipeline corrosions could be broadly classified as internal and external corrosions. While the environmental conditions around the pipeline are responsible for the external corrosion (Soares et al, 2009), the internal corrosion is mainly caused by the fluid flowing through the pipeline and the pipe's geometry. Corrosion may also be caused or facilitated by the activities of microorganisms living within or on the pipe wall (Picioreanu and Loosdrecht, 2002; Reyes et al., 2008).

Table 2.20: Pipeline failure by cause in some developed countries ([a] DOT, 2005; [b] Cribb, 2003; [c] Mokrousov, 2008)

Cause	Contribution (%)			
	USA[a]		Canada[b]	Russia[c]
	Liquid Pipeline	Gas Pipeline	Gas Pipeline	Gas Pipeline
Corrosion	19.26	41.25	57	31
Natural forces	-	-	12	
Defective Weld	8.61	-	15	
Incorrect operation	3.28	-		5
Defective pipe	4.51	-	8	12
Outside damage	23.36	28.75	4	23
Equipment Malfunction	9.02	11.25		
Construction defects				29
Others	31.97	18.75	4	

Corrosion of the internal wall of a gas pipeline signifies the presence of significant partial pressures of CO_2 and/or H_2S. This occurs when the pipe wall is exposed to water and contaminants in the gas such as oxygen (O_2), dihydrogen sulphide (H_2S), carbon-dioxide (CO_2) or chloride ion (Cl^-). On a weight percentage or weight fraction basis, O_2 is more dissolved to ordinary steels than either CO_2 or H_2S (Stress,

2003). Although, the probability of having appreciable concentrations of O_2 inside a gas transmission line is apparently quite low, a small partial pressure of O_2 can produce surprisingly high internal corrosion rates in steel pipes than that containing liquid water.

2.8.1 Chemistry and electrochemistry of corrosion

Electrochemical process involves the transfer of electrons from one chemical species to another. Metal atoms characteristically lose or give up electrons through oxidation reaction (Equation 2.7) which takes place at the anode (Nakajima et al, 2008) or reduction reaction (Equation 2.8) taking place at the cathode (Nakajima and Tajima, 2009).

$$M \rightarrow M^+ + ne^-$$
$$Fe \rightarrow Fe^{2+} + 2e^- \qquad \text{Equation 2.7}$$
$$Al \rightarrow Al^{3+} + 3e^-$$

Most metals undergo corrosion in acid solutions that have high concentration of hydrogen ion (H^+) which reduced to hydrogen gas, H_2 through reduction process (Equation 2.8).

$$2H^+ + 2e^- \rightarrow H_2 \qquad \text{Equation 2.8}$$

For an acid solution having dissolved oxygen, reduction according to Equation (2.9) may occur (Miah and Ohsaka, 2009) whereas, for a neutral or basic aqueous solution in which oxygen is dissolved, reduction according to Equation (2.10) is mostly favored (Xu et al, 2009a).

$$O_2 + 4H^+ + 4e^- \rightarrow 2H_2O \qquad \text{Equation 2.9}$$
$$O_2 + 2H_2O + 4e^- \rightarrow 4(OH^-) \qquad \text{Equation 2.10}$$

For multivalent ions, reduction may occur by decreasing its valence state through acceptance of an electron (Equation 2.11) or by totally reducing itself from an ionic state to a neutral metallic state (Equation 2.12). Two or more of the reduction processes may occur simultaneously.

$$M_n^+ + e^- \rightarrow M^{(n-1)+} \qquad \text{Equation 2.11}$$

$$M_n{}^+ + ne^- \rightarrow M \hspace{4cm} \text{Equation 2.12}$$

However, corrosion by chemical reaction does not involve electron transfer. In this case, the metal is attacked by a diluted acid (e.g HCl) to evolve hydrogen gas (Equation 2.13).

$$Fe + 2HCl \rightarrow FeCl_2 + H_2 \hspace{3cm} \text{Equation 2.13}$$
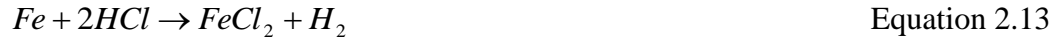
2.8.2 Classification of corrosion

Corrosion can be generally classified into three major categories while the corrosion through microbial activities could be the fourth group. The first group belongs to those that can be readily identified by visual examination; this includes uniform corrosion, localized corrosion and galvanic corrosion. In the second group are those that require further examination for identification. They include erosion-corrosion, cavitations corrosion, fretting corrosion (these three are classified under velocity corrosion), intergranular corrosion and dealloyed corrosion. The third group which involves cracking form of corrosion and high-temperature corrosion are those that can only be confirmed through the use of microscope(s). Another form apart from these three general groups is the hydrogen ion induced corrosion (Heppner and Evitts, 2008). Each of these corrosion groups is uniquely initiated.

2.8.2.1 Pitting and Crevice Corrosions

Crevice and pitting corrosions are related because of their familiar mechanisms and they both require stagnant water, Cl^- and O_2 or CO_2. They are confined to a point or small area that develops in highly localized areas on the metal surface (Pardo et al, 2008). This results in the development of cavities or "holes" that may range from deep cavities of small diameters to relatively shallow depressions in the material (Figures 2.17 and 2.18).

Pitting corrosion is frequently observed in both the sweet and sour fields. It is very difficult to detect, predict or design against at the plant design stage. Through its gradual formation, the products from the corrosion cover the cavities, hence, making the small narrow pit unnoticed. However, this small pit is capable of collapsing the whole pipeline structure.
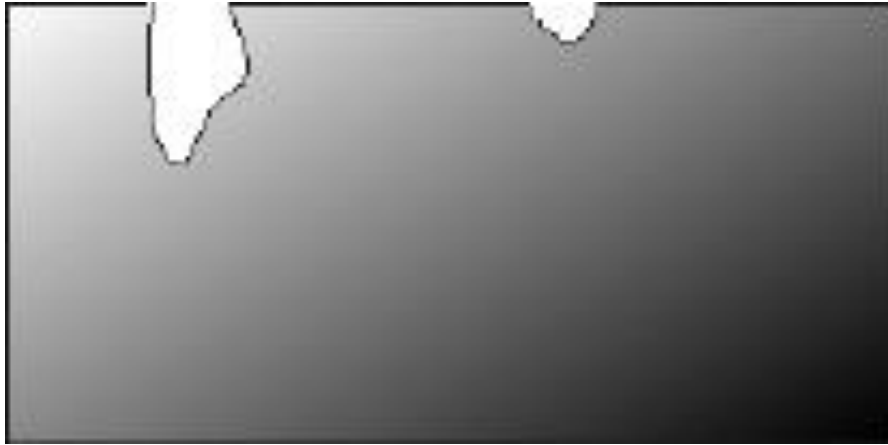
Figure 2.17: A metal attacked by pitting corrosions (Obanijesu et al, 2010c)

Crevice corrosion is formed by contact with adjacent piece of the same or another metal with a non-metallic material. When this occurs, the intensity of attack is usually more severe than on surrounding areas of the same surface (Kennell and Evitts, 2009). It is mostly formed under a shielded area such as under gaskets, washers, insulation material, fastener heads, surface deposits, disbonded coatings, threads, lap joints and clamps.

Figure 2.18: A metal attacked by crevice corrosions (Obanijesu et al, 2010c)

Chloride ions and operating temperature influence pitting formation, thus, offshore pipelines are more prone to this corrosion type since sea water contains sodium

chloride which could be produced with wet gas from the reservoir. Stagnant fluid inside the tubing can also easily initiate pitting corrosion and crevice attacks, especially, if particles settle out of the liquid. Stainless steel Type 304 can be attacked by pitting corrosion inside the sea at $10^{O}C$ even, at low chloride level, while Type 316 which is more resistant to pitting can easily be attacked by crevices or at a slightly increased temperature.

2.8.2.2 Stress-corrosion cracking (SCC)

SCC corrosion (Figure 2.19) can be accelerated by residual internal stress in the metal or external applied stress. Residual stresses are produced by deformation during fabrication, by unequal cooling from high temperature and by internal structural arrangements involving volume change.
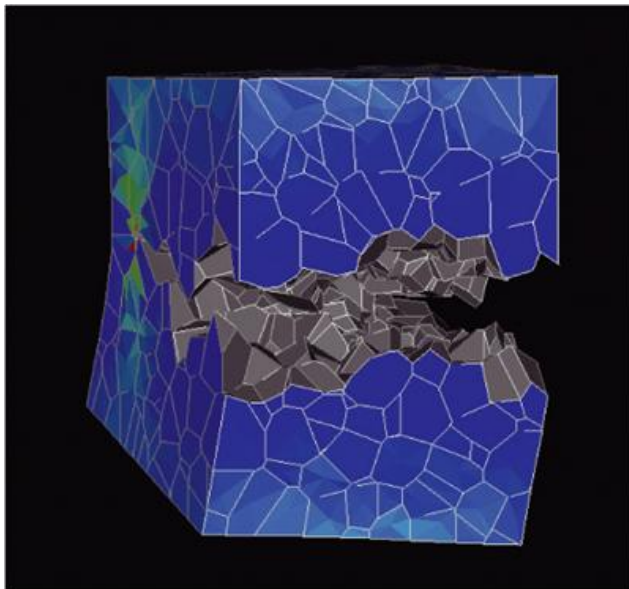
Figure 2.19: Three-dimensional reproduction of SCC shape (Itakura et al, 2005)

The steel pipeline is composed of many crystals of about 0.05mm (Itakura et al, 2005; Choi et al, 2009) whose temperature is always kept high to prevent hydrate formation and/or the liquefaction of some other components during operation. This may generate irradiation inside the steel especially at a high temperature, thus, subjecting the material to tensile stress in a corrosive environment.

This problem increases at pH$\geq$8 but decreases at pH$\leq$6 (Guo et al, 2002). When SCC occurs, its intricate crack shape follows the interface between these grains in a zigzag

manner. There can be multiple cracks in the pipeline, thus, making the study of SCC progression in a pipelength very crucial for the pipe's safety assessment.

2.8.2.3 Erosion, Cavitations and Fretting Corrosions

These corrosions occur as a result of high velocity flow of fluid inside the pipe. The processes of initiation for both erosion and cavitations corrosion have been fully explained in sections 2.7.1 and 2.7.2.

Fretting corrosion damage (Figure 2.20) is induced by repeatedly moving a load across a surface at a relatively high velocity (Park et al, 2008). It is experienced at rough contact surfaces that are exposed to vibration during transportation because the interface of the two highly loaded metal surfaces will be moving against each other. The protective film on the surfaces is removed by the rubbing action and exposes fresh, active metal to the corrosive action of the immediate environment. This problem is experienced in the oil and gas pipelines as the motion of the fluid inside the tube causes a lot of vibration due to the contact of the weight of the fluid with the inner surface of the tubing.
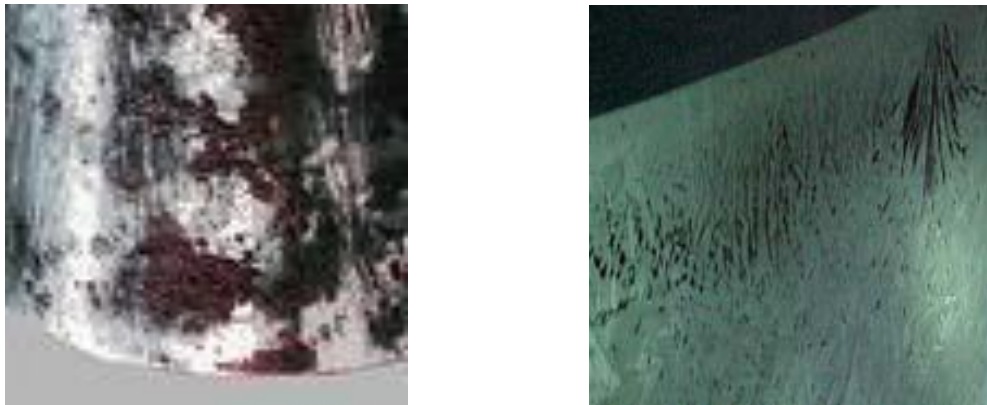
Figure 2.20: Fretting corrosion on metal plates (ILZRO, 2009)

Erosion-corrosion (Figure 2.15) has been rated in the top five most prevalent forms of corrosion damage in the oil and gas industry (Rajahram et al., 2009). The industries transporting slurries and other particle-laden liquids in pipes through offshore and marine technologies spend millions of pounds every year to repair material damage from this corrosion type (Meng et al, 2007).

2.8.2.4 Uniform corrosion of carbon steel

Uniform corrosion (Figure 2.21) is the least damaging form of corrosion in that it is predictable if the corrosion rate is known. This is a corrosion process exhibiting uniform thinning that proceeds without appreciable localized attack and commonly occur on metal surfaces having homogenous chemical composition and microstructure. As the corrosion occurs uniformly over the entire surface of the metal component, it can be practically controlled by cathodic protection, use of coatings or paints, or simply by specifying a corrosion allowance.

Figure 2.21: Uniform corrosion of structural steel (KSC, 2009)

2.9 Factors Influencing Gas Pipeline Corrosion

The nature and extent of gas pipeline corrosion are functions of the gas pH, present oxidizing agent(s), the system temperature, operating pressure, the fluid velocity, the pipe wall's shear stress, size of available particles, the gas composition and the gas viscosity amongst others (Maier et al, 2007; Mercier and Barthes-Labrousse, 2009).

2.9.1 pH

Corrosion rate of most metals is affected by pH (Zhao et al, 2008) which promotes the galvanic corrosion in metals and alloys (Tada et al., 2004). For pH related corrosions, the corrosion rate of acid- soluble metals such as iron is controlled by the rate of transport of oxidizers (usually dissolved oxygen) to the metal surface whereas the amphoteric metals such as aluminum and zinc dissolve rapidly in either acidic or basic solutions. However, corrosion of noble metals such as gold or platinum is not appreciably affected by pH. The Hydrocarbon pipelines are susceptible to corrosion–

induced stress and stress corrosion cracking at high pH (Guo et al, 2002; Song, 2009).

2.9.2 Oxidizing agents

Oxidizing agents are often powerful accelerators of corrosion. In their study based on monoethanolamine (MEA) system, Veawab and Aroonwilas (2002) indicated bicarbonate ion (HCO_3^-) and water (H_2O) as primary oxidizing agents while Stack et al (2003) revealed oxygen as a contributor to erosion-corrosion in aqueous slurries. In many cases, the oxidizing power of a solution is its most important single property in promoting corrosion. When oxygen is involved, there is a rapid reaction between the O_2 and the polarizing layer of atomic hydrogen absorbed on the oxide layer and this reaction rapidly removes the polarizing layer.

2.9.3 Temperature

Like most other chemical reactions, corrosion rate increases with temperature since ionic mobility increases with temperature, thus, leading to conductance increase (Niklasson et al, 2008; Krishnan et al, 2008; Ezuber, 2009). The process temperature and pressure govern the solubility of the corrosive species in the fluid. These species include oxygen, carbon-dioxide (or hydrogen sulfide in case of sour field), chlorides and acetic acid amongst others. From the rule of thumb, reaction rate doubles between the temperature rises of 20^OF to 50^OF. This linear increase stops along the line partly due to a change in the oxide film covering the surface. Temperature also has secondary effects through the influence on the solubility of air (O_2), which is the most common oxidizing substance influencing corrosion.

2.9.4 Fluid Velocity

The fluid velocity plays a great role in corrosion rate (Aw et al, 2008; Stack and Abd El-Badia, 2008; Badiea and Mohana, 2009). When the velocity is very high, the available particles in the fluid impact upon the inner wall and remove the protective oxide layer as well as erode the exposed metals. This causes erosion-corrosion with time. Also, when H_2O is involved, water velocity of 30 to 40 ft per second initiate corrosion since increase in the relative movement between a corrosive solution and a metallic surface frequently accelerate corrosion.

2.9.5 Wall shear stress

Wall shear stress highly influence hydrodynamically induced corrosion such as erosion corrosion (Boutoudj et al, 2008; Demoz and Dabros, 2008; Chaal et al, 2009). In pipeline industry, natural gas is frequently transferred at turbulent flow in order to increase the transportation efficiency at a minimized cost. Particles and other geometrical changes in the flow give rise to higher shear stress though abrasion. This leads to drag (skin friction) which eventually induced corrosion of the inner wall by wearing off the protective coatings.

2.9.6 Particle size

The size of the particle traveling with the gas inside the pipeline network plays a significant role in initiating corrosion (Lau et al, 2008; Pardo et al, 2009). Erosion and cavitations corrosions are among the identified corrosion types that could be initiated by the particle size distributions. Niu and Cheng (2008) and Xu et al (2009b) established that particles are capable of initiating erosion-corrosion by using sand and Nano-Particle-Reinforced Ni Matrix Composite Alloying Layer respectively while Obanijesu et al (2010a) established the capability of hydrate clathrates in gas pipeline to initiate the erosion, cavitation, galvanic and electrolytic corrosions depending on the formation stage, the point of contact, the gas velocity and composition.

2.9.7 Chemical Composition and Concentration

Composition and concentration play significant roles in the corrosion rate of a gas pipeline. While Zhao et al, (2008) established that ion concentrations of a conveyed fluid aids Stress Corrosion Cracking (SCC), various relationships between corrosion rates of pipes and the composition and concentration have also been established by other researchers (Gonzalez-Rodriguez et al, 2008; Hamdy (2008); Skrifvars et al., 2008; Montemor et al, 2009).

The influence of pH and concentration on corrosion rate is best understood through electrochemical reaction. At any considered pH, the pipe corrosion rate increases with concentration of non metallic components of the gas. This is so as the corrosion behavior of the metallic alloys is governed by a partially protective surface film, with the corrosion reactions occurring predominantly at the break or imperfection of the

partially protective film. The implication is that, the fraction of film free surface increases with decreasing bulk pH and with increasing fluid non metallic ion concentration. This is consistent with the known tendency of non metallic ions to cause film breakdown and the known instability of the metallic hydroxides in solutions with pH less than 10.5.

2.9.8 The Gas Viscosity

This has been an area where researchers have not really developed, Ricciardiello and Roitti (1972) was likely to be the most recently available literatures on this area before Obanijesu et al (2010b). However, science can easily be used to support this claim. Viscosity is the resistance of a liquid to shear forces and hence to flow (Obanijesu and Omidiora, 2009). This is a quantity expressing the magnitude of internal friction in a fluid, as measured by the force per unit area resisting uniform flow. Thus, the higher the viscosity, the lower the mobility and higher the time of surface interaction between the fluid's properties and the pipe inner surface to facilitating corrosion initiation.

2.10 Consequences of Pipeline Failures on the Industry

Pipeline failure is the malfunction of the pipe body due to metallurgical or processing abnormalities. It can be a leak or rupture. Leakage is a small opening, crack or hole in the pipeline causing loss of pipeline products, but not immediately impairing the line operation. Small leaks due to fractured or small corrosion holes often lead to leak rates usually less than 1% of flow and go unnoticed for weeks. Medium leaks are caused by fractures that remained narrow. This usually takes place by the worn gaskets and valve stem packing. These leaks are not large enough to cause a loss of working line pressure. Large leaks result in rapid loss of working line pressure that generates an alarm to the dispatcher even without a leak detection system (LDS). However, rupture is the instantaneous tearing or fracturing of pipe material, this immediately impairs the operation of the pipeline.

The spate of accidents in the pipeline industry has attracted a significant level of awareness in safety and loss prevention, and has earned considerable public and regulatory attentions globally. A case study of a typical offshore platform in the North Sea, UK showed that the amount of gas present in a 150 km long and 0.4 m

diameter pipeline at 100 bars could be as much as 637,000 kg (Mahgerefteh et al, 1997). This represents an enormous source of energy release, which in the event of Full Bore Rupture (FBR) poses the risks of general and extreme fire exposure to all personnel in open platform areas and also undermines platform safety.

Though, hydrate formation has been established as a flow assurance problem to gas industry, corrosion is of higher consequences. Apart from the ability of both problems to collapse the offshore pipeline systems (Gbaruko et al, 2007; Netto et al, 2007; Netto, 2009), corrosion would further deteriorate the integrity of the pipe material which may necessitate a total replacement (Shipilov and May, 2006; Adib et al, 2007). The impacts of pipeline failure on the industry could be classified into economic, safety and environmental consequences.

2.10.1 The Economic Impacts

The economic consequence of pipeline accidents includes the cost of product loss; the public, private and operator property damage costs, and the cleanup/recovery cost (Restrepo et al, 2009). Two of the six categories included in a 'gravity scale' are related to the cost of production losses and the cost of environmental cleanup (Papadakis et al, 1999). The economic impact of such accident is experienced by both the consumer and the industry.

2.10.1.1 Economic impacts on the consumers

Raw natural gas from reservoir is normally treated at gas plants with ethanolamine and diethanolamine amongst other chemicals during the sweetening process before the final transport to customers. The unrecoverable trace amounts of these chemicals escape into the product gas stream because of their vapour pressures (Mokhatab et al, 2006). When corrosion takes place within the pipe, these chemicals would react with the exposed carbon alloyed to form chelation with metals used to construct the pipeline. The resulting products (Figure 2.22) then travel downstream with the sales gas to the client terminal (consumers) where, it will be used for cooking and other required domestic and industry applications.

At the client terminals, the gas often burns with discolorations, with reduction in heat value and potential health hazard implications. Apart from the significant heat value loss, cancer and memory loss are few of the resulting health hazards. This will

subject the client to further economic loss in taking care of their health afterward. Also, the client will end up using more gas to achieve the desired level of cooking or application.

a) Copper-ethanolamine chelate   b) Copper-diethanolamine chelate
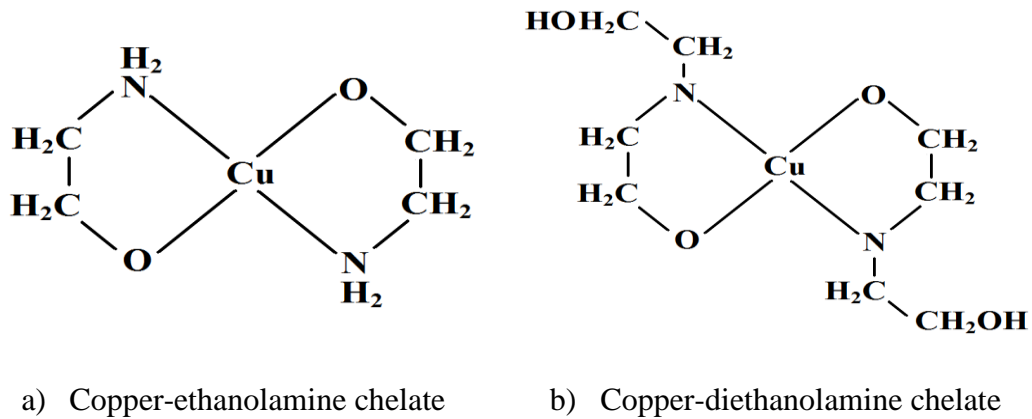
Figure 2.22: The copper chelates that flow with gas stream to consumers (Obanijesu et al, 2011d)

Chelates are typically more stable than other metal-ligand complexes (Hunt et al (2011) which contributes largely to the complex remaining finely entrained in the product gas. This is further bolstered by the hydroxyl group co-ordination in ethanolamine which greatly reduces steric strain. Grigoryan et al, (2003) reported that Copper-alkanolamines are stable at limits of ambient temperatures, and hence typical transport temperatures of $45^{\circ}C$ are within stability bounds. It is apparent that thermodynamic conditions favour the formation and stability of these copper chelates.

Hunt et al (2011) applied Equation (2.14) to determine the mass percentage of ethanolamine (MEA) and diethanolamine (DEA) respectively, required to produce a 0.5MJ/kg reduction in natural gas higher heating value (HHV). This was further extended to nickel-ethanolamine and iron-ethylenediaminetetraacetic acid (EDTA) chelates.

$$HHV = 0.3491[C] + 1.1783[H] + 0.1005[S] - 0.1034[O] - 0.0151[N] - 0.0211[Ash]$$

Equation 2.14

2.10.1.2 Economic impacts on the industry

Hydrate prevention costs the gas industry about US$1 million per mile (Jassim and Abdi, 2008) while the pipelines eventual rupture costs the industry an extra cost on welding, product loss and loss of production time.

Fingerhurt and Westlake (2000) reported that the total length of high pressure gas transmission lines in North America alone (USA and Canada) was more than 480,000km, and estimated the outage cost, in case of rupture from any of the pipelines between $500,000 and $1,000,000 per day. This loss can be recorded for a rupture from both hydrate and corrosion. However, corrosion presents a worse scenario by introducing a further cost of assets' capital replacement value which can be estimated by applying the average cost as given by Parker (2004). This costing method gave the capital replacement cost for 36in and 42in pipelines as $1,767,710 per mile and $1,977,644 per mile respectively with the cost distributed as material 26%, labor 45%, Right of Way 22% and Misc. 7%. The miscellaneous included the cost on surveying, engineering, supervision, contingencies, allowances, overhead and filing fees.

Applying this on existing 305,438 km (190,899 miles) of natural gas pipeline in the United States, additional pipeline replacement costs for USA and Canada as a result of corrosion are US$337 - US$378 billion and US$193 – US$216 billion respectively. For offshore productions, these estimations exclude other considerations such as location, climatic conditions, political situations as well as specific requirements such as the need for a barge for pipe laying, sea depth and wave function. In actual fact, Fingerhurt and Westlake (2000) put the total replacement cost for the whole North American pipelines at over US$3 trillion.

A review on effects of corrosion on US economy showed that corrosion of metals and alloys cost U.S. companies and consumers approximately $300 billion per year with about 1% of it ($3bn) coming from the pipeline industry (Battelle, 1996). After much attempts to reduce corrosion problems, Thompson and Vieth (2003) later put the new annual cost on corrosion from the same country at $276bn (representing 3% of annual GDP) with $8.6bn coming from oil and gas transmission pipelines. Considering this economic trend, the cost implication of corrosion on USA pipeline industry alone has increase from $3bn to $8.6bn within a short period of 8 yrs (1995-

2003). Since 2003 however, the country has embarked on various new gas projects which have reasonably increased the number and length of existing pipelines. Globally likewise, there is a sharp increase in the number of onshore and offshore transboundary pipelines from gas rich countries to those lacking the hydrocarbon due to increase in population and gas demand. These pipelines have been generally subjected to conditions favoring various corrosion accidents with related consequences (Table 2.21). The product loss alone from the pipeline failure of September 17, 1999 at Ekakpamre, Nigeria was estimated at over $10 billion dollars (Obanijesu et al, 2006).

Table 2.21: Some global pipeline accidents from corrosion and consequences (Obanijesu et al, 2010)

Date	Location	Nature of Accident	Damage Caused
03-02-09	Shah Oilfield, Al Gharbia, UAE	Corrosion led to a leakage on a pipeline carrying 50,000 barrel of oil per day; thus, releasing H_2S gas to the environment before explosion.	3 killed by inhaling high concentration of H_2S gas.
19-08-00	Carlsbad, New Mexico USA	A 30-in diameter natural gas pipeline ruptured due to severe internal corrosion (pitting) and exploded.	12 members of the same family killed, 3 vehicles burnt and 2 nearby steel suspended bridges damaged. Property and losses totaled $998,296.
08-08-96	Lively, Texas, USA	An 8-in diameter LPG pipeline transporting Liquid butane burst due to inadequate corrosion protection.	2 men killed, 25 families evacuated, damages cost over $217,000.
04-03-65	Louisiana, Tennessee, USA	Gas transmission pipeline exploded from stress corrosion cracking.	17 killed.

The Varunus Island Explosion of 3rd of June 2008 offered a perfect case study on the economic implication of a total pipeline failure. As of then, Western Australia was consuming approximately one petajoule of gas per day with 35% supply from the Varanus Island while the remaining 65% was supplied by other North West shelf companies.

The accident (Figure 2.23) occurred when one pipeline failed and caused an explosion which severed three adjacent pipelines. This led to stoppage of all operations at the processing plant and resulted in cutting gas supply to Western Australia by a third (Logan, 2008). Industries and the general populous were also asked to reduce their gas and power usage to account for the shortfalls in supply. Subsequently, all possible gas power stations switched to alternative fuels such as diesel and coal with associated coordination to ensure supplies of these fuel stocks. This necessitated the hurried rebuilding of a shattered turbine; also, the mothballed Muja AB power units and all coal fired power stations that were undergoing routine winter maintenance were brought online.

Figure 2.23: Veranus Island pipeline explosion (Cutler, 2010)

With industry and household power usage dropping by 28858 megawatt hours, North West Shelf supplies were increased by 100 terajoules per day while the Verve

Energy workers freed a further 100 terajoules of gas for other industry by bringing the Muja 7, Collie A and Kwinana B coal fired power generators back online. However, heavy consumers of natural gas had to reduce their production or stop entirely as related products such as CO_2 and N_2 from CSBP (a major chemical and fertilizer producer in Western Australia) were in short supply due to gas interruption. Small industries were harder hit with many customers receiving little or no gas supplies. Gas flow from the Varanus Island processing plant was partially restored by August 8th. The cost to the Western Australian economy from this incident was estimated to be AUS$2.5 billion, equating to 0.5% reduction in gross state product (Eggleston et al, 2008).

2.10.2 Safety consequences

Pipeline blow-outs always endanger human life and subject the pipeline operators working on the platform as well as the community to severe safety risks which are predominantly death. Notably is the Bellingham, Wash pipeline accident of June 10, 1999 where 250,000 gallons of gasoline from a ruptured large transmission pipeline spilled into a nearby creek and ignited. This led to the death of three young individuals, eight injuries, and over US$45 million worth of property damaged (PHMSA, 2009).

Also, the pipeline explosion of December 19, 2010 at a Petroleos Mexicanospumping station in Central Mexico resulted in over 27 deaths, 50 injuries and destruction of 32 houses.

Again, the Piper Alpha offshore pipeline accident of 6th July 1988 at North Sea (Figure 2.24) clearly demonstrated the catastrophic consequence. The accident started when the failure of a primary propane condensate pump led to an explosion. Within 20 minutes of the failure, the gas risers (pipes between 24 and 36 inches in diameter) on the platform carrying gas at 2000 pounds per square inch (1,406,139.16kg/m^2) burst and created inferno. 167 out of the 226 personnel died with 109 from smoke inhalation (Coombs, 2003). The fire was visible up to 85 miles away and the heat felt at 1 mile away. Almost the whole production platform melted to sea level. It was further estimated that the energy released during this tragedy was equal to 1/5th of the UK energy consumption at the period. The experience from this

accident can never be forgotten in gas industry and it is still regarded till today as the global worst offshore pipeline accident ever.

A: Before the fire   b) During burning

c) Final platform stage   d) Memorial status

Figure 2.24: The North Sea Piper Alpha accident (Obanijesu et al, 2010)

Nigeria has a long history of devastating experience from various pipeline accidents. Over 2000 people were burnt to death in the Jesse pipeline disaster of 15th December, 1998 (Obanijesu et al, 2006). Consequent upon the death of many parents in this fire, several children were left orphaned and some parents widowed. Among the survivors, many suffered severe burns and damaged internal organs as a result of inhalations of fumes and smoke; thus, becoming liabilities because they were unable to fend for themselves any longer. In July 2000, another pipeline explosion outside

the city of Warri caused 250 deaths while an explosion in Lagos in December 2000 killed at least 60. A pipeline fire incidence at Alagbado in Lagos on December 26, 2006 resulted in over 500 people been burnt to death (Figure 2.25).

Figure 2.25: Human deaths from Alagbado pipeline fire (Obanijesu et al, 2009)

A similar pipeline explosion occurred at Ijegun in Lagos on May 16, 2008 after a bulldozer struck a pipeline. The fire spread to surrounding homes and schools with occupants inside. More than 15 homes and 20 vehicles were completely burnt. The Nigerian Red Cross claimed that over 100 people died (Figure 2.26) with a pregnant woman and her 4-year-old son among the dead. Eight out of sixteen primary school students that were trampled upon died the following day at hospital while three residents were killed after being run over by vehicles whose drivers attempted to flee the fire zone. Table 2.22 further shows some of the global pipeline accidents that result into human deaths.

Table 2.22: Some global major pipeline accidents (Obanijesu et al, 2010)

Date	Location	Nature of Accident	Damage Caused
05-05-09	Rockville, USA	Natural gas pipeline explosion.	Homes were evacuated in a one-mile area of explosion.
16-05-08	Ijegun, Lagos, Nigeria.	A bulldozer accidentally struck an oil pipeline which eventually exploded.	100 deaths. 15 homes and 20 vehicles burnt.
01-11-07	Carmichael, USA	Propane pipeline explosion.	2 deaths, 5 injured.
26-12-06	Lagos, Nigeria.	A vandalized oil pipeline exploded	Over 500 deaths.
30-07-04	Ghislenghien, Belgium	Explosion of a major natural gas pipeline.	23 killed, 122 injured.
2003	Chongqing, China	A gas well blew out releasing toxic sour gas cloud to the environment.	243 deaths.
21-10-00	Colombia	Pipeline explosion.	43 deaths.
10-06-99	Bellingham, Washington.	A gasoline pipeline ruptured. 250,000 gallons of gasoline escaped into a creek and resulted into fire.	3 deaths, 8 injured, over $45 million property damages.
21-11-96	San Juan PR	Liquid natural gas line explosion due to employee's negligence in responding to leak.	33 people killed.
09-11-93	Nam Khe Village, East of Hanoi.	A 9-year-old boy lit a match while scooping fuel from broken underground pipe leading to explosion	45 deaths.
01-03-98	Ecuador	Pipeline explosion and fire at Ecuador's largest oil pipeline.	11 deaths, 80 injured.
18-10-98	Jesse Village Delta, Nigeria	Oil pipeline explosion while villagers were scooping fuel from a ruptured pipeline.	Over 2000 deaths.
04-06-89	Ufa, Russia	The gas leaking from an LPG pipeline was detonated by two passing trains.	645 deaths.
03-06-89	Russia	Liquefied natural gas Pipeline explosion	575 deaths.
23-06-89	Eastern Pakistan	Gas Pipeline ruptured and exploded.	12 killed; hundreds injured.
03-10-89	Gulf of Mexico	Submerged Gas pipeline exploded.	11 deaths.
28-10-93	Las Tejeria, Venezuela	Telephone crew laying fiber optic cable ruptured natural gas pipeline beneath highway leading to explosion	36 deaths.
1982	Amoco field, Canada	A high profile blowout releasing sour gas for 67 days.	2 human and hundreds of cattle death.

Figure 2.26: Human deaths from Ijegun pipeline accident (Obanijesu et al, 2009)

2.10.3 Environmental consequences

The threats posed by a gas pipeline failure on the environment depend on the quality and quantity of gas released, operating pressure, failure mode and the immediate environment. There could be severe damage and debris throw due to stored energy released by the failure, vapour cloud explosion, release of toxic gases (e.g. H_2S, VOCs, SO_2, e.t.c), asphyxiation and thermal radiation, hydrate formation in water body, dissolution of components, loss of human lives and livestock, climate change as well as flammability amongst others (Stevens, 2003; Sonibare et al., 2005; Obanijesu and Macaulay, 2009). A catastrophic failure of pipeline at its usual operating pressure may cause surface damage within 50 feet of rupture while an oil and gas pipeline of over 800 mm in diameter and over 40 km long may affect sensitive ecosystems or change the lifestyle of local populations.

Generally, the impacts are felt in all the four environmental matrices which are the soil, vegetation, water and air as expatiated below.

2.10.3.1 Soil and Vegetation Impacts

A discharge of gas from an underground pipe would drive out the oxygen from the soil in the vicinity thus killing plants. Large areas of arable land get destroyed as a result of gas pipeline failure and the resulted fire out-breaks with degree of damage to soil depending on the level of contamination. The soil becomes less fertile as a subsequent of nutrients essential to plants growth becoming scarce while those that are more toxic to plants becoming more available. The effect on soil microorganisms may persist for several years. This adversely impacts on plant growth rate.

2.10.3.2 Impacts on Water Quality

A failure along a submerged offshore pipeline will strongly release natural gas into the water body as bubbles with high volume of gas. This generates a plume (McGinnis et al, 2005) which is guided by four main mechanisms of transport. These are the vertical bubble transport (bulk flow), vertical turbulent diffusion, dissolution of components and horizontal advection by ambient currents (Obanijesu and Mosobalaje, 2008). These gas flow patterns are controlled by laws (including Fick's law of diffusion and Brownian law of motion) to cause hazardous impacts on the ecosystems. Some impacts on the marine lives are explained below.

The immediate flow pattern upon failure is the vertical bubble transport which is the transport of gas molecules due to the bulk flow (flux). It is a convective transfer and governed by principle of mass conservation. Natural gas boils at $-162^{O}C$, hence, its release at this rate and condition will result into formation of hydrates within the water body (Obanijesu and Macaulay, 2009). The hydrates cause problems ranging from behavioral nature such as fish excitement, increased activity, and scattering in the water as well as to chronic poisoning depending on the quantity of the gas and the total period of exposure (Patin, 2004).

When discharged into water body, the water soluble components such as H_2S and CO_2 dissolve and are transported into the ocean. The dissolution and stripping are responsible for the noticeable changes in bubble size in a typical plume. Specifically, the discharged fluid increases the hydrocarbon content of swamps, streams or rivers, and also acidifies the water course. Dissolved CO_2 indirectly affects seawater

temperature, salinity, ice-cover, turbulence and current while all these abiotic effects have biotic consequences (US DOE, 1985).

The acidified water could be taken up by plants within the watercourse through their roots to impair their growth. Also, the dissolved acidic gases alter the pH of the sea water which is eventually taken in by the sea animals; this reduces their reproduction rate which also reduces their availability for human consumption, thereby leading to increase in price. Through the bioaccumulation process, man takes in the poisoned fish and this could be very detrimental to his health.

2.10.3.3 Air Pollution

Due to high pressure of discharge at the point of offshore failure and insolubility of most of the components, the gas is ultimately released to the atmosphere at a particular distance either through vertical transport or by water inversion. This causes air pollution and could further lead to deaths. Typical of this accident is the Lake Nyos, Cameroon, incidence of August 1986 where an enormous volume of CO_2 was released from a collapsed underwater pipeline to atmosphere by water inversion. 1700 people and livestock up to 25km away from the point of discharge were killed (Clarke, 2001). Another example is the Lake Monoun incidence of 1984 where a smaller release of CO_2 killed 37 people (Steven, 2000). Air pollution is of greater environmental concern in pipeline failure because of the nature of transported fluid. It affects the air quality through climate change, poisoning and fire amongst others.

2.10.3.3.1 Climate Change

Considering WAGP project as an example, Nigerian natural gas contains between 68% and 90% methane (CH_4). Upon offshore failure, it would take millions of years for the CH_4 to oxidize in the water by bacteria (Dickens, 2001). But this is not achievable considering the pressure at which the gas is been discharged from the point of failure, hence, it will reach the water surface shortly and the large volume of CH_4 will escapes into the atmosphere.

With 8.4years global mean atmospheric lifetime (Prather et al, 1995), 12years perturbation lifetime (Schimel et al, 1996) and average transport distance by wind in the lower atmosphere of 500 – 1000 km per day (NEGTAP, 2001), it is easy to see

how the substantial quantity of CH$_4$ will be exchanged between countries in Africa. Any full bore rupture along the pipelength will negatively impact on the whole continent if left unattended to within three day.

CH$_4$ is a greenhouse gas (GHG) which aids climate change. The dangers posed by atmospheric abundance of CH$_4$ which increase from 1520ppb in 1978 to 1745ppb in 1998 (Prather and Ehbalt, 2001) has led to global desired declination observed annually over the last three decades. Global Warming Potential (GWP) increase in CH$_4$ production from energy source (in Tg (CH$_4$/yr)) has been estimated at 75 (Fung et al, 1991), 97 (Hein et al, 1997), 110 (Lelieveld et al, 1998), 89 (Houweling et al, 1999) and 109 (Olivier et al, 1999). Based on its atmospheric burden and climatic impacts (Alcamo, 1994), CH$_4$ was among the GHGes listed in the Kyoto Protocol of 11 December 1997 and enforced on 16 February 2005. Definitely, any accidental discharge of natural gas through WAGP project will jeopardize the treaty on the global climate.

Apart from being a direct threat, CH$_4$ oxidizes in stratosphere with OH, Cl and O leading to in-situ source of stratospheric water vapor (equation 2.15)

$$CH_4 + O_3 \rightarrow CH_3^{\cdot} + OH + O_2$$
$$CH_4 + OH \rightarrow CH_3 + H_2O \qquad \ldots\ldots\ldots\ldots\ldots\ldots \quad (2.15)$$
$$CH_3 + Cl \rightarrow CH_3Cl$$
$$CH_4 + Cl \rightarrow CH_3Cl + H^{\cdot}$$
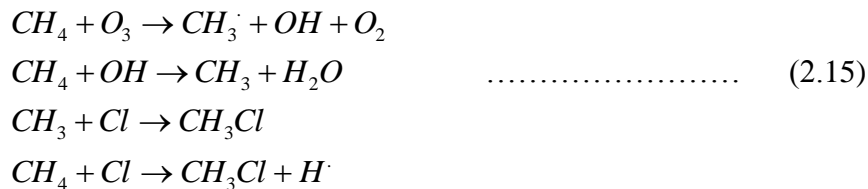
Oxidation of CH$_4$ is a source of mid-stratospheric H$_2$O and currently causes its abundance to increase from about 3ppm at the tropopause to about 6ppm in the upper stratosphere. Water vapor in the lower stratosphere is a very effective GHG. Baseline levels of stratospheric H$_2$O are controlled by temperature of the tropical tropopause, a parameter that changes the climate (Moyer et al, 1996; Rosenlof et al, 1997; Dessler 1998; Mote et al, 1998). Finally, stratospheric ozone depletion increases tropospheric OH (Bekki et al, 1994; Fuglestvedt et al, 1994) which reacts with CH$_4$ to produce more water vapor. CH$_4$ also reacts with Cl atoms in the troposphere (Singh et al, 1996) as shown in Equation (2.15).

Climate change impacts negatively on fish population and aquatic life. It was responsible for the drastic declination in the availability of king crab stock in the

Eastern North Pacific which include Eastern Bering Sea and Gulf of Alaska (Wooster, 1982) and the rapid disappearance of California Sardine (Ueber and McCall, 1982) amongst others.

2.10.3.3.2   *Flammability and VOC Discharge*

Natural gas is 35% lighter than air; it therefore dissipates into air to explode or otherwise burn in the presence of ignition source. The fumes escaping from the fire are carcinogenic and have other direct and indirect impacts on human health.

The fire resulting from the ignition (Figure 2.27) always introduces VOCs into the atmosphere. VOCs have been determined to be human risk factors in urban environment (Sonibare et al, 2005), as well as primary contributors to the formation of photochemical oxidants (Seguel et al 2012). To reduce anthropogenically produced O_3, and human risk, their (VOCs) presence in the environment must be reduced (Huang et al, 2012). Human exposure to certain level of some of these compounds could increase cancer risk (Ramirez et al, 2012) and their existence in high concentration have been found to have negative impact on outcome of pregnancy (Yang et al, 2002; Chun-Yuh et al, 2004). Cape (2003) confirmed that adverse effects of VOCs on vegetation in urban areas cannot be rejected; reproductive processes (flowering and seed production) were found to be most sensitive.

Figure 2.27: Resulting fire from Elume pipeline failure (EFR, 2000)

Leaf water content and photosynthetic efficiency were identified by Cape et al (2003) as additional parameters by which impacts of VOCs on plants can be determined. Water quality can be reduced by VOCs (Johnson et al, 2003) while soil can equally be affected if their ambient concentrations exceed certain level (Kim et al, 2001). Benzene, Toluene and Xylene (BTX, some common VOCs) could be of great risk to the environment if their emissions are not adequately controlled. They were found to affect luteal function in females exposed to such emissions (Chen et al, 2000) and Gamo et al (2003) identified them as part of the 12 major environmental pollutants in Japan. Chronic Benzene exposure may result in DNA break in bone marrow cells and peripheral blood lymphocytes and decrease the activities of antioxidative enzymes (Zhongha et al, 2003).

2.10.3.3.3 Release of toxic gas

Toxic gases are release from gas pipeline accidents and could lead to human death amongst several other hazards. In 1982, a high-profile blow out at an Amoco well in Western Canada spewed sour-gas cloud for 67 days, killing two workers and hundreds of cattle. In 2003, a blown out gas well near the city of Chongqing in Central China clouded the environment and the released toxic gas killed 243 people through inhalation. Hydrogen sulfide (H_2S) is a corrosive material that is frequently associated with pipeline failure at sour fields, the gas combines with other chemicals in a pipeline to produce microbial reduced corrosion (tiny cracks that are not detectable with the naked eye but can leak deadly quantities of gas). H_2S exists in many gas fields especially in Asian countries such as India, China, Pakistan, etc. Noteworthy is the Shah natural gas field in India that contains up to 30% H_2S.

Similar fields with such high sour gas are Bah, Asab and the offshore Hail fields (all in India). The H_2S gas is heavier than air (OSHA, 2005) and can travel along the ground to easily cause respiratory failure and brain damage even at low concentration. The threshold for human tolerance to this gas is very low. It is estimated to be less than 20ppm (GAEI, 2009) and the fatality of the gas as a killer has been recorded to be high worldwide.

Conclusively, the impacts of pipeline failure on the four environmental matrices (soil, water, air and vegetation) are interwoven and can only be appreciated by

considering real-life scenarios. Some of the existing and projected scenarios are discussed below.

Many of the existing and proposed gas pipelines are routed through critical wildlife and wild lands. An example is the $2.23billion worth 3056-kilometres-long Bolivia-Brazil pipeline. The 20 year contract pipeline is expected to transport 8 million m^3 for the first 7 years and l6 million m^3 for the remaining 13years (Pató, 2000). The pipeline runs through the Amazon River Basin which contains the world's largest tropical forest and almost half of the planet's terrestrial biodiversity. This is the largest basin in the world and covers about 4,195 miles long and 2,720,000 square miles in area. Specifically, the river basin includes 15,000 tributaries and sub-tributaries, four of which are in excess of 1,000 miles long each. Any failure from such pipelines will result in release of toxic gas or fire which in addition to affecting the community living could add to the destruction of the tropical ecosystems, loss of species and specimens, degradation of soil, water, air and destruction of basic infrastructures. Most importantly, it could add to the extinct of this wildlife.

The Niger-Delta region of Nigeria is another perfect case study to showcase the environmental consequences of pipeline failure. Nigeria is the world's 6th largest oil producer and 7th for natural gas with an average production rate of 2.5 million barrels per day and 4 billion cubic feet per day respectively. Her proven hydrocarbon reserves had been estimated at 35 billion barrels of crude oil and 5.24 trillion cubic meters of gas, while her undiscovered gas reserves was estimated at 8.5 − 16.99 trillion cubic meters (Oyekunle, 1999; Gbenga Biobaku & Co., 2008). However, these resources that account for over 90% of the country's revenue are located in the Niger-Delta region (Sonibare and Akeredolu, 2006), thus, majority of the existing pipeline networks in Nigeria are located in this region. The Niger-Delta region is described as one of the largest wetlands in the world covering an area of over 70,000 square kilometers (Groundwork, 2003) with a number of ecological zones that range from sandy coastal ridge barriers, brackish or saline mangrove, freshwater, permanent and seasonal swamps, forests as well as lowland rain forests. The total population of the region is over 30 million people in long settled communities spreading through nine states of the Nigerian federation, this accounted for about 20% of Nigeria's total population. The population density of the region is also among the highest in the world with 265 people per kilometer squared. Fishing,

hunting and subsistence agriculture are the major occupation of the people while the oil and gas industry is the major industrial sector. Some of the recorded pipeline failures (Table 2.23) included the Jones Creek of March 27th, 1998 where a pipeline failure spilled 840,000 barrels of crude oil into the environment (Doyle, 2002). In 1998, a pipeline leakage in Bayelsa State spilled 800,000 barrels of oil into the nearby farmlands and rivers. On 19th June 2003 also, a pipeline failure at Onicha Amaiyi-Uhu Village of Abia State caused a fire outbreak where over 200 deaths were recorded while the only drinking water serving the village was adversely polluted (Akinola, 2004). Again, Mobil Producing had a pipeline failure in 1998 that discharged 840,000 barrels of crude into the environment with adverse impact on the soils in the communities near Qua-Iboe. The spill completely extinguished the local fauna and flora including periwinkles – a major food source for the local people. Furthermore, a typical product loss from a pipeline accident in Nigeria resulted in contaminated soil with clay (34%), gravel (5%), heavy soil (16%), peat (12%), sand (6%), and others (18%) of average composition. 4.7% of the product loss resulted in ignition (Advantica, 2002; Onianwa, 1995).

Generally, most of the farmlands in Niger-Delta region can no longer produce good harvest and the ecosystem has equally been negatively affected as a result of environmental degradation arising from numerous pipelines failures and perpetual gas flaring. Fishing is no longer lucrative for the same reason and strange diseases that defy medical explanations are emerging.

Table 2.23: Some major pipeline accidents in Nigeria and consequences (Obanijesu et al, 2006)

Date	Location	Nature of Accident	Damage caused
15-04-04	Obeakpu village, Rivers State	Shell pipeline vandalized by youths resulting into fire	15 deaths. 13 injured.
26-09-03	Atlas cove, Lagos	Saboteur resulting to fire	Some injured.
29-08-03	Gio Village, Rivers State	Shell ruptured crude oil pipeline caught fire	Farmlands destroyed. The only river polluted. The village covered with smoke and soot.
19-06-03	Onicha Amaiyi-Uhu, Abia State	Fuel scooping from a vandalized pipeline resulted into fire.	Over 200 deaths. Iyi-Eruru, the only drinking water polluted.
12-02-02	Amukpe, Delta State	NNPC pipeline leaking from valve resulted into fire	4 deaths.
2001	Atlas Cove, Lagos State	Leaking PPMC pipeline resulted into fire	500 deaths.
Dec 2000	Lagos	Pipeline explosion	Over 60 deaths.
Nov 2000	Ebute-Ero, Lagos State	Pipeline failure resulted to fire	Over 70 deaths.
30-11-00	Lagos	A fractured pipeline caught fire near a fishing village	50 deaths.
08-11-00	Elume, Delta State	Fire erupted from PPMC pipeline that leaked for 4 months.	Several communities affected. Farmlands, rivers and aquatic lives destroyed. Ibada-Elume bridge collapsed. The stream polluted with diesel. NEPA transmission line burnt/cut.
July 2000	Warri-South, Delta State	Fuel scooping from a leaking pipeline resulted into explosion and fire	40 deaths.
July 2000	Ethiope-West, Delta State	Fuel scooping from a leaking pipeline resulted into explosion and fire	15 deaths
10-07-00	Egborode, Delta State	Ruptured Pipeline burst into fire	3000 death. Omugba, the only water source polluted. Over 30 km affected. Farmlands, forest and crops roasted
July 2000	Warri City, Delta State.	Pipeline Explosion	250 deaths
10-07-00	Adeje, Delta State	A damaged oil pipeline resulted into fire.	Over 300 deaths.
July 2000	Okpe, Delta State	Fuel scooping from a leaking pipeline resulted into explosion and fire	230 deaths. 30 missing. Farmlands destroyed

Table 2.23 (Contd.)

Date	Location	Nature of Accident	Damage caused
July 2000	Umuichichi/ Umunigbode, Abia State	Pipeline failure resulted into fire	Over 50 deaths.
July 2000	Iffie/Ajala, Delta State	Pipeline failure resulted into fire	Over 80 deaths.
09-07-00	Oviri Court, Delta State	Vandalized pipeline resulted into fire	Over 300 deaths.
Jun 2000	Ogwe-Asa, Abia State	Pipeline failure resulted into fire	Undetermined number of deaths.
Mar 2000	Adeje Village, Delta State	Pipeline failure resulted into fire	250 deaths.
14-03-00	Osisioma Ngwa Village, Abia State	Pipeline failure resulted into fire	50 deaths.
Jan 2000	Ogwo, Abia State	Vandalized pipeline burst into fire	Several lives lost
26-12-99 to Apr 2000	Adeje Village, Delta State	Fuel pipeline leaked continuously for over 4 months	Destruction of farmland. The smell of petrol in air made breathing difficult. This eventually resulted into catarrh and cough.
17-09-99	Ekakpamre, Delta State	Ruptured Shell BP pipeline caught fire.	Lives, animals, fishes and properties destroyed. River and land polluted.
Jun 1999	Aketedo, Lagos	Pipeline failure resulted into fire	30 deaths.
Oct 1998	Jesse Town, Delta State	Explosion and fire while scooping fuel from NNPC vandalized pipeline	Over 1200 deaths. Farmlands, trees, forests, crops and fauna roasted. Pollution of river body.
17-10-98	Idjerhe, Delta State	Leaking pipeline caught fire.	Over 500 deaths. Lives, farmlands, houses and other properties destroyed.
27-03-98	Jones Creek	Pipeline failure	840000 barrels of crude spilt into the environment.
1998	Bayelsa	Pipeline failure	800000 barrels spilt into the environment

2.11 Corrosion inhibition

Various types of inhibitors are being applied by pipeline industry to minimize corrosion along the internal wall of pipelines during gas transport. These inhibitors are generally organic and inorganic in nature (Ryu and Lee, 2012; Teryusheva et al, 2012). They include hexamine (Vashi and Naik, 2010), phenylenediamine (Abd El Rehim et al, 2010), dimethylethanolamine (Muller and Fischer, 2006), nitrites (Loto, 2012), cinnamaldehyde and condensation products of aldehydes (Kandepi and Narender, 2012; Seiad et al, 2012), amine (imines) (Khaled et al, 2005; Aiad et al, 2011), chromates (Sangeetha et al, 2011), phosphates, hydrazine and ascorbic acid amongst others (Rani and Basu, 2011).

The suitability of each chemical for a task in hand depends on many factors such as the material of the pipeline under consideration, the nature of the substances they are added into and the operating conditions such as temperature and pressure. The inhibitors could be anodic in nature or cathodic, the anodic inhibitors form a passivation layer on the metal surface thus, preventing its oxidation while cathodic inhibitors retard the corrosion by inhibiting the reduction of water to hydrogen gas. However, corrosion inhibitors have surfactants properties and some surfactants have been established to promote hydrate by increasing the gas content and the formation rate (Zhong and Rogers, 2000; Ricaurte et al, 2012).

2.12 Project Focus and other Contributions to knowledge

Hydrate formation cannot be totally prevented along the offshore gas pipeline due to various favourable thermodynamic conditions. As mentioned in section 2.6, these hydrates have been established by Obanijesu et al (2010; 2011) to be able to initiate corrosions along the pipelength. Also, corrosion inhibitors are equally applied to the gas stream in order to minimize corrosion during the transportation; however, the corrosion inhibitors have some surfactants properties in nature. Surfactants have been established to be hydrate promoters through various studies, therefore, there is may be a possibility for these surfactant properties of corrosion inhibitors to aid hydrate formation. However, all the reported research has not been studying this possibility, hence the uniqueness of this work. This work addressed these issues through various laboratory investigations. Once established, it means that the gas

industry is directly engaged in-between these two flow assurance problems. Efforts to solve one will conveniently promote the other, hence, the need to find a way to break away from the cyclic problems. This study further investigated the application of some gases to reduce the hydrate formation temperature. Any achievement on this will go a long way in minimizing hydrate-corrosion problems for the industry. This will help to save millions of dollars for the industry each year, increase production time which will lead to more profitability, reduce the environmental and safety risk of the operation thereby improve the operational conditions of the pipeline industry.

3. Corrosion Inhibitors as Hydrate Promoters

3.1 General Background

In response to the flow assurance issue raised in Chapter 2.12, this chapter properly investigated the use of corrosion inhibitors to aid the promotion of gas hydrate formation during the natural gas transport through offshore (underwater) pipelines. This investigation is divided into two separate studies. The first study which is reported in this chapter, investigated the ability of corrosion inhibitors to promote hydrate formation along deepwater gas pipeline. The study, carried out at 100bar and 500ppm in a cryogenic sapphire cell at static condition involved the use of five different corrosion inhibitors with different sizes, structures, active functional groups, and affinity for water molecules. This study is significant since there is no existing literature on it. The results obtained established the need for further investigation in this research. This further investigation is reported in chapter four.

3.2 Introduction

Inhibition of corrosion along the inner wall of pipelines during natural gas transportation is a major investment in the gas industry due to the implications of corrosion problems on flow assurance. Corrosion has been established to be specifically responsible for 57% of oil & gas pipeline ruptures in Canada (Cribb, 2003) and about 50% of worldwide pipeline failures with a replacement cost of about $1,767,710 and $1,977,644 per mile for 36' and 42' pipelines respectively (Parker et al, 2004). In 1995 alone, corrosion of metals and alloys cost U.S. companies and consumers approximately $300bn with 1% ($3bn) coming from the pipeline industry (Battelle, 1996); this cost increased for pipeline industry within the same country to $8bn by 2003 (Thompson and Vieth, 2003).

Australia with good quality of natural gas (Table 3.1) is susceptible to sweet corrosion. Millions of dollars are annually invested on corrosion inhibition through chemical injections into the flow lines during the gas transportations and sponsorship of various researches to improve the performance of these chemicals.

Corrosion inhibitors are generally organic and inorganic in nature. The suitability of each chemical for a task depends on many factors such as the pipe's material of

construction, the nature of the substance that the inhibitor is added into, the gas composition and the operating conditions such as temperature and pressure. The inhibitors could be anodic in nature or cathodic. While the anodic inhibitors form a passivation layer on the metal surface thus preventing its oxidation, the cathodic inhibitors retard the corrosion by inhibiting the reduction of water to hydrogen gas. However, most of these inhibitors have similar chemical properties and structures to the established hydrate formation promoters in gas pipelines.

Table 3.1: Some Australian gas field compositions at platform separators (Pack, 2011)

Component	North West Shelf gas (mol %)	Timor Sea gas (mol %)
Methane	84.120	79.543
Ethane	4.282	8.137
Propane	1.733	1.746
i-Butane	0.345	0.158
n-Butane	0.532	0.133
i-Pentane	0.213	0.023
n-Pentane	0.193	0.012
n-Hexane	0.132	0
Carbon dioxide	2.513	6.146
Nitrogen	5.938	4.102

Hydrate formation along offshore gas pipelines is always aided by the favourable thermodynamic conditions of the producing environment, which are the gas transportation at a very high pressure and the low deepwater temperature of about $4^{o}C$. With the presence of these conditions, the low paraffinic homologous composition of the gas (C_1-C_4) and/or the impurities present in the gas (such as H_2S, CO_2, etc) combine(s) with the available water vapour at the liquid/gas interphase in the presence of weak Van der Waals forces to form hydrates. If not quickly removed, the hydrate grows along the line and blocks the inner orifice of the pipe, hence, leading to pressure build-up along the line and eventual rupture. Hydrates, which have been costing the gas industry millions of dollars annually on prevention have been established to be promoted by surfactants (Karaaslan and Parlaktuna, 2000; Mandal and Laik, 2008). Some of the established hydrate promoters with surfactant

properties include tetra butyl ammonium chloride (Prasad et al, 2009) and Tetra-*n*-butyl ammonium bromide (Sun et al, 2008).

Of the five surfactants' classifications, the cationic surfactants are the most expensive due to the high pressure hydrogenation reaction carried out during their synthesis. However, due to their ability to adsorb on negatively charged substrates to produce antistatic and hydrophobant effects, they are of most value as corrosion inhibitors. Technically, it is observed that most of the corrosion inhibitors used in the gas fields either belong to the cationic surfactant group or have similar chemical structures with some members in the group.

Several studies have been carried out to investigate the properties and efficiencies of various corrosion inhibitors (Bentiss et al, 2000; Aljourani et al, 2009) but none of the existing literatures have investigated the ability of these chemicals to promote hydrate formation, hence, the significance of this study. This study investigated the possibility of corrosion inhibitors to promote hydrate formation along deepwater gas pipelines. Five chemicals from the most regularly used inhibitors for sweet corrosions in gas fields (Table 3.2) are investigated due to its significance since carbon dioxide (CO_2) corrosion is caused by carbonic acid (H_2CO_3) and remains one of the major problems associated with the oil and gas industry (Marco et al, 2001).

Table 3.2: The list of inhibitors used for the study

Inhibitor	Abbreviation	Molecular Formula	Mol. Wt. (g/mol)
2-mercapto pyrimidine	MP	$C_4H_4H_2S$	112.15
Cetylpyridinium chloride	CPC	$C_{21}H_{38}NCl.H_2O$	358.07
Dodecylpyridinium chloride	DPC	$C_{17}H_{30}ClN$	283.88
Thiobenzamide	TB	$C_6H_5CONH_2$	121.14
Benzl dimethyl hexadecylammonium chloride	BDHC	$CH_3(CH_2)_{15}N(CH_3)_2CH_2C_6H_5.Cl$	396

2-mercaptopyrimidine (MP) is a derivative of Pyrimidine. Pyrimidine is a heterocyclic compound containing nitrogen atoms at positions 1 and 3 in six-membered ring structure molecule. Nandeesh and Sheshadri (1991) reported the corrosion inhibitory effect of MP on copper. Cetylpyridinium chloride (CPC) is a cationic quaternary ammonium compound with anti-microbial properties and an IUPAC naming of 1-Hexadecylpyridinium chloride. It is a white powder with 80-83°C as melting point. The inhibitory effect of CPC on acid corrosion of low carbon steel was studied by Atia and Saleh (2003). Dodecylpyridinium Chloride (DPC) is a Heterocyclic Quarternary Ammonium Salts and cationic surfactant that undergoes complex formation with multicharged anionic planar substances (Murakani, 2004). Thiobenzamide (TB) is a sulphur-containing organic compounds used as a corrosion inhibitor (Zcan and Dehri, 2004). Finally, Benzyl dimethyl Hexadexyl Ammonium chloride (BDHA) is a Quaternary ammonium compounds with colour ranging from white to creamy crystalline powder and the melting point of 54-58°C. It is freely soluble with pH of 6.0-8.5 (10% solution), non-reactive, slightly inflammable but stable under ordinary conditions. Marco et al (2001) studied the adsorption behavior of this chemical as a corrosion inhibitor on mild steel in CO_2 saturated brine media.

3.3 Methodology

3.3.1 Reagent, Materials and Equipment

Natural gas containing 20% CO_2 (Table 3.3) was prepared by the BOC Pty Australia. The industrially prepared specific composition was necessary to maintain constant composition throughout the experimentation period. Purified water was obtained from a Milli-Q†-system (MQ-H$_2$O). MQ-H$_2$O is double-distilled, ultrapure laboratory grade water that is filtered and purified by reverse osmosis method.

The five inhibitors were prepared from their various fresh stocks at CORR_CERT centre of Curtin University and the experiments were conducted at static condition inside a cryogenic sapphire cell (Figure 3.1) in the Clean Gas Technology Section of Curtin University, Perth, Australia. The cryogenic sapphire cell equipment is made up of piston pump, pneumatic pump, sapphire cell unit, valves, two cameras and other fittings. The equipment was manufactured by ST (Sanchez Technology) France and operates at a temperature range of -160 ^{o}C – 60 ^{o}C (with accuracy of $\pm$ 0.10^{o}C)

and pressure range of 1bar – 500bar (with accuracy of ± 0.5bar). The specified accuracies were given by the manufacturers with the equipment.

Table 3.3: Composition of the studied natural gas

Component	Concentration (%)
CH_4	70.90
C_2H_6	5.00
C_3H_8	3.00
$n-C_4H_{10}$	0.94
$n-C_5H_{12}$	0.10
N_2	0.06
CO_2	20.0
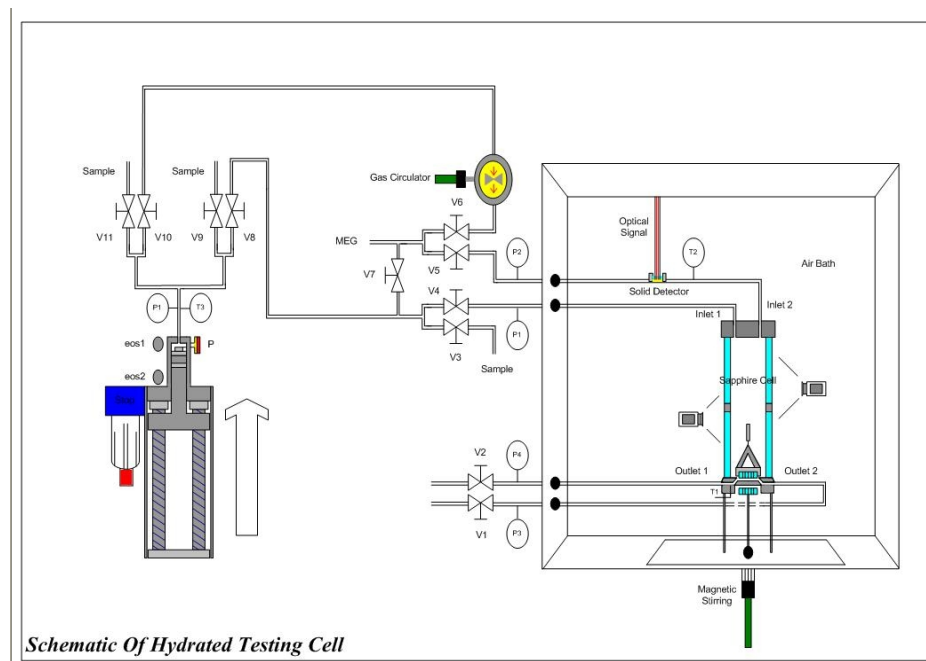
Figure 3.1: Schematic of the sapphire cell (Sucortseva et al, 2009; Obanijesu et al, 2012a)

The sapphire cell unit (Figure 3.2) is an inner glass cell of 60ml for liquid/gas interaction and has a magnetic stirrer which could be regulated to a desired speed. A thermocouple is screwed to the top of the cell to read the gas phase temperature (or TOP TEMPERATURE) and another to the bottom to read the liquid phase temperature (or BOTTOM TEMPERATURE) during an experiment. For each

experiment, the cell was properly cleaned and vacuumed in order to drastically minimize experimental errors. To achieve this, the cell is firstly depressurized by direct venting to the atmosphere followed by opening the cell door to critically clean the glass cell with MQ-H$_2$O. The internal wall of the glass cell was then completely dried with air using a booster pump in order to minimize water retainment and the glass cell was finally secured with nuts at both ends. The cell door was then closed and securely locked while the whole cell was vacuumed and the inlet valves tightly closed.
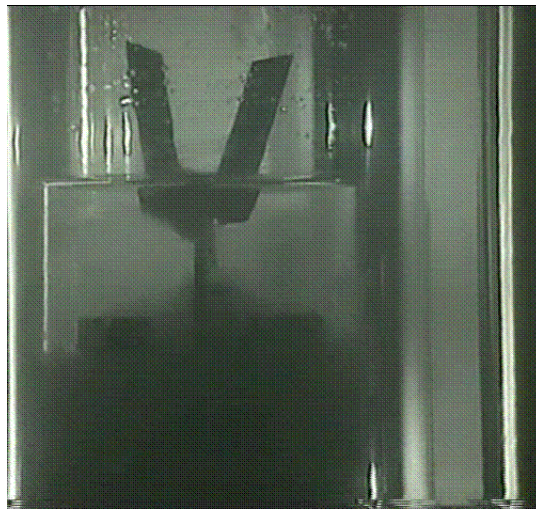
Figure 3.2: Liquid-gas interaction section in the sapphire cell (Obanijesu et al, 2012a)

During the experiment, the cell temperature was controlled using Falcon-E4378-Curtin-Cryogenic Cell software which was a temperature regulator at constant pressure, (Temperature search method), this software operates using the ideal gas law as as $\frac{PV}{T} = nR$. With this, Temperature depends on number of dissolved moles at constant pressure. The cell pump was controlled for pressure regulation using Workbench V-5-Gas pump-Pressure software; the pump's motor speed was always set to 100% for utmost efficiency. Finally, the cell's temperature and pressure were monitored through the Texmate Meter Viewer software which displays the operating pressure and the temperatures (TOP and BOTTOM) inside the cell at each time. The Falcon, Workbench and Texmate Meter Viewer softwares were connected to a computer and the whole process is controlled/regulated through a computer monitor. Progress of each experiment was monitored through the two cameras attached to the

81

Cryogenic Sapphire Cell while the generated data were automatically logged by the system.

3.3.2 The gas preparation for laboratory experimentation

500ml cylindrical sampling bottles, made of steel were each vacuumed with a 2-stage Edwards Rotation pump with an AC motor of 50Hz, Voltage of 220/240V and speed of 1425rpm. Each cylinder was then filled with fresh natural gas composition using a pressure transducer which is connected to power source with a cable of Type Gefion PI205. Each filled bottle is fitted to the manifold line and the whole system is again vacuumed. The gas was compressed into the Sapphire cell through V9 (Figure 3.1) while 5ml of already prepared liquid phase solution was injected into the cell through V5. The liquid phase solution was either MQ-H_2O (for blank experiment or 0ppm concentration) or a required corrosion inhibitor whose concentration was prepared using

$$M_1V_1 = M_2V_2 \hspace{4cm} \text{Equation 3.1}$$

Where

M_1 is the concentration of the available inhibitor (ppm), M_2 is the concentration of required solution (ppm), V_1 is the volume of inhibitor (ml) and V_2 is the volume of solution (ml).

All lines (including the manifold line and the piston pump) were then connected to the sapphire cell and finally vacuumed.

3.3.3 General Experimental Operations

The system's pressure was raised within the desired pressure using both the booster and piston pumps while the WORKBENCH software was used to fix for specific operating pressure. The cell was heated up to $35^{o}C$ as a reference point temperature (thus, giving the study a baseline for data generation), the heater was then turned off and the experimental SET-POINT TEMPERATURE (T_{set}) was fixed to $10^{o}C$. The chiller was then switched on and the experiment commenced. At the commencement of each experiment, the BOTTOM TEMPERATURE (T_B) and TOP TEMPERATURE (T_{Top}) were recorded. The T_B represented the temperature of the liquid phase in the cell while T_{Top} was that of the gaseous phase. As the cooling

progressed, changes in the T_{Top}, T_B, and AIR BATH TEMPERATURE (T_{AB}) were automatically logged (in milliseconds) by the Falcon software for retrieval after each experiment. Other external observations such as the interphase condition (clear or cloudy), the point when the wall of the sapphire cell started turning (or fully turned) cloudy; the temperature where the first hydrate particle was formed, the agglomeration, growth and behaviour; the foaming properties, the point where the stirrer stops rotating due to complete hydrate blockage and the reduction rate of the liquid volume in the cell, were recorded into a log-book. These information points were also recorded through the video cassette recorder (VCR) embedded into the computer software for the study. At the end of each experiment, the hydrate formation temperature was recorded while the automatically logged data were downloaded.

3.3.4: Experimental Procedure

The experiments were conducted at 100bar. Before the commencement of the experiments, HYSYS software was used to investigate the compositional phase behavior of the gas at 100 bar for various temperatures. This was to investigate if the gas will remain gaseous at a very low temperature and maintain a constant composition throughout the study. This was important since the experiments were to be conducted at winter period; at a very low temperature, CO_2 gas can undergo partial condensation to give the gas mixture different composition at different experiment based on the environmental conditions.

HYSYS software was also used to predict the formation temperature of the gas composition at 100bar to give a rough formation temperature point for the blank studies in order to save time during the experiment. A blank experimental study was carried out to establish the hydrate formation temperature point. This was conducted by introducing 1200ml of the gas mixture through the manifold into the system and then pressurized with 5ml of MQ-H_2O (liquid phase) in the 60ml sapphire cell at 100bar while the temperature was gradually reduced till the first point where hydrate was formed. The gas/liquid mixture in the cell represents blank mixture. The value from this experiment served as the baseline temperature (T_{Blank}).

After establishing the hydrate formation temperature at blank condition, 500ppm of MP was prepared using Equation (3.1) to form the newly desired mixture of liquid

phase (blank+inhibitor). 5ml of the prepared 500ppm solution was injected into the sapphire cell through V5 while 1200ml of the gas was compressed in through V9 and the experiment repeated at 100bar till hydrate is formed, this generate a new formation temperature (T_{New}). This same experimental procedure was repeated for the other inhibitors, one at a time. Deviation in temperature ($T_{Deviation}$) was obtained by comparing the (T_{Blank}) with (T_{New}). The difference in value for each showed how much the inhibitor impacted on the formation temperature along the offshore gas pipeline.

To evaluate the performance of the equipment and ascertain accuracy of the generated experimental data, the blank study was repeated three times while some of the experiments (with inhibitors) were selected at random for replication; it was observed that the same results were obtained. Fluid leakages were also prevented during the experimentations in order to minimize errors; this was done by threading a Teflon tape along the outlet part of each valve and soap tested before starting the experiment. Furthermore, parallax error was avoided during the preparation of liquid phase solutions. Again, there was no source for the liquid head in the cell to fluctuate throughout the experiments. Statistical analysis on the generated data gave the maximum experimental error of 1.299%; this clearly showed that the data obtained were accurate within the limits of experimental errors since the probability limit (confidence level) is above 95%.

3.4   Results and Discussions

3.4.1   Promotion of hydrate formation

The deviation in the formation temperature for all the investigated inhibitors was calculated using Equation (3.2) and the results plotted as shown in Figure 3.3.

$$T_{Deviation} = T_{New} - T_{blank}$$ Equation 3.2

Where

T_{blank} is the Formation temperature for the blank experiment and T_{New} is the Formation temperature for (blank + Inhibitor).

From Figure 3.3, it is established that corrosion inhibitors generally promote hydrate formation along deepwater natural gas pipelines by increasing the formation

temperature. This development is best explained through their surfactant and hydrogen bonding properties.
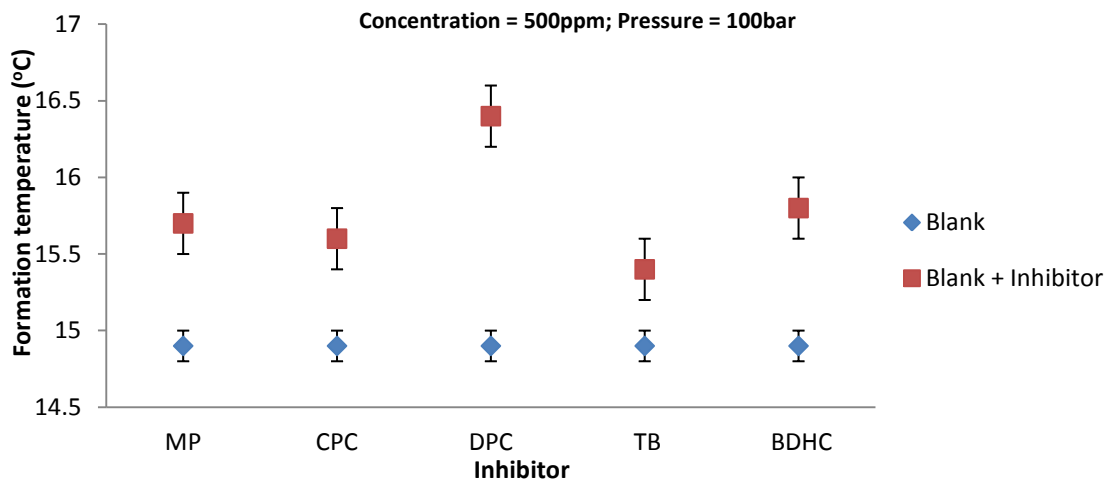
Figure 3.3: Hydrate formation temperature trend for the investigated inhibitors

3.4.1.1 Effects of the inhibitors' surfactant properties on formation temperature

It was not surprising that all the investigated corrosion inhibitors aided hydrated formation since all corrosion inhibitors are surfactants and surfactants have generally been established to be hydrate promoters (Sun et al, 2003b; Gayet et al, 2005; Wu et al, 2011). A surfactant (also known as "surface-active agent") is a chemical that stabilizes mixtures of hydrocarbon and water by reducing the surface tension at the interface between the fluids' molecules. Because the fluids do not dissolve in each other, the present surfactant keeps the entire fluids mixture from separating into layers, thus, affecting surface characteristics of the system by increasing the contact of the two materials involved (wettability). There are generally five types of surfactants which are anionic, non-ionic, amphoteric, polymeric and cationic surfactants (Huntsman, 2010) with their production rates and utilization shown in Table 3.4.

Corrosion inhibitors are mostly cationic surfactants. The cationic surfactants are more expensive than (and hence, rarely used compared to) the anionic surfactants due to the high pressure hydrogenation reaction carried out during their synthesis. However, due to their ability to absorb on negatively charged substrates to produce antistatic and hydrophobant effects, they are of most value as corrosion inhibitors.

85

Table 3.4: The surfactant types and their world production rates (Salager, 2002)

The Surfactant Type	World Production (%)
Anionic	50
Nonionic	45
Others	5

Cationic surfactants dissociate in aqueous solution into anion and cation but exhibits positively charged head groups and have anti-static properties (Salagar, 2002)**.** Anti-static property of a material is its ability to minimize the generation of static charges without depending upon the material's resistivity (ESD, 2009). Large proportion of this surfactant group corresponds to nitrogen compounds such as fatty amine salts and quaternary ammoniums, with one or more long chain of the alkyl type often coming from natural fatty acids. Karaaslan and Parlaktuna (2000) experimentally investigated the effects of surfactants on hydrate formation kinetics and established that the hydrate formation rate is increased by anionic surfactants at all concentrations while cationic surfactants increase the formation rate at low concentrations; whereas, corrosion inhibitors (which are also cationic surfactants) are generally introduced at low concentrations into the gas stream during transportation through pipelines, thus, behaving as proposed by Karaaslan and Parlaktuna (2000).

3.4.1.2 Contributions of the material orientation

Surfactants are amphiphilic substances by exhibiting double affinity defined from physico-chemical point as polar-apolar duality (Salagar, 2002). An amphiphilic molecule consists of two ends where the first end is a polar (hydrophilic) group with heteroatoms contents such as O, S, P, or N included in the functional groups. The other apolar (hydrophobic or lipophilic) end however is generally a hydrocarbon chain of alkyl or alkylbenzene, atimes, with halogen or non-ionized oxygen atoms. When in hydrocarbon-water mixture, the surfactant migrates to the interface and orientates in such a way that the hydrophilic end is placed in water while the hydrophobic end lies in the hydrocarbon, thus, reducing the tension at the interface through the surface activities. The hydrophilic end is always regarded as the head while the lipophilic end is the tail.

Just like surfactant where the hydrophilic end is placed in water and the hydrophobic end lies in the hydrocarbon in a hydrocarbon-water mixture, corrosion inhibitors when injected into a gas pipeline system have their hydrophilic end adsorbed (attached) to the pipe wall because of the high intensity HOMO structure while the hydrophobic end (carbon chain length) in the gas stream. In this case, the metal surface which is a conductor of electricity acts like water (which is also an electricity conductor). This enables the inhibitors to prevent any interaction between the water molecules in the gas stream and the pipeline, thus, inhibiting corrosion by spreading themselves throughout the entire pipe surface. However, the hydrophobic end within the gas stream encourage the gas components to dissolve more into the water molecules present in the gas stream to promote hydrate formation. This is due to the strong interaction between the carbon in the corrosion inhibitor and the methane present in the gas stream (Daimaru et al, 2007).

3.4.1.3 Hydrogen bonding Contributions

Gas clathrates (Figures 3.4a and 3.4b) exist due to the ability of H_2O molecules to assemble through hydrogen bonding and form polyhedral cavities.
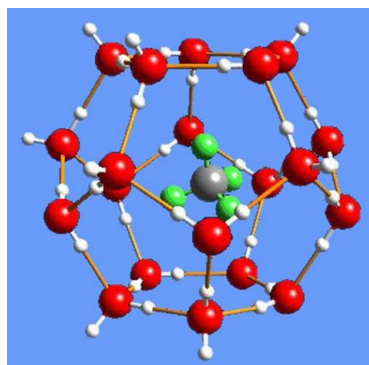
Fig. 3.4a: Schematic drawing of natural gas clathrate structure where a methane molecule is encaged by a lattice of water molecules.
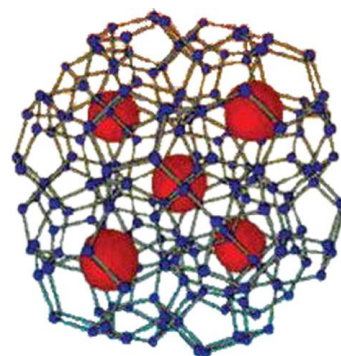
Fig. 3.4b: Methane clathrate dual structure.

Figure 3.4: Methane hydrate structures (Mahajan et al, 2007)

According to Vysniauskas and Bishnoi (2003) and Zhong and Rogers (2000), the hydrate formation mechanism in a water-gas system depends on the hydrogen-bonded water molecules clustering with the solutes of the hydrocarbon gas to form hydrate crystals at certain concentration and size. In each water molecule, the two hydrogen atoms are separated at an angle of $108^{\circ}C$ as a result of the hydrogen bonds

formed with oxygen (Caroll, 2009); this results in the formation of polyhedral cavities between several H_2O molecules. The solute molecules (CH_4, CO_2, etc) are then trapped in- between the cavities to form the required hydrate type.

Just like water molecule which is able to form hydrate because of its hydrogen bonding property, all amphiphiles exhibit hydrogen bonding abilities (Ali and Saha, 2001). Corrosion inhibitors are amphiphiles, hence, their ability to exhibit hydrogen bonding property in their solid and/or liquid states. For the five investigated inhibitors, MP (Figure 3.5) has the ability to form a dimensional chain complex due to the existence N....H hydrogen bonding (Ma et al, 2005).
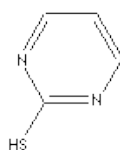
Figure 3.5: The chemical structure of MP.

The inhibitor also owns a de-protonated heterocyclic thioamide group (N-C-S)⁻ that makes it to act as an S or N-bridging ligand. Okazaki et al (1976) strongly confirmed the hydrogen bonding ability of CPC by experimenting with chloroform. Observation of the chemical structure (Figure 3.6) shows the ability of the inhibitor to form N—H bond.
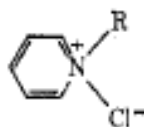
Figure 3.6: The chemical structures of CPC.

Akba and Batigoc (2008) confirmed the hydrogen bonding ability of DPC (Figure 3.7) while Saeed et al (2011) and Al-Kady et al (2011) equally confirmed the hydrogen bonding properties of TB and BDHA (Figure 3.8) respectively.
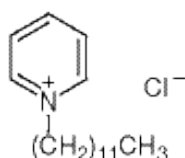
Figure 3.7: Chemical formula DPC

88
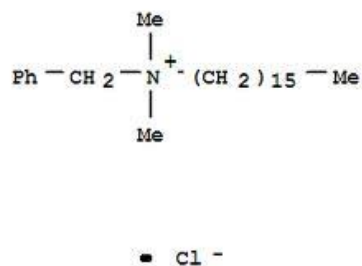
Figure 3.8: Chemical formula for BDHA

3.4.2 Impact of Different Inhibitors on Formation Temperature.

The variation in promotion rate of different corrosion inhibitors on gas hydrate formation temperature was investigated based on the formation trends observed in Figure 3.3. This variation was necessary to study the impact of different types of corrosion inhibitors on offshore pipeline systems. It was observed that at the same inhibitor concentration, liquid volume and operating pressure, all the inhibitors increased the formation temperature with a trend of DPC > BDHC > MP > CPC > TB (Figure 3.9).

These results show that corrosion inhibitors aid promotion of hydrate formation at different rates. This characteristic may depend on cumulative effects of many factors such as their sizes and structural distributions, active functional groups and affinity for water molecules which eventually impact on their hydrogen bonding properties and electronegativity.
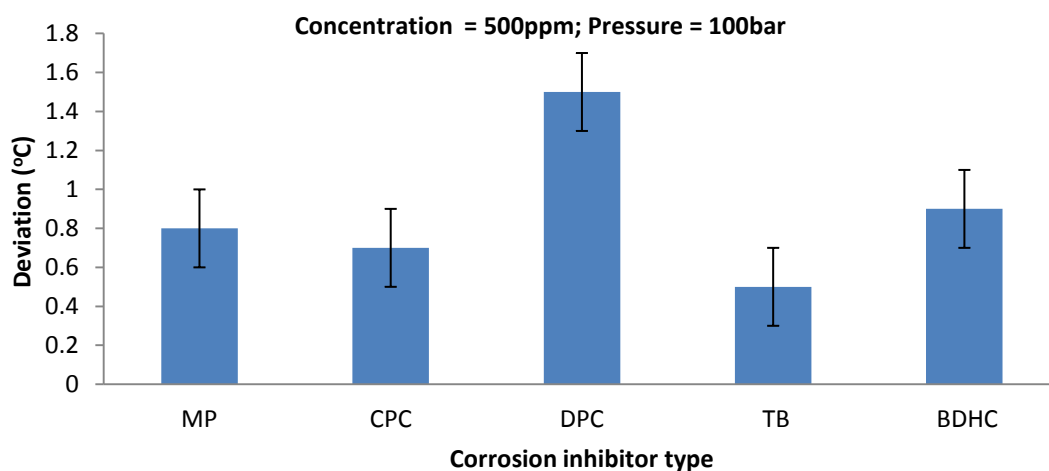
Figure 3.9: Formation temperature deviation of different inhibitors.

3.4.2.1 Structural Distribution

The apolar (hydrophobic or lipophilic) end of corrosion inhibitors is generally known to be hydrocarbon chain of alkyl or alkylbenzene, and sometimes with halogen or non-ionized oxygen. The different sizes of this end for different inhibitors give them structures that are responsible for their different molecular aggregations; this gives each inhibitor unique chemical, physical and other phenomena ability. As cationic amphiphiles molecules, they possess non-polar hydrocarbon chains ending with methyl group; nitrogen; chloride and sulphide to enable them form onium and counterion structures (Vongbupnimit et al, 1995). By determining the distance between the active atom(s) at the outermost shell and the nucleus, the structure and size of each inhibitor therefore affects its electronegativity since the active electrons of some of the inhibitors have direct exposure to the nucleus while for others, the active electrons at the outermost shell have been shielded from the direct contact.

The electronegativity of a substance has a direct influence on the impact of its hydrogen bonding type, the higher the electronegativity, the stronger the bond type. Electronegativity is a function of atomic radius, number of electrons in the outermost shell. The farther the electrons attached to the outermost shell from the influence of the nucleus charge, the easier it is to draw it away and the weaker the hydrogen bond that could be formed. The types and strength of the resulting hydrogen bonding will impact the average bond length, bond angle, the molecular packing and the torsion angles.

3.4.2.2 Active functional group

The polar (hydrophilic) group of each inhibitor contains heteroatom(s) such as O, S, P, or N which determines its impact on hydrate formation temperature through the type(s) of hydrogen bonding exhibited while in solution. The type of functional group will further determine whether the formed bonding will be polar covalent, ionic or ionic with covalent character in nature.

While forming hydrate, MP (Figure 3.5) serves as a bridging ligand coordinate to a crystal structure which is stabilized by N···H, O—H···O and O—H···S (Li et al, 2010). However Lima et al (2006) used Second- and fourth-order M ller-Plesset perturbation theory and thermodynamic perturbation theory implemented on a Monte

Carlo N_pT simulation to show that the SH is more stable in gas phase while NH type is more stable in solution. From their structure likewise, CPC (Figure 3.10) can form N⋯H and H⋯Cl bond types; DPC (Figure 3.11) forms N⋯H, H⋯O and H⋯Cl; TB (Figure 3.12) forms S⋯H and N⋯H and BDHA (Figure 3.13) forms N⋯H and H⋯Cl.

Figure 3.10: Another structural representation of CPC
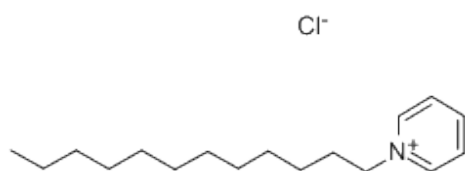
Figure 3.11: Another structural representation of DPC
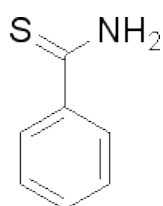
Figure 3.12: The chemical structures of TB.
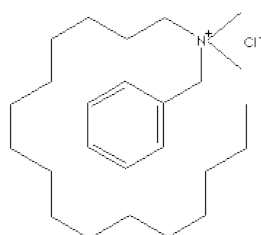
Figure 3.13: The chemical structure of BDHA.

3.4.2.3 Affinity for water

Also, the affinity of each inhibitor for water molecules affects its level of promotion; the more the affinity, the more the promotion ability. This affects the inhibitor's hydration ability to forming more hydrogen bond with water by taking more water

molecules into the complex three dimensional structures which will confine the gas into its cage (matrix) to form $X.H_2O$, $X.10H_2O$ and/or $X.50H_20$ where X is a particular inhibitor. The strength of the hydrogen bonds to be formed will be determined by the accessibility of the hydrogen atom(s) to the required site which thus encourages electrolyte selectivity through stericity and Nucleophelicity.

Considering cumulative effects of the structural distribution, active functional group and affinity for water based on above explanations, the hydrate formation pattern as observed can be justified. DPC which is shows the strongest ability contains both the Cl^- and N^+ groups that can react very fast with water molecules because of highly polar and strong hydrogen bonding properties which have higher affinity for water molecules meeting the thermodynamic energy needed for the breaks and formations. BDHA also contains these two groups, it however has a large non-polar part that restricts interaction with water because of increase in apolar character which involves London dispersion force (instantaneous dipole). Though, MP is expected to have more affinity for water compared with DPC due to it's readily solubility property, DPC and BDHA however show more polar character comparatively. Finally, although CPC also has Cl^- and N^+ groups in its structure and expected to be readily soluble and reactive with water like DPC; the hydrophobic end however is very large.

3.4.3 Hydrate Formation Patterns

3.4.3.1 The blank formation patterns.

The hydrate formation patterns for the blank and the five inhibitors were studied through physical observations. At the blank concentration (Figure 3.14a), the formed hydrate started building at the gas phase and grew gradually at the gas phase (Figure 3.14 b-d); while the liquid volume was gradually reducing till the whole cell become blocked (Figure 3.14d-f).
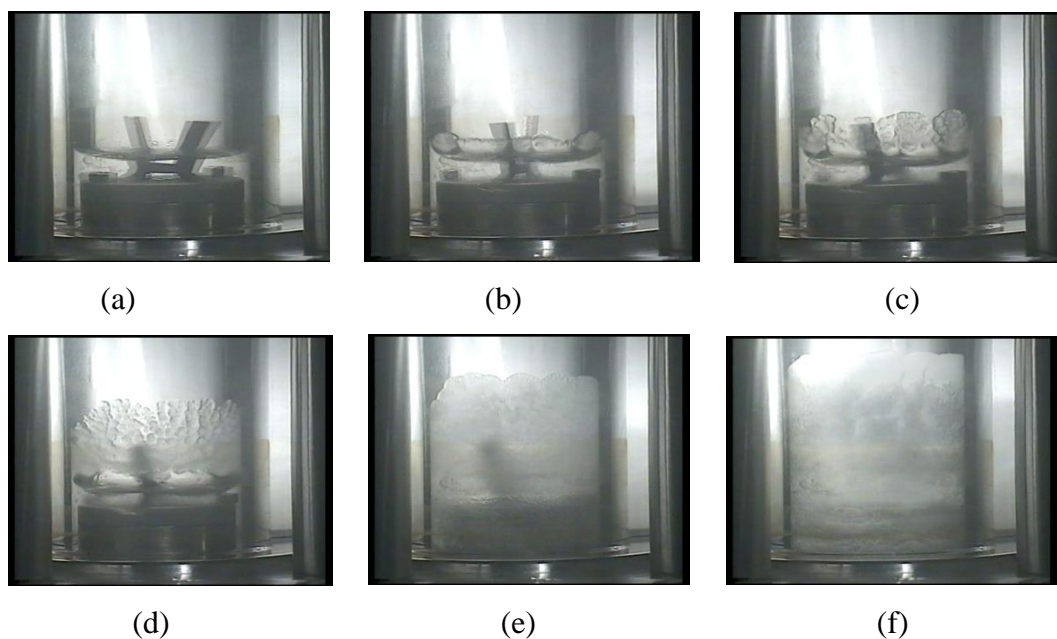
Figure 3.14: Captured images of hydrates at blank concentration

3.4.3.2 The formation patterns for MP

The hydrate for MP is initially formed thinly at the interphase without agglomerating for about 6 mins (Figure 3.15b); it then started forming disjointedly, block by block and piece by piece at the glass surface at a very low rate. During the growth (Figure 3.15 c-f), the hydrate seemed suspended in the gas phase away from the liquid phase with the top building sky-like with snow colour.
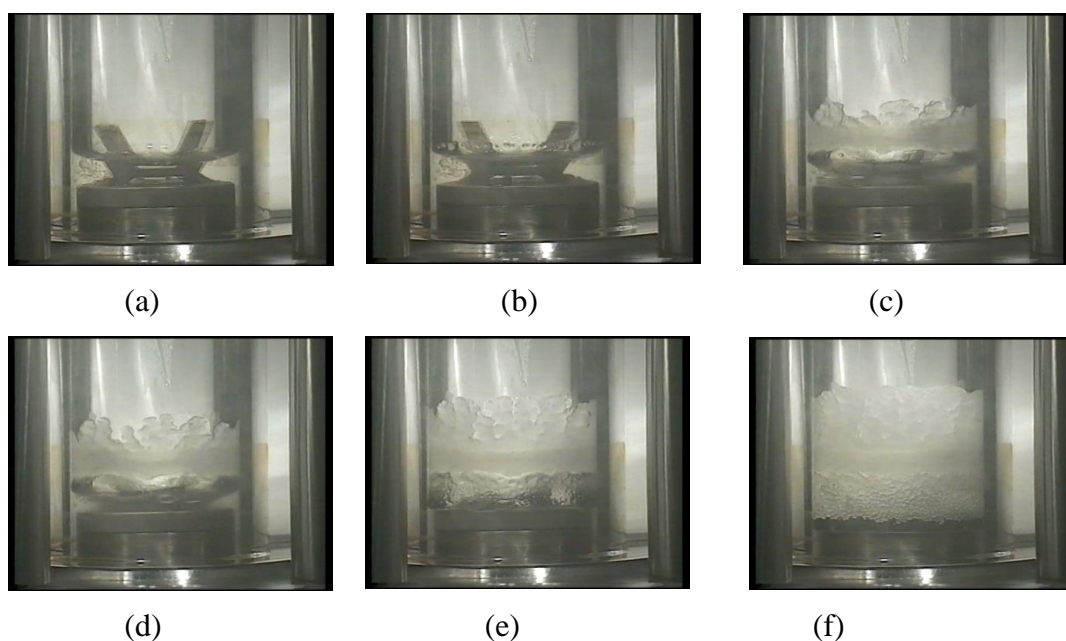
Figure 3.15: Captured images of hydrates formed by MP

3.4.3.3 The CPC formation patterns.

At the formation temperature, CPC's hydrates were initially formed at the interphase in chips form (Fig 3.16b). They then dissolved within two minutes into the liquid phase (Figure 3.16c) and started growing gradually but at a slow rate (Figure 3.16d).

(a)
(b)

(c)
(d)
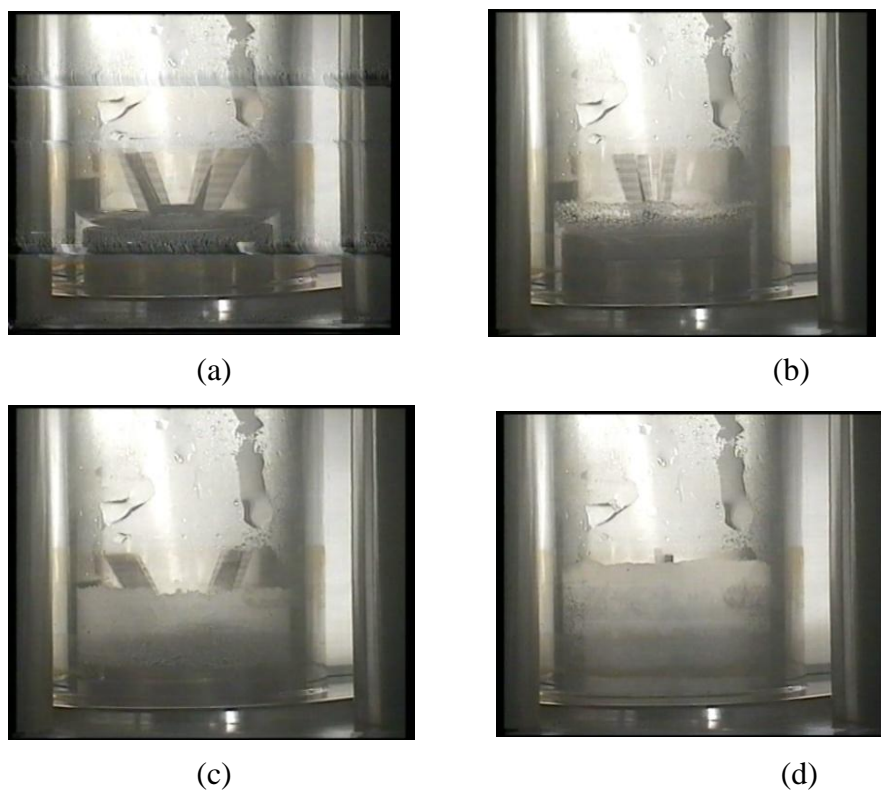
Figure 3.16: Captured images of hydrates formed by CPC

3.4.3.4 Formation patterns for DPC

The hydrate for DPC initially started growing slowly for the first 7mins after which the growth rate increased rapidly (Figure 3.17a-f). The growth rate was so alarming and the whole glass column was blocked within the next 4mins while the stirrer stopped rotating 1min after. For this chemical, it is observed that the liquid disappearance rate and the hydrate formation rate are very much higher when compared with the other four inhibitors.

(a)　　　　　　　　(b)　　　　　　　　(c)

(d)　　　　　　　　(e)　　　　　　　　(f)
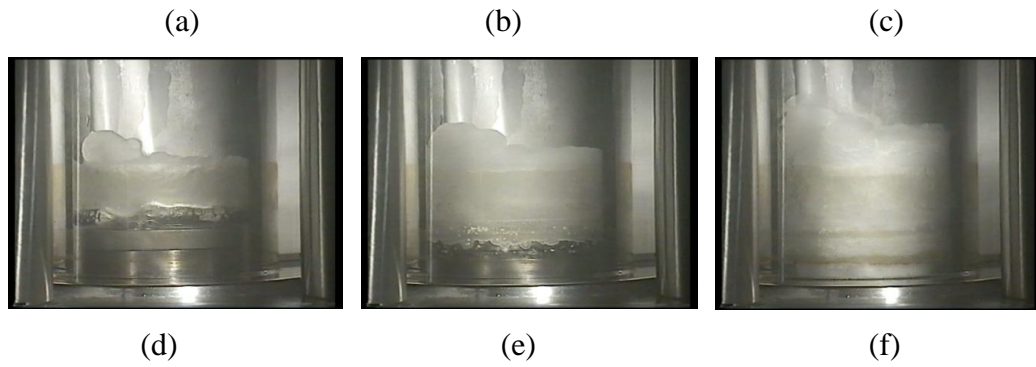
Figure 3.17: Captured images of hydrates formed by DPC

3.4.3.5 The formation patterns for TB

The hydrate for TB, which was as white as snow, was formed at the interphase (Figure 3.18a-b), and then started growing upward along the cell glass column at the gas phase without mixing with the liquid phase (Figure 3.18c-d). The growth rate at the gas phase was rapid while the liquid phase was slightly turning cloudy and disappearing downward till it finally vanished (Figure 3.18d-e). Throughout, this experiment, the hydrate never collapsed into the liquid phase but solidified in the gas phase and grew.

(a)　　　　　　　　(b)　　　　　　　　(c)

(d)　　　　　　　　(e)
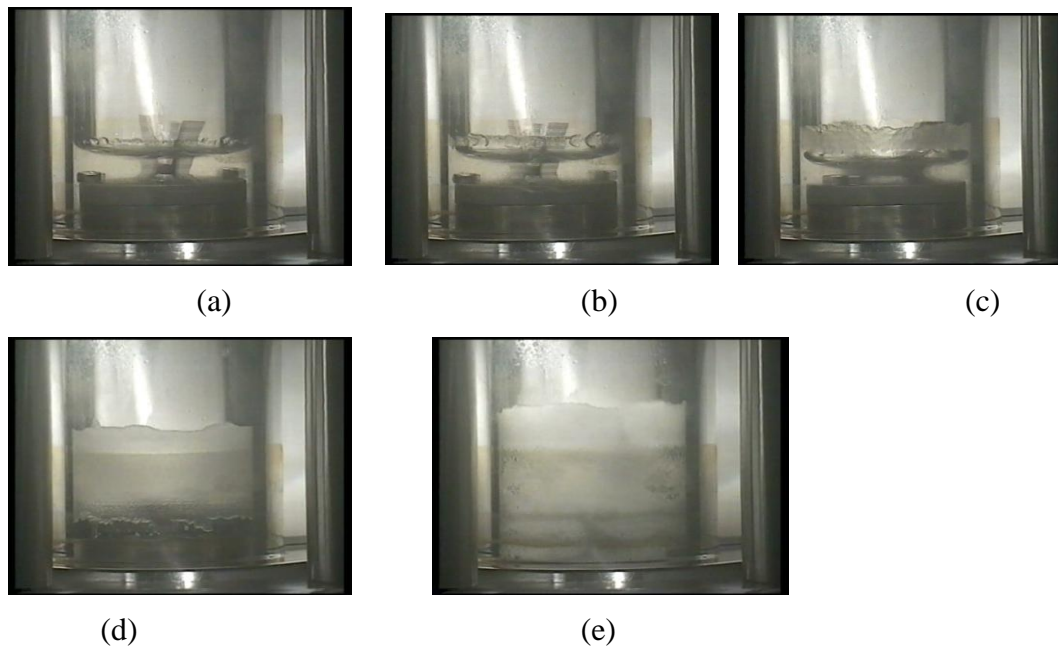
Figure 3.18: Captured images of hydrates formed by TB

95

3.4.3.6 The formation patterns for BDHC

The BDHC's hydrate was observed to form rapidly by breaking into chips and mixing with the liquid phase (Figure 3.19a-d). This was followed by the hydrate growing inside the liquid as flocs, breaking up and adding up to the existing hydrates (Figure 3.19e-f). The hydrate grow rate for this inhibitor was observed to be higher than those of the other inhibitors except for the DPC.

(a) (b) (c)

(d) (e) (f)
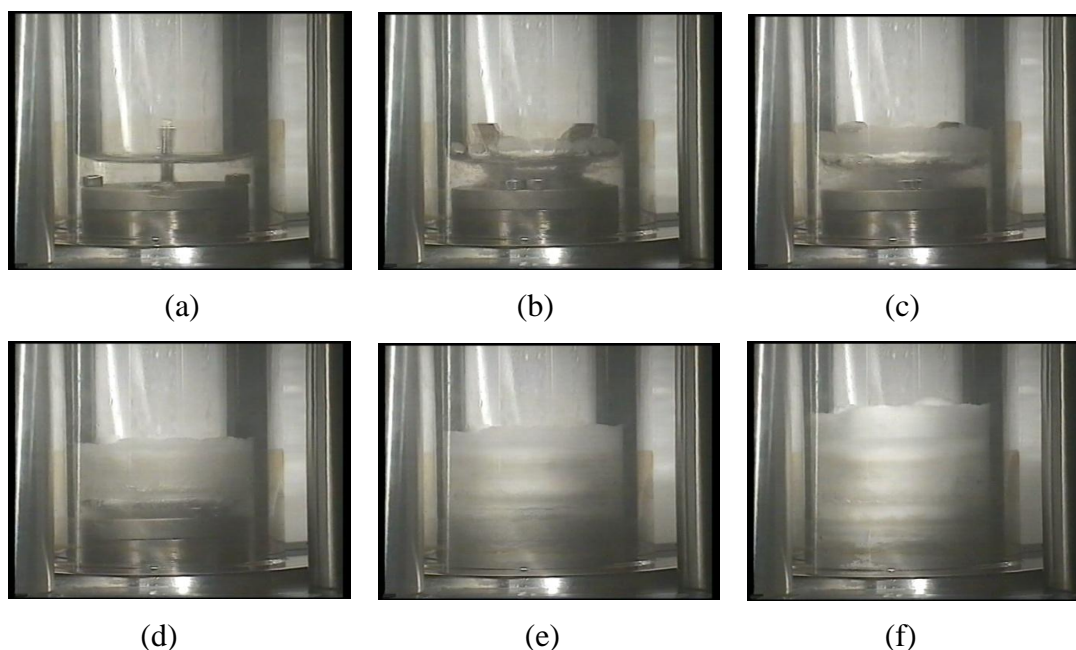
Figure 3.19: Captured images of hydrates formed by BDHC

3.5 Conclusions

This study has successfully established the ability of corrosion inhibitors to generally promote hydrate formation along the deepwater gas pipelines. This has strong consequences on flow assurance policy of the industry through creation of one problem while solving the other. It has further established that the inhibitors promote the hydrate at different rates probably based on their structural distributions, active functional groups and affinity for water molecules which eventually impact on their hydrogen bonding properties and electronegativity. Based on the experimental results, care must be taken in the use of DPC by the industry at deepwater facilities due to its alarming ability to aid the hydrate promotion compared to other inhibitors. Essentially, this study has brought a new focus to corrosion-hydrate relationship as well as establishes the need for comprehensive investigations along this area of

research interest. Further studies should be conducted on the growth and dissociation rates. Also, other inhibitors with similar structural distribution and active functional groups with DPC should be investigated for any correlation.

4. Hydrate Promotional Behaviour of DPC

4.1 Background

This chapter reports a further study conducted subsequent to the laboratory discoveries reported in chapter three. It was conducted on Dodecylpyridinium Chloride based on its remarkable promotion ability as reported in the chapter three. This further study was carried out on the inhibitor at pressure range of 50 - 150bar and concentration range of 0 - 10,000ppm in order to establish its behaviors under different operating conditions.

4.2 Introduction

DPC is one of the chemicals commonly used in the gas industry to remarkably extend the shelf-life of process equipment through inhibition of carbon-dioxide corrosion (Pandarinathan et al, 2011). It is a cationic surfactant (with a molecular weight of 283.88g/mole and melting point of 66-70°C) that inhibits corrosion by adsorbing onto the active anodic and cathodic sites of the metal, and by forming bilayers, thus, classifying it as a mixed type inhibitor.

DPC adsorbs onto the pipe surface both chemically and physically (Durnie et al, 2005) through electrostatic adsorption and π-electron sharing (Durnie et al, 2003), although, the exact mechanism remains unknown (Likhanova et al, 2010). Where physical adsorption dominates, DPC molecules can associate to form bilayers depending on its concentration and chain length (Fuerstenau and Jia, 2004).

4.2.1 Corrosion Inhibition Mechanism

DPC exhibits mixed type inhibition properties by inhibiting corrosion both at anodic and the cathodic sites (Frignani and Trabanelli, 1999; Saleh, 2006). The important difference between the two sites is that physical adsorption occurs on the anodic sites, while chemical adsorption occurs on the cathodic sites (Likhanova et al, 2010). At anodic sites where iron is dissolved into the solution through electrochemical processes, DPC molecules slow down the dissolving rate through physical adsorption by generating ions with localised adsorption occurring initially, followed by the formation of monolayers and bilayers. The van der Waal forces between the

alkyl chains help to achieve a closely packed film at the metal surface, thus, increasing the inhibition effectiveness.

At the cathodic site however, iron is oxidised. Without the corrosion inhibitor at this site, hydronium ions are adsorbed and hydrogen gas is desorbed. With the presence of the inhibitor however, its pyridinium head, being quite large compared to hydrogen, is able to cover a relatively large area of the steel surface. The pyridinium head bonds to the steel surface through the pi electrons in the aromatic ring and the free electron pair that is present on the nitrogen. The compound then accepts an electron from the metallic surface to achieve electroneutraility.

4.2.2 Factors influencing Inhibition Efficiency

These factors can broadly be distinctly classified into two, which are the operating conditions and material properties. Operating conditions include the operating temperature, pressure, pH, inhibitor concentration, flow rate and CO_2 concentration. These have effects on the corrosion rate of steel.

Also, the internal properties of a corrosion inhibitor determine its effectiveness. These properties include the alkyl chain length, ring size, type of head, bond type, bond strength, contact angle and unit cell structure and parameters. The physical structure of DPC consists of a pyridine head, a twelve long carbon chain and a chloride ion. The twelve-long carbon chain, often called a fatty chain, consists of carbons bonded together by single sigma bonds. The pyridine head is similar to that of benzene molecule, but with a nitrogen ion substituted into the ring (Figure 3.9).

4.2.3 Study Justification

Recent laboratory study by Obanijesu et al (2012a) however revealed that care should be taken in the use of DPC by the gas industry at deepwater facilities due to its ability to aid hydrate promotion compared to other corrosion inhibitors. This behaviour was justified by the presence of the Cl^- and N^+ groups that could react very fast with water molecules due to highly polar and strong hydrogen bonding properties, thus, making it to have higher affinity for water molecules to meet the thermodynamic energy needed for the breaks and formations.

This study was carried out at 50bar, 100bar and 150bar since many offshore transmission and distribution operations are performed around these pressures. These encourage rapid hydrates formation, growth and agglomerate. These pressures are practically justified considering that the Line 300B that ruptured during pressure test in USA on 20th October 2011 was transmitting natural gas at 52.19bar (757psi) (Derbeken, 2011). This 34-inch pipeline runs from Arizona boarder to Milpitas and it is operated by Pacific Gas and Electric Company (PG&E). Typically, natural gas is transported through pipelines at 100bar and above (Mahgerefteh et al, 2011). The gas is transported through interstate pipelines at pressures up to 103.42 bar (1500psi) in order to reduce its volume by about 600 times and propel it through the pipeline (NG, 2011); while a compression of about 200bar (20MPa) is required for its transportation as fuel (Matranga et al, 1992).

4.3 Methodology

4.3.1 Reagent, Materials and Equipment

This study was carried out inside the Cryogenic Sapphire Cell at the Clean Gas Technology Unit of Curtin University, Australia using exactly the same reagents, materials and equipment as explained in chapter 3.3 but with little modifications. The modifications include the use of DPC only for this study and the use of a range of pressures and concentrations. 10000ppm fresh stock of DPC was prepared at CORR_CERT centre of Curtin University and diluted to the required concentration for each experiment. Also, the experiments were conducted at 50bar, 100bar and 150bar, these variations automatically led to more preliminary studies before the commencement of the experiments and other modifications to the experimental procedure are explained below

4.3.2 Preliminary Study

Before the experimentation, HYSYS software was used to investigate the formulated gas phase behaviour at various temperatures ranges for 50bar, 100bar and 150bar respectively (Table 4.1).

This investigation was necessary before the experiment in order to establish if the gas will remain gaseous at a very low temperature and maintain a constant

composition throughout the study since the experiment was to be performed during winter period. At a very low temperature, CO_2 gas can undergo partial condensation to give the gas mixture different composition at different experiment based on the environmental conditions (weather).

Table 4.1: HYSYS prediction on the gas composition's phase behaviour

Temperature (^{O}C)	Pressure (bar)		
	50	100	150
5	Gas	Gas	Gas
0	Gas	Gas	Gas
-5	Gas	Gas	Gas
-10	Gas	Gas	Gas
-15	Gas	Gas	Gas

4.3.3 Experimentation

HYSYS software was used to predict the formation temperature of the gas composition at the chosen pressures for rough formation temperature points for the blank studies in order to save time during the experiment (Figure 4.1).
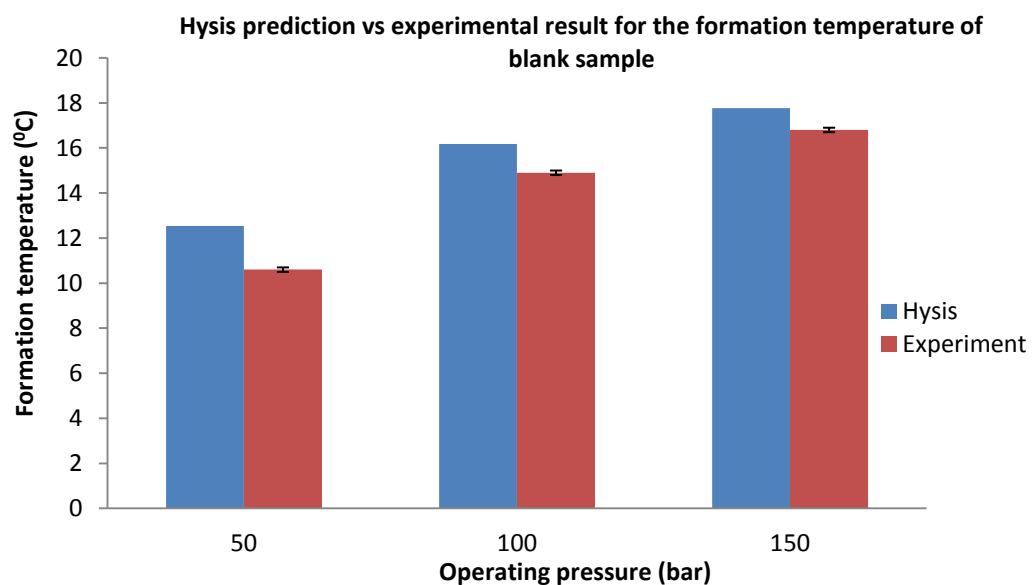
Figure 4.1: HYSYS prediction vs experimental result for the formation temperature at blank concentration.

Blank studies were then carried out experimentally at each of these set pressures to locate the hydrate formation temperature point (Figure 4.1). This was carried out by introducing a specific volume of gas as required by each pressure under study with 5ml of MQ-H$_2$O into the cell before carrying out the experiment. The formed gas/liquid mixture in the cell represents blank mixture. The value from this experiment served as a baseline for the deviation from the experiments to be conducted with the addition of the corrosion inhibitors. Introduced volume at 50, 100 and 150bar were 600ml, 1200ml and 1500ml respectively.

500ppm of DPC was prepared from the 10000ppm stock with a beaker, a pipette and Milli-Q water using the dilution factor calculated as equations (4.1-4.3).

$$M_1V_1 = M_2V_2 \hspace{4cm} \text{Equation 4.1}$$
$$V_2 = \frac{M_1V_1}{M_2} \hspace{4cm} \text{Equation 4.2}$$

Therefore, the required MQ-H$_2$O for dilution V_3 is given as

$$V_3 = V_2 - V_1 \hspace{4cm} \text{Equation 4.3}$$

Where

M_1 is the concentration of the available inhibitor (ppm); M_2 is the concentration of required solution (ppm); V_1 is the volume of inhibitor (ml) and V_2 is the volume of solution (ml).

5ml of the prepared solution was injected into the system through V5 while 1200ml of the gas was compressed in through V9. The newly formed gas/liquid mixture in the cell represents (blank+inhibitor) mixture and the experiment repeated at 100bar until hydrate was formed. This same experimental procedure was repeated three times to ascertain accuracy of the result.

The deviation in temperature T_D for each experiment was calculated as

$$T_D = T_{New} - T_{Blank} \hspace{4cm} \text{Equation 4.4}$$

Where

T_{Blank} is the formation temperature for the blank experiment; T_{New} is the formation temperature for (blank + Inhibitor) experiment.

To ascertain accuracy of the generated experimental data, the blank study was repeated three times while some of the experiments were selected at random for repetition; it was observed that the same results were obtained. . Fluid leakages were also prevented during the experimentations in order to minimize errors; this was done by threading a Teflon tape along the outlet part of each valve and soap tested before starting the experiment. Furthermore, parallax errors were avoided during the preparation of liquid phase solutions by reading the values at the bottom of meniscus. At the concentrations where the cell solution became very foamy before commencement of experiment, the cell was heated to high temperature of $45^{O}C$ to obtain clear solution and clear interphase. The system was then cooled to the reference Temperature of $25^{O}C$ before conducting the experiment.

Also, explosion was avoided through complete venting of the whole system before vacuuming the gas cylinders. This was compulsory noting that, venting the system after completion of each experiment usually left 3bar in the line, which must be totally bleeded before fixing the vacuuming pump to the line. This remaining pressure (3bar) was always bled off by opening all the valves connected to the lines for about 60 seconds. Furthermore, care was taken to prevent hydrate blockage along the manifold line as this usually leads to pressure drop in the cell. This was experienced two times during the experiments and they have to be repeated for certainty. Whenever hydrate blocked the line, the sensors along the line would no longer receive data from the pump, thus, preventing data transmission to the sensors in the cell. If this should occur in the industry, explosion is inevitable as the line operator would have been reading low pressure as generated by the system and his efforts to increase the pressure to 'normal' operating pressure would result into over-pressurization.

Due to all these precautions, the statistical analysis on the generated data gave the maximum experimental error of 1.823%; this clearly showed that the data obtained were accurate within the limits of experimental errors since the probability limit (confidence level) is above 95%.

4.3.4 Concentration Profile

Due to observed high hydrate promotion rate of DPC, a concentration profile was investigated in order to study the inhibitor's behavious at different pressures and

concentrations. First, concentration profile for the inhibitor at 50 bar was developed. This was carried out by introducing a solution of (blank+inhibitor) at a required concentration prepared using Equations 4.1 – 4.3 into the Sapphire cell and the experiment was carried out. The considered concentrations of 1000ppm, 2000ppm, 3000ppm, 5000ppm and 10000ppm were prepared from the fresh stock each at a time for experimentation. This wide concentration range was used for both academic and industrial applications. Industrially, 200ppm is the maximum applied concentration due to cost implication on operation; however, it is important to academically study the trend at higher concentrations in order to study the possibility of the chemical to serve as hydrate inhibitor at such concentration(s). For each experiment, 5ml of the prepared concentration (in ppm) and 600ml of the fresh gas were fed into the cell and the experiment carried out at 50bar till hydrate is formed. The formation temperature was recorded and the cell cleaned. The experiment was then repeated at 100bar and 150bar for each of these concentration ranges. 1200ml and 1500ml gas volume were introduced into the sapphire cell respectively for the experimentations at 100bar and 150bar. The hydrate formation temperatures were properly recorded and the cell cleaned after each experiment. The complete set of experimental data generated at these three pressures were analysed for the Pressure-Concentration matrix. Many of these experimental conditions were randomly selected for repetition in order to ascertain the accuracy and duplicability of the results.

4.3.5 Location of Critical/Peak Operating Concentration

While the effectiveness of a corrosion inhibitor depends on fluid composition, quantity of water, and flow regime, the quantity of corrosion inhibitor required for gas line is a function of the chemical price, pipe dimension, the length of the pipeline, the desired film thickness, the quantity and the quality of the transported natural gas (Whited, 2003; Schlumberger, 2011). This quantity, which is displaced down the lines between pigs, is estimated by Schlumberger (2011) as

$$V = L * D * 0.0798 * Dft \hspace{4cm} \text{Equation 4.5}$$

Where

V is the vol (l); L is the length (km); Dft is the Desired film thickness (ml)

However, the chemical concentration should play a critical role since this study has established that there is variation in hydrate influence at varying concentration and pressure; hence, the need to establish the critical operating concentration. The critical (or peak) operating concentration is that concentration at which the highest formation temperature is recorded. Hydrate could easily be promoted along the pipeline system at this concentration due to the corrosion inhibitor's influence. Operating at critical concentration should be avoided at all cost due to the safety and economic impacts on the industry. Continual operation at this concentration means that, the industry has to invest in the continual removal of the hydrate blocks within the line in order to prevent full-bore rupture of the pipeline. Since it has been observed through the pressure-concentration matrix that at all pressure, the formation temperature dropped between the concentrations of 500ppm and 1000ppm (Figure 4.7), definitely, the peak could not be within this range. Further studies were carried out to investigate whether the concentration falls between 0ppm (blank) and 500ppm. This was done by carrying out the experiments at the mid-point concentration of 250ppm for the three pressures. The results (Figure 4.2) established that, at all pressures, the influence on formation temperature at 250ppm was higher than both at 0ppm and 500ppm, hence, the conclusion that the critical concentration lies between 0ppm and 500ppm.
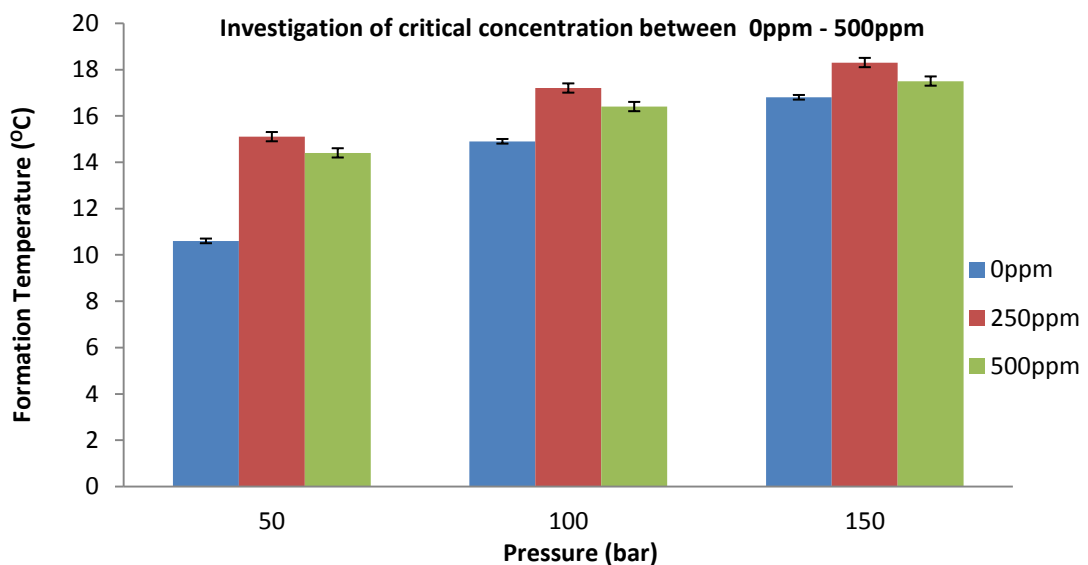
Figure 4.2: Investigation of critical operating concentration of DPC

The experiment was repeated on DPC solutions between the blank (0ppm) and 500ppm at 50ppm interval (0, 50, 100, ..., 450, 500). Each concentration was studied

at a time inside the cryogenic cell at 100bar and the results recorded. The 100bar pressure was selected for this study because, 150bar is very dangerous when considering safety factors, whereas, at 50bar, the hydrate formation temperature was more difficult to locate and the formed hydrate grew too slowly for recognition.

4.4 Results and Discussions

4.4.1 Hydrate Formation Ability

At all inhibitor concentrations for the three experimented pressures, it was observed that hydrate was always formed at temperatures above those for blank studies; this shows that DPC promotes hydrate formation at all concentrations. This is a negative influence on gas industry since the chemical is introduced into the gas stream to assist in solving a flow assurance problem by minimizing corrosion along the pipeline network; due to this negative influence however, the same pipeline is subject to hydrate formation which is another flow assurance problem. Either way, the outcome will result into loss of product, environmental degradation and other economic losses apart from the political issues depending on the sensitivities of the terrain and neighbouring habitat.

Throughout the experiment, the liquid phase never turned cloudy for all concentrations and pressures until the formation period and hydrate always started to form at the gas (Figure 4.3), the hydrates are very clear and ice-like in colour.

| 1000ppm at 50bar | 2000ppm at 100bar | 3000ppm at 50bar |

         5000ppm at 100bar   10000ppm at 150bar
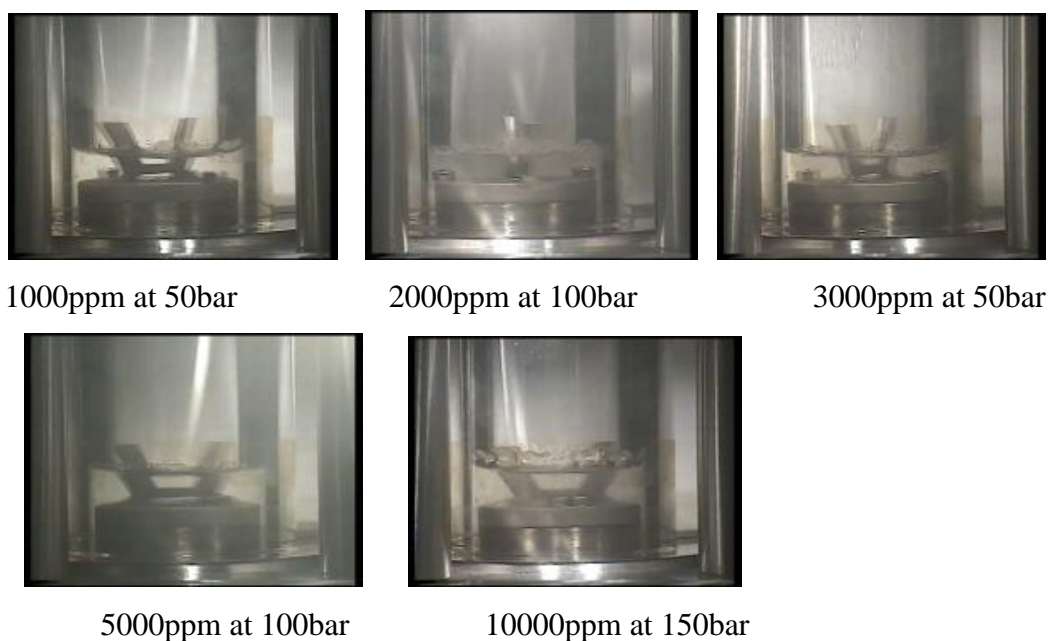
Figure 4.3: Images of hydrates formed at various concentrations and pressures.

The liquid phase takes a long time to completely disappear as the hydrate turned into slurry and built-up very slowly in the glass cell.

It was also observed that the inhibitor was very foamy regardless of the concentration, the foaming ability however reduced with increase in concentration except for 5000ppm (Figure 4.4). Also, the formed hydrate flake at this concentration failed to completely block the glass orifice. Furthermore, unlike other concentrations, the stirrer keeps rotating at 5000ppm even after all the liquid had turned into hydrate. All these showed that 500ppm could be a special concentration to the chemical. After further differential results were obtained at this concentration, it was later believed to be the Critical Micelle Concentration (CMC) for the chemical.

| 1000ppm at 100bar | 2000ppm at 100bar | 3000ppm at 100bar |

| 5000ppm at 100bar | 10000ppm at 100bar |
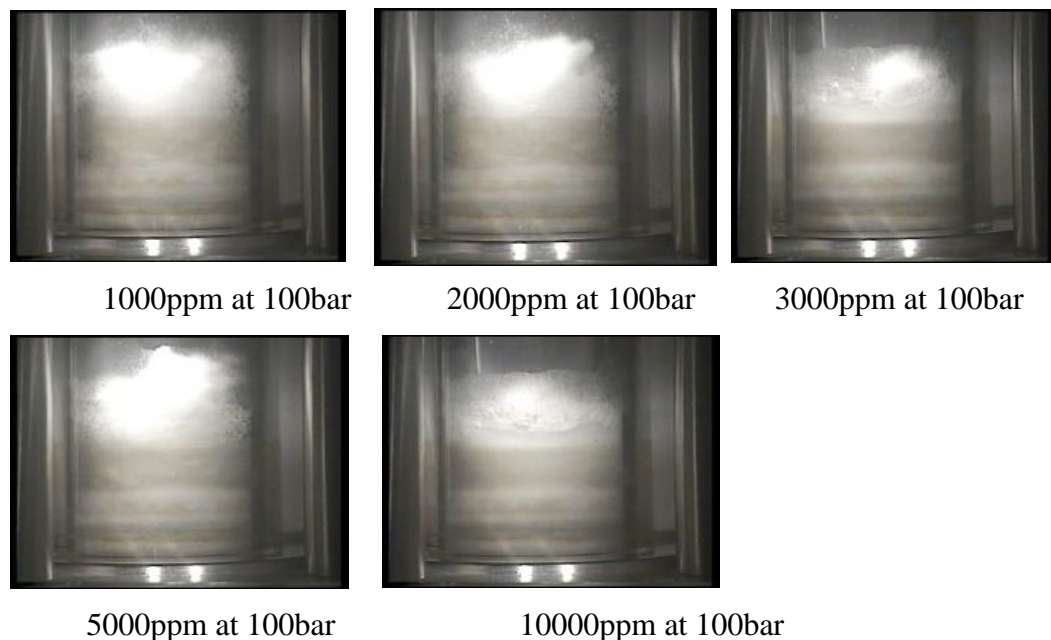
Figure 4.4: Decreasing foaming property with concentration except at 5000ppm

Critical Micelle Concentration (CMC) is that concentration where all the available molecules of a surfactant in solution go into micellization. Micellization is the submicroscopic aggregation of surfactant molecules (DPC for this study) that are dispersed in a liquid colloid. This aggregation is formed at each polar (hydrophilic) end of the molecules that are in direct contact with the surrounding liquid to form micelles, and this leads to sequestration of existing hydrophobic tails within the micelle centre. These polar ends are capable of forming hydrogen bonding. The shape and size of each micelle is determined by the molecular geometry of the

surfactant molecules and the solution conditions such as the pH, temperature, surfactant concentration, and the ionic strength. For any given surfactant, CMC is strongly dependant on temperature, pressure and concentration (Hara et al, 2004; Metha et al, 2005). Surface tension is strongly influenced below CMC but remains relatively constant once CMC is reached. Korotkikh and Kochurova (2006) gave the CMC value for DPC at 20^0C as $1.78*10^{-2}$M and gave those of 25^0C, 30^0C, 35^0C and 40^0C as $1.75*10^{-2}$M, $1.36*10^{-2}$M, $1.97*10^{-2}$M and $2.15*10^{-2}$M respectively.

It was further observed that the inhibitor remained foamy even after the hydrate might have stopped the stirrer from working due to total blockage of the orifice (Figure 4.5).

| Towards blockage | Towards blockage | Towards blockage |

| About to block | Foamy at blockage |
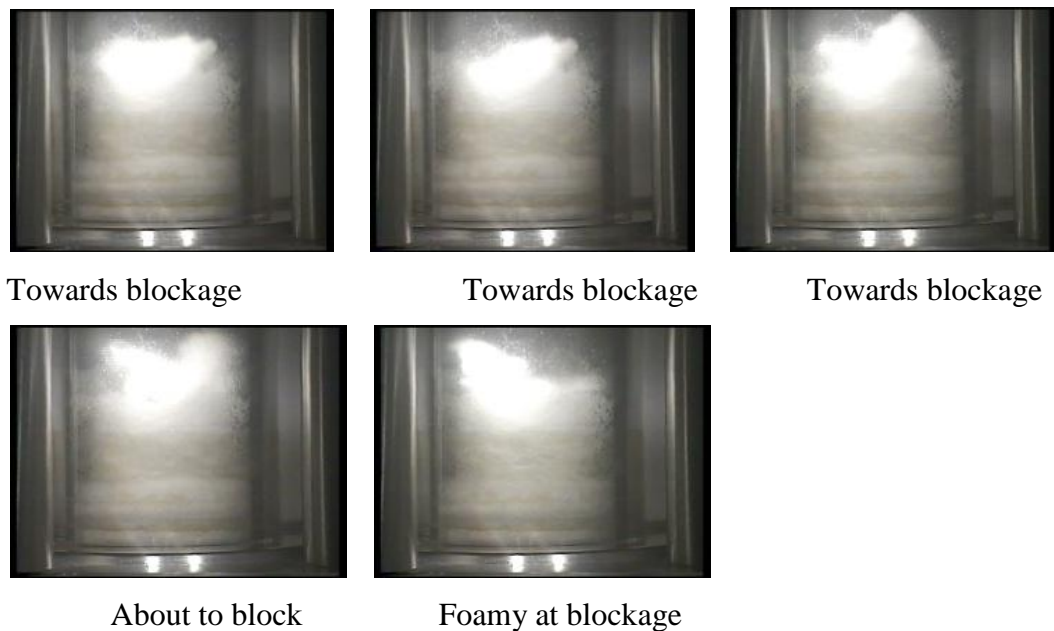
Figure 4.5: Foam growth with time at 3000ppm and 150bar.

At each pressure, it was further observed that the liquid disappearance rate decreased with increase in concentration. At 100bar and 1000ppm for instance, over 80% of the liquid had disappeared within 5 minutes after formation whereas at the same pressure but 5000ppm and 10000ppm, it took 12 and 15 minutes respectively to have this same quantity to disappear. Likewise, the hydrate growth rate followed the same trend. These suggest the possibility of using this chemical to aid the transportation and storage of natural gas in slurry form. This research area was investigated by Gudmundsson and Børrehaug (1996), Javanmardi et al (2004) and Rogers et al (2005) as a means of solving hydrate problems. Recently, Wang et al (2010)

conducted a similar study using tetrahydrofuran, while Delahaye et al (2011) conducted a similar work to study the rhelogical properties of CO_2 hydrate slurry flow using surfactants and antiagglomerants as additives.

For both 100bar and 150bar, the blockage time decreases with increase in concentration. At 100bar for instance, it was observed that at 1000ppm, the stirrer stopped working due to total blockage of the glass orifice at 18minutes after formation time whereas, the stirrer stopped at 28 minutes and 32 minutes respectively for 5000ppm and 10000ppm respectively. This means that at very high concentration, DPC exhibited some hydrate inhibition properties which might make it a useful additive for transporting natural gas at such concentration. This might further support the potential of using the chemical in natural gas transportation in slurry form.

It was further observed that increase in agitation (stirring) rate could prolong the hydrate growth rate. At 150bar as an example, when the rate was very slow, the hydrate was formed at 17.3^OC; however, when the rate was significantly increased, the flocs dissolved into the liquid completely and later started to form again at 16^OC. This might have to do with the combined influences of pressure, temperature, agitation and particle size on the gas solubility which could be explained as follows.

According to kinetic theory, reduction in kinetic energy was experienced by the gas-liquid system as temperature dropped towards the hydrate formation point. This resulted in reduction in the molecules' motion that eventually led to reduction in the rate at which the gas molecules escaped from the solution since there was already a reduction in the rate that the intermolecular bonds broke up. This effectively increased the gas solubility. The gas solubility is further enhanced by the 150bar at which the study is conducted. At this high pressure, Henry's Law is obeyed and the gas molecules are further pushed into the liquid; hence, the initially obtained hydrate formation temperature of 17.3^OC.

When the agitation rate was increased however, the solubility now depended on the particle size. The existing fine hydrate particles had more exposed surface area to the surrounding solvent. The solute (hydrate particles) then dissolved rapidly into the liquid since agitation brought the available fresh solvent into contact with the surface of the solute. As the temperature dropped further to 16^OC, another hydrate formation

temperature was reached based on the new agitation rate. At this point, the hydrate agglomerated and grew to form an 'ice' that blocked the glass orifice.

Agitation and particle size can only affect the solute (hydrate) dissolution rate but cannot influence the saturation point, this phenomenon could further be investigated as related to deepwater natural gas pipeline in order to understand the hydrate growth process.

4.4.2 Specific Observations at Various Operating Pressures

During the experimentation, specific observations were made that were unique to the operating pressures. There were some unique to 50bar while others were unique to the high pressure range of 100bar and 150bar. These are discussed below.

4.4.2.1 Specific observations at 100bar and 150bar

Experiments for all concentrations at 100bar and 150bar followed the same observed trends. At all concentrations, hydrates were generally formed at the interphase and grew along the gaseous phase (Figure 4.6) while the liquid disappeared downward.

   10000ppm and 150bar   10000ppm and 100bar

Figure 4.6: Images showing the hydrate growth in gas phase.

At Initial stage after formation, each time hydrate flocs were formed within the liquid phase, they would quickly rise to the interphase (this hardly happened and required a very good observation to notice); with time however, the flocs started to dissolve in the liquid thus, turning it into slurry and the floc particles became noticeable in the liquor or as the hydrate agglomerated and grew. The growth pattern might have been influenced by concentration and pressure (Figure 4.7).

| 3000ppm and 100bar | 5000ppm and 100 bar | 5000ppm and 150 bar |
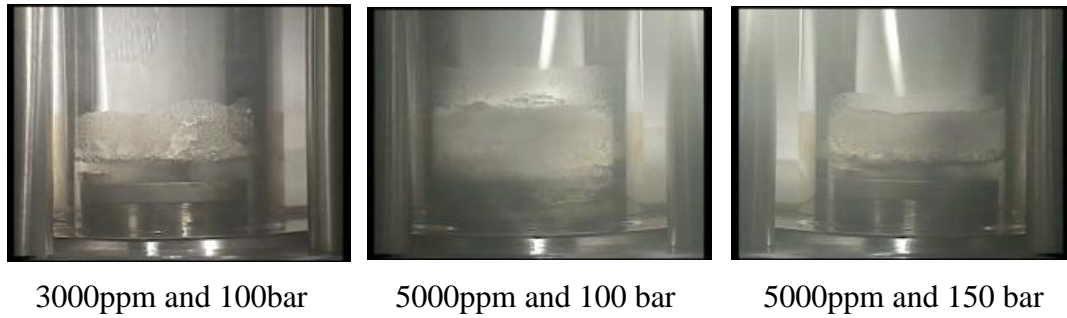
Figure 4.7: Formation of flocs in the liquid phase

As the temperature continued to drop, the hydrate slurry turned into flakes up to about 0.5^OC below the formation temperature. Within this period, the hydrate growth rate was generally slow. At about 0.5^OC below formation temperature however, the temperature started to rise but suddenly dropped sharply while approaching the formation temperature. Within this period, the hydrate growth rate was noticed to increase sharply and completely block the whole glass orifice within a very short period of time at a temperature varying between 0.3^OC and 0.5^OC away from formation temperature. This trend was noticed for all concentrations except for 10000ppm where the temperature dropped to 1^OC below the formation temperature before it started rising again. Again, at 10000ppm for both 100bar and 150bar, it was observed that at some point, the formed hydrate collapsed inside the liquid and started rebuilding and growing until the blockage time (Figure 4.8).

| Initial stage | Collapsed | Rebuilding |
| Growing | Growing | Final growth |
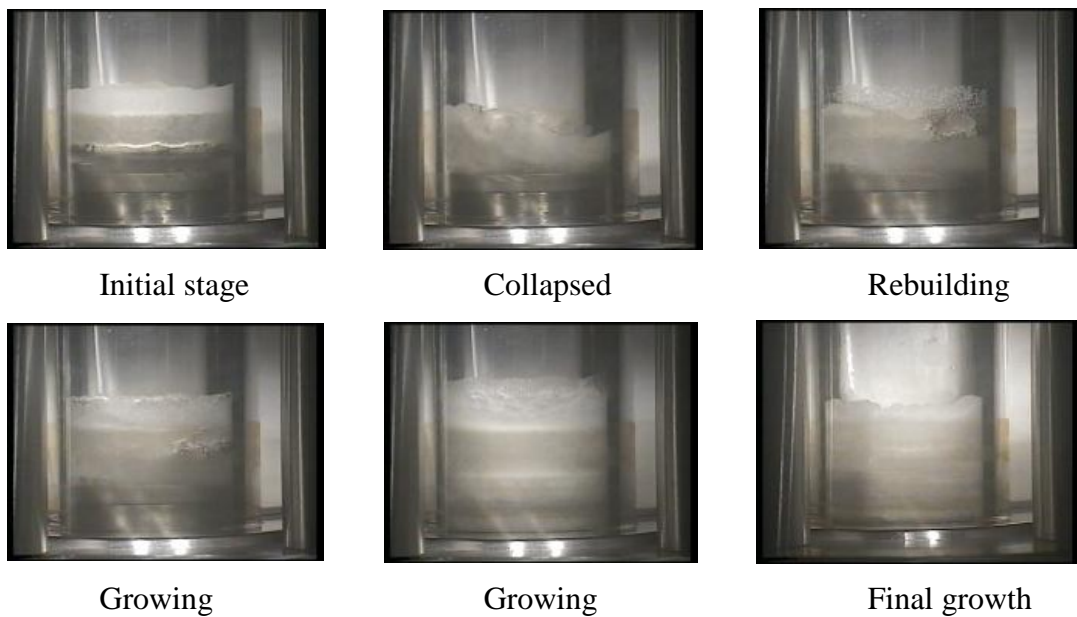
Figure 4.8: The collapsing and rebuilding trend at 100bar and10000ppm

4.4.2.2 Specific observation at 50 bar

At each concentration, hydrates were generally formed at lower temperature compared to those of higher pressures. After formation, the temperature is generally reduced to a very low value compared to those at 100bar and 150bar before the hydrates agglomerate, even despite that, the growth rate is noticed to be very very slow comparatively. This is an indication that hydrate growth rate may be directly proportional to operating pressure. The hydrates, independently formed in bits, formed a 'ring' at various spots and cycle round the glass wall at interphase while growing. At a pressure mostly between 2^OC - 3^OC below the formation temperature, the temperature usually increased sharply due to heat transfer process taking place at this point. This resulted in the hydrates completely filling the glass orifice which in turn blocked the glass and stopped the stirrer within 4-6 minutes.

4.4.3 Concentration Profile

The concentration-pressure matrix study carried out on DPC showed a unique trend at all the pressures (Figure 4.9). From the figure, it is observed that though, at same the concentration but different pressures, the formation temperature was different; however, a look at the results from the three pressures gave a similar 'camel back' structure with that of 100bar more obvious. Generally, the formation temperature increases sharply from 0ppm to 500ppm and then reduced at 500ppm to 2000ppm and then starts to increase at 3000ppm; however, a sharp increase was noted at 5000ppm before a final drop at 10000ppm.

The experiment for 5000ppm was repeated to confirm the noticed sharp increase as against the normal on-going reduction trend and the same result was obtained. This increase may be due to the effect of change in the hydrate formation rate beyond the critical micelles concentration (CMC). According to Zhong and Rogers (2000), at a concentration above its CMC, the formation rate of gas hydrate in a static system increases in multiple times (over 700).
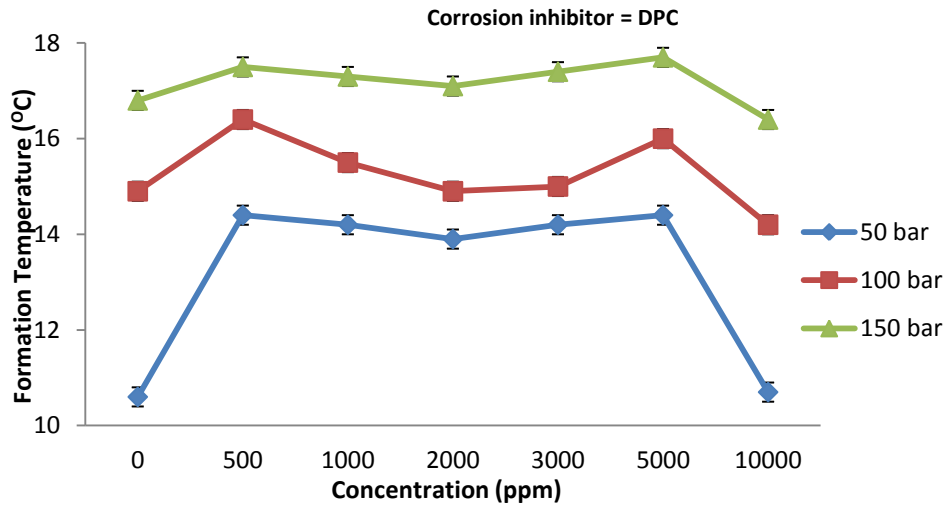
Figure 4.9: Concentration–pressure matrix showing similar structure at all pressures.

4.4.4 Critical Operating Concentration

Because of the very significant saddled structure observed at 100bar, this pressure was used to further investigate the trend in relationship between concentration and formation temperature in the concentration range of 0-500ppm. From Figure 4.10, it could be proposed that the critical operating concentration for DPC at 100bar is 200ppm. This result suggests that the gas industry should avoid the use of this chemical around this concentration for the deepwater pipeline in order to prevent hydrate promotion. All points close to this value may have the same effect which could easily lead to full bore rupture and the subsequent consequences.
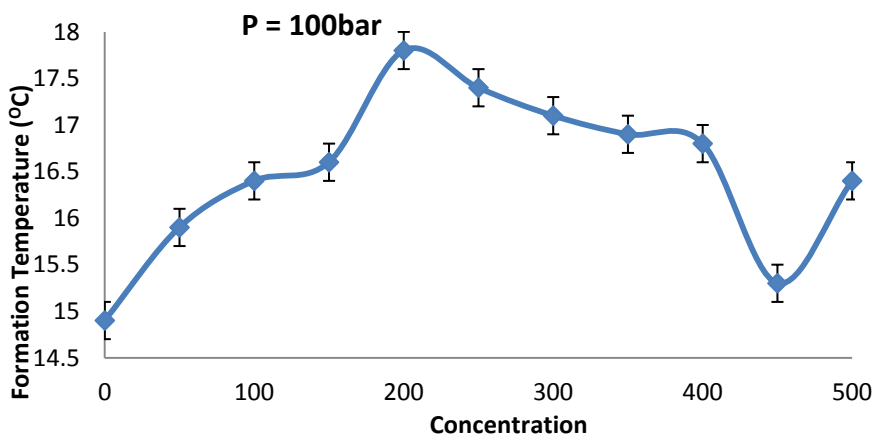
Figure 4.10: Result establishing the peak concentration for CPC as 200ppm.

4.4.5 Pressure Effect on Formation Temperature Point

The pressure effect on formation temperature was studied from two angles. First, the pressure effect on the hydrate promotion ability of corrosion inhibitors was studied and noted to reduce with increase in operating pressure. As an example, analysing the generated data between the blank (0ppm) and 500ppm at different pressures showed that while the difference in formation temperature (deviation value) at 50bar is $3.8^{o}C$, it is $1.5^{o}C$ and $0.7^{o}C$ at 100bar and 150bar respectively. Also, this study showed that at any concentration, the hydrate formation temperature increases with operating pressure (Figure 4.11). This perfectly agreed with the scientifically established findings (Ganji et al, 2007; Palmer and King, 2008; Moraveji et al, 2010).
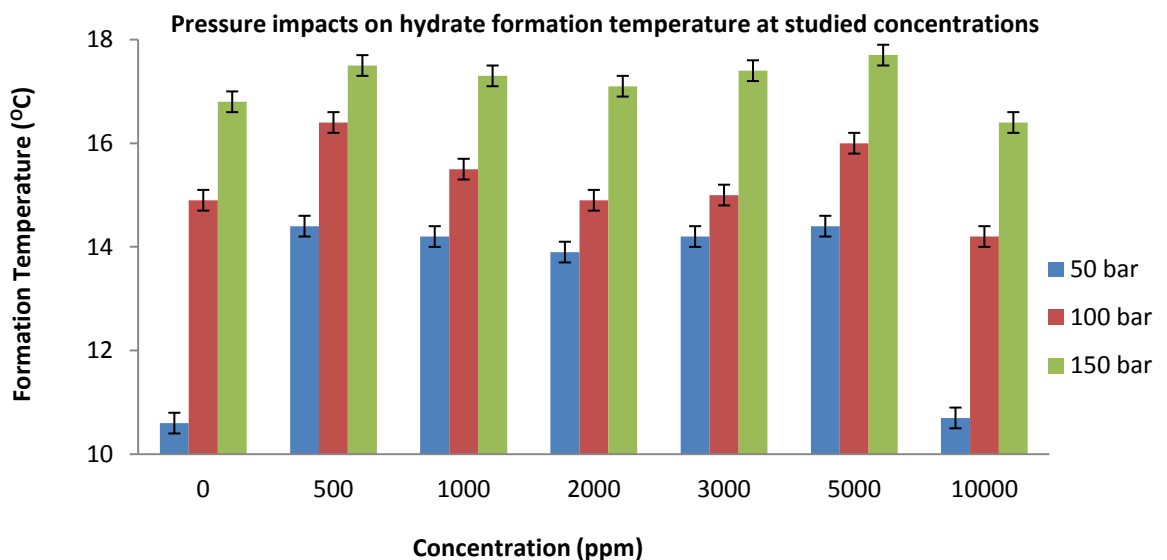
Figure 4.11: Pressure impacts on formation temperature at studied concentrations.

4.5 Conclusions

This study has shown that care should be taken in the use of DPC as corrosion inhibitor at deepwater gas facilities due to its significant ability to aid hydrate promotion. The resulting hydrates from this influence were very foamy at all investigated concentrations and pressures. This specifically showed that some surfactant properties of the chemical were highly influential at all stages of the hydrate formation. It was observed however that this foaming ability decreased with concentration except at 5000ppm where anomalous behaviour was generally observed probably due to the CMC influence. The combined influence of pressure,

temperature, agitation and particle size were noticed on hydrate solubility. At all the investigated pressures, it was also realized that DPC prolonged the complete blockage of the glass orifice at 10000ppm. This special characteristic may suggest the potentiality in applying the chemical as an additive for natural gas transportation and storage in slurry form. Besides, it may further suggest the possibilities of using the chemical as corrosion and hydrate inhibitor along offshore gas pipeline at very high concentrations. Though the usage as both the corrosion and hydrate inhibitor could be expensive, it could be cost effective since it would serve a dual purpose and there would be no further need to add another hydrate inhibitor.

Finally, this study has further confirmed the need to investigate the hydrate formation ability of the corrosion inhibitors that are used along the deepwater natural gas pipeline.

5. Hydrate-Corrosion Model: Development and Simulation

5.1 Background

Chapters 3 and 4 have established the ability of corrosion inhibitors to aid in the promotion of gas hydrate within the offshore natural gas pipelines. Considering Chapter 2.6 that suggested that gas hydrates can initiate internal corrosion along the same pipelength with time, it is then necessary to consider measures to handle this possibility. Preventive and corrective options are the only available options. The preventive options are always better since they are easy to control with no future repercussions. This chapter considered development of a predictive model as a preventive measure.

5.2 Introduction

Hydrate formation along a long natural gas pipeline has been established as a potential initiator of different types of internal corrosion along the pipe-length based on the formation stage and point (Obanijesu et al, 2011b). These corrosions may lead to disintegration of the pipe's properties and eventually result into the pipe's leakage or full-bore rupture. Apart from the enormous economic implications on the operating company, the conveyed fluid upon escape to the environment poses the risk of fire, reduction of air quality and other health hazards.

This work theoretically developed an empirical model on natural gas corrosion rate with gas hydrate as the corroding agent. The model considered carbon steel pipelines (with iron as alloyed metal) conveying natural gas at different temperatures, pHs, fugacities and wall shear stresses and is based on turbulent flow (Re › 2300), closed system and homogenous phase conditions. This model, with emphasis laid on the thermodynamic properties of the gas composition is a preventive model which will enable prediction of the pipe's shelf-life.

5.3 Existing Corrosion Rate Monitoring Methods

In recognition of the dangers posed by corrosion to gas pipeline, various methods have been proposed by scientists to minimize its occurrence. These methods can broadly be classified as preventive and corrective measures and many of them are

presently in use in the industry while several studies are still going on globally for improvement. One of the corrective techniques is the use of on-line electrical resistance (ER) probes for instantaneous corrosion velocity readings (Huang and Ji, 2008; Saravanan et al, 2009). These readings are linked to computer software systems over a determined period to establish an accurate corrosion rate. This method allows for a continuous monitoring without multiple exposures to transferred fluid. However, it is subject to fouling and may not read pitting corrosion (Pickthall et al, 2011). Also, this method has a slow reaction time and there is a need to obtain a balance between the sensitivity and the probe lifespan.

Pigging is another corrective method commonly used in the pipeline industry. A pig is used to scrape off the corroded surface of the inner portion of hydrocarbon transporting pipeline but eventually reduces the pipe's thickness. Guided wave corrosion detection (Konstantinidis et al, 2006; Clarke et al, 2010; Croxford et al., 2010) could have been a valid substitute for smart pigging considering the recent advances in the technology which makes it more reliable on unpiggable process lines, road crossing and overhead (gantry lines). It however has an accuracy of location detection problem among others (ETF, 2011). Also, it is only applicable in buried lines but not on a subsea line where the probes are exposed.

Predictive model development is a preventive measure. It predicts the likely shelf-life of the pipe for the industrial use on planning the replacement time. Both the CO_2 corrosion (sweet corrosion) and H_2S corrosion (sour corrosion) are major concern in the application of carbon and low alloy steels which are still the principal construction materials offering economy, availability and strength (Nesic et al, 2004). In practice, localized corrosion is the most dangerous mode of attack and can result in serious failures, hence, the need to predict the occurrence. Localized corrosion of metals is stochastic in nature (Williams et al, 1985, Bertocci et al, 1986; Gabrielli et al, 1990; Wu et al, 1997; Frankel and Sridhar, 2008; Caleyo et al, 2009; di Caprio et al, 2011) and it is believed to relate to two stochastic processes: the breakdown of the passive film and repassivation of the exposed area (Bettocci et al, 1986; Hashimoto et al, 1992; Stockert and Bohni, 1989; Pistdrius and Burstien, 1992; Gabrielli and Keddam, 1992; Pujar et al, 2007; Estupinan-Lopez et al, 2011; Montesperelli and Gusmani, 2011). The probabilistic characters of localized attack make a stochastic approach to its study attractive. Gunaltum (1996) proposed a

localized corrosion prediction model, which applies a turbulence factor to general corrosion rate, assuming the flow to be the main parameter initiating localized attack. Schmitt et al (2000) developed a probabilistic model for prediction of flow-induced localized corrosion. It is well known however that there are other environmental factors such as pH, temperature, partial pressure of the corroding agent (Sun et al, 2003a) amongst others, causing carbon steel to undergo rapid, localized corrosion and therefore, a model that could predict it should take all these into account.

van Hunnik et al (1996) developed a two-dimensional (2-D) stochastic algorithm to simulate the morphology of localized attack (Equation 4.1). The rule-based algorithm operated on the assumption that the morphology of corrosion attack depended on the balance of two processes: corrosion (leading to metal loss) and precipitation (leading to metal protection). This balance was effectively quantified using a single parameter: the scaling tendency ST:

$$ST = \frac{R_{FeCO_3}}{CR}$$ Equation 5.1

Where

R_{FeCO_3} is the precipitation rate of iron carbonate (mm/yr) and CR is the corrosion rate (mm/yr)

The algorithm produced a wide range of acceptable corrosion surface morphologies. Though, there was not much physico-chemical contents built into the algorithm, the appearance of the 2-D corroded surface, including the one with localized attack was rather similar to what is seen in Scanning Electron Microscope (SEM) images of corroded steel samples (Plates 5.1 and 5.2).

However, the model's strength (the requirement of only one input: the ST) turns out to be its weakness since knowing the ST was not straight forward. ST depends on both the precipitation rate and corrosion rate, and neither is easy to predict as they depend on many other factors including water chemistry, steel composition, surface electrochemistry and transport of species in the solution.
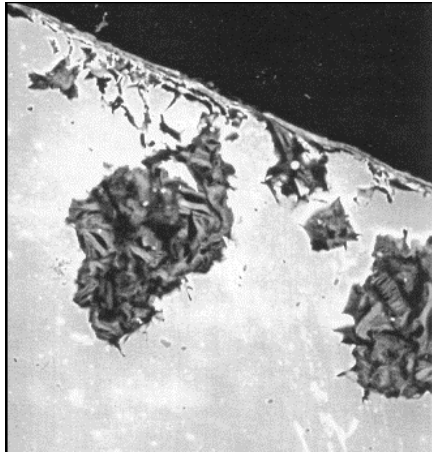
Figure 5.1: SEM image of the corroded steel surfaces taken from the study of CO_2 corrosion in multiphase flow (Nesic et al, 2004)
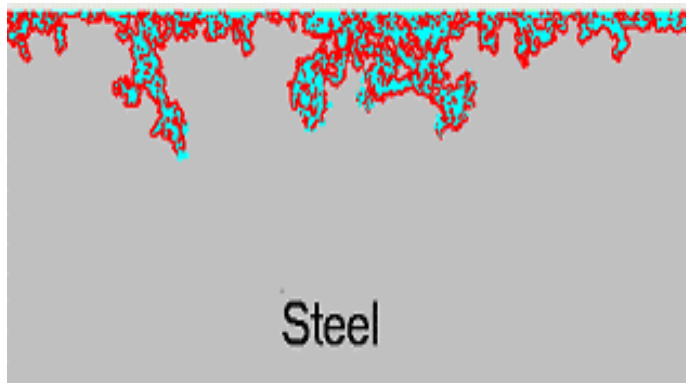
Figure 5.2: Simulated metal surface morphology following moderate precipitation leading to a partially protective film and localized corrosion. ST = 0.53 (Nesic et al, 2004)

Nesic et al (2004) modified the van Hunnik et al (1996) to enable simulation of a broader variety of localized corrosion morphologies found in practice. The 2-D algorithm, which used ST as the only input parameter was connected with the 1-D mechanistic model of CO_2 corrosion so that the morphology of localized attack can be predicted as a function of primitive parameters such as temperature, pH, partial pressure of CO_2, velocity, etc. The model which was on uniform corrosion, stretched from the steel surface though the pores of a surface film and mass transfer boundary layer, ending in the turbulence bulk of the solution. The concentration of each species was governed by a species conservation (mass balance) equation. The model equation was finally presented as

$$\frac{\partial(\varepsilon C_j)}{\partial t} = \frac{\partial}{\partial x}\left(\varepsilon^{1.5} D_j^{eff} \frac{\partial C_j}{\partial x}\right) + \varepsilon R_j \qquad\qquad \text{Equation 5.2}$$

Where

$\dfrac{\partial(\varepsilon C_j)}{\partial t}$ is the accumulation term; $\dfrac{\partial}{\partial x}\left(\varepsilon^{1.5} D_j^{eff} \dfrac{\partial C_j}{\partial x}\right)$ is the net flux; εR_j is the

source or sink due to chemical reaction; C_j is the concentration of species j

(kmol/m^3); ε is the porosity of the film; D_j^{eff} is the Effective diffusion coefficient

of species j (which include both the molecular and the turbulent components, m^2/s);

R_j is the source or sink of species j due to all the chemical reactions in which the

particular species is involved, kmolm^{-3}s^{-1}); t is the time, (s) and x is the spatial

coordinate (m).

Based on the results of its simulation, the model postulated that partially protective films were all that was needed to trigger localized attack; this was in agreement with the experimental study of Sun et al (2003a). The shortcoming in the model was the neglect of electromigration component in the transport equation. An assumption that its contribution to the overall flux of species was small as the cumulative contribution from various species could be significant. Also, turbulent convention was replaced with turbulent diffusion as the former was difficult to determine explicitly in turbulent flow. This will however affect the final output of the model. Further improvement and adjustment on this model was reported through Xiao and Nesic (2005).

Song et al (2007) developed a micro-mechanics based corrosion model to predict the service life of reinforced concrete (RC) structure. The corrosion model consisted of a chloride penetration model (Equation 5.3) to evaluate the initiation of corrosion, an electric corrosion cell model (Equation 5.4) and an oxygen diffusion model to evaluate the rate and the accumulated amounts of corrosion products (Equation 5.5).

$$\alpha_i \frac{\partial C_{Cl}}{\partial t} + div J_{Cl} + Q_{Cl} = 0 \qquad\qquad \text{Equation 5.3}$$

Where

α_i is the specific capacity; C_{Cl} is the amount or concentration of chlorine ions; J_{Cl} is the diffusion flux of chloride ions; Q_{Cl} is the sink term and t is the time.

$$R_{Corr} = \phi S \frac{M_{Fe} i_{corr}}{Z_{Fe} F} (kgm^{-2}s^{-1})$$

Equation 5.4

Where

ϕ is Porosity of the porous media; S is the Saturation; M_{Fe} is the Molecular weight of iron; i_{corr} is Corrosion current density; Z_{Fe} is Number of electric charge of iron and F is the Faraday number.

$$\frac{\partial}{\partial t} \left\{ \phi \left[(1-S)\rho_{gO_2} + S\rho_{dO_2} \right] \right\} + div J_{O_2} - Q_{O_2} = 0$$

Equation 5.5

Where

ϕ is the Porosity of the porous media; S is the Degree of saturation of the porous media; ρ_{gO_2} is the Density of dissolved O_2 in pore water (kg/m^3); ρ_{dO_2} is the Density of gaseous O_2 (kg/m^3); J_{O_2} is the Total flux of dissolved and gaseous O_2 (kg/m^2.s); Q_{O_2} is the Sink term that represents the rate of consumption due to corrosion (kg/m^{3}s) and t is the Time (s).

A corrosion cracking model (Equation 5.6) was then combined with the three models to evaluate the critical amount of corrosion product required for initiating cracking in covered concrete. By implementing the model into a finite element analysis program, a time and space dependent corrosion analysis and a service life prediction of RC structures due to chloride attack are simulated.

$$W_{rust} = W_{Crit} = \pi D \frac{\rho_{st}\rho_{rust}}{\rho_{st} - \kappa\rho_{st}} \left\{ [d_o - d_s] \right\}$$

Equation 5.6

Where

W_{rust} is the Accumulated corrosion amount; W_{Crit} is the Critical amount of corrosion products; ρ_{st} is the Density of steel; ρ_{rust} is the Density of rust; d_o is the Original

diameter; d_s is the Displaced steel (i.e. diameter of displacement) and D is the Material thickness.

Classifying deterioration process due to corrosion into initiation period, propagation period, acceleration period and deterioration period with service life defined as the time for the corrosion initiation, the model predicted corrosion rate of a pipe at submerged zone exposed to marine environment over a period of ten (10) years. The model, however, could have overestimated the chloride content to be penetrated into the RC structure, hence, underestimated the service life of the concrete structure.

Development of refined corrosion wastage models is another interesting aspect in corrosion science. This is so since the quality of any analysis on collapse and reliability depends to a large degree on corrosion model. Southwell et al (1979) proposed linear and bilinear models for corrosion wastage that were considered appropriate for design purposes while Melchers (2001) suggested a steady state trilinear and another power function for corrosion wastage. Yamamoto and Ikegami (1998) proposed a three-stage corrosion model based on analysis data collected from plate thickness measurements. Soares and Garbatov (1999) proposed a non-linear model that described the growth of corrosion wastage in three phases: durability of coating, transition to visibly obvious corrosion with an exponential growth, and the progress and leveling of such corrosion. Sun et al (2001) and Sun and Yong (2003) used the same mathematical formulation of Soares and Garbatov (1999) to describe the corrosion rate instead of corrosion wastage. Qin and Cui (2002) assumed that the corrosion rate is defined by equating the volume of pitting corrosion to uniform corrosion. The corrosion model of Paik et al (2003) also categorized the corrosion behaviour into three phases. The model of Ivanov et al (2003) assumed that the transition phase of non-linear thickness reduction increases with time by a linear relation. A different probabilistic model was developed by Melchers (2003a) which divided the corrosion process into four stages: initial corrosion, oxygen diffusion controlled by corrosion products and micro-organic growth, aerobic activity with limited food supply, and anaerobic activity. Wang et al (2003) collected a very large databank of measurements of thickness of ships to derive regression relations of corrosion wastage as a function of time that provides a consistent fitting to the collected data. Garbatov et al (2005) use the model of Soares and Garbatov (1999) to

fit the data from Wang et al (2003) and found that the nonlinear model represents the data very well. Though, all the above mentioned models derive the duration of the coating system, or in a broader sense, the time to initiation of the corrosion process, they all assumed time as a unique parameter and defined various corrosion phases but none of them accounted for the influences of the contributing environmental factors.

To improve on these models, Soares et al (2005) studied the effects of different marine environmental factors as being identified by Melchers (2003b and 2003c) on the corrosion behavior of steel plated totally immersed in salt water. They proposed a new corrosion model based on a nonlinear time-dependent function. The model accounted for the effects of various environmental factors, including salinity, temperature, dissolved oxygen, pH and flow velocity. During the model development, influences of salt content, temperature, dissolved oxygen, pH water velocity and coating breakdown as given in Equations 5.7 - 5.12 respectively were considered

$$f(S_r) = \frac{\gamma}{\varepsilon(2\pi)^{\frac{1}{2}}(S_r + \delta)} \exp\left[-\frac{\ln(S_r + \delta) - \beta^2}{2\varepsilon^2}\right]$$

$$S \geq 0$$

Equation 5.7

Where

$f(S_r)$ is the Corrosion rate correction factor for salinity (Corrosion rate at actual salinity/Corrosion rate at nominal condition); S_r is the Salinity ratio (Actual salinity/nominal salinity); γ is the A constant introduced as a magnification factor $(\gamma \geq 0)$; δ is the a constant introduced to adjust a truncated portion $(\delta \geq 0)$; β is a constant corresponding to mean value of the distribution and ε is a constant corresponding to the standard deviation of the distribution.

$$f(T_r) = cT_r + d$$

Equation 5.8

Where

$f(T_r)$ is Corrosion rate correction factor for temperature (Corrosion rate at actual temperature/Corrosion rate at nominal temperature); T_r is the Temperature ratio

(Actual temp/nominal temp); c is a constant representing the slope of the $f(T_r) - T_r$ relationship and d is the The constant representing the $f(T_r)$ value at zero T_r

$$\ln(O_2) = A_1 + A_2\left(\frac{100}{T}\right) + A_3 \ln\left(\frac{T}{100}\right) + A_4\left(\frac{T}{100}\right) + S\left[B_1 + B_2\left(\frac{T}{100}\right) + B_3\left(\frac{T}{100}\right)^2\right]$$

(ml/L)   Equation 5.9

Where

T is the Temperature (^{O}K); S is the Salinity {Part per thousand ($\%_{oo}$)}; and A_1, A_2, A_3, A_4, B_1, B_2, B_3 are Constants to be found in Kester (1975)

$$f(pH) = k10^{-(npH)}$$ Equation 5.10

Where

$$f(pH) = \frac{Corrosion \text{ rate correction factor for pH (corrosion rate at actual pH)}}{Corrosion \text{ } rate \text{ } at \text{ } nominal \text{ } pH}$$

k, n = Constants

$$f(V_r) = \lambda\left[1 - \exp\frac{v + \theta}{1 + \theta}\ln\left(1 - \frac{1}{\lambda}\right)\right]$$ Equation 5.11

Where

$f(V_r)$ is the Corrosion rate correction factor for velocity; V_r is the Velocity ratio; λ is the Magnification factor $(\lambda \geq 0)$; v is the Velocity and θ is an introduced constant to adjust the truncated portion of the distribution $(\theta \geq 0)$

$$SR = 1 - e^{\frac{-t}{\tau_o}}$$ Equation 5.12

Where

SR is the Saturation ratio; τ_o is the Constant controlling the slope at (t=0) and $\frac{1}{\tau_o}$ is the Slope at t=0

Equations 5.7 – 5.12 were synchronized to give a model on a long term effect of the environmental factors as

124

$$d_L(t) = \sum_{i=1}^{n} P_i d_{c,i}(t) = \sum_{i=1}^{n} f_{i,j} d_{n,j}(t)$$

Equation 5.13

Where

P_i is the Weighting factor representing the relative duration of the ith stationary period along the lifetime of material; and $d_{c,i}$ is the short-term corrosion wastage of the ith period.

This model has an advantage over most others because instead of providing only the average corrosion wastage, it also provided information about how the corrosion changed with respect to the associated environmental factors. However, the model was too cumbersome to solve.

Also, further studies have shown that metals could be corroded through microbial activities (Geesey, 1991; Schwermer et al, 2008; Little and Lee, 2009). It was discovered that patchy bacterial colonies could enhance corrosion by formation of differential aeration cells. The possible oxygen depletion at the metal surface in the areas covered with biofilms, combined with a higher oxygen concentration in the zones exposed to bulk aqueous phase, may create differential aeration cell which could lead to intensification of local corrosion rate under the biofilm. Moreover, anaerobic bacteria could later colonize the biofilm, producing corrosion substances like acids (Videla, 1996). Picioreanu and Loosdrecht (2002) developed a three-dimensional mathematical model to investigate interactions between aerobic biofilms and a metal surface, and to clarify conditions under which the onset of localized corrosion caused by anaerobic microorganisms is likely to occur. The model includes transport of seven chemical species (O_2, Fe^{2+}, Fe^{3+}, HO^-, H^+, Na^+ and Cl^-) by diffusion and migration, electrochemical reactions at the metal surface, and homogenous reaction in solution. Material balances for a small liquid volume element were developed for all the seven chemical species as

$$D_i \nabla^2 C_i^2 + D_i \frac{Z_i F}{RT} \nabla(C_i \nabla \Phi) + \sum_{j=1}^{I} S_{i,j} r_j = 0$$

$$i = 1, 2, 3 \dots \dots 7$$

Equation 5.14

Where

Φ is the Electric potential (V); D_i is the Diffusion coefficient ($m^2 s^{-1}$); Z_i is the charge (e^-/mol); F is the Faraday constant (96487 C/e^-); R is the Universal constant ($Jmol^{-1}k^{-1}$); $S_{i,j}$ is the Stoichiometric coefficient of species i in the jth homogenous reaction; r_j is the Rate ($molm^{-3}s^{-1}$) and ∇ is the Divergence operator written in 3-D Cartesian coordinates.

The system was solved using classical Newton-Raphson procedure and Jacobian matrix computed with the symbolic package from MATLAB. The model results show that the degree of metal coverage with bacteria significantly influences the heterogeneity of the corrosion pattern. The results equally show that in certain region of the parameter space, formation of differential aeration cells leads to localized enhancement of corrosion under biofilm colonies, although the average corrosion rate decreases by decreasing oxygen concentration. The model however assumed amongst others, a steady-state operation, isothermal system and that physical parameters (e.g. diffusion coefficient) were constant, which are not likely to be accomplished in real-life situation.

5.4 Hydrate Corrosion Rate Modeling

Of the entire existing corrosion model, none has focus on developing a model on hydrate-corrosion relationship. In actual fact, there was no known existing literature identifying the possibility of hydrate chips to initiate corrosion along the natural gas pipeline till 2010 when a paper was presented on this area by Obanijesu et al (2010). This chapter develops a predictive model on internal corrosion rate resulting from hydrate formation along the offshore segment of natural gas pipeline. The model is developed based on the Norsok method and application of the thermodynamic properties of the possible hydrate composition. The hydrate composition is based on the recommendation of Abdel-Aal et al (2003) that water is of 90% composition of the hydrate lattice while other components constitute 10%. The other component in this work is taken to be the natural gas composition used in the laboratory as given in Chapter three of this thesis.

5.5 Model Development

From the laboratory studies conducted on the specially prepared 20% CO_2 natural gas composition, it had been deduced from Chapter three that the hydrate formation temperature range from 10°C and 18°C for the operating pressure range 5 Mpa (50 bar) and 15 Mpa (150 bar).

At the operation condition of 5°C ≤ T ≤ 15°C, NORSORK STANDARD (2005) proposed a corrosion rate equation as

$$C_{rt=} K_T * f_T^{0.36} * \left(\frac{S}{19}\right)^{0.146+0.0324(log f_T)} * f(pH)_T \qquad \text{Equation 5.15}$$

K_T is a constant with values at various temperatures given in Table 5.1.

Table 5.1: Constant K_T at different temperatures (NORSORK STANDARD, 2005)

Temperature (°C)	K_T Value (dimensionless)
5	0.42
15	1.59
20	4.762
40	8.927
60	10.695
80	9.949
90	6.250
120	7.770
150	5.203

5.5.1 Calculation of the pH factor ($f(pH)_T$)

The pH factor within this operating temperature range is given as

$$f(pH)_T = 2.0676 - (0.2309 * pH) \qquad \text{Equation 5.16}$$
$$3.5 \le pH \le 4.6$$
Or
$$f(pH)_T = 4.986 - (01.191 * pH) * (0.0708 * pH^2) \qquad \text{Equation 5.17}$$
$$4.6 \le pH \le 6.5$$

5.5.2 Calculation of the Wall Shear Stress (S)

Wall shear stress is a parameter to be accounted for when modeling corrosion rate. High shear stress may cause a mesa corrosion attach (Singh and Krishnathasan, 2009; Nyborg, 2010). The wall shear stress is a function of friction factor at the specific temperature (f_T), mixture density (ρ_m) and superficial velocity (U_m). It is given by NORSORK STANDARD (2005) as

$$S = 0.5 * \rho_m * f_T * U_m \qquad \text{Equation 5.18}$$

Where

$$f_T = 0.001375 \left[1 + \left(20000 \frac{k}{D} + 10^6 \frac{\mu_m}{\rho_m U_m D} \right)^{0.33} \right] \qquad \text{Equation 5.19}$$

The mixture density, mixture velocity and mixture viscosity are calculated as

$$\rho_m = \sum \rho_{m_i} = \sum(\rho_L \lambda + \rho_G(1 - \lambda)) \qquad \text{Equation 5.20}$$

$$U_m = \sum U_{m_i} = \sum(U_L^s + U_G^s) \qquad \text{Equation 5.21}$$

$$\mu_m = \sum \mu_{m_i} = \sum(\mu_L \lambda + \mu_G(1 - \lambda)) \qquad \text{Equation 5.22}$$

Where λ is given as

$$\lambda = \frac{Q_L}{Q_L + Q_G} \qquad \text{Equation 5.23}$$

5.5.3 The formation fugacity

Apart from the water molecule, every other molecule in the hydrate is gaseous. However, at high pressure, an ideal gas situation can no longer be assumed, hence, the partial pressure of individual gas should be multiplied by its fugacity constant. The general equation for the fugacity of the multi-component hydrate can be expressed as

$$f = \sum f_i = \sum(a * P_i) \qquad \text{Equation 5.24}$$

The partial pressure P_i is found using

$$P_i = \frac{Mass\ flow\ of\ component\ i\ in\ the\ gas\ stream\ (kmoleh^{-1}) * Total\ pressure}{Total\ mass\ flow\ in\ the\ gas\ phase\ (kmoleh^{-1})} \qquad \text{Equation 5.25}$$

The fugacity coefficient (a) as a function of temperature and pressure is given by Waard et al (1991) as

$$a = 10^{P*(0.0031-\frac{1.4}{T})} \qquad\qquad P \le 250 \ bar \qquad\qquad \text{Equation 5.26}$$

$$a = 10^{2.5*(0.0031-\frac{1.4}{T})} \qquad\qquad P > 250 \ bar \qquad\qquad \text{Equation 5.27}$$

Since a is constant for the system, then,

$$f = \sum f_i = a * \sum(P_i) \qquad\qquad\qquad \text{Equation 5.28}$$

However, Equation (5.26) was applied for this study since most pipeline operations are carried out below 250 bar coupled with the fact that hydrates could even be formed at the pressure as low as 28 bar (Moudrakovski et al, 1999).

5.6 Model Simulation

The composition of the natural gas used for this study is presented in Table 5.2a. For the appropriate simulation of the model as applied to hydrate formation, an assumption of 90% water composition in the total hydrate as given by Abdel-Aal et al (2003) was used to compute Table 5.2b. The computational method is shown in Equation 5.28.

$$X_{GHC} = \frac{Total\ Hydrate - Water\ content}{Total\ Hydrate} * X_{NGC} \qquad\qquad \text{Equation 5.28}$$

Where

X_{GHC} is the Mole fraction of gas X in the hydrate; X_{NGC} is the Mole fraction of gas X in the natural gas stream and Water content is 90%.

5.6.1 Calculation of the Fluid Fugacity

The fugacity of a fluid is given by Smith et al (2008) as

$$\ln \frac{f}{P} = \frac{\Delta G}{RT} \qquad\qquad\qquad \text{Equation 5.29}$$

Therefore, for a multi-component stream

$$\ln \frac{f_i}{P_i} = \frac{\Delta G_i}{RT} \qquad\qquad\qquad \text{Equation 5.29a}$$

Re-arrangement of this gives

$$f = \Sigma \left(P_i * e^{\left(\frac{\Delta G_i}{RT}\right)} \right)$$

Equation 5.29b

Table 5.2: The hydrate composition used for the study

Component	Natural gas component (mole %) [a]	Hydrate component (mole %) [b]
CH_4	70.90	7.090
C_2H_6	5.00	0.500
C_3H_8	3.00	0.300
n-C_4H_{10}	0.94	0.094
n-C_5H_{12}	0.10	0.010
N_2	0.06	0.006
CO_2	20	2.000
H_2O (l)	--	90.000

[a] Natural gas formulation in use for the on-going laboratory experiments.

[b] Calculated values using Equation 5.28 based on Abdel-Aal et al (2003).

A component's Gibb-free energy is a state property which is expressed as

$$\Delta G_i = \Delta H_i - T\Delta S_i$$

Equation 5.30

Where each component's enthalpy change (ΔH_i) is given as

$$\Delta H_i = \int_{T_o}^{T} C_{p_i} dT$$

Equation 5.31

And ΔS_i, a component's entropy change is expressed as

$$\frac{\Delta S_i}{R} = \int_{T_o}^{T} \frac{C_{p_i}}{R} dT - \ln \frac{P_i}{P_o}$$

Equation 5.32

Equations 5.30 – 5.32 are property related only and completely independent of the process causing the change of state. C_{p_i} is temperature dependent however and expressed as

$$\frac{C_{p_i}}{R} = A_i + B_i T + C_i T^2 + D_i T^{-2}$$

Equation 5.33

Thermodynamically, the temperature dependence of Equation 5.33 allows for the integration of Equation 5.31 and Equation 5.32 to give more simplified equations for the enthalpy change and entropy change respectively as

$$\frac{\Delta H_i}{R} = A_i T_o (\tau - 1) + \frac{B_i}{2} T_o{}^2 (\tau^2 - 1) + \frac{C_i}{3} T_o{}^3 (\tau^3 - 1) + \frac{D_i}{T_o}\left(\frac{\tau - 1}{\tau}\right) \qquad \text{Equation 5.34}$$

$$\frac{\Delta S_i}{R} = A_i ln\tau + \left[B_i T_o + \left(C_i T_o{}^2 + \frac{D_i}{\tau^2 T_o{}^2}\right)\left(\frac{\tau + 1}{2}\right)\right](\tau - 1) - ln\frac{P_i}{P_o} \qquad \text{Equation 5.35}$$

Where

$$\tau = \frac{T}{T_o} \qquad \text{Equation 5.36}$$

A, B, C and D are the characteristics of a particular fluid and are of constant values for specific fluid regardless of operating conditions. Either C or D is zero depending on the fluid. $\frac{C_{p_i}}{R}$ is dimensionless, thus, the unit of C_p depends mainly on the unit of R chosen. The values of A, B, C and D for the gases present in hydrate composition for this study are presented in Table 5.3

5.6.2 Calculation of the wall shear stress

Equations 5.18 to 5.23 are necessary to calculate the wall shear stress. However, ρ_G and ρ_L are respectively given by NS (2005) as

$$\rho_G = \frac{627.1047 * P * \rho_g}{Z * (460 + T_f)} \qquad \text{Equation 5.37}$$

For multi-component fluid therefore,

$$\rho_G = \Sigma \rho_{G_i} = \Sigma \frac{627.1047 * P_i * \rho_{g_i}}{Z_i * (460 + T_f)} \qquad \text{Equation 5.37b}$$

$$\rho_L = \emptyset \rho_w + \rho_G (1 - \lambda) \qquad \text{Equation 5.38}$$

The only liquid for this study is water; therefore, ρ_L is not a multicomponent parameter. The data to calculate the hydrate density are presented in Table 5.4.

Table 5.3: Values of the constants in $\frac{C_{p_i}}{R} = A_i + B_i T + C_i T^2 + D_i T^{-2}$ (Smith et al, 2005)

Component	A	B (10^3)	C (10^6)	D (10^{-5})
CH_4	1.702	9.081	-2.164	0.000
C_2H_6	1.131	19.225	-5.561	0.000
C_3H_8	1.213	28.785	-8.824	0.000
$n\text{-}C_4H_{10}$	1.935	36.915	-11.402	0.000
$n\text{-}C_5H_{12}$	2.464	45.351	-14.111	0.000
N_2	4.982	1.195	0.000	-0.792
CO_2	5.457	1.045	0.000	-1.157
H_2O (l)	8.712	1.250	0.000	-0.180

Table 5.4: Values for the mol. wt, ρ and ρ_g for the hydrate components ([a] TET, 2011a; [b]TET, 2011b)

Component	Molecular wt (Kg/Kmol)	ρ (NTP) (Kg/m^3)	ρ (STP) (Kg/m^3)	ρ_g
CH_4	16.043 [a]	0.668 [a]	0.717 [a]	0.5537 [b]
C_2H_6	30.07 [a]	1.264 [a]		1.0378 [b]
C_3H_8	44.09 [a]	1.882 [a]		1.5219 [b]
$n\text{-}C_4H_{10}$	58.1 [a]	2.489 [a]	2.500 [a]	2.0061 [b]
$n\text{-}C_5H_{12}$				2.487 [b]
N_2	28.02 [a]	1.165 [a]	1.2506 [a]	0.9669 [b]
CO_2	44.01 [a]	1.842 [a]	1.977 [a]	1.5189 [b]
H_2O (l)	18.016 [a]	0.804 [a]	0.804 [a]	

Furthermore, the compressibility factor for each component, Z_i, can be calculated using the Ptizer Correlations for the Second Virial Coefficient given as

$$Z_i = Z_i{}^o + w_i Z_i{}'$$
Equation 5.39

Where

$$Z_i{}^o \text{ and } Z_i{}' = f(T_{r_i}, P_{r_i})$$
Equation 5.40

$$T_{r_i} = \frac{T}{T_{c_i}}$$

Equation 5.41

$$P_{r_i} = \frac{P}{P_{c_i}}$$

Equation 5.42

Thermodynamically for a multi-component system, $Z_i{}^o$ and $Z_i{}'$ can be respectively represented as

$$Z_i{}^o = 1 + B_i{}^o \frac{P_{ri}}{T_{ri}}$$

Equation 5.43

$$Z_i{}' = B_i{}' \frac{P_{ri}}{T_{ri}}$$

Equation 5.44

Where $B_i{}^o$ and $B_i{}'$ are given by

$$B_i{}^o = 0.083 - \frac{0.422}{T_{ri}{}^{1.6}}$$

Equation 5.45

$$B_i{}' = 0.139 - \frac{0.172}{T_{ri}{}^{4.2}}$$

Equation 5.46

Substituting Equations 5.43, 5.44, 5.45 and 5.46 into Equation 5.39 gives

$$Z_i = 1 + \left(0.083 - \frac{0.422}{T_{ri}{}^{1.6}}\right) \frac{P_{ri}}{T_{ri}} + w_i \left(0.139 - \frac{0.172}{T_{ri}{}^{4.2}}\right) \frac{P_{ri}}{T_{ri}}$$

Equation 5.47

Therefore

$$Z = \Sigma Z_i = \Sigma \left\{ 1 + \left(0.083 - \frac{0.422}{T_{ri}{}^{1.6}}\right) \frac{P_{ri}}{T_{ri}} + w_i \left(0.139 - \frac{0.172}{T_{ri}{}^{4.2}}\right) \frac{P_{ri}}{T_{ri}} \right\}$$

Equation 5.48

The required values for w_i, T_{c_i} and P_{c_i} for the hydrate components are presented in Table 5.5.

The associated water in the hydrate is considered incompressible; hence, the liquid superficial velocity is given as

$$U_L{}^S = \frac{Q_L}{A}$$

Equation 5.49

Also, the gas superficial velocity is expressed as

$$U_G{}^S = \left(\frac{Q_G}{A}\right) Z \left(\frac{T}{T_{std}}\right)$$

Equation 5.50

Table 5.5: Corresponding values of w_i, T_{c_i} P_{c_i} for the hydrate components (Smith et al, 2005)

Component	w	T_c (/K)	P_c (/bar)
CH_4	0.012	190.60	45.99
C_2H_6	0.100	305.3	48.72
C_3H_8	0.152	369.8	42.48
$n\text{-}C_4H_{10}$	0.200	425.1	37.96
$n\text{-}C_5H_{12}$	0.252	469.7	33.70
N_2	0.038	126.2	34.00
CO_2	0.224	304.2	73.83
H_2O (l)	0.345	647.1	220.55

μ_w is expressed by Lide (2006) as a function of temperature only as

$$\mu_w = 10^{\left(\frac{1301}{(998.333+8.1855(T-20)+0.00585(T-20)^2)}\right)-1.30233} * 10^{-3} \qquad 0°C \leq T \leq 20°C$$

Equation 5.51

While

$$\mu_w = 1.002 * \left(10^{\left(\frac{1.3272(T-20)-0.001053(T-20)^2}{(T+105)}\right)} * 10^{-3}\right) \qquad 20°C \leq T \leq 100°C$$

Equation 5.52

However, equation 5.51 was considered for this study since the temperature range used for this study is within this region. Also, since the main liquid in the hydrate is water while the other component(s) which might liquefy within this temperature range at a very high pressure are infinitesimal, μ_L is assumed to be equal to μ_w i.e.

$$\mu_L = \mu_w \qquad \qquad \text{Equation 5.53}$$

The gas viscosity (μ) for the hydrate fluid was calculated using the Sutherland's viscosity law with 3-co-efficient (FLUENTS Incorporated, 2001; Roux et al, 2008) expressed as

$$\mu_G = \mu_o \left[\left(\frac{T}{T_o} \right)^{\frac{3}{2}} \frac{T_o + S}{T + S} \right]$$

<div align="right">Equation 5.54</div>

Where

μ is the Viscosity in $Kg/m - s$; μ_o is the a reference value in $Kg/m - s$; T_o is the a reference Temperature (K); T is the static Temperature (K); S is the Effective Temperature also known as Sunderland constant which, is the characteristic of the gas (K).

Other set of data used to evaluate the model's performance include pH, specific gravity, water density and others as stated in Table 5.6. At moderate temperature and pressure, values for the reference points in Equation 5.54 are presented in Table 5.7. Sutherland gave the viscosity law in 1893 from a kinetic theory by using an idealized intermolecular-force potential. The solution flowchart for the simulation is displayed in Appendix A.

Table 5.6: Other parameters used to test the model

Parameter	Value
T_o, Ambient temperature T_o (K)*	298.15
T_o, temperature at zero degree (K)*	273.15
T_{std}, Temperature at standard condition, K (^{o}F)*	288.70 (60)
Operating temperature, T (°C)**	5, 6, 7, 8, ……, 13, 14, 15
Operating pressure (MPa)**	5, 7, 9, 11… 21, 23, 25
P_o Atmospheric pressure (KPa)*	101.33
Typical liquid rate in pipelines, Q_L (m^3/day)***	100
Typical gas rate in pipelines, Q_G (m^3/day)***	10200
pH range****	3.5 - 6.5
D, pipe diameter (inches)***	12, 18, 24, 30, 36, 42, 48
K, Pipe roughness (m)****	50*10^{-6}

Where

* are from Smith et al (2005); ** are assumed based on the experimental results and others factors; *** are typical natural gas flowrate in a pipe (CNL, 2007) and **** are obtained from NORSORK STANDARD (2005).

Table 5.7: The values for Sutherland's reference points (FLUENTS Incorporated, 2001)

Parameter	Value
μ_o	$1.7894 * 10^{-5}$
T_o	273.11
S	110.56

5.7 Result and Discussions

The trend of the results obtained from the model agreed comparatively with various existing predictions models and experimental works.

The effect of temperature and wall shear stress on corrosion rate as predicted by the model at 100bar and pH of 5.0 was presented as Figure 5.3. The Figure showed that the corrosion rate increases with temperature; this perfectly agreed with various existing related experimental and predictive models (Liu and Weyers, 1998; Popova et al, 2003; Chen and Mahadevan, 2008; Nyborg, 2010; Obot and Obi-Egbedi, 2010; NPF 2011a). This could be attributed to the temperature's secondary effects through its influence on the solubility of the corroding agent which is the most common factor influencing corrosion. This further showed that a change in operating temperature would affect many other factors influencing corrosion rate.
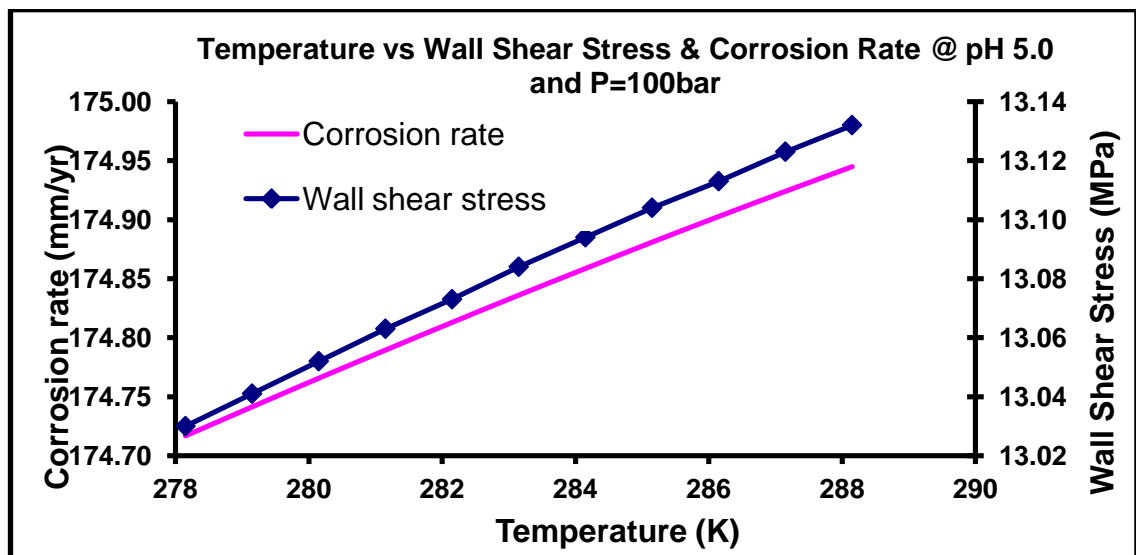
Figure 5.3: Temperature against wall shear tress and corrosion rate at pH=5.0 and 100bar

Specifically, Figure 5.3 showed that within the studied hydrate formation temperature range and 100bar, the minimum corrosion rate for the transportation pipeline is about 175mm/yr (0.48mm/day) while the wall shear stress is also increasing at high rate. This is alarming since at this rate, the pipeline may be subject to permanent failure within weeks due to continuous usage of the pipeline. This is true since hydrate chips will be increasing in size and this will initiate more pitting and crevice corrosions.

Also, the Figure agreed with related studies to show that corrosion rate increases with the wall shear stress (Ahammed and Melchers, 1997; Vlachos et al, 1997; Wharton and Wood, 2004). Corrosion can be accelerated by stress through either residual internal stress in the pipe or externally applied stress (Ginzel and Kanters, 2002; Mochizuki, 2007). Residual stresses are usually produced by deformation during the pipeline fabrication, unequal cooling from high temperature and /or the internal structure arrangements that involve the volume change. The geometrical changes and any obstacles in the flow regime also give rise to higher shear stress. Again, the the different flow regimes and geometrical obstacles may generate flunctuation in shear stress at those points where the shear stress peaks may be considerably higher than the average shear stress.

As the operating pressure increases, the erosion-corrosion rate increases while the velocity loss also increases (Figure 5.4). The obtained pressure-corrosion rate relationship is true considering the thermodynamic properties of hydrate formation (Sarshar et al, 2010). Increasing the operating pressure would lead to increase in velocity along the pipe-length, this would increase agitation in the transport fluid which would aid hydrate formation through turbulence (Moon et al, 2003; Anderson et al, 2007; Wenji et al, 2009). At choke also, temperature drop will be experienced through Joule Thompson effects to further promote the formation (Harun and Watt, 2009) while the presence of welded spots (elbows, tee, etc), dirt, scales, slits and sands along the pipe will make good nucleation sites and the available free-water will be an enhancer due to gas-water interface. With time, the formed hydrates will increase in quantity and size through agglomeration inside the pipeline. This will cause reduction in the pipe's orifice, thus, resulting into velocity loss. This ultimately results into line plugging, pressure build-up and eventual pipeline rupture.
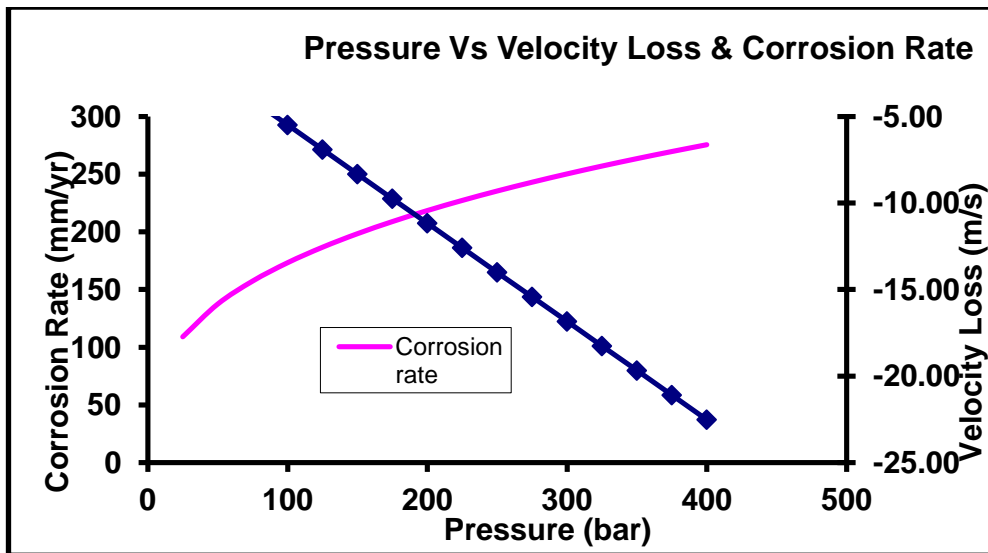
Figure 5.4: Pressure against velocity loss and corrosion rate at 15°C and pH=5.0

The impact of pH on the eventual corrosion rate along the longitudinal section of a pipeline depends on the soluble corroding agent and the type of metal used for the pipe's construction. If the metal is acid soluble, the corrosion rate is controlled by the rate of transport of available oxidiser to the metal surface. Amphoteric metals such as aluminium and zinc dissolve rapidly in acidic or basic solutions to aid corrosion while noble metals such as gold and platinum are not appreciably affected by pH.
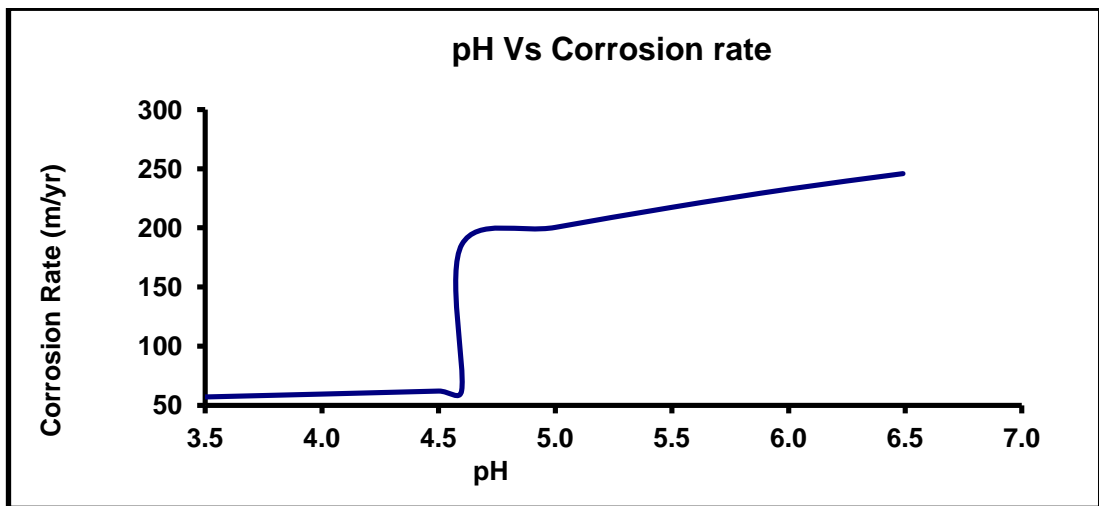
Figure 5.5: Impact of pH on corrosion rate

Figure 5.5 perfectly agreed with NPF (2011b) that pH hardly influences corrosion rate of iron within the pH region of 4 - 10. Within this range, corrosion rate of iron is relatively independent of pH for it is governed mostly by the rate at which oxygen

would react with the absorbed atomic hydrogen. This will depolarize the pipe's surface and allow continuation of the reduction reaction.

Ferrous oxide (FeO) is however soluble below pH of 4 and would dissolve upon formation rather than being deposited on the metal surface for film formation. The pipe's surface will directly be in contact with the acid solution due to an absence of the protective film, and this will result in sharp increase in corrosion rate. At this lower pH range, corrosion rate is dependent on both the depolarization of oxygen and hydrogen evolution since hydrogen will be produced in the acid solution at this lower pH range. Above pH of 10, corrosion rate decreases with an increase in pH probably due to the increase in reaction rate of oxygen with hydrated FeO ($Fe(OH)_2$) to form a more protective FeO in the oxide layer.

The sharp variation noticed at pH of 4.6 in Figure 5.5 is due to the change in the corrosion modelling formula at this point as indicated by Equations 5.16 and 5.17. This further confirmed the activeness of the developed MATLAB code for simulation.

5.8 The Limitations of the Model

Since the parameters needed for the model are subjective to various operating conditions and often change with distance within the pipe-length, the model could be thought of as being a point corrosion rate model. Nonetheless, since the model makes use of some physical data such as temperature and pressure, other parameters such as concentration, composition e.t.c. could be assumed to be constant over a few kilometers to reduce the iteration of measurement. This assumption could be costly.

Also, where gases such as CO_2, H_2S, O_3, and other organic and inorganic gases are present, this model should be modified to accommodate the contributions of each agent to corrosion rate of the pipeline.

Finally, the generated results from this model were calculated without full consideration being given to corrosion inhibitors, like the introduction of glycol. When these inhibitors are present (which is common in pipeline systems) their effects must be evaluated separately.

5.9 Conclusions

The model adequately predicted the pipe's shelf-life due to corrosion initiated through hydrate formed within a pipeline transporting natural gas at deepwater location and its effectiveness is confirmed by the ability of its plotted trends which agree with existing literatures. The resulting corrosion rates from this model increased with temperature, pressure and wall shear stress. This is in agreement with the existing mathematical and experimental reports, hence, the reliability of this predictive model. The resulting corrosion rate from hydrates could be as high as 174mm/yr (0.48mm/day). This is extremely alarming compared to the industry's aim to operate below 2mm/yr. At this rate, a pipeline would be subjected to full bore rupture within some days if corrective actions are not quickly taken. This extreme increase in corrosion rate will negatively impact operation by reducing the pipe-shelf life as well as the pipe's integrity. Also, increase in operating pressure increases the hydrate formation temperature. This increase in temperature will have secondary effects through its influence on the solubility of the corroding agent(s). Since CO_2 as the corroding agent for this study is very soluble in the formation water, any change in temperature would have resulting effects on other factors influencing the corrosion rate.

Again, an increase in operating pressure increases the erosion-corrosion rate as well as the velocity loss along the pipeline system. Finally, further work should be done on improving this model to accommodate other operating conditions experienced during the gas transport operation.

6. Application of Component Interactions for Gas Hydrate Inhibition

6.1 Background

Chapter 5 has shown that the rate at which gas pipelines corrode as a result of hydrate formation is significantly very high, hence, the need to investigate some avenues of inhibiting the formation. Corrosion rate highly depends on gas composition, therefore, there is need to investigate the contributions of the components before a deceleration options could be ascertained. CH_4 and CO_2 are the major components for sweet gas (and Australian fields majorly produce sweet). These two gases are also strong guests for Type I gas hydrates. Using 'Temperature Search' method, this chapter investigated the consequences of CH_4 and CO_2 varying compositions in gas stream on formation temperatures. Finally, the use of pure H_2 and N_2 gases to inhibit the resulting effects was investigated. This chapter goes a long way in proposing a solution that could help the gas industry to minimize the pertinent hydrate problems that have besieged the industry for several years.

6.2 Introduction

The quality of natural gas at a particular location is measured by its methane (CH_4) content, the higher the CH_4 content, the better the gas field. This is informed by the industrial desire for gases $\geq96\%$ CH_4 composition as sales gas as a result of its high caloric value as fuel which is the quantity of heat produced by its combustion. Studies have shown that gas hydrates are formed due to interactions between water and the gas components. These interactions could be functions of gas composition, concentration and operating conditions.

Various studies have been conducted on component interactions within the resulting gas hydrates. Snell et al (1961) investigated the initial hydrate conditions for C_2H_4-H_2O and CH_4-C_2H_4-H_2O systems. They finally compared the experimental and predicted hydrate forming conditions for several mixtures of CH_4-C_2H_4-C_3H_6-H_2O hydrate formation systems. Again, Ma et al (2001) used the "pressure search" method to study the $CH_4+C_2H_4$ and $CH_4+C_3H_6$ interactions in a cylindrical

transparent sapphire cell and finally presented valuable data that could be used to test the existing hydrate models and softwares. Furthermore, Fray et al (2010) measured three-phase (ice + clathrate hydrate + vapour) equilibrium in a water system with xenon (Xe), CO_2 and CH_4 as guest species. The generated results were used to determine the empirical laws that could be used to calculation the equilibrium pressure of pure Clathrates at all temperatures. Using the 'Pressure search' method, Li et al (2010c) also reported the ability of Tetrabutyl Ammonium Bromide to remarkably reduce the equilibrium hydrate formation pressure of CO_2+H_2 hydrate.

This study primarily investigated the CH_4+CO_2 gas mixture because Australia gas fields have been identified to be rich in high level of CO_2 content. A typical example is the Gorgon Project with 14% CO_2 content as explained in Chapter 2. This CO_2 would have passed through the underwater pipeline systems before the separation at Barrow Island is carried out.

'Temperature search' method was employed for this study and all the experiments were conducted in a cylindrical transparent sapphire cell. This method allows the gas industry to operate at any desired pressure while the hydrate formation temperature is controlled. By this, there will be no restriction to the operating conditions of the industry, hence, no negative impact on the net profit margin except for the additional investments resulting from utilizing any recommendations from this study.

6.3   Methodology

6.3.1   Reagent, Materials and Equipment

This study was carried out inside the same Cryogenic Sapphire Cell at the Clean Gas Technology Unit of Curtin University, Australia as explained in chapter 3.3 but with several modifications. The modifications included preparation of CH_4+CO_2 mixtures, $CO_2 +H_2$ mixtures, CH_4+H_2 mixtures, $CH_4+CO_2+N_2$ mixtures and $CH_4+CO_2+H_2$ mixture for investigations. All the gases used are industrial grades and the hydrate formation temperature was monitored for each set of experiment at 100bar, 125bar, 150bar, 175bar and 200bar.

6.3.2: Preliminary Study

HYSYS software was used to initially predict the hydrate formation temperature of each gas mix at the chosen pressures for estimates. This assisted in saving experimentation time.

6.3.3 Preparation of Experimental Gas Mix

CH_4 and CO_2 gases were used for the first set of studies while H_2 and N_2 were subsequently added to these gases for further investigations. Each gas mix was prepared by the following two steps. The first step was achieved by the use of a transducer to fill a specific gas into a 500cc cylinder bottle and the second step was by weighing the quantity of the gas in the bottle. The second step was necessary to confirm the accuracy of the first step. Subsequent steps were taken as well before the experimental runs.

When filling a specific gas, a cylinder steel bottle was first vacuumed and weighed with an electrical weighing balance. The 500cc bottles were then filled with the gas using an electrical transducer that was fitted to the main gas cylinder at one end and the bottle at the other end. While other gases were filled directly from the main gas cylinder to the bottle, CO_2 gas had to be heated to 60^oC before filling in order to prevent CO_2 gas from undergoing partial condensation during experimentation.

The quantity of each gas needed for each experiment was determined as a calculated ratio following the general gas equation principles as shown in Equations $6.1 - 6.13$.

The general gas equation is given as

$$P_n V_n = n_n RT \hspace{4cm} \text{Equation 6.1}$$

Where
P_n is the Pressure of gas component n (bar); V_n is the Volume of gas component n (cc); n_n is the Number of mole of component n (mol); T is the Desired operating Temperature (^oC) and R is the Universal gas constant (lit.barK^{-1}mol^{-1}).

In case of two gas mix (CO_2 and H_2 for example),

$$P_{CO_2} V_{CO_2} = n_{CO_2} RT \hspace{4cm} \text{Equation 6.2}$$

$$P_{H_2}V_{H_2} = n_{H_2}RT \qquad\qquad \text{Equation 6.3}$$

Dividing Equation (6.2) by Equation (6.3) gives

$$\frac{P_{CO_2}V_{CO_2}}{P_{H_2}V_{H_2}} = \frac{n_{CO_2}}{n_{H_2}} \qquad\qquad \text{Equation 6.4}$$

Since the volume of the cylinder to be used is fixed, then,

$$V_{CO_2} = V_{H_2} \qquad\qquad \text{Equation 6.5}$$

This implies that

$$\frac{P_{CO_2}}{P_{H_2}} = \frac{n_{CO_2}}{n_{H_2}} \qquad\qquad \text{Equation 6.6}$$

Equation (6.6) was then used to work out the quantity of each gas to be pressurized into the sapphire cell at a certain gas mix.

Consider 20% mol of CO_2 and 80% mol of H_2, and taking 100 moles as basis, then

$$\frac{P_{CO_2}}{P_{H_2}} = \frac{n_{CO_2}}{n_{H_2}} = \frac{20}{80} = \frac{1}{4} = 0.25 \qquad\qquad \text{Equation 6.7}$$

$$P_{H_2} = 4P_{CO_2} \qquad\qquad \text{Equation 6.8}$$

$Total\ Pressure\ (P_T) = Summation\ of\ Partial\ Pressures$ i.e.

$$P_T = \sum_{i=1}^{N} P_i \qquad\qquad \text{Equation 6.9}$$

For this system therefore

$$P_T = P_{CO_2} + P_{H_2} \qquad\qquad \text{Equation 6.10}$$

Though, the experiments were conducted inside the sapphire cell in bar, the available laboratory gauge could only measure in psi, thus, the need for conversion.

According to Smith et al (2007)

$$1\ bar \equiv 14.7psi \qquad\qquad \text{Equation 6.11}$$

Therefore a successful operation at 80% H_2 and 20% CO_2 gas composition and 100bar requires 294psi (20 bar) of CO_2 and 1176psi (80 bar) of H_2.

After using the calculated pressure ratio to fill the cylinder bottles with the desired gases, weight was used to confirm accuracy before the experimentation. This was achieved by weighing the bottles again to calculate the weight difference as shown in Equation 6.12 with a typical example given as Table 6.1.

$$m_D = m_f - m_i \qquad \text{Equation 6.12}$$

Where

m_i is the initial weight before filling the cylinder, m_D is the Weight of the gas filled into the cylinder (Mass difference) and m_f is the final weight after filling the cylinder.

Table 6.1: Typical measured values for H_2 and CO_2 mixture during the experiments

Cylinder 1			Cylinder 2			Cylinder 3		
Empty (E)	E + H_2	H_2	E	E + H_2	H_2	E	E + CO_2	CO_2
1276.98	1278.68	1.70	1597.50	1599.21	1.71	1359.20	1377.79	18.59
P (psi)	793		P (psi)	782		P (psi)	394	

The accuracy of the filled in gases was determined by the ratio of the weighed differences as given by Equations 6.13 – 6.20.

$$Number\ of\ moles\ (n) = \frac{mass\ of\ the\ substance\ (m)}{Molar\ mass\ of\ the\ substance\ (M)} \qquad \text{Equation 6.13}$$

For CO_2 and H_2 for instance,

$$n_{CO_2} = \frac{m_{CO_2}}{M_{CO_2}} \qquad \text{Equation 6.14}$$

$$n_{H_2} = \frac{m_{H_2}}{M_{H_2}} \qquad \text{Equation 6.15}$$

From 6.13 and 6.14, the weight ratio is given by

$$\frac{n_{CO_2}}{n_{H_2}} = \frac{\frac{m_{CO_2}}{M_{CO_2}}}{\frac{m_{H_2}}{M_{H_2}}} = \frac{m_{CO_2}}{M_{CO_2}} * \frac{M_{H_2}}{m_{H_2}} \qquad \text{Equation 6.16}$$

Molar masses for the two gases are given respectively as

$$M_{CO_2} = 44 g/mol; \quad M_{H_2} = 2 g/mol \qquad \text{Equation 6.17}$$

Therefore, Equation 6.15 becomes

$$\frac{n_{CO_2}}{n_{H_2}} = \frac{m_{CO_2}}{44} * \frac{2}{m_{H_2}} \qquad \text{Equation 6.18}$$

For 20% mol CO_2 + 80% mol H_2 as earlier calculated in section 6.3.4, the mass ratio will be

$$\frac{m_{CO_2}}{44} * \frac{2}{m_{H_2}} = \frac{20}{80} \qquad \text{Equation 6.19}$$

$$\frac{m_{CO_2}}{m_{H_2}} = 5.5 \qquad \text{Equation 6.20}$$

This simply means that, filling the cylinders A and B for CO_2 (20% mol) and H_2 (80% mol) respectively, increase in weight A (W_A) will be 5.5 times that in W_B where W_i is the weight of gas component i.

As an example from Table 6.6, the pressure ratio was calculated as

Quantity of CO_2 (psi) $= \qquad 394$

Quantity of H_2 (psi) $\qquad = \qquad 793 + 782 = 1575$

Therefore,

$$\frac{P_{CO_2}}{P_{H_2}} = \frac{394}{1575} = 0.25016 \qquad **$$

The mass ratio was calculated as

Total mass of $CO_2 \qquad = \qquad 18.59$

Total mass of $H_2 \qquad = \qquad 1.70 + 1.71 = 3.41$

Therefore,

$$\frac{m_{CO_2}}{m_{H_2}} = \frac{18.59}{3.41} = 5.4516 \qquad ***$$

Comparing the values from Equation (**) with Equation (6.7) with further comparison of Equation (***) with Equation 6.20 confirmed the accuracy of this gas

mix. These calculations and confirmations were repeated for all the gas mixes throughout the experimentation.

6.3.4 The study of Hydrate formation points

Prepared gas mixtures containing CH_4, CO_2+H_2, CH_4+CO_2, $CH_4+CO_2+N_2$ and $CH_4+CO_2+H_2$ were individually fed into the sapphire cell, each at an experimentation time through V9 (Figure 3.1) while 5ml of Millin-Q water (the liquid phase solution) was injected into the cell through V5. The system was heated up to T_B of 25 ^{o}C, operating pressure was set at 100 bar while the T_{set} was set at 15°C. The experiment commenced by switching on the system while the T_{set} was gradually and systematically reduced through the cooling system. The chillers was switched off immediately the hydrate particles were noticed in order to stop further supply of external cooling to the system, the formation temperature was recorded and the hydrate behaviours were visually observed. The beginning and end of dissociation studies were then carried out and recorded as explained in section 6.3.7. This set of experiments was then repeated for the same gas composition at 125bar, 150bar, 175bar and 200bar respectively and all the data recorded. The system was then purged, vented and cleaned before changing the gas composition.

6.3.5 The Experimental Sequence

The experimental study sequence was divided into two separate parts. The first part considered the consequences CH_4 and CO_2 compositions in natural gas mix. The second part considered the application of H_2 and N_2 gases for inhibition purposes. This was carried out by addition of these two gases (one at a time) to the CH_4+CO_2 gas mixtures. These two gases were considered because H_2 does not form hydrate at any pressure and temperature while N_2 can only form hydrates at a very high pressure. Each of the following was investigated.

a. CH₄ hydrate study

Experiments were conducted on industrially prepared methane gas in the sapphire cell at 100bar, 125bar, 150bar, 175bar and 200bar. The experiments were divided into three parts which included a study on the formation temperature, beginning of dissociation and the end of dissociation. All generated data were properly recorded and stored.

147

b. *CO_2 hydrate study*

Studies were carried out on CO_2 hydrates. This very study was technical due to the ability of CO_2 to undergo partial condensation at a very low temperature. To solve this problem, hydrogen gas was mixed with the desired percent of CO_2 gas. Initially, 10% mol CO_2 was mixed with 90% mol H_2 gas for experimentation. This was later changed to 20%CO_2 +80%H_2. H_2 gas was considered as a mix because H_2 gas forms hydrate at about 2000bar, therefore, it is inert at these experimented pressures. By this claim, the gas would have absolutely no effect on the hydrate formation point of the CO_2 gas.

c. *CH_4+CO_2 hydrate study*

After the individual studies, a gas mix of CH_4 and CO_2 was then fed into the sapphire cell to enable a study on typical natural gas composition in the pipelines.

d. *CH_4+H_2 hydrate study*

Effect of hydrogen gas on CH_4 hydrate formation temperature was study at all the pressures. This is necessary to investigate the impact(s) of H_2 gas on CH_4 hydrate properties.

e. *CH_4+CO_2+H_2 hydrate study*

H_2 gas was later added to the CH_4+CO_2 mixture and the hydrate formation temperatures were studied at all experimental pressures. This was to investigate the impact of H_2 gas on real natural gas environment.

f. *CH_4+CO_2+N_2 hydrate study*

Another round of experiments were conducted by adding N_2 gas to the CH_4+CO_2 mixture and the hydrate formation temperatures studied at all experimental pressures. This was also to investigate the impact of N_2 gas on real natural gas environment.

6.3.6 Beginning and end of dissociation study

Beginning and end of dissociation study was carried out on each composition under study. Beginning of dissociation point is the temperature where the first solid

hydrate turns to liquid while end of dissociation is that point where the last hydrate solid turns to liquid form.

These were determined for each composition through physical observations. Immediately the hydrate was formed, the chiller was switched off to prevent further supply of external cooling effects to the system and the system temperature was allowed to rise on its own accord till the hydrate begins to dissociate. This required heat needed to raise the temperature was naturally transferred from the environment to the enclosed system. The temperature where the first liquid was formed was recorded while the heating continues till all the solid turned to liquid. The final temperature was also recorded.

6.3.7 Instrumental Analysis of Gas Composition

After each experiment, the compositions of the gas in the cell were instrumentally analysed in order to compare with that estimated. The estimation was carried out through calculation and filling the cylinders at the calculated ratios using the pressure transducer while the actual value was measured using a gas transmitter.

The gas transmitter used for the analysis was a PolyGard (R) Transmitter manufactured by MSR in Germany with serial number No: 38/08. It was an AT-A2-3400-4-001 model with 100% Vol. CH_4. It had an alarm controller system attached with model MGC-03-02-02-9-110005011. The alarm system which was also manufactured by the same company had a serial number of 03-31/08. The equipment had a rating of 230V, AC/0.1VA and input of 4-20mA. To analyse, a rubber tube was connected from the outlet part of the cell to the inlet part of the analyzer. The gas inside the cell was then gradually released for the transmitter to read. The gas composition, displayed in percentage was read off and the value compared to the previous estimated value for precision.

6.3.8 Precautions

All the experimental and equipment precautions stated in section 4.3.3 were observed. Further precautions taken for this study included carrying out pressure test on the cell before starting the experiments. This was carried out to make the system leak-proof. A leak within the system could lead to discharge of hazardous gas(es) to the environment and/or explosion in the laboratory when operating at high pressure.

The pressure test was carried out after the system had earlier been decoupled and sent for a proper industrial cleaning. The system was coupled back, vacuumed, filled with N_2 gas, and pressurized at 150bar for 30 minutes. Generally, the system pressure used to increase at the initial stage of pressurization. The leakage is bound to be noticed either during the pressurizing because at a point, there will be a sudden drop in cell pressure. Alternatively, after reaching the 150bar, the cell pressure would start dropping after few minutes. A chemical "Gas and Air Leak Detector" was sprayed at all joints to enable location of the leaking point or joint. In case this failed, the system would need to be re-pressurized but this time, some sections of the system would be closed while others left opened in order to isolate the leaking point(s). To achieve this, the whole system was sectionalized into the feeding unit, the piston pump unit and the cell unit. After locating a leak, the point would be tightened and the pressure test repeated till a stable pressure was achieved for the 30 minutes period.

Also, since the gas composition was used for a set of pressure range, it could have been wise enough to just reduce the operating pressure for the next experiment. This would have dissociated the hydrates formed at higher temperature. However, wrong results would have been generated if this was done because the gas composition would not have been at equilibrium. To prevent this error, the cell was heated to

$30\,^{\circ}C$ and left for about 2 hours before the next experimentation. The heating to such temperature released all the gas that had dissolved into the liquid phase while the

2-hr time lag allowed both the liquid and gaseous phases to be at equilibrium with one another before the next experiment. After these precautions, the statistical analysis on the generated data gave the maximum experimental error of 1.68%. This was acceptable since the confidence level was above 95%. This confirmed the accuracy of the generated data set.

6.4   Results and Discussions

6.4.1   Validity of generated data set

The validity of the generated data sets for all the conducted gas mix was investigated. This was carried out by plotting them all on a chart (Figure 6.1) and

their trends compared with those on similar study presented by Ma et al (2001) and Li et al (2010c). For each gas mixture from this study (regardless of the components), the formation temperature increases with pressure, and this trend is in perfect agreement with those from existing literatures. This validity test indicated that this study is reliable within the limit of experimental errors.
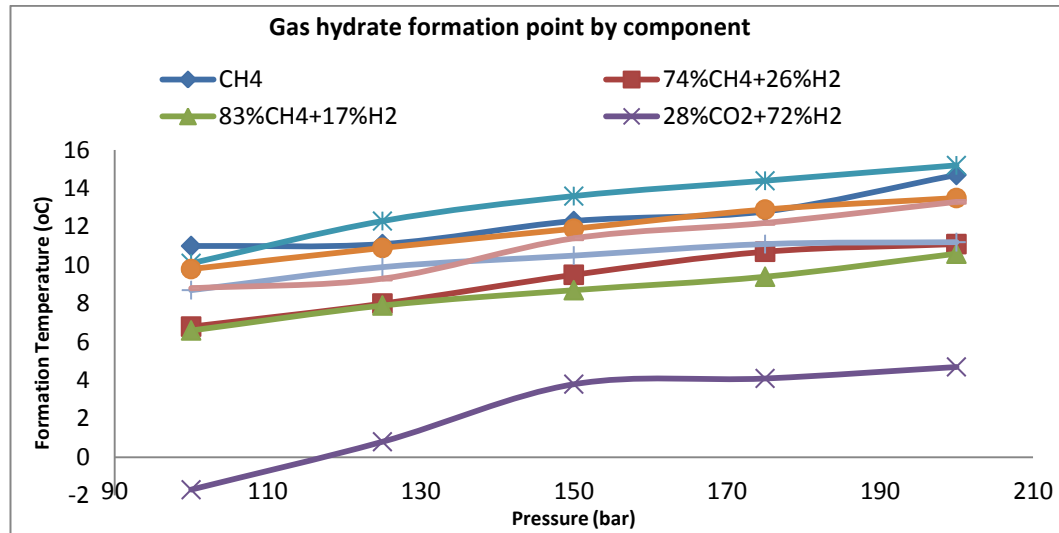
Figure 6.1: Gas hydrate formation point by component

6.4.2 Studying the characteristics of pure CO_2 hydrates

This study was conducted by investigating the hydrate formation characteristics of 10% CO_2 and 20% CO_2. It was observed that the 10%CO_2 did not form hydrate even at 200bar whereas the 20%CO_2 formed. Figure 6.2 showed that CO_2 form hydrate at comparatively low temperatures and high pressures. At pressures close to 100bar, the chart showed that CO_2 might not form hydrate till the whole liquid is solidified. However, exception to all these took place when the gas was mixed with CH_4 as obtainable in natural gas.

At all pressures, the hydrate particles started forming inside the liquid and travelled to the interphase in the tangential form according to the direction of agitation. The formation was very rapid with the particles independent of one another. 5 minutes after, the particles started to form slurries that look like 'corn flakes' and suspended at the interphase. However, the growth rate, even at 200bar, was very slow to the extent that, the particles were still independent at 0^oC. Visual observation showed that the hydrates were thinly deposited at the wall of the glass within a short

thickness of about 1 mm while others kept moving within the liquid phase. The stirring rate was later increased vigorously to study the impact but there was not change. The same observations were made at other pressures for this composition; however, different formation temperatures were obtained as a function of pressure (Figure 6.2). While the hydrates were pronouncedly noticed at 150bar and above, it was hardly noticed at 125bar and was formed below 0^oC at 100bar.
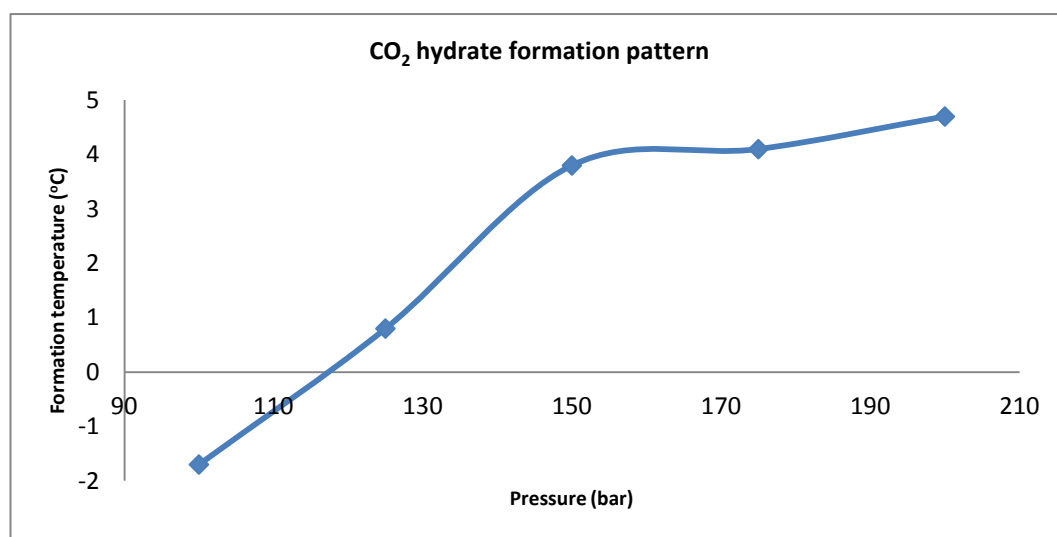
Figure 6.2: A chart on CO_2 hydrate formation pattern

6.4.3 Methane and methane mixture hydrates

This study was conducted to understudy the implications of having other components with methane gas in the pipeline during natural gas transport.

The characteristics of hydrates generated from CH_4 and its mixture with CO_2 and H_2 are presented as Figure 6.3. Pure CH_4 showed a strong ability to form hydrate at all experimented pressures. This is justified by its small molecular size range of 4.4-5.4 Å which is capable to occupy the small and large cages to form Type I hydrate. Though, CO_2 also falls within the same molecular size range, it could not exhibit this same hydrate formation behavior with CH_4 due to its solubility. CO_2 is readily soluble in water while CH_4 is sparingly soluble.

At about 110bar however, the hydrate forming part of CO_2 gas became suddenly activated when mixed with CH_4. Figure 6.2 showed that the CH_4+CO_2 mixture is more hydrate prone compared to CH_4 gas at all pressures above 110bar. This might be due to the combine property effects of the two guests on hydrate formation point.

152

Also, the Figure clearly showed the inhibition ability of H_2 gas by seriously reducing the hydrate formation temperature at all pressure. The ability to this could be attributed to the fact that hydrogen forms hydrate at a very high pressure of about 2000bar but not these pressure and temperature. Introduction of H_2 gas also discourage agglomeration of the hydrates.
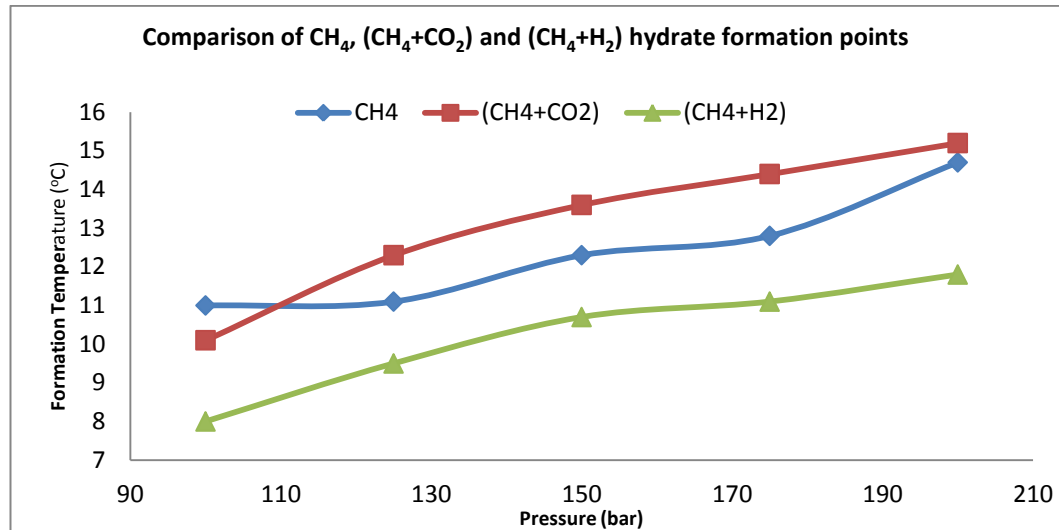
Figure 6.3: Hydrate characteristics of methane and gas mixtures.

For 100% CH_4, the formed hydrate was very whitish like snow. It was formed at the interphase as tiny flocs that gradually increased in size and kept building up downward into the liquid. At all pressures, the hydrate particles rapidly agglomerated to produce slurry, which solidified to block the whole orifice within a period range of 5 minutes at 100bar and 3 minutes at 200bar. This showed that the uncontrolled presence of CH_4 within natural gas is very 'poisonous' to pipeline industry.

The hydrates from CH_4+CO_2 were formed within the waterbody but quickly travelled to settle at the water-gas interphase. The hydrate cloud was usually formed within the waterbody and travelled fast to the interphase to join and stick to the existing hydrate particles for fast agglomeration. The growth rate at all pressures was observed to be significantly very high. At 200bar and T_{set} of 5^oC, the whole liquid turned to hydrate block within 8 minutes of spotting the first hydrate particle and further 3 minutes stopped the stirrer (blocked hydrate formation). This showed that gas within this compositional value could be extremely troublesome for pipelines in Australia at winter period. Various analyses have shown that Australian gas fields,

already known to have high CO_2 problem, operate at a composition within this range (Roarty, 2008; Cook, 2009; Ferronato et al, 2010).

The agitation rate was significantly increased at 175bar in order to study the effects on formation temperature and agglomeration rate. It was noticed that the formed hydrates quickly dissolved back into the liquid. This showed that agitation rate played a significant role by breaking the tension at the interphase to allow more interaction between the liquid and gaseous phases. This enabled more gas molecules to be available and dissolve in the liquid to promote hydrate formation.

Furthermore, the hydrates from CH_4+H_2 mixture generally formed in thin paper sheet forms within the liquid and travelled with the water in flow direction. The agglomeration rate was very low while the formed hydrates were deposited at the interphase; however, they never stick together. The agglomeration rate was very insignificant at 100 and 125bar. To successfully study the sea conditions (about 4^OC), the system temperature was dropped to 0^oC at each pressure while the agglomeration condition was continually monitored. Despite this extremely low temperature, the hydrate growth rate was still very slow and retained its 'thin paper' form without sticking together.

6.4.4 Studying the effects of H_2 concentration on methane hydrates

This study was conducted as a preliminary investigation on the inhibition ability of pure H_2 gas. It involves experimenting with two different CH_4+H_2 gas mix with different concentrations. The results were then compared with those generated from the experiments conducted on pure CH_4.

The results confirmed the high tendencies of pure H_2 gas to inhibit hydrate formation temperature (Figure 6.4). At all pressures, the hydrate formation temperature was remarkably reduced when H_2 was added.

The expectation would have been for the formation temperature to further reduce when H_2 concentration increased in the mixture, surprisingly; this was not the case as can be observed in the Figure. This suggested the possibility of optimal effective concentration for the inhibition ability.
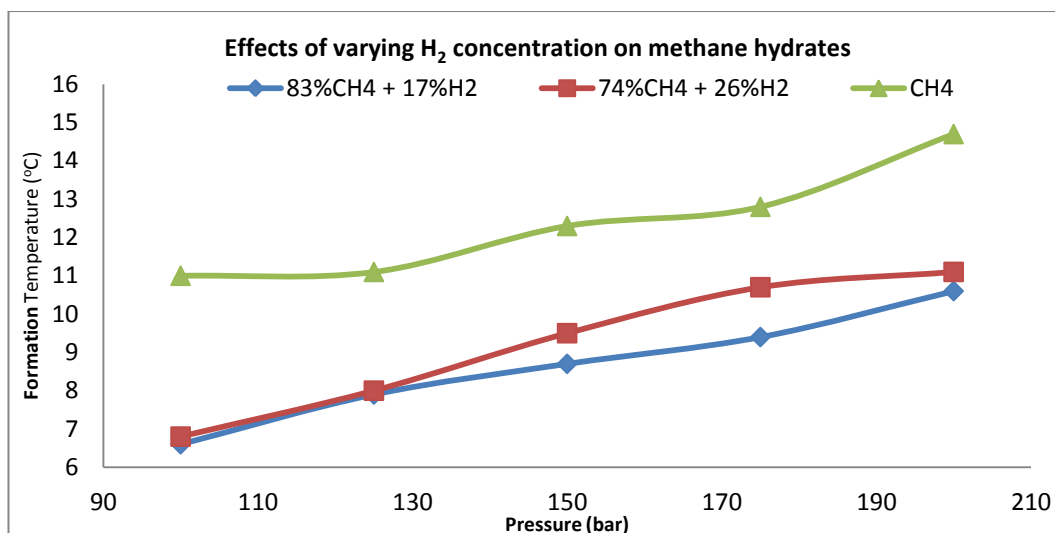
Figure 6.4: Effects of varying H_2 concentration on methane hydrates

6.4.5   The effects of concentration variation on sweet gas hydrates

The effect of concentration variation of the hydrates from sweet natural gas was studied through the CH_4+CO_2 gas mixture. This study was important considering the variations in gas composition from field to field and from region to region. Knowledge from this study would assist in predicting the hydrate expectations from a field based on the gas composition. A set of experiment was conducted on two different gas mixtures with the same compositions but 2% concentration variation. The experiments were conducted at the five pressure points.

From Figure (6.5), it could be seen that the presence of CO_2 in the gas mixture reduced the hydrate formation temperature. Considering the CH_4+CO_2 gas mix, the difference in the hydrate formation point at each pressure is significantly large despite just a slight variation of 2% in their concentrations (Figure 6.5).

Further observation of Figure 6.5 showed that the gas mix with 22%CO_2 concentration was able to promote hydrate more than that of 20%CO_2; this may probably be due to the combined hydrate promotional effects of the individual component. It could be further noticed from the Figure that the difference increases with pressure. This gives more credence to the explanation from section 6.4.2 that CO_2 gas has the ability to display greater hydrate promotional tendencies at higher pressures.
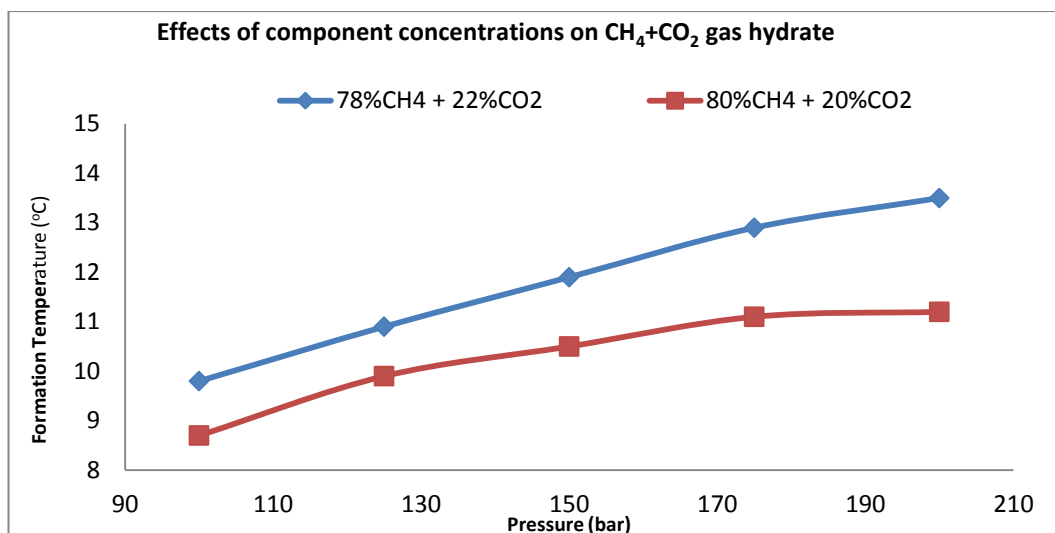
Figure 6.5: Effects of concentration variation on CH_4+CO_2 gas hydrates

6.4.6 The effects of N_2 and H_2 on hydrates formation temperature

Effects of N_2 and H_2 on hydrate formation temperature were individually studied in order to investigate their abilities to inhibit the formation of gas hydrates. A positive achievement in this area would suggest a cost effective process of handling this flow assurance problem along the deepwater pipelines. For the first study, $10\%N_2$ was added to 100% (CH_4+CO_2) and then normalized to final 100%. A gas mixture, prepared based on the normalized composition was then studied in the sapphire cell at all the five pressures for the formation temperatures, beginning of dissociation and end of dissociation. After this set of experiments, the cell was vacuumed, thoroughly cleaned and vacuumed again. These same experiments were repeated for 10% H_2. The results were processed for analysis and comparison, and finally presented as Figure 6.6.

The effects of the two gases on gas hydrate were glaringly shown in the Figure 6.6. The two gases were able to remarkably reduce the formation temperature at all pressures. However, the reduction ability of H_2 gas was very much significant compared to N_2 gas (Figure 6.7).

156
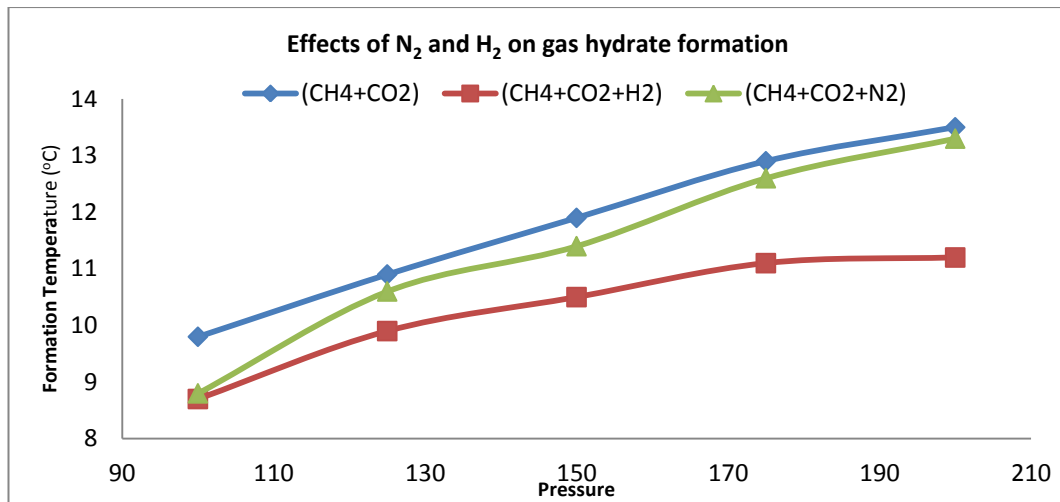
Figure 6.6: Effects of pure N_2 and H_2 gases on gas hydrate formation.
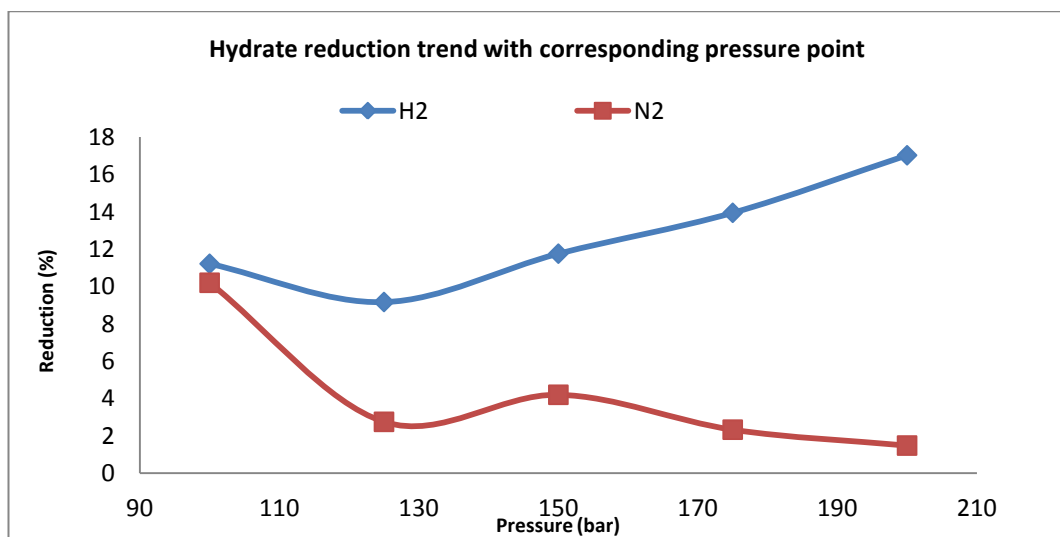
Figure 6.7: Comparison of inhibition trend between H_2 and N_2

The sharp difference in the hydrate inhibition capability of the two gases may be due to their abilities to individually form gas hydrate. N_2 gas, with small molecules forms Type II hydrate at a relatively higher pressure above the experimented pressures but can still form hydrate within other higher operating pressures practice at gas fields during the gas transportation. However, H_2 gas can never form hydrate at any natural gas transportation conditions. H_2 gas can form hydrates at extremely high pressure of about 2000bar because its molecules are too small and usually leaked out of hydrate cage, thus, reducing the amount that could be stored. By extension, these individual properties affect their interactions with natural gas during the hydrate formation process.

157

The observed downward and upward trend for the Nitrogen gas in Figure 6.7 may be due to diffussional resistance at higher pressures. At lower pressure, nitrogen molecules could move more easily between the hydrates. However, increasing the pressure causes the hydrate particles to become more compact and then proxy between the particles will decrease; this will result in increase of the diffusional resistance to the nitrogen molecules. However, at these higher pressures, hydrogen molecules are small enough to still penetrate. This justification should be further investigated experimentally.

Further laboratory observations showed that hydrates produced after adding each of these two gases were very tiny with low agglomeration rates. In actual fact, agglomeration was not taking place at all for H_2 mixture at all pressures. The floating hydrates remained in tiny bits throughout. For N_2, agglomeration was hardly noticed at 100bar while the rate was almost ignorable at other investigated pressure points up to 4° below the formation temperature. The formed hydrate particles were only floating at the liquid phase without any agglomeration. The hydrates were very distinct while the liquid phase was very clear.

Though, this could be pointing towards the preference for H_2 gas as inhibitor, however, care must be taken by considering other factors such as safety, cost implications, material availability and recovery before a final decision could be taken. Any dissociation of H_2 as a result of partial pressure would easily initiate internal corrosion along the pipeline; whereas, N_2 as an inert gas is less dangerous.

6.4.7 Study on software prediction accuracy

Industrially, there are many available software packages in use to predict the hydrate formation temperatures for both gas and liquid mixtures. Some of these packages include HYSYS, PVTsim, OLGA, e.t.c. This thesis conducted this part of the study on HYSYS since it was the Software used to roughly estimate the formation temperatures before the laboratory experimentations. This study was conducted by comparing the outputs from HYSYS software to those generated from the experimental sets. The HYSYS outputs were generated through the Hydrate envelope in the software after supplying the composition, concentrations and other operating conditions while the experimental data were generated through the

Sapphire cell equipment with strict precautions. For a robust study, the experimental aspect included investigating the hydrate formation temperature, the beginning of dissociation and the end of dissociation on four different types of gas mixtures.

All the results as shown in Figure 6.8 (a-d) gave exactly almost the same trends. The Figures revealed that the HYSYS predictions are closely the same with the values obtained as end of dissociation. It can then be deduced that the software has been predicting the end of dissociation value instead of the actual hydrate formation point. Nevertheless, this ability of the Software to predict values that are a bit higher could be viewed as a preventive guide to the industry.
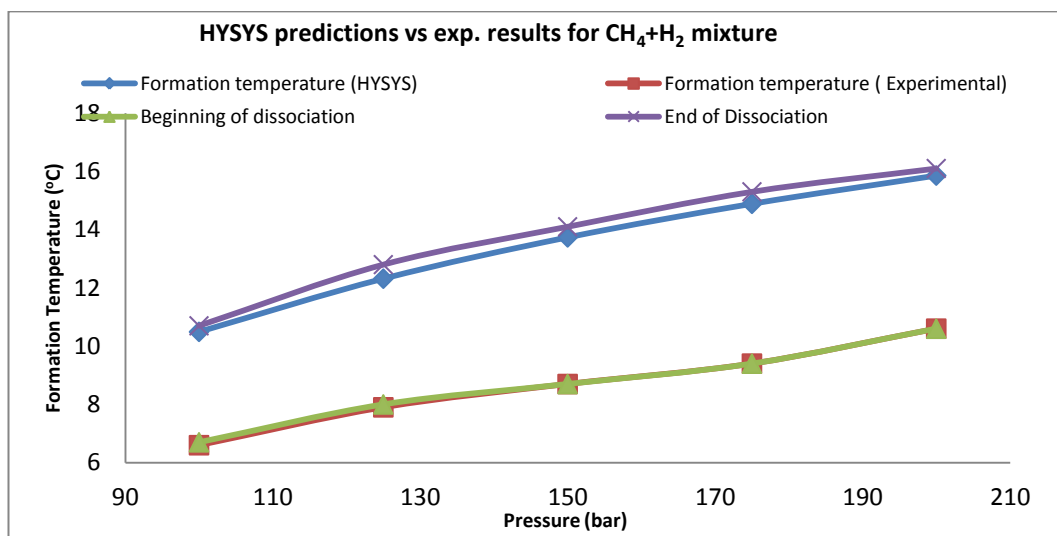
Figure 6.8a: Comparing the HYSYS and experimental results for CH_4+H_2
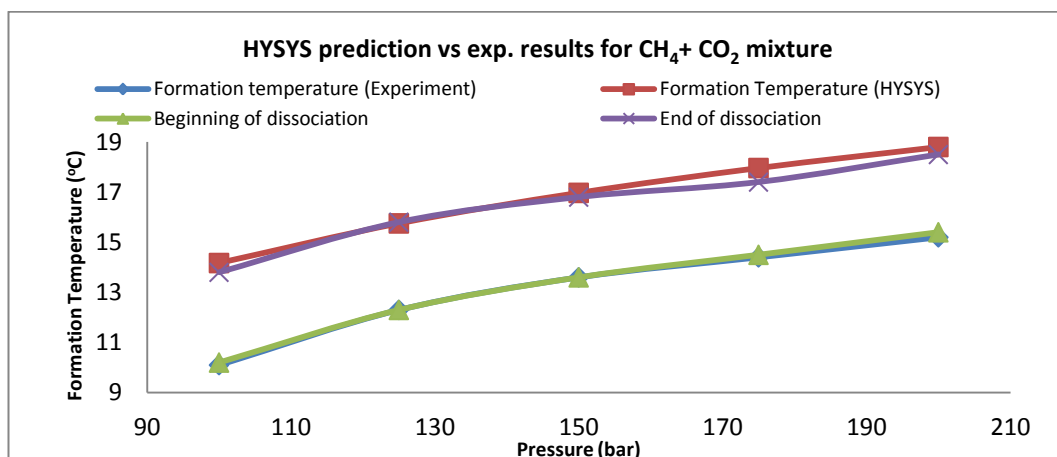
Figure 6.8b: Comparing the HYSYS and experimental results for CH_4+CO_2
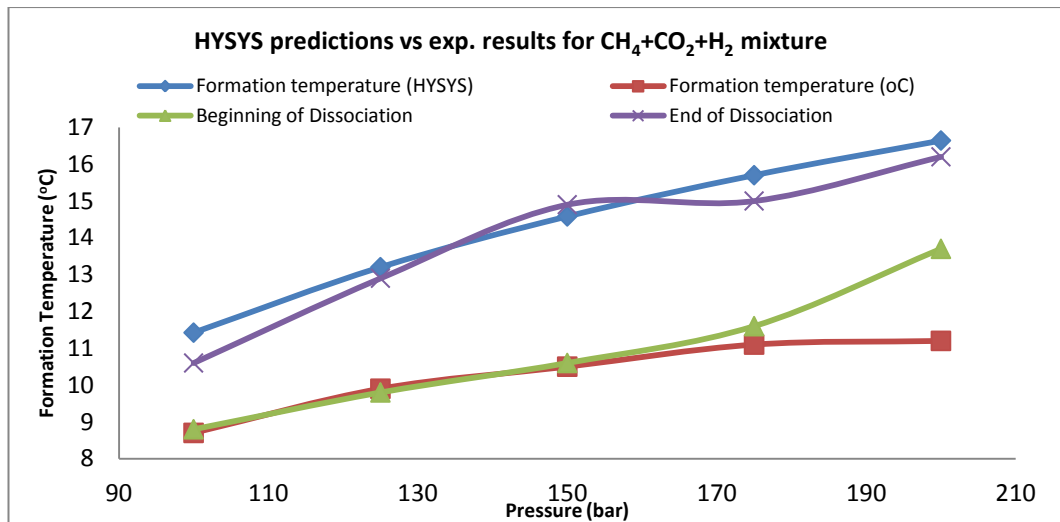
Fig. 6.8c: Comparing the HYSYS and experimental results for $CH_4+CO_2+H_2$
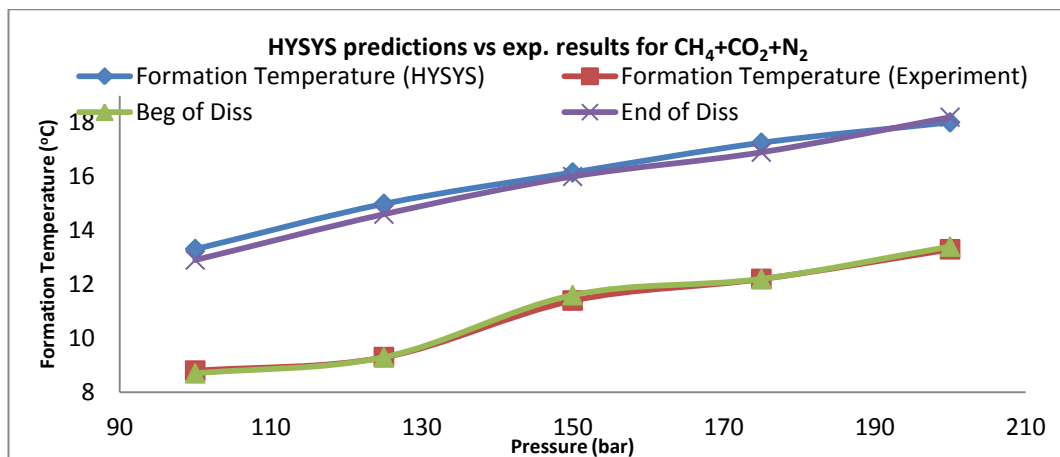
Figure 6.8d: Comparing the HYSYS and experimental results for $CH_4+CO_2+N_2$

Also, the experimental results showed that the hydrate formation temperature is closely equal to the temperature of the beginning of dissociation. This is thermodynamically correct because the amount of heat the system lost to the surrounding at the hydrate formation point (through the cooling process) would be the same amount gained at the point where the hydrate would start to melt.

Water molecules could appear in gaseous, liquid or solid (ice) state. The liquid molecules could move through rotation, vibration and translation motions while the ice molecules could only vibrate due to rigidity of the structure. Gas hydrates are Ice-like. During the experimentation, the water-gas system released latent heat to the surrounding at the point of changing from liquid phase to hydrate. This slowed down the hydrogen bonds till the liquid could no longer rotate (freezing point), thus, the

160

formation of gas hydrate. For the hydrate to dissociate (the beginning of dissociation), latent heat was absorbed from the surrounding. This enabled the hydrate to go from higher ordered state to the lower one by weakening the hydrogen bonds between the hydrate molecules.

Temperature remained constant throughout the phase changes (solidification or melting) because the available energy was used either to loosen or tighten the hydrogen bonds. The entire hydrogen bonds must be broken (in case of melting) or tightened (in case of solidification) before further energy could be used to increase the temperature.

6.5   Conclusions

This study has successfully investigated the implications of component interactions of CH_4, CO_2, CH_4+CO_2, $CH_4+CO_2+N_2$ and $CH_4+CO_2+H_2$ gas mixtures on hydrate formation temperature. It was discovered that CH_4 played key roles on hydrate formation patterns during natural gas transportation through offshore pipeline system, the higher the CH_4 content in a natural gas mix, the higher the risk of hydrates promotion. The resulting CH_4 hydrates grew very fast and blocked the pipe's orifice within a short period of formation. It was also discovered that CO_2 does not form hydrate at low concentrations. However, its presence in CH_4+CO_2 gas mix showed its remarkable ability to aid hydrate formation. This is not surprising since it is also a former with ability to form Type I hydrate.

 Furthermore, the study confirmed the ability of pure N_2 and pure H_2 gases to significantly inhibit the formation of gas hydrate; however, H_2 experimentally showed a more promising characteristic. This was ascribed to the fact that H_2 gas only forms hydrate at an extremely high pressure of 2000bar and above. This pressure range is far above the operating pressure range for gas transport; thus, making it to behave as an inert gas at all the investigated pressures. However, safety factors, material availability, cost implication and recovery from stream should be further investigations for these two gases in order to choose the better option.

7. Conclusions and Recommendations

This chapter is divided into conclusions and recommendations. The conclusion part highlights the various conclusions generated from the different sections of the study while the recommendation part proposes two potential PhD studies for future investigation.

7.1   Conclusions

This thesis extensively evaluated the implications of corrosion and hydrate formation along underwater natural gas pipelines systems on the industry. Experimental studies were conducted to assess the links between these two flow assurance problems, these included several laboratory experiments to investigate the ability of corrosion inhibitors to promote hydrate formation along the offshore/cold region pipelines due to similar chemical and structural properties. Based on the findings, a comprehensive mathematical model was developed to predict the corrosion rate as a result of the formed gas hydrate. Finally, another set of experimental study was carried out to investigate the ability of H_2 and N_2 gases to inhibit the formation of hydrate along the gas pipeline. The study comprises of four parts which are summarized below.

7.1.1   Impacts of Corrosion and Hydrate Formation on the Industry

Pipeline industry is searching for all possible means to minimize the occurrence of these two flow assurance problems during operations as a result of their economic, safety, health and environment implications. Some existing and proposed global natural gas pipeline networks systems were considered while the causes of these two flow assurance problems were thoroughly evaluated. The full impacts of any failure along the pipelength as a result of any of these problems were presented with the support of many case studies. This was followed by descriptions and analyses of the existing prevention measures. Finally, it was established that gas hydrate could initiate corrosion. This is one of the major contributions of this work to knowledge.

 The conclusions of this part of the study included:

- Increase in natural gas demands due to economical and increased population purposes have driven the industry to deepwater (offshore) regions in search of this energy source.

- Attempts to Prevent hydrate formation along these pipelines annually cost millions of dollars to the industry while its eventual occurrence was equally fatal. Unfortunately, all existing preventive measures could only minimize its occurrence but cannot stop its promotion along the pipelength.

- Through extensive literature search, this study successfully justified a need to investigate the ability of the corrosion inhibitors to promote hydrate formation. This was due to the observed similar chemical and structural properties between the corrosion inhibitors and established hydrate promoters. This has been outside the existing general research on hydrates.

- Finally, this study has successfully recommended a need to investigate the ability of gas hydrates to initiate different types of internal corrosions along gas pipelines. This research area is also completely new.

7.1.2 Corrosion-Hydrate Relationships (Experimental Assessments)

This is another major contribution to knowledge from the thesis because all known literature have not considered this research area. Ability of corrosion inhibitors to promote hydrate formation was experimentally investigated. Five corrosion inhibitors commonly used in the gas industry were studied in a cryogenic sapphire cell at 500ppm and 100bar. They were all discovered to aid hydrate formation but at different rates. DPC was further studied at different pressures and concentrations due to its significant promotional ability compared with other investigated inhibitors.

The conclusions of this part of the study included:

- Corrosion inhibitors generally promote hydrate formation along the deepwater natural gas pipeline due to their surfactant properties and hydrogen bonding distributions within their chain lengths.

- They however promote at different rates based on their different structural distributions, active functional groups and affinity for water molecules. These properties affect the hydrogen bonding and electronegativity properties of individual inhibitor.

- Care should be taken in using DPC as a corrosion inhibitor along the deepwater gas pipelines due to its significant ability to aid hydrate formation.

- The resulting hydrates from DPC are foamy at all operating pressures and concentrations. This showed that the surfactant properties of this chemical are highly influential during operation.

- Hydrate formation temperature is directly proportional to the operating pressure.

- The CMC for DPC is about 5000ppm due to various anomalous behaviours observed at this particular concentration compared to other concentrations.

- At all pressures, the liquid disappearance rate and the hydrate growth rate for DPC decreases with increase in concentration. This suggests the potential of using the chemical as an additive for natural gas transportation and storage in slurry form.

- At high concentrations, DPC prolonged the complete blockage of the glass orifice. This strengthens the potential of the chemical to serve as both the corrosion and hydrate inhibitors at high concentrations such as 10000ppm and above.

7.1.3 Corrosion-Hydrate Relationships (Mathematical Assessment)

A predictive corrosion rate model was mathematically developed to further assess the resulting problems from the established corrosion-hydrate relationships. This study area is entirely new, hence, the need for an extensive literature search on the existing corrosion models. Finally, a model was developed and validated by comparing the generated results with the outputs from other corrosion models. This new model again serves as another contribution to knowledge from this work.

The conclusions from this part of the study included:

- The resulting corrosion rates increased with temperature, pressure and wall shear stress. This perfectly agreed with all existing mathematical and experimental reports, hence, the reliability of this predictive model.

- The resulting corrosion rate from hydrates alone could be as high as 174mm/yr. This is extremely alarming compared to the industry's aim to operate below 2mm/yr. At this rate, a pipeline would be subjected to full bore rupture within some days if corrective actions are not quickly taken.

- This extreme increase in corrosion rate will negatively impact on operation by reducing the pipe-shelf life as well as the pipe's integrity.

- Increase in operating pressure increases the hydrate formation temperature. This increase in temperature will have secondary effects by influencing the solubility of the corroding agent(s) and other factors affecting the corrosion rate.

- Increase in operating pressure also promotes the initiation of erosion-corrosion as well as increases the rate of velocity loss along the pipeline.

7.1.4 The Gas Component Interactions

The final stage of this thesis searched for some means to inhibit hydrate promotion within the pipeline system. The investigation was carried out by initially studying the interactions between different components of natural gas, and then followed by investigating the ability of H_2 and N_2 gases to achieve the inhibiting feat.

This final part is another major contribution to knowledge from this work and successfully place both academic and commercial values on the entire thesis. These are clearly shown in the recommendations section.

The conclusions from this part of the study included:

- The higher the CH_4 content in a natural gas mix, the higher the risk of hydrate formation along the deepwater pipeline networks. The resulting hydrates from this component agglomerate very fast to block the pipe's orifice.

- Regardless of the operating pressure, CO_2 does not form hydrate at very low concentrations.

- Addition of H_2 and/or N_2 to CH_4 and CO_2 mixture significantly reduced the formation temperature at all operating pressures and concentrations. This confirmed that the two gases can individually serve as hydrate inhibitor along the deepwater natural gas pipelines.

- H_2 gas has better inhibition capability compared to N_2. This is attributed to the fact that pure H_2 gas forms hydrate at extremely high pressure and low temperature whereas, pure N_2 gas will form hydrate at a very low temperature but relatively very low pressure.

165

7.2   Recommendations

Further studies should be conducted on the types of corrosion that could be initiated by gas hydrates along the inner wall of underwater pipelines and the likely points of initiation. Also, further studies on the use of H_2 and N_2 gases as hydrate inhibitors are highly recommended for further investigation. The importance of the two recommended studies is highlighted below.

7.2.1 Laboratory Investigation on the Corrosion Patterns

This thesis has presented (through extensive literature review) that resulting hydrates could initiate different types of corrosion within the internal wall of gas pipelines; therefore, there is a need to experimentally authenticate this discovery and understand the patterns and the extent of damages that could be caused at each point. Figure 7.1 was designed by the author for consideration. It involves cutting a typical gas pipeline with various pits that could be caused by hydrate particles during the gas transport. This alone could be the basis for a Ph.D. thesis in the area.
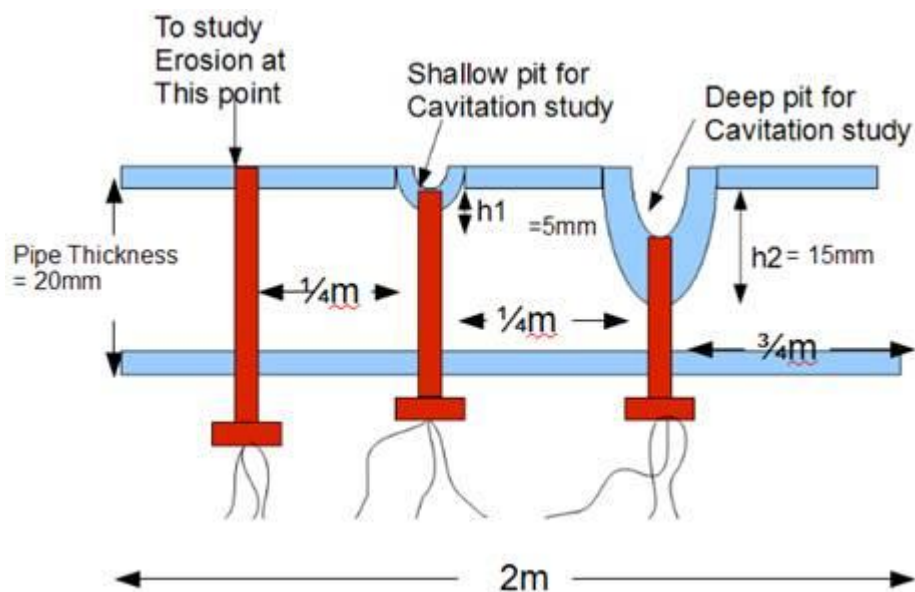
Figure 7.1: Proposed diagram for corrosion-hydrate interaction study

7.2.2   Investigations on Applicability of H_2 and N_2 as Hydrate Inhibitors

In-depth investigations should be conducted on the abilities of H_2 and N_2 gases to inhibit the formation of gas hydrate based on the observations from the latest part of this work. From what this thesis has achieved so far, it would have been more

appropriate to recommend H_2 gas instead of N_2 gas because of its hydrate inhibition capability which is more significant compared to that of N_2. However, this could be negated by the cost implications and reactivity properties of the two gases. Pure N_2 gas can be obtained from the atmosphere thus, an initial cost of plant installation for processing is all that is required and the freely obtained N_2 gas would thereafter be passed through the pipe-length with the raw natural gas. In other hand, H_2 gas has to be obtained from another source (through a process) before passing through the pipeline; this simply means that, using H_2 gas will involve the initial cost of installation, the continual processing cost from the source and other operational costs. To prevent the continuous processing of fresh H_2, the gas can be recycled after separation at the exit; however, this will require additional pipelines which will also add to the cost of production.

Also, N_2 gas can easily be separated from the natural gas compared to H_2 gas. This means that after successfully transporting the natural gas through the pipeline system, more capital will be required to separate H_2 gas from the stream and this will add to the cost of production. Again, passing H_2 gas along the pipeline might be dangerous for the safety of the pipeline system because any dissociation of the gas as a result of partial pressure will easily initiate corrosion along the pipe-length.

The procedures itemized below might assist in achieving this goal;

1. Application of N_2 gas at various concentrations.
2. Application of H_2 gas at various concentrations.
3. Application of N_2 and H_2 mixed at various concentrations.
4. Engineering design for installing the required inhibitor at the inlet point. The design should consider the inhibitor and the natural gas as the feeds into the pipeline. This should involve material of construction, the feed rate, the feed point(s), etc.
5. Engineering design for the required separation at the outlet of the pipeline.

From the foregone, it can be seen that this recommendation could also form the basis for another Ph.D. thesis in this area.

REFERENCES

Abd El Rehim, S.S, Sayyah, S.M., El-Deeb, M.M., Kamal, S.M and Azooz, R.E. (2010), "Poly(o-phenylenediamine) as an inhibitor of mild steel corrosion in HCl solution", *Materials Chemistry and Physics*, Vol. 123, Iss. 1, pp. 20–27

Abdel-Aal, H.K., Aggour, M. and Fahim, M.A. (2003), "Petroleum and Gas Field Prosessing", Marcel Dekker Inc., New York, USA.

Adib, H., Jallouf, S., Schmitt, C., Carmasol, A. and Pluvinage, G. (2007), "Evaluation of the Effect of Corrosion Defects on the Structural Integrity of X52 Gas Pipelines Using the SINTAP Procedure and Notch Theory", *International Journal of Pressure Vessels and Piping*, Vol. 84, Is. 3, pp. 123-131

Advantica (2002), "Ukopa Pipeline Fault Database: Pipeline Product Loss Incidents (1961-2000)", 2nd Report of UKOPA Fault Database Management Group, Advantica Report Reference R4798. pp 22

Ahammed, M. and Melchers, R.E. (1997), "Probabilistic Analysis of Underground Pipelines Subject to Combined Stresses and Corrosion", *Engineering Structures*, Vol. 19, Iss. 12, pp. 988-994.

Aiad, I., Ahmed, S. M. and Dardir . M. M. (2011), "Synthesis and some applications of Anionic Palmitic Acid Schiff Base Salt Surfactants", *Journal of American Science*, Vol. 7, Iss. 1, pp. 799-807

Akba, H., and Batigoc, C.D. (2008), "Micellization of Dodecylpyridinium Chloride in Water–Ethanol Solutions", *Colloid Journal*, Vol. 70, Iss. 2, pp. 127–133.

Akinola, T., (2004), "Pipeline Vandalization and Oil Scooping in the Niger Delta and Others" African Conservation FORUMS, http://www.africanconservation.org/ accessed in Jan, 2006

Al-Adel, S., Dick, J.A.G., El-Ghafari, R. and Servio, P. (2008), "The effect of biological and polymeric inhibitors on methane gas hydrate growth kinetics", *Fluid Phase Equilibria*, Vol. 267, Iss. 1, pp. 92-98.

Alcamo, J (1994), "IMAGE 2.0: Integrated Modelling of Global Climate Change", Special Issue of Water, Air and Soil Pollution, Vol. 76, pp. 1-2

Ali, M., and Saha, S. (2011), "Hydrogen-Bonded Large Molecular Aggregates of Charged Amphiphiles and Unusual Rheology: Photochemistry and Photophysics of Hydroxyaromatics Dopants", *In:* K. Han, G. Zhao (Eds.), Hydrogen Bonding and Transfer in the Excited State, John Wiley and Sons, U.K., pp. 711-747.

Aljourani, J., Raeissi, K., and Golozar, M.A. (2009), "Benzimidazole and its Derivatives as Corrosion Inhibitors for Mild Steel in 1M HCl Solution", *Corrosion Science*, Vol. 51, Iss. 8, pp. 1836–1843.

Al-Kady, A.S., Gaber, M., Hussein, M.M. and Ebeid, E.M. (2011), "Nanostructure-Loaded Mesoporous Silica for Controlled Release of Coumarin Derivatives: A Novel Testing of the Hyperthermia Effect", *European Journal of Pharmaceutics and Biopharmaceutics*, Vol. 77, Iss. 1, pp. 66–74.

Amao, L (2004), "ChevronTexaco Pressing Nigerian Gas Monetization Plans", Oil and Gas Journal, Nigeria, 23 Mar. 2004, http://ogje.pennnet.com/news/news_display.cfm?Section=NEWS&ArticleID=19601 accessed in Jan 2012

American Gas Association (1986), "Natural Gas Application for Air Pollution Control", Nelson E. Hay, Editor; The Fairmount Press Inc., Lilburn, Pp 1 – 41.

Anderson, R. Chapoy, A. and Tohidi, B. (2007), "Phase Relations and Binary Clathrate Hydrate Formation in the System H_2-THF-H_2O", *Langmuir*, Vol. 23, Iss. 6, pp. 3440-3444.

Atia, A.A. and Saleh, M.M. (2003), "Inhibition of Acid Corrosion of Steel using Cetylpyridinium Chloride", *J. of Applied Electrochemistry*, Vol. 33, Iss. 2, pp. 171-177.

Aw, P.K., Tan, A.L.K., Tan, T.P. and Qiu, J. (2008), "Corrosion Resistance of Tungsten Carbide Based Cermet Coatings Deposited by High Velocity Oxy-Fuel Spray Process", *Thin Solid Films*, Vol. 516, Is. 16, pp. 5710-5715.

Badiea, A.M. and Mohana, K.N. (2009), "Effects of Temperature and Fluid Velocity on Corrosion Mechanism of Low Carbon Steel in Presence of 2-Hydrazino-4,7-dimethylbenzothiazole in Industrial Water Medium", *Corrosion Science*, Vol. 51, Is. 9, pp 2231-2241.

Bai, Y. and Bai, Q. (2005), "Hydrates", Subsea Pipelines and Risers, pp. 357-382

Battelle (1996) "Economic Effects of Metallic Corrosion in the United States: A 1995 Update", Battelle Columbus Report to Specialty Steel Industry of North America, USA: Battelle Institute.

Bekki, S, Law, K.S and Pyle, J.A (1994), "Effect of Ozone Depletion on Atmospheric CH_4 and CO Concentrations", *Nature*, 371, 595-597

Bentiss, F., Traisnel, M. and Lagrenee, M. (2000), "The Substituted 1,3,4-Oxadiazoles: A New Class of Corrosion Inhibitors of Mild Steel in Acidic Media", *Corrosion Science*, Vol. 42, Iss. 1, pp. 127-146.

Bertocci, U., Koike, M., Leigh, S., Qiu, F and Yang, G (1986), "A Quasi 2-D Localized Corrosion Model", *J. Electrochem Soc.*, Vol. 133, pp. 1782-1790.

Boutoudj, M.S., Ouibrahim, A., Barbeu, F., Deslouis, C. and Martemianov, S. (2008), "Local Shear Stress Measurements with Microelectrodes in Turbulent Flow of Drag Reducing Surfactant Solutions", *Chemical Engineering and Processing: Process Intensification*, Vol. 47, Iss. 5, pp. 793-798.

Brkić, D. and Tanasković, T.I. (2008), "Systematic Approach to Natural Gas Usage for Domestic Heating in Urban Areas", *Energy*, Vol. 33, Is. 12, pp. 1738-1753

Buddy I (2004), "BPA Membership", Pipeline and Gas Technology, June 2004

Caleyo, F., Velazquez, J.C., Valor, A. and Hallen, J.M. (2009), "Markov Chain Modelling of Pitting Corrosion in Underground Pipelines", *Corrosion Science*, Vol. 51, Iss. 9, pp. 2197–2207

Cape, J.N. (2003), 'Effects of Airborne Volatile Organic Compounds on Plants", *Environmental Pollution*, Vol. 122, Iss. 1, pp. 145 – 157.

Cape, J.N., Leith, I.D., Price, D.N., Brown, A.R., and Sharpe, A.D. (2003), "Effects of VOCs on Herbaceous Plants in an Open-Top Chamber Experiment", *Environmental Pollution*, Vol. 124, Iss. 2, pp. 341 – 353.

Carrol, J.J. (2009), "Natural Gas Hydrates - A Guide for Engineers", 2nd Edition, Gulf Professional Publishing, USA.

Chaal, L., Albinet, B., Deslouis, C., Al-Janabi, Y.T., Pailleret, A. Saidani, B. and Schmitt, G. (2009), "Wall Shear Stress Mapping in the Rotating Cage Geometry and Evaluation of Drag Reduction Efficiency using an Electrochemical Method", *Corrosion Science*, Vol. 51, Is. 8, pp 1809-1816.

Chapoy, A., Haghighi, H., Burgass, R. and Tohidi, B. (2010), "Gas Hydrates in Low Water Content Gases: Experimental Measurements and Modelling using the CPA Equation of State", *Fluid Phase Equilibria*, Vol. 296, Iss. 1, pp. 9–14

CHCMT (2009), "Erosion and Cavitation Corrosions", Cli Houston Corrosion Material Technology, Texas, USA.

Chen, D and Mahadevan, S. (2008), "Chloride-induced Reinforcement Corrosion and Concrete Cracking Simulation", *Cement & Concrete Composites*, Vol. 30, Iss. 3, pp. 227–238.

Chen, H., Song, L., Wang, X., and Wang, S. (2000), "Effect of Exposure to Low Concentration of Benzene and Its Analogous on Luetal Function of Female Workers", *Wei Sheng Yan Jiu*, Vol. 29, Iss. 6, pp. 351 – 353.

Chevron Australia (2008), "Gorgon Baseline Survey", Corporate Report, Perth, Australia.

Chevron Australia (2009), "Gorgon Gas Devolopment Revised and Expanded Proposal: Barrow Island Nature Reserve." Corporate Report, Perth, Australia.

Chevron Australia (2011b), "Reservoir Carbon Dioxide Injection" Corporate Article, Perth, Australia.

Chevron Australia (2012) "Downstream: Gas Processing Facility" http://www.chevronaustralia.com/ourbusinesses/gorgon/downstream.aspx (accessed on January 19th, 2012).

Chun-Yuh, Y., Chih-Ching, C., Hung-Yi, C., Chi-Kung, H., Trong-Neng, W., and Po-Ya, C. (2004) "Increased Risk of Preterm Delivery among People Living Near the Three Oil Refineries in Taiwan", *Environment International*, Vol. 30, Iss. 3, pp. 337 – 342

Clarke, T (2001), "*Taming Africa's killer lake*", Nature, V. 409, p. 554-555, February 2001.

Clarke, T., Simonetti, F. and Cawley, P. (2010) "Guided Wave Health Monitoring of Complex Structures by Sparse Array Systems: Influence of Temperature Changes on Performance", *Journal of Sound and Vibration*, Vol. 329, Iss. 12, pp. 2306–2322

Clough Limited Australia (2012), "Gorgon DOMGAS Pipeline Installation" Accessed on 20th January, 2012 from http://www.clough.com.au/images/UpstreamOilGas/PDF/DOMGAS_Pipeline_OG193 a.pdf.

CNL (2007), "Natural Gas Operation Factsheet", Chevron (Nigeria) Limited, Lagos, Nigeria.

Colomba, L. (2010), "Gorgon Natural Gas Project", Thesis, Norwegian Institute of Science and Technology, Norway.

Cook, P.J. (2009), "Demonstration and Deployment of Carbon Dioxide Capture and Storage in Australia", *Energy Procedia*, Vol. 1, Iss. 1, pp. 3859–3866

Coombs, V. (2003), "Fire in the Oil and Gas Industry: Case Study – The Petrotrin Oil Refinery". http://www.disaster-info.net/ accessed in Jan 2010.

Cordesman, A.H. and Al-Rodhan, K.R. (2006), "The Changing Dynamics of Energy in the Middle East", 1st Edition, Greenwood Publishing Group Inc., USA. ISBN 0-275-99188-1 (set).

Cribb, R. (2003), "Danger Below: When Pipelines Go Bad", Toronto Star, Canada. Available from http://www.corrosion-club.com/pipelines.htm (accessed on July 12, 2011).

Croxford, A.J., Moll, J., Wilcox, P.D. and Michaels, J.E (2010), "Efficient Temperature Compensation Strategies for Guided Wave Structural Health Monitoring", *Ultrasonics*, Vol. 50, Iss 4-5, pp. 517–528.

CSIRO (2011), "A holistic approach to solving corrosion problems", Accessed on 24 November 2011 from http://www.csiro.au/science/Corrosion-Research.html

Cwiklik, L. and Devlin, J.P. (2010), "Hindering of Rotational Motion of Guest Molecules in the Type I Clathrate Hydrate", *Chemical Physics Letters* , Vol. 494, Iss. 4-6, pp. 206-212

Daimaru, T., Yamasaki, A., and Yanagisawa, Y. (2007), "Effect of Surfactant Carbon Chain Length on Hydrate Formation Kinetics", *Journal of Petroleum Science and Engineering*, Vol. 56, Iss. 1-3, pp. 89–96.

Das, M.C., Ghosh, S.K., Sanudo, E.C., and Bharadwaj, P.K. (2009), "Coordination polymers with pyridine-2,4,6-tricarboxylic acid and alkaline-earth/lanthanide/transition metals: synthesis and X-ray structures", *Dalton Trans*., 2009, 1644–1658

Delahaye, A., Fournaison, L., Jerbi, S. and Mayoufi, N. (2011), "Rheological Properties of CO_2 Hydrate Slurry Flow in the Presence of Additives", *Ind. Eng. Chem. Res.*, Vol. 50, Iss. 13, pp 8344–8353.

Demoz, A. and Dabros, T. (2008), "Relationship between Shear Stress on the Walls of a Pipe and an Impinging Jet", *Corrosion Science*, Vol. 50, Is. 11, pp 3241-3246.

Derbeken, J.V. (2011), "Utilities: Major PG&E Gas Line Ruptures During Hydro Test", Hearst Communications Inc., New York. Accessed on 28th December 2011 from http://articles.sfgate.com/2011-10-25/news/30322862_1_pg-e-officials-longitudinal-seam-compressor-station

Dessler, A.E (1998), "A Reexamination of the 'Stratospheric Fountain' Hypothesis", *Geophys. Res. Lett.*, Vol. 25, pp. 4165-4168

di Caprio, D., Vautrin-Ul, C., Stafiej, J., Saunier, J., Chaussé, A., Féron, D. and Badiali, J.P. (2011), "Morphology of Corroded Surfaces: Contribution of Cellular Automaton Modelling", *Corrosion Science*, Vol. 53, Iss. 1, pp. 418–425

Dickens, G (2001), "On the Fate of Past Gas: What Happens to Methane Release from a Bacterially Mediated Gas Hydrate Capacitor?", Geochem. *Geophys. Geosyst.*, 2, 2000GC000131

Doyle, J. (2002), "Riding the Dragon: Royal Dutch Shell and the Fossil Fire" Environmental Health Fund, Washington D.C. p 178

DRET (2009), "Energy in Australia", Department of Resources, Energy and Tourism, Canberra ACT 2601, Australia Government, pp 1-104

DSD (2010), "Gorgon Project Factsheet" Department of State Development, Perth, Australia.

Du, Q., Chen, Y. and Li, S. (2007), "Mathematical model for natural gas hydrate production by heat injection", *Petroleum Exploration and Development*, Vol. 34, Iss. 4, pp. 470–473, 487.

Durnie, W., De Marco, R., Jefferson, A. and Kinsella, B. (2003), "In situ SERS Study of the Adsorption of Inhibitors of Carbon Dioxide Corrosion", *Surface and Interface Analysis*, Vol. 35, Iss. 6, pp. 536-543.

Durnie, W., De Marco, R., Kinsella, B., Jefferson, A. and Pejcic, B. (2005), Predicting the Adsorption Properties of Carbon Dioxide Corrosion Inhibitors Using a Structure-Activity Relationship. *Journal of the Electrochemical Society*, Vol. 152, Iss. 1, pp. B1-B11.

EFR (2000), "PPMC Pipeline Spill Sparks Fire", ERA Field Report Number 73   Nov. 16,   2000, www.waado.org/Environment/OilFires_2000/ElumeRiverFire/ERAReport.html

Eggleston, A., Adams, J., Bushby, D., Johnston, D. and Joyce, B. (2008), "Coalition Senators' Dissenting Report", Parliament of Australia, Canberra.

Encarta, (2004), "Petroleum", Encarta Encyclopedia Photo Researchers, Microsoft Corporation, U.S.A.

Equid, D. (2008), "Challenges of the Jansz Deepwater Tieback", *Deep Offshore Technology International Conference & Exhibition*, Perth Convention Exhibition Centre, Australia, December 3-5.

Equitable (2004), "Equitable Hires Meter-reading Firm", Pipeline and Gas Technology, June 2004

EPA (1997), "Ground Transportation Industry", United States Environmental Protection Agency, EPA/310-R-97-002. USA.

ESD (2009), "Electrostatic Discharge", Glossary of ESD Terms, Accessed on 28th August, 2011 from http://www.interfacebus.com/glossary-of-terms-esd-definition.html.

Estupinan-Lopez, F.H. Almeraya-Calderon, F., Bautista Margulis, R.G., Zamora, M.A.B., Martínez-Villafane1, A., Ch., J.U. and Gaona-Tiburcio, C. (2011), "Transient Analysis of Electrochemical Noise for 316 and Duplex 2205 Stainless Steels under Pitting Corrosion", *Int. J. Electrochem. Sci.*, Vol. 6, pp. 1785 – 1796

ETF (2011), "Guided Wave –v- Smart Pigging", Corrosion Engineering Technical Support Forum and Mutual Help System for Engineering, http://www.eng-tips.com/viewthread.cfm?qid=156660. Retrieved on 16 December, 2011

Ezuber, H.M. (2009), "Influence of Temperature and Thiosulfate on the Corrosion Behavoir of Steel in Chloride Solutions Saturated in CO_2", *Materials & Design*, Vol. 30, Is. 9, pp 3420-3427.

Felder, R. and Dones, R. (2007), "Evaluation of Ecological Impacts of Synthetic Natural Gas from Wood Used in Current Heating and Car Systems", *Biomass and Bioenergy*, Vol. 31, Iss. 6, pp. 403-415

Ferronato, M., Gambolati, G., Janna, C. and Teatini, P (2010), "Geomechanical Issues of Anthropogenic CO_2 Sequestration in Exploited Gas Fields", *Energy Conversion and Management*, Vol. 51, Iss. 10, pp. 1918–1928

Fingerhut, M., and Westlake, H. (2000), "Pipeline fitness-for-purpose certification", Corrosion Prevention & Control March, pp. 3–14. Accessed on November 24, 2009 from http://www.corrosion-club.com/pipelines.htm

FLUENT Incorporated (2005), "Viscosity as a Function of Temperature", Accessed from

http://sydney.edu.au/engineering/aeromech/AMME4210/old_manuals/manuals/fluent_ help/html/ug/node300.htm on 12th December, 2011.

Frankel, G.S. and Sridhar, N. (2008), "Understanding Localized Corrosion", *Materialstoday*, Vol. 11, Iss. 10, pp. 38-44.

Fray, N., Marboeuf, U., Brissaud, O. and Schmitt, B. (2010), "Equilibrium Data of Methane, Carbon Dioxide, and Xenon Clathrate Hydrates below the Freezing Point of Water. Applications to Astrophysical Environments", *J. Chem. Eng. Data*, Vol. 55, Iss. 11, pp 5101–5108

Frignani, A. and Trabanelli, G. (1999), "Influence of Organic Additives on the Corrosion of Iron-Based Amorphous Alloys in Dilute Sulfuric Acid Solution", *CORROSION*, Vol. 55, Iss. 7, pp. 653-660.

Frostman, L.M., Thieu, V., Crosby, D.L. and Downs, H.H. (2003), "Low-Dosage Hydrate Inhibitors (LDHIs): Reducing Costs in Existing Systems and Designing for the Future", International Symposium on Oilfield Chemistry, Society of Petroleum Engineers, Houston, Texas, 5-7 February.

Fu, S.B., Cenegy, L.M. and Neff, C.S. (2001), "A Summary of Successful Field Application of a Kinetic Hydrate Inhibitor", International Symposium of Oil Field Chemistry, SPE Conference, Paper SPE 65022, Houston, Texas, Feb. 13-16.

Fuerstenau, D.W. and Jia, R. (2004), "The Adsorption of Alkylpyridinium Chlorides and Their Effect on the Interfacial Behavior of Quartz", *Colloids and Surfaces A: Physiochemical and Engineering Aspects*, Vol. 250, Iss. 1-3, pp. 223-231.

Fuglestveld, J.S, Jonson, J.E and Isaksen, I.S.A (1994), "Effects of Reduction in Stratospheric Ozone on Tropospheric Chemistry Through Changes in Photolysis Rates", *Tellus*, Vol. 46B, pp. 172-192

Fung, I, John, J, Lerner, J, Matthew, E, Prather, M, Steeler, L.P and Fraser, P.J (1991), "Three-Dimensional Model Synthesis of the Global Methane Cycle", *J. Geophys. Res.*, Vol. 96, pp. 13033-13065

Gabrielli, C., Huet, F., Keddam, M., and Oltra (1990), "Application of Phase Shifting Interferential Microscopy to Pitting Corrosion", *CORROSION*, Vol. 46, Iss. 4, 266-278

Gabrielli, C., and Keddam, M., (1992), "Quantitative Evaluation of General Corrosion of Type-304 Stainless Steel in Subcritical and Supercritical Aqueous Solutions via Electrochemical Noise Analysis", *CORROSION*, Vol. 48, 794-802.

GAEI (2009), "Workplace Health and Safety Bulletin – Hydrogen Sulphide at the Work Site" Document, CH 029, Government of Alberta, Employment and Immigration, Canada, pp 1-17. Accessed online on 20-12-09 from http://employment.alberta.ca/documents/WHS/WHS-PUB_ch029.pdf.

Gamo, M., Oka, T., and Nakanishi, J. (2003), "Ranking the Risks of 12 Major Environmental Pollutants that Occur in Japan", *Chemosphere*, Vol. 53, Iss. 4, pp. 277 − 284.

Ganji, H., Manteghian, M. And Mofrad, H.R. (2007), "Effect of Mixed Compounds on Methane Hydrate Formation and Dissociation Rates and Storage Capacity", *Fuel Processing Technology*, Vol. 88, Iss. 9, pp. 891-895.

Gao, S. (2009), "Hydrate Risk Management at High Watercuts with Anti-agglomerant Hydrate Inhibitors", *Energy & Fuels*, Vol. 23, pp. 2118–2121

Gazzard, J. (2008a), "Aviation and climate change: Can alternative fuel save the day?", Aviation Environment Federation, London, UK.

Gazzard, J. (2008b), "Pros and contrails", Aerospace Testing International, UKIP Media & Events Abinger House, Dorking Surrey, United Kingdom

Garbatov, Y, ,Soares, C.G, and Wang, G (2005), "Non-linear Time Depandent Corrosion Wastage of Deck Plates of Ballast and Cargo Tanks of Tankers", *Proceedings of the 24th International Conference on Offshore Mechanics and Arctic Engineering*, ASME, Paper OMAE2005-67579.

Gaverick, L. (1994), "Corrosion in the Petrochemical Industry", 1st Edition, *ASM International*, Metal Park, Ohio, USA.

Gayet, P., Dicharry, C., Marion, G., Graciaa, A., Lachaise, J. and Nesterov, A. (2005), "Experimental Determination of Methane Hydrate Dissociation Curve up to 55 MPa by using a Small Amount of Surfactant as Hydrate Promoter", *Chemical Engineering Science*, Vol. 60, Iss. 21, pp. 5751-5758

Gbaruko, B.C., Igwe, J.C., Gbaruko, P.N. and Nwokeoma, R.C. (2007), "Gas Hydrates and Clathrates: Flow Assurance, Environmental and Economic Perspectives and the Nigerian Liquified Natural Gas Project", *Journal of Petroleum Science and Engineering*, Vol. 56, Is. 1-3, pp. 192-198

Gbenga Biobaku & Co. (2008), "Investing in Nigeria's Oil and Gas Industry", Babafemi Osoba Crescent, Victoria Island, Lagos, Nigeria.

Geesey, G.G. (1991), "Biofouling and Biocorrosion in Industrial Water Systems", Springer-Verlag, Berlin, pp. 1-220

Gelb, B.A. (2006), "Russian Oil and Gas Challenges", Congressional Research Service, Report Order Code RL 33212, Washington, USA, pp. 1-15

Ginzel, R.K. and Kanters, W.A. (2002), "Pipeline Corrosion and Cracking and the Associated Calibration Considerations for Same Side Sizing Applications", *The e-Journal of Nondestructive Testing*, Canada, Vol 7, No7.

Grigoryan, S., A. Manukyan, A. Hayrapetyan, A. Arzumanyan, A. Kuzanyan, Y. Kafadaryan, and E. Vardanyan, E. (2003), "A New Way of Preparing the Y-Ba-Cu-O High Temperature Superconductor Using the Sol-Gel Method", *Superconductor Science and Technology*, Vol. 16, pp 1202-1206.

Gonzalez-Rodriguez, J.G., Mejia, E., Rosales, I., Salinas-Bravo, V.M., Rosas, G., and MArtinez-Villafañe, A. (2008), "Effect of Heat Treatment and Chemical Composition on the Corrosion Behavoiur of Ni-Al Intermetallics in Molten (Li+K) Carbonate", *Journal of Power Sources*, Vol. 176, Issue 1, pp. 215-221.

GreenAir (2009), "The search for alternative aviation fuels: understanding the challenge", Greenair Communications, London, U.K.

Groundwork (2003), "Shell International's Legacy of Pollution and Damage", Pietermaritzburg, South Africa. http://www.groundwork.org.za/Pamphlets/Shell.htm

Gudmundsson, J.S. and Børrehaug, A. (1996), "Frozen Hydrate for Transportation of Natural Gas", *2nd International Conference on Natural Gas Hydrate*, Toulouse, France, June 2-6, pp. 415-422.

Gunaltun, Y.M. (1996), "Integrated CO_2 Corrosion-Multiphase Flow Model", *CORROSION*, Paper No. 27, NACE International, Houston, Texas.

Guo, X.J., Gao, K.W., Qiao, L.J. and Chu, W.Y. (2002), "The Correspondence between Susceptiblity to SCC of Brass and Corrosion-Induced Tensile Stress with Various pH Values", *Corrosion Science*, Vol. 44, Is. 10, pp 2367-2378

Hadler, A.B., Ott, L.S. and Bruno, T.J. (2009), "Study of azeotropic mixtures with the advanced distillation curve approach", *Fluid Phase Equilibria*, Vol. 281, Iss. 1, pp. 49-59

Hamdy, A.S. (2008), "The Effect of Surface Modification and Stannate Concentration on the Corrosion Protection Performance of Magnesium Alloys", *Surface and Coatings Technology*, Vol. 203, Is. 3-4, pp. 240-249.

Hao, Y., Bo, Q. and Chen, Y (2006), "Laboratory investigation of pressure development of natural gas hydrates", *Petroleum Exploration and Development*, Vol. 33, Iss. 2, pp. 217–220.

Hara, K., Baden, N. and Kajimoto, O. (2004), "Pressure Effect on Water Solvation Dynamics in Micellar Media", *Journal of Physics: Condensed Matter*, Vol. 16, Iss. 14, pp. 1207–1214.

Harun, A.F., and Watt, N. (2009), "Bringing the 1st BP Operated Subsea to Shore Gas Field into Production: Flow Assurance Lessons Learned", *Asia Pacific Oil and Gas Conference & Exhibition*, Society of Petroleum Engineers, Jakarta, Indonesia, 4-6 August.

Hashimoto, M., Miyajima, S. and Murata, T. (1992), "An Experimental Study of Potential Fluctuation during Passive Film Breakdown and Repair on Iron", *Corrosion Science*, Vol. 33 Iss. 66, pp. 905-915.

Hashimoto, S, Murayama, S., Sugahara, T., Sato, H., and Kazunari Ohgaki, K. (2006), "Thermodynamic and Raman spectroscopic studies on H_2+tetrahydrofuran+water and H_2+ tetra-n-butyl ammonium bromide+water mixtures containing gas hydrates", *Chemical Engineering Science*, Vol. 61, Iss. 24, pp. 7884-7888

Hein, R, Crutzen, P.J and Heinmann, M (1997), "An Inverse Modeling Approach to Investigate the Global Atmospheric Methane Cycle", *Global Biogeochem. Cycles*, Vol. 11, pp. 43-76

Heppner, K.L. and Evitts, R.W. (2008), "Modelling of the Effect of Hydrogen ion on the Crevice Corrosion of Titanium", *Environment-Induced Cracking of Materials*, pp 95-104.

HGMCE (2004), "Glossary of Corrosion Related Terms", The Hendrix Group: Material and Corrosion Engineers, http://www.hghouston.com/c.html, Retrieved on 16 Jan, 2010.

Hill, Z (2005), "LNG Will Supply More Than 20% of US Gas by 2025", *NAFTA Journal*, Year 56, No 6, pp 220

Hook, M., R. Hirsch, R. and K. Aleklett. K. (2009), "Giant Oil Field Decline Rates and their Influence on World Oil Production", *Energy Policy*, Vol. 37, Iss. 6, pp. 2262-2272.

Hosa, A., Esentia, M., Stewart, J. and Haszeldine, S. (2011), "Injection of CO_2 into Saline Formations: Benchmarking Worldwide Projects", *Chemical Engineering Research and Design*, Vol. 89, Iss. 9, pp. 1855-1864

Houweling, S, Kaminski, T, Dentener, F, Lelieveld, J and Heinmann, M (1999), "Inverse Modeling of Methane Sources and Sinks Using the Adjoint of a Global Transport Model", *J.Geophys. Res.*, Vol. 104, pp. 26137-26160

Huang, Y. and Ji, D. (2008), "Experimental Study on Seawater-Pipeline Internal Corrosion Monitoring System", *Sensors and Actuators B*, Vol. 135, Iss. 1, pp 375–380

Huang, B.X., Xue, W.C., Wang, Y.Z. and Zhang, T. (2012), "Review of Theory and Practice on Natural Gas Hydrate", *Advanced Material Research*, Vol. 361-363, pp. 149-160

Huang, C., Chen, C. H., Li, L., Cheng, Z., Wang, H.L., Huang, H.Y., Streets, D.G, Wang, Y.J, Zhang, G.F. and Chen, Y. R. (2011), "Emission inventory of anthropogenic air pollutants and VOC species in the Yangtze River Delta region, China", *Atmospheric Chemistry and Physics*, Vol. 11, pp. 4105–4120

Hunt, D., Akindeju, M.K., Obanijesu, E.O., Pareek, V. and Tade, M.O. (2011), "Potential Impacts and Modeling the Heat Value Loss Due to Chelation in Natural Gas Processing and Transport" *Elsevier 21ˢᵗ European Symposium on Computer-Aided Process Engineering*, (Part B), pp. 1573-1577

Huntsman (2010), "Chemical Types by Surfactant Class", Huntsman Performance Products, Woodloch Forest Drive, Woodlands, TX, USA.

IEA (2001), "World Energy Outlook – 2001 Insights, Assessing Today's Supplies to Fuel Tomorrow's Growth", International Energy Agency, October 2001

IEA (2010), International Enery Agency, "Key World Energy Statistics". Paris: SOREGRAPH.

ILZRO (2009), "Fretting Corrosion (Transit Abrasion) on Galvanized Sheet", The International Lead Zinc Research Organization, Durham, North California, USA.

Imperial Venture Corp (1998), "Natural Gas Utilization Study: Offshore Newfoundland", A Report Prepared for Atlantic Canada Opportunity Agencies and Newfoundland Oceanic Industies Association, pp 1-85

IPCC Climate Change (2001): Mitigation. A Report of Working Group III of the Intergovernmental panel on Climate Change. Sixth Session held in Accra, Ghana.

Itakura, M.; Kaburaki, H.; Arakawa, C. (2005), "Branching mechanism of intergranular crack propagation in three dimensions", *Phys. Rev.*, Vol. 71, Issue 5, pp 5102 -5105.

Ivanov, L., Spencer, J. and Wang, G. (2003), "Probabilistic Evaluation of Hull Structure Renewals for Aging Ships", *Proceedings of the 8ᵗʰ International Marine Design Conference* (IMDC), Athens, Greece, 5-8 May, pp 393-406

Jacobs, S, (2002), "Pipeline Factors Affecting Gasoline Prices", Federal Trade Commission Conference, Washington DC, May 8-9, 2002, pp. 1-23.

Jacobson, L.C. and Molinero, V. (2010), "A Methane-Water Model for Coarse-Grained Simulations of Solutions and Clathrate Hydrates", *J. Phys. Chem*. Vol. 114, pp. 7302–7311

Janovic, Z (2005), "Oil and Petrochemical Processes and Products", Hrvatsko, drustvo za goriva I maziva, Zagreb, Croatia, pp 1-427

Jassim, E. and Abdi, M.A. (2008), "A CFD-Based Model to Locate Flow Restriction Induced Hydrate Deposition in Pipelines", Manuscript OTC 19190, *Offshore Technology Conference*, Houston, Texas, USA, 5-8 May, 2008

Javanmardi, J., Nasrifar, K. and Moshfeghian, M. (2004), "Economic Evaluation of Natural Gas Hydrate as an Alternative for Natural Gas Transportation", *GPA-GCC Chapter-12th Technical Conference*, World Petroleum Congress, Kuwait, May 5th, pp. 1-14

Joelsson, A. and Gustavsson, L. (2009), "District Heating and Energy Efficiency in Detached Houses of Differing Size and Construction", *Applied Energy*, Vol. 86, Is. 2, pp. 126-134

Johnson, R.L., Thoms, R.B., and Zogorski, J.J. (2003), "Effects of Daily Precipitation and Evapotranspiration Patterns on Flow and VOC Transport to Groundwater along a Watershed Flow Path", *Environ Sci. Technol*, Vol. 37, Iss. 21, pp. 4944 – 4954.

Kamimura, A, Guerra, S.M.G. and Sauer, I.L. (2006), "On the Substitution of Energy Sources: Prospective of the Natural Gas Market Share in the Brazilian Urban Transportation and Dwelling Sectors", *Energy Policy*, Vol. 34, Is. 18, pp. 3583-3590

Kandepi, V.V. and Narender, N. (2012), "Synthesis of N-heterocyclic Compounds over Zeolite Molecular Sieve Catalysts: An Approach Towards Green Chemistry", Catalysis Science & Technology, Manuscript accepted for publication and available online at http://pubs.rsc.org/en/content/articlepdf/2012/cy/c2cy00162d

Kang, S. and Wang, J. (2010), "Kinetic Behaviors of CO_2 Hydrates in Porous Media and Effect of Kinetic Promoter on the Formation Kinetics", *Chemical Engineering Science*, Vol. 65, Iss 5, pp. 1840–1845

Karaaslan, U. and Parlaktuna, M. (2000), "Surfactants as Hydrate Promoters?", *Energy & Fuels*, Vol. 14, Iss. 5, pp. 1103-1107

Karimi, A. and Abdi, M.A. (2009), "Selective Dehydration of High-Pressure Natural Gas using Supersonic Nozzles", *Chemical Engineering and Processing: Process Intensification*, Vol. 48, Is. 1, pp. 560-568.

Kelland, M.A., Monig, K., Iversen, J. E. and Lekvam, K (2008), "Feasibility Study for the Use of Kinetic Hydrate Inhibitors in Deep-Water Drilling Fluids", *Energy & Fuels*, Vol. *22*, Iss. 4, pp 2405–2410

Kennell, G.F. and Evitts, R.W. (2009), "Crevice Corrosion Cathodic Reactions and Crevice Scaling Laws", *Electrochimica Acta*, Vol. 54, Is. 20, pp 4696-4703.

Kester, D. (1975), "Dissolved Gases Other Than CO_2", Chemical Oceanography, Vol. 1, 2nd Edition, J.P Riley and Skirrow, G. (Editors), Academy Press, New York, pp. 497 - 556.

Khaled, K.F., Babić-Samardžija, K. and Hackerman, N. (2005), "Theoretical Study of the Structural Effects of Polymethylene Amines on Corrosion Inhibition of Iron in Acid Solutions", *Electrochimica Acta*, Vol. 50, Iss. 12, pp. 2515–2520

Kim, H., Annabel, M.D., and Rao, P.S. (2001), "Gaseous Transport of Volatile Organic Chemicals in Unsaturated Porous Media: Effect of Water-Partitioning and Air-Water Interfacial Adsorption", *Environ. Sci. Technol.*, Vol. 35, Iss. 22, pp. 4457 – 4462.

Klerke, A., Christensen, C.H., Norskov, J.K. and Vegge, T. (2008), "Ammonia for hydrogen storage: challenges and opportunities", *Journal of Materials Chemistry*, Vol. 18, Iss. 20, pp. 2304-2310

Konstantinidis, G., Drinkwater, B.W. and Wilcox, P.D. (2006), "The Temperature Stability of Guided Wave Structural Health Monitoring Systems", *Smart Mater. Struct.*, Vol. 15, No. 4, pp. 967–976

Korotkikh, O.P. and Kochurova, N.N. (2006), "Micelle Formation in Aqueous Dodecylpyridinium Chloride", *Russian Journal of Applied Chemistry*, Vol. 79, No. 7, pp. 1204 - 1206.

Krishnan, V., Bharani, S., Kapat, J.S, Sohn, Y.H. and Desai, V.H. (2008), "A Simplistic Model to Study the Influence of Film Cooling on Low Temperature Hot

Corrosion Rate in Coal Gas/Syngas Fired Gas Turbines", *International Journal of Heat and Mass Transfer*, Vol. 51, Is. 5-6, pp. 1049-1060.

KSC (2009), "Uniform Corrosion", Corrosion Technology Laboratory, Kennedy Space Centre, NASA, USA.

Lain, S., Broder, D., Sommerfeld, M. and Goz, M.F. (2002), "Modelling hydrodynamics and turbulence in a bubble column using the Euler–Lagrange procedure", *International Journal of Multiphase Flow*, Vol. 28, Iss. 8, pp. 1381–1407

Lau, N.T., Chan, C.K., Chan, L.I., and Fang, M. (2008), "A Microscopic Study of the Effects of Particle Size and Composition of Atmospheric Aerosols on the Corrosion of Mild Steel Corrosion", *Corrosion Science*, Vol. 50, Is. 10, pp. 2927-2933

Lelieveld, J, Crutzen, P.J and Dentener, F.J (1998), "Changing Concentration, Lifetime and Climate Forcing of Atmospheric Methane", *Tellus*, Vol. 50B, pp. 128-150

Li, B., Li, W., Ye, L., Hou, G.F. and Wu, L.X. (2010), "Metal-Organic Compounds: Poly[di-l2-aqua-l4-chlorido-l4-(2-mercaptopyrimidine-4,6-diolatoj4O:O:O0:O0)-disodium(I)]", *Acta Cryst.,* Vol. E66, pp. 1-5

Li, S., Fan, S., Wang, J., Lang, X. and Wang, Y. (2010), "Semiclathrate Hydrate Phase Equilibria for CO_2 in the Presence of Tetra-n-butyl Ammonium Halide (Bromide, Chloride, or Fluoride)", *J. Chem. Eng. Data*, Vol. 55, Iss. 9, pp 3212–3215

Li, X.S., Xia, Z.M., Chen, Z.Y., Yan, K.F., Li, G. and Wu, H.J. (2010c), "Equilibrium Hydrate Formation Conditions for the Mixtures of CO_2 + H_2 +Tetrabutyl Ammonium Bromide", *J. Chem. Eng. Data*, Vol. 55, pp. 2180–2184

Li, Y. and Duan, Y. (2012), "Treatment of Wastewater Containing High Concentration Ammonia-Nitrogen by Electrochemical Oxidation Process", *Advanced Materials Research*, Vols. 393-395, pp. 1587-1590

Liang, S. and Kusalik, P.G. (2010), "Explorations of Gas Hydrate Crystal Growth by Molecular Simulations", *Chemical Physics Letters*, Vol. 494, Iss. 4-6, pp 123-133

Lide, D.R (2006), "CRC Handbook of Chemistry and Physics" 87th Edition, CRC Press Inc, Boca Raton, Fl, U.S.A.

Likhanova, N. V., Dominguez-Aguilar, M. A., Olivares-Xometi, O. and Nava-Entzana, N. (2010), "The Effect of Ionic Liquids with Imidazolium and Pyridinium Cations on the Corrosion Inhibition of Mild Steel in Acidic Environment", *Corrosion Science*, Vol. 52, Iss. 6, pp. 2088-2097.

Lima, M.C.P., Coutinho, K., Canuto, S. and Rocha, W.R. (2006), "Reaction Mechanism and Tautomeric Equilibrium of 2-Mercaptopyrimidine in the Gas Phase and in Aqueous Solution: A Combined Monte Carlo and Quantum Mechanics Study", *J. Phys. Chem.*, Vol. 110, Iss. 22, pp. 7253-7261.

Little, B.J. and Lee, J.S. (2009), "Microbiologically Influenced Corrosion", Kirk-Othmer Encyclopedia of Chemical Technology, John Wiley & Sons, Inc., pp. 1-3

Liu, T. and Weyers, R.W. (1998), "Modeling the Dynamic Corrosion Process in Chloride Contaminated Concrete Structures", *Cement and Concrete Research*, Vol. 28, No. 3, pp. 365–379

Liu, Y., Liu, X. and Liu, D. (2007), "Applications of geophysical techniques to gas hydrate prediction", *Petroleum Exploration and Development*, Vol. 34, Iss. 5, pp. 566–573

Logan, F. (2008) "Opening Statement to the Senate Standing Economics Committee" on Inquiry into Matters Relating to the Gas Explosion at Varanus Island, Perth, Australia.

Lopez, D. A., Perez, T. and Simison, S. N. (2003), "The Influence of Microstructure and Chemical Composition of Carbon and Low Alloy Steels in CO_2 Corrosion: A State of the Art Appraisal", *Materials and Design*, Vol. 24, Iss. 8, pp. 561-575.

Lorenzo, M.D. (2009), "The Hydra Flow Loop: A Tool for Testing the Hydrates Behavior in Gas Pipelines", R & D Seminar Organized by National Research Flagship/Commonwealth Scientific and Industrial Research Organization (CSIRO), Australian Resources Research Center Building, Perth, Australia

Loto, C.A. (2012), "Electrode Potential Evaluation of Effect of Inhibitors on the Electrochemical Corrosion Behaviour of Mild Steel Reinforcement in Concrete in H_2SO_4", *J. Mater. Environ. Sci.*, Vol. 3, Iss. 1, pp. 195-205

Ma, C.F., Chen, G.J., Wang, F., Sun, C.Y. and Guo, T.M. (2001), "Hydrate Formation of (CH_4+C_2H_4) and (CH_4+$C3H_6$) Gas Mixtures", *Fluid Phase Equilibria*, Vol. 191, pp. 41-47

Ma, C., Shi, Y. and Jiang, Q. (2005), "Syntheses, Characterizations and Crystal Structures of New Triorganotin Complexes with 2-Mercaptopyrimidine and 4-amino-2-mercaptopyrimidine", *Heteroatom Chemistry*, Vol. 16, Iss. 1, pp. 69-75

Mahajan, D., Taylor, C.E. and Mansoori, G.A. (2007), "An Introduction to Natural Gas Hydrate/Clathrate: The Major Organic Carbon Reserve of the Earth", *Journal of Petroleum Science and Engineering*, Vol. 56, Iss. 1-3, pp. 1–8.

Mahgerefteh, H, Saha, P. and Economou, I.G (1997). "A Study of the Dynamic Response of Emergency Shutdown Valves following Full Bore Rupture of Gas Pipelines", *Trans IchemE*, Vol. 75 (b), pp. 201-209

Mahgerefteh, H., Jalali, N. and Fernandez, M.I. (2011), "When Does a Vessel Become a Pipe?", *AIChE J*, Vol. 57, No. 12, pp. 3305-3314.

Mahmut, K.A. (2005), "Major Utilization of Natural Gas in Turkey", *Energy Exploration and Exploitation*, Vol. 23, No. 2, Issue 16, Multi-Science Publishing Co. Ltd, pp. 125-140 (16)

Maier, N., Nickel, K.G. and Rixecker, G. (2007), "High Temperature Water Vapor Corrosion of Rare Earth Disilicates (Y, Yb, Lu)$_2$ Si_2O_7 in the Presence of $Al(OH)_3$ Impurities", *Journal of the European Ceramic Society*, Vol. 27, Issue 7, pp 2705-2713

Mainusch, S., Peter, C.J., de Swaan, A.J., Javanmardi, J. and Moshfeghian, M. (1997), "Experimental Determination and Modelling of Methane Hydrates in Mixtures of Acetone and Water", *J. Chem. Eng. Data*, Vol. 42, pp. 948-950

Makino, T., Yamamoto, T., Nagata, K., Sakamoto, H., Hashimoto, S., Sugahara, T. and Ohgaki, K. (2010), "Thermodynamic Stabilities of Tetra-n-butyl Ammonium Chloride + H_2, N_2, CH_4, CO_2, or C_2H_6 Semiclathrate Hydrate Systems", *J. of Chem. Eng. Data*, Vol. 55, Iss. 2, pp 839–841

Makogon, Y. F. 1997. Hydrates of hydrocarbons: Pennwell Corp.

Mandal, A. and Laik, S. (2008), "Effect of the Promoter on Gas Hydrate Formation and Dissociation", *Energy & Fuels*, Vol. 22, Iss. 4, pp. 2527–2532

Marco, R.D., Durnie, W., Jefferson, A. and Kinsella, B. (2001), "Surface Analysis of Adsorbed Carbon Dioxide Corrosion Inhibitors", *Corrosion Science Section, NACE International*, Vol. 57, No.1, pp. 9-18

Martın, A. and Peters, C.J (2009), "Hydrogen Storage in sH Clathrate Hydrates: Thermodynamic Model", *J. Phys. Chem*. Vol. B 2009, Iss. 113, pp. 7558–7563

Matranga, K.R., Myers, A.L. and Glandt, E.D. (1992), "Storage of Natural Gas by Adsorption on Activated Carbon", *Chemical Engineering Science*, Vol. 47, Iss. 7, pp. 1569-1579

Mathiesen, T., Nielsen, T.S., Haugen, T., Espelid, B., Hummelgaard, P. and Vilpponen, K. (2004), "Improved Method for ASTM G48 Corrosion Testing of Welds", NT Technical Report, Report No. TR 548, Nordic Innovation Centre, Oslo, Norway, pp. 1-58.

Megraud, F., Neman-Simha, V. and Brugmann, D. (1992), "Further evidence of the toxic effect of ammonia produced by Helicobacter pylori urease on human epithelial cells", *Infect Immun*., Vol. 60, Iss. 5, pp. 1858-1863

Mehrian, T., de Keizer, A., Korteweg, A.J. and Lyklema, J. (1993), "Thermodynamics of Adsorption of Dodecylpyridinium Chloride on Na-kaolinite", *Colloids and Surfaces A: Physicochemical and Engineering Aspects*, Vol. 73, pp 133-143.

Melchers, R. (2001), "Probabilistic Model of Corrosion for Reliability Assessment and Maintenance Planning", *Proceedings of the 20th International Conference on Offshore Mechanics and Arctic Engineering*, OMAE2001/S&R-2108

Melchers, R. (2003a), "Modeling of Marine Immersion Corrosion for Mild and Low alloy Steels – Part 1 Phenomenological Model", *CORROSION*, Vol. 59, Iss 4, pp. 319-334

Melchers, R. (2003b), "Mathematical Modeling of the Diffusion Controlled Phase in Marine Immersion Corrosion of Mild Steel", *Corrosion Science*, Vol. 45, Iss. 5, pp. 923-940

Melchers, R. (2003c), "Effect on Marine Immersion Corrosion of Carbon Content of Low Alloyed Steels", *Corrosion Science*, Vol. 45, Iss. 11, 2609-2625

Meng, H., Hu, X. and Neville, A (2007), "A Systematic Erosion-Corrosion Study of Two Stainless Steels in Marine Conditions via Experimental Design", *Wear*, Vol. 263, Is. 1-6, pp 355-362.

Mercier, D. and Barthés-Labrousse, M.G. (2009), "The role of chelating agents on the corrosion mechanisms of aluminium in alkaline aqueous solutions", *Corrosion Science*, Vol. 51, pp 339-348.

Metha, S.K., Bhasin, K.K., Chauhan, R. and Dham, S. (2005), "Effect of Temperature on Critical Micelle Concentration and Thermodynamic Behavior of Dodecyldimethylethylammonium Bromide and Dodecyltrimethylammonium chloride in Aqueous Media", *Colloids and Surfaces A: Physicochemical and Engineering Aspects*, Vol. 255, Iss. 1-3, pp. 153-157

MetOcean. Final MetOcean Design Criteria Gorgon MOG and Revised Export Jetty Corporate, Perth, Western Australia: *MetOcean*, 2006.

Miah, R. and Ohsaka, T. (2009), "Kinetics of Oxygen Reduction Reaction at Tin-Adatom-Modified Gold Electrodes in Acidic Media", *Electrochimica Acta*, Vol. 54, Is. 24, pp 5871-5876.

Mochizuki, M. (2007), "Control of Welding Residual Stress for Ensuring Integrity against Fatigue and Stress–Corrosion Cracking", *Nuclear Engineering and Design*, Vol. 237, Iss. 2, pp. 107–123

Mokhatab, S., W. A. Poe, and J. G. Speight. 2006. Handbook of Natural Gas Transmission and Processing. Edited by M. Saeid, A. P. William and G. S. James. Burlington: Gulf Professional Publishing.

Montemor, M.F., Pinto, R. and Ferreira, M.G.S. (2009), "Chemical Composition and Corrosion Protection of Silane Films Modified with CeO_2 Nanoparticles", *Electrochimica Acta*, Vol. 54, Is. 22, pp. 5179-5189

Montesperelli, G. and Gusmano, G. (2011), "Electrochemical Noise for Corrosion Detection", *Corrosion Reviews*, Vol 29, Iss.5-6, pp. 247–252

Moon, C., Taylor, P.C., and Rodger, P.M. (2003), "Molecular Dynamics Study of Gas Hydrate Formation", *American Chemical Society*, Vol. 125, Iss. 16, 4706-4707

Moraveji, M.K., Sadeghi, A., Fazlali, A. and Davarnejad, R. (2010), "Effect of an Anionic Surfactant on the Methane Hydrate Formation: Induction Time and Stability", *World Applied Science Journal*, Vol. 9, Iss. 10, pp. 1121-1128.

Morikawa, T. (2008), "Natural Gas and LNG Supply/Demand Trends in Asia Pacific and Atlantic Markets", Report FY2007, *The Institute of Energy Economic*, Japan, pp. 1-28

Mote, P.W, Dunkerton, T.J, McIntyre, M.E, Ray, E.A, Haynes, P.H and Russel, J.M (1998), "Vertical Velocity, Vertical Diffusion and Dilution by Midlatitude Air in the Tropical Lower Stratosphere", *J. Geophys. Res.*, 103, 8651-8666

Moudrakovski, I.L., Ratcliffe, C.I., McLaurin, G.E, Simard, B. and Ripmeester, J.A. (1999), "Hydrate Layers on Ice Particles and Superheated Ice: A ^{1}H NMR Microimaging Study", *J. Phys. Chem. A*, Vol. 103, Iss. 26, pp 4969–4972

Moyer, E.J, Irion, F.W, Yung, Y.L and Gunson, M.R (1996), "ATMO Stratospheric Deuterated Water and Implications for Troposhere-Stratosphere Transport", *Geophys. Res. Lett.*, 23, 2385-2388

MSDS (2009), "Instant FAME/Instant Anaerobe Methods - Methanol", Section 1 – Chemical Product and Company Identification, *Material Safety Data Sheet*, 19th June, pp. 1-6

Muller, B. and Fischer, S. (2006), "Epoxy Ester Resins as Corrosion Inhibitors for Aluminium and Zinc Pigments", *Corrosion Science*, Vol. 48, Iss. 9, pp. 2406–2416

Murakani, K. (2004), "Complex Formation between Dodecylpyridinium Chloride and Multicharged Anionic Planar Substances", *Langmuir*, Vol. 20, Iss. 19, pp. 8183-8191

Nakajima, A, Doi, Y, Fuchigami, T and Tajima, T. (2008), "Indirect Anodic Oxidation Based on the Cation Exchange Reaction between (Earth) Metal Halides and Solid-Supported Acids", *Journal of Electroanalytical Chemistry*, Vol. 623, Is. 2, 15 pp 177-180.

Nakajima, A. and Tajima, T (2009), "Anodic Oxidation of Organic Compounds Based on the Cation Exchange Reaction between KBF4 and Solid-Supported Acids", *Electrochemistry Communications*, Vol. 11, Is. 2, pp 305-308.

Nandeesh, L.S. and Sheshadri, B.S. (1991), "Inhibitory Effect of 2-Mercapto Pyrimidine on Corrosion of Copper Single Crystal Planes in $0·1$ M H_2SO_4", *Journal of Chemical Sciences,* Vol. 103, No. 6, pp. 763-775.

NEGTAP (2001) "Transboundary Air Pollution: Acidification Eutrophication and Ground-Level Ozone in the UK", National Expert Group on Transboundary Air Pollution, Department for Environment, Food and Rural Affairs (DEFRA), UK, pp 1

Nesic, S, Xiao, Y. and Pots, B.F.M. (2004), "A Quasi 2-D Localized Corrosion Model", *CORROSION*, NACE, Paper No. 04628, Houston, Texas, pp 1-16

Netto, T.A., Ferraz, U.S. and Botto, A. (2007), "On the Effect of Corrosion Defects on the Collapse Pressure of Pipelines", *International Journal of Solids and Structures*, Volume 44, Issues 22-23, November 2007, Pages 7597-7614

Netto, T.A. (2009), "On the Effect of Narrow and Long Corrosion Defects on the Collapse Pressure of Pipelines", *Applied Ocean Research*, Vol. 31, Iss. 2, pp. 75-81

NG (2011), "The Transportation of Natural Gas", Natural Gas.Org, Accessed on 25th October 2011 from http://www.naturalgas.org/naturalgas/transport.asp

Niklasson, A., Johansson, L. and Svensson, J. (2008), "The Influence of Relative Humidity and Temperature on the Acetic Acid Vapour-Induced Atmospheric Corrosion of Lead", *Corrosion Science*, Vol. 50, Is. 11, pp 3031-3037.

Niu, L. and Cheng, Y.F (2008), "Synergestic Effects of Fluid Flow and Sand Particles on Erosion-Corrosion of Aluminum in Ethylene Glycol-Water Solution", *Wear*, Vol. 265, Is. 3-4, pp. 367-374.

NORSORK STANDARD (2005), "CO_2 Corrosion Rate Calculation Model", Norwegian Technological Standards Institute, Oscarsgt. 20, Majorstural, NORWAY.

NPF (2011a), "Factors Affecting General Corrosion Rate", Nuclear Power Fundamentals, Integrated Publishing, http://www.tpub.com/content/doe/h1015v1/css/h1015v1_115.htm, Retrieved on 16 Dec., 2011

NPF (2011b), "Effect of pH on the Corrosion Rate of Iron in Water", Integrated Publishing, http://www.tpub.com/content/doe/h1015v1/css/h1015v1_117.htm, Retrieved on 16 Dec., 2011.

Nyborg, R. (2010), "CO_2 Corrosion Models for Oil and Gas Production Systems", *Corrosion 2010 Conference & Expo*, NACE International, San Antonio, TX, March 14 - 18, Paper No. 10371, pp. 1-20

Obanijesu, E.O. and Sonibare, J.A. (2005), "Natural Gas Flaring and Environmental Protection in Nigeria", *NAFTA Journal*, Year 56, No 7, pp 287-294

Obanijesu, E.O., Sonibare, J.A., Bello, O.O., Akeredolu, F.A. and Macaulay, S.R.A. (2006), "The Impact of Pipeline Failures on the Oil and Gas Industry in Nigeria", *Engineering Journal of University of Qatar*, Qatar, Vol. 19, pp 1-12

Obanijesu, E.O. and Mosobalaje, O.O. (2008), "Concentration Profile Simulation on Natural Gas Accidental Release from a Submerged Offshore Pipeline", *NAFTA Journal*, Year 59, No 9, pp 419-431

Obanijesu, E.O. (2009), "Modeling the H_2S Contribution in Corrosion Rate of Natural Gas Pipeline", *Energy Sources Part A: Recovery, Utilization and Environmental Effects*, Vol. 31, Iss. 4, pp 348-363

Obanijesu, E.O. and Macaulay, S.R.A. (2009), "West African Gas Pipeline (WAGP) Project: Associated Problems and Possible Remedies", E.K Yanful (Ed), *Chapter 2, Appropriate Technology for Environmental Protection in the Developing World*, Springer Books, Netherlands, pp 101–112

Obanijesu, E.O. and Omidiora, E.O. (2009), "Velocity Profile Simulation for Natural Gas underneath Waterbody following a Full-Bore Rupture of an Offshore Pipeline", *NAFTA Journal*, Year 60, No 11, pp 610-614.

Obanijesu, E.O., Pareek, V. and Tade, M.O. (2010a), "Hydrate Formation and its Influence on Natural Gas Pipeline Internal Corrosion Rate", SPE-128544, *Asia-Pacific Oil and Gas Conference and Exhibition*, Society of Petroleum Engineers, Mumbai, India, January 20-22.

Obanijesu, E.O., Pareek, V., Gubner, R and Tade, M.O. (2010b), "Corrosion Education as a Tool for the Survival of Natural Gas Industry", *NAFTA Journal*, Year 61, No 12, pp 541-554.

Obanijesu, E.O., Pareek, V., Gubner, and Tade, M.O. (2010c), "Corrosion Education as a Tool for the Survival of Natural Gas Industry", <u>*Presented during Research & Development Seminar*</u>, Curtin University, Perth, Australia, November, 2010

Obanijesu, E.O., Akindeju, M.K., Pareek, V. and Tade, M.O. (2011a), "Modeling the Natural Gas Pipeline Internal Corrosion Rate as a Result of Hydrate Formation", <u>*Elsevier 21st European Symposium on Computer-Aided Process Engineering*</u>, (Part B) pp. 1160-1164.

Obanijesu, E.O., Pareek, V., Gubner, R and Tade, M.O. (2011b), "Hydrate Formation and its Influence on Natural Gas Pipeline Internal Corrosion Rate", *NAFTA Journal,* Year 62, No 5-6, pp 164-173.

Obanijesu, E.O., Pareek, V., Barifcani, A., Gubner, R. and Tade, M.O. (2011c), "Influence of Corrosion Inhibitors on Hydrate Formation Temperature", *3rd Regional Materials Technology Conference*, Imperial Palace Hotel, Miri, Malaysia, April 26-27.

Obanijesu, E.O., Tade, M.O., Pareek, V., Gubner, R. and Barifcani, A. (2011d), "Pipeline Engineering in Oil and Gas Industry: Importance and Problems", *Presented during Research & Development Seminar*, Curtin University, Miri Campus, Malaysia, April 28

Obanijesu, E.O., Gubner, R., Barifcani, A., Pareek, V. and Tade, M.O. (2012a) "Experimental Investigations on the Influence of Corrosion Inhibitors Commonly used

in Offshore Natural Gas Pipelines on Hydrate Formation Temperature", Submitted to *Chemical Engineering Communications*, on January 11th, 2012.

Obanijesu, E.O., Gubner, R., Barifcani, A., Pareek, V. and Tade, M.O. (2012b), Investigations on the Impacts of Dodecylpyridinium chloride as a CO_2 Corrosion Inhibitor for Subsea Natural Gas Pipeline Networks, To be submitted to *Chemical Engineering Science*, Elsevier.

Obot, I.B. and Obi-Egbedi, N.O. (2010), "Adsorption Properties and Inhibition of Mild Steel Corrosion in Sulphuric Acid Solution by Ketoconazole: Experimental and Theoretical Investigation", *Corrosion Science*, Vol 52, Iss. 1, pp.198–204

Okazaki, M., Hara, I. and Fullyema, T. (1976), "Spectroscopic Studies of Surfactant Solubility. 1. Formation of Hydrogen Bonding between Surfactants and Chloroform", *The Journal of Physical Chemistry*, Vol. 80, Iss. 1, pp. 64-68

Olivier, J.G.J, Bouwman, A.E, Berdowski, J.J.M, Veldt, C, Bloos, J.P.J, Visschedijk, A.J.H van der Maas, C.W.M and Zasndveld, P.Y.J (1999), "Sectorial Emmision Inventories of Greenhouse Gases for 1990 on a Per Country Basis as Well as on 1x1*", Envir. Sci. Policy*, Vol. 2, pp. 241-263

OME (2002), "Assessment of Internal and External Gas Supply for the EU, Evaluation of the Supply Costs of New Natural Gas Supply Projects to the EU and an Investigation of Related Financial Requirements and Tools", Executive Report, Observatoire Mediterraneen De L'Energie, Nanterre, France, pp 1-17

Onianwa, P.C (1995) "Petroleum Hydrocarbon Pollution of Urban Topsoil in Ibadan City, Nigeria", *Environment International* Vol. 21, Iss. 3, pp. 341 – 343.

OSHA (2005), "OSHA Fact Sheet: Hydrogen Sulfide (H_2S)", Occupational Safety and Health Administration, U.S. Department of Labor, DSG 10/2005, www.osha.gov. Accessed online on 20-12-09 at http://www.osha.gov/OshDoc/data_Hurricane_Facts/hydrogen_sulfide_fact.pdf.

Oyekunle, L.O. (1999), "Gas Flaring in Nigeria and Environment Pollution Control", In: Natural Gas: The Energy for the Next Millennium, *29th Annual Conference of Nigerian Society of Chemical Engineers*, Kaduna, Nigeria

Pack, D.J. (2011), Gas Measurement and Auditing Property Ltd, Kalamunda, Western Australia.

Paik, J. Lee, J., Hwang, J and Park, Y. (2003), "A Time-Dependent Corrosion Wastage Model for the Structures of Single and Double Hull Tankers and FSOs and FPSOs", *Marine Technology*, The Society of Naval Architects and Marine Engineers, New Jersey, Vol. 40, Iss. 3, pp. 201-217

Palmer, A.C. and King, R.A. (2008), "Subsea Pipeline Engineering", 2nd Ed., PennWell Corporation, Oklahoma, USA, pp. 1 – 624

Pandarinathan, V., Lepková, K. and Gubner, R. (2011), "Inhibition of CO_2 Corrosion of 1030 Carbon Steel Beneath Sand-Deposits", Paper 11261, *CORROSION 2011 Conference & Expo*, NACE International, Houston, USA, March 13 – 17

Papadakis, G.A., Porter, S. and Wettig, J. (1999), "EU Initiative on the Control of Major Accident Hazards Arising from Pipelines", *Journal of Loss Prevention in the Process Industries*, Vol. 12, Iss. 1, pp 85.90.

Papavinasam, S., Doiron, A., Panneerselvam, T. and Revie, R.W. (2007), "Effect of Hydrocarbons on the Internal Corrosion of Oil and Gas Pipelines", *Corrosion*, Vol. 63, Is. 7, pp. 704-712.

Pardo, A., Merino, M.C., Coy, A.E., Viejo, F., Arrabal, R. and Matykina, E. (2008), "Pitting Corrosion Behaviour of Austenitic Stainless Steels − Combining Effects of Mn and Mo Additions", *Corrosion Science*, Vol. 50, Is. 6, pp. 1796-1806.

Pardo, A., Merino, S., Merino, M.C., Barroso, I., Mohedano, M., Arrabal, R. and Viejo, F. (2009), "Corrosion Behaviour of Silicon-Carbide-Particle Reinforced AZ92 Magnesium Alloy", *Corrosion Science*, Vol. 51, Is. 4, pp 841-849.

Parfomak, P.W. (2004), "Pipeline Security: An Overview of Federal Activities and Current Policy Issues", Congregational Research Services, The Library of Congress, U.S. (Feb 5).

Park, Y.W., Sankara-Narayanan, T.S.N. and Lee, K.Y. (2008), "Fretting Corrosion of Tin-Plated Contacts", *Tribology International*, Vol. 41, Is. 7, pp. 616-628.

Parker, N.C. (2004), "Using Natural Gas Transmission Pipeline Costs to Estimate Hydrogen Pipeline Costs", Research Report UCD-ITS-RR-04-35, Institute of Transportation Studies, University of California, Davis.

Parker, N.C. (2004), "Using Natural Gas Transmission Pipeline Costs to Estimate Hydrogen Pipelien Costs.", Institute of Transportation Studies, University of California, Davis, Research Report UCD-ITS-RR-04-35, pp 1-85.

Patin S (2004a), "Gas impact on fish and other marine organisms", Retrieved June 19, 2009 from http://www.offshore-environment.com/gasimpact.html.

Patin, S. (2004b) "Environmental Impact of the Offshore Oil & Gas Industry", Retrieved June 19, 2009 from http://www.offshore-environment.com /naturalgas.html.

Pató, Z (2000), "Piping the Forest: A Case Study of the Bolivia-Brasil Gas Pipeline", CEE Bankwatch Network, January 2000.

PHMSA (2009), "Remembering Bellingham: Pipeline Accident Plays Huge Role in Restructuring DOT's Pipeline Safety Program", Pipeline and Hazardous Materials Safety Administration, *U.S. Department of Transportation*, Vol.3, No.3, pp 1-15.

Picioreanu, C. and Loosdrecht, M.C.M (2002), "A Mathematical Model for Initiation of Microbiologically Influenced Corrosion by Differential Aeration", *Journal of Electrochemical Society,* Vol. 149, Iss. 6, pp. B211-B223

Pickthall, T., Rivera, M., McConnell, M. and Vezis, R. (2011), "Corrosion Monitoring Equipment, A Review of Application and Technique", Paper 11280, *Corrosion 2011 Conference and Expo*, Houston, Texas, March 13-17, pp. 1-16.

Pilavachi, P.A., Stephanidis, S.D., Pappas, V.A. and Afgan, N.H (2009), "Multi-criteria Evaluation of Hydrogen and Natural Gas Fuelled Power Plant Technologies", *Applied Thermal Engineering*, Vol. 29, Is. 11-12, pp. 2228-2234

Pistdrius, P.C and Burstein, G.T (1992), "Metastable Pitting Corrosion of Stainless Steel and the Transition to Stability", *Philos. Trans. R. Soc. Lond*., A341, pp. 531-559

Popova, A., Sokolova, E., Raicheva, S. and Christov, M. (2003), "AC and DC Study of the Temperature Effect on Mild Steel Corrosion in Acid Media in the Presence of Benzimidazole Derivatives", *Corrosion Science*, Vol. 45, Iss. 1, pp. 33–58

Prasad, P.S.R., Sugahara, T., Sum, A.K., Sloan, E.D. and Koh, C.A. (2009), "Hydrogen Storage in Double Clathrates with tert-Butylamine", *The Journal of Physical Chemistry A*, Vol. 113, Iss. 24, pp. 6540–6543

Prather, M, Derwent, R, Ehhalt, D, Frazer, P, Sanhueza, E and Zhou, X (1995), "Other Tracer Gases and Atmospheric Chemistry In: Climate Change 1994, [Houghton, J.T, MeiraFilho, L.G, Bruce, J, Hoesung L, Callander, B.A, Haites, F, Harris, N and Maskell, K (ed)] Cambridge University Press, UK, pp 73-126

Prather, M and Ehhalt, D (2001), "Atmospheric Chemistry and Greenhouse Gases: In Climate Change 2001- The Scientific Basis (2001) [Contribution of Working Group 1 to the Third Assessment Report of the Intergovernmental Panel on Climate Change] Cambridge University Press, UK, 239-287

Pujar, M.G., Anita T., Shaikh H., Dayal, R.K. and Khatak, H.S. (2007), "Analysis of Electrochemical Noise (EN) Data Using MEM for Pitting Corrosion of 316 SS in Chloride Solution", *Int. J. Electrochem. Sci.,* Vol. 2, pp. 301 – 310

Qin, S and Cui, W. (2002), "Effect of Corrosion Models on the Time-Dependent Reliability of Steel Plated Elements", *Marine Structures*, Vol. 16, Iss. 1, pp 15-34

Railroad Commission of Texas (2008), "Barnett Shale Information – Updated July 30, 2010", On-line document: http://www.rrc.state.tx.us/barnettshale/index.html

Rajahram, S.S., Harvey, T.J. and Wood, R.J.K. (2009), "Erosion-Corrosion Resistance of Engineering Materials in Various Test Conditions", *Wear*, Vol. 267, Iss. 1-4, pp. 244-254

Ramirez, N., Cuadras, A., Rovira, E., Borrull, F. and Marce, R.M. (2012), "Chronic Risk Assessment of Exposure to Volatile Organic Compounds in the Atmosphere near the Largest Mediterranean Industrial Site", *Environment International*, Vol. 39, Iss. 1, pp. 200–209

Rani, B.E.A. and Basu, B.B.J. (2011), "Green Inhibitors for Corrosion Protection of Metals and Alloys: An Overview", *International Journal of Corrosion*, Vol. 2012, pp. 1-15

RCEBC (2009), "I.T. Super Models: European Oil and Gas from Exploration to End Users", Roadbridge Civil Engineering and Building Contractor", Issue 2, Schofield Publishing Ltd, Norwich, U.K.

Restrepo, C.E, Simonoff, J.S and Rae Zimmerman, R. (2009), "Causes, cost consequences, and risk implications of accidents in US hazardous liquid pipeline infrastructure", *International Journal of Critical Infrastructure Protection*, Vol. 2, pp. 38 – 50

Reyes, A., Letelier, M.V., De la Iglesia, R., González, B and Lagos, G (2008), "Microbiologically Induced Corrosion of Copper Pipes in Low-pH Water", *International Biodeterioration & Biodegradation*, Vol. 61, Iss. 2, pp 135-141.

Ricciardiello, F. and Roitti, S. (1972), "The Corrosion of Fe and Ag in S Liquid at Low Temperature, Effect of S Viscosity", *Corrosion Science*, Vol. 12, Is. 8, pp. 651-659.

Roarty, M. (2008), "Australia's Natural Gas: Issues and Trends", Science, Technology, Environment and Resources Section, Department of Parliamentary Services, Parliament of Australia, no. 25, ISSN 1834-9854, pp. 1-22

Roberge, P.R. (2008), "Corrosion Engineering: Principle and Practise", 1st Ed., The McGraw-Hill Companies Inc., New York, pp. 1 – 754

Rogers, R.E., Zhong, Y., Arunkumar, R., Etheridge, J.A., Pearson, L.E., McCown, J. and Hogancamp, K. (2005), "Gas Hydrate Storage Process for Natural Gas", *GasTIPS*, Winter, pp. 14-18

Rojey, A., Jaffret, C., Cornot-Gandolphe, S., Durand, B., Jullian, S. and Valais, M. (1997), "Natural Gas: Production, Processing, Transport", Imprimerie Nouvelle, Saint-Jean-de-Braye, France.

Rosenlof, K.H, Tuck, A.F, Kelly, K.K, Russel, J.M and McCormick, M.P (1997), "Hemispheric Asymmetries in Water Vapor and Interferences about Transport in the Lower Stratosphere", *J. Geophys. Res.*, Vol. 102, pp. 13213-13234

Roux, A., Gicquel, L.Y.M, Sommerer, Y. and Poinsot, T.J. (2008), "Large Eddy Simulation of Mean and Oscillating Flow in a Side-Dump Ramjet Combustor", *Combustion and Flame*, Vol. 152, Iss. 1-2, pp. 154-176.

Roymech (2009), "Properties Of Gases", Accessed on 24th November, 2009 from http://www.roymech.co.uk/Useful_Tables/Matter/Prop_Gas.htm

Ryu, H.S. and Lee, H.S. (2012), "Study of Anti-corrosion Properties of Organic and Inorganic Inhibitors by Electrochemical Treatment in Aqueous Solution", *Advanced Materials Research*, Vol. 415 – 417, pp. 2070-2073

Saeed, A., Erben, M.F., Shaheen, U. and Flörke, U. (2011), "Synthesis, Structural and Vibrational Properties of 1-(4-Fluorobenzoyl)-3-(Isomeric Fluorophenyl)thioureas", *Journal of Molecular Structure*, Vol. 1000, Iss. 1-3, pp. 49–57

Saipem (2004), "Saipem to Lay Dolphin Line", Pipeline and Gas Technology, USA, June.

Salagar, J.L. (2002), "Surfactants: Types and Uses – Teaching Aid in Surfactant Science and Engineering", Laboratory of Formulation, Interfaces, Rhelogy and Processes, Version #2, FIRP Booklet #E300-A, Universidad De Los Andes, Merida-Venezuela. pp 1-50

Saleh, M. M. (2006), "Inhibition of Mild Steel Corrosion by Hexadecylpyridinium Bromide in 0.5M H_2SO_4", *Materials Chemistry and Physics*, Vol. 98, Iss. 1, pp. 83-89.

Sangeetha, M., Rajendran, S., Muthumegala, T.S. and Krishnaveni, A. (2011), "Green Corrosion Inhibitors-An Overview", Zastita Materijala, Vol 52, Iss. 1, pp. 3-19

Saravanan, K., Kumar, K. and Palaniswamy, N. (2009), "Corrosions, Condition Monitoring and Rehabilitation of Concrete Structures", *Corrosion Reviews*, Vol. 27, Iss. Supplement, pp. 213–286.

Sarshar, M., Fathikalajahi, J. and Esmaeilzadeh, F. (2010), "Experimental and Theoretical Study of Gas Hydrate Formation in a High-Pressure Flow Loop", *The Canadian Journal of Chemical Engineering*, Vol. 88, Iss. 5, pp. 751-757

Scheiner, S. and Hellmich, C. (2007), "Stable Pitting Corrosion of Stainless Steel as Diffusion-Controlled Dissolution Process with a Sharp Moving Electrode Boundary", *Corrosion Science*, Vol. 49, Is. 2, pp. 319-346.

Schimel, D, Alves, D, Enting, I, Heinmann, M, Joos, F, Raynaud, D, Wigley, T, Prather, M, Derwent, R, Ehhart, D, Frazer, P, Sanhueza, E, Zhou, X, Jonas, P, Charlson, R, Rodha, H, Sadasivan, S, Shine, K.P, Fouquart, Y, Ramaswamy, V, Solomon, S, Srivinasan, J, Albritton, D, Isaksen, I, Lal, M and Wuebbles, D (1996), "Chapter 2, Radioactive Forcing of Climate Change", In: Climate Change 1995: The Science of Climate Change, Contribution of Working Group 1 to the Second Assessment Report of the Intergovernmental Panel on Climate Change, Cambridge University Press, UK, pp 65-131

Schlumberger (2011), "Corrosion Inhibitor KI-3882* High Film Persistent, Batch-type Corrosion Inhibitor Designed to Control Corrosion in Oil Production Systems", Houston Texas, U.S.A, pp 1-2. Accessed on 3rd November, 2011 from http://www.slb.com/~/media/Files/miswaco/product_sheets/ki_3882.ashx

Schmitt, G., Bosch, C., Mueller, M. and Siegmund, G. (2000), "A Probabilistic Model for Flow Induced Localized Corrosion", *CORROSION*, Paper No. 49, NACE International, Houston, Texas.

Schwermer, C.U., Lavik, G., Abed, R.M.M., Dunsmore, B., Ferdelman, T.G., Stoodley, P., Gieseke, A. and Dirk de Beer, D. (2008), "Impact of Nitrate on the Structure and Function of Bacterial Biofilm Communities in Pipelines Used for Injection of Seawater into Oil Fields, *Applied and Environmental Microbiology*, Vol. 74, No. 9, pp. 2841–2851

Scientific and Industrial Research Organization (CSIRO), Australian Resources Research Center, Perth, Australia.

Seguel, R.J., Morales S.R.G.E. and Leiva G. M.A. (2012) "Ozone weekend effect in Santiago, Chile", *Environmental Pollution*, Vol. 162, pp. 72-79

Seiad, L.L., Villemin, D., Bar, N. and Hachemiˈ M. (2012), "Solvent-Free Condensation of Methyl Pyridinium and Quinolinium Salts with Aldehydes Catalyzed by DBU", *Synthetic Communications*, Vol. 42, Iss. 5, pp. 650–657

Shell (2004), "Shell to Sell Gulf of Mexico System", Pipeline and Gas Technology, USA, June.

Singh, B. and Krishnathasan, K. (2009), "Pragmatic Effects of Flow on Corrosion Prediction", *Corrosion 2009 Conference & Expo*, NACE International, Atlanta, GA, March 22 – 26, Paper No. 09275, pp. 1-29

Singh, H.B, Thakur, A.N, Chen, Y.E and Kanakidou, M (1996), "Tetrachloroethylene as an Indicator of Low Cl Atom Concentrations in the Troposhere", *Geophys. Res. Lett.*, 23, 1529-1532

Shipilov, S.A. and May, L.L (2006), "Structural Integrity of Aging Buried Pipelines Having Cathodic Protection", *Engineering Failure Analysis*, Vol. 13, Is. 7, pp. 1159-1176

Shukla, P.R., Dhar, S., Victor, D.G. and Jackson, M. (2009), "Assessment of Demand for Natural Gas from the Electricity Sector in India", *Energy Policy*, Vol. 37, Is. 9, pp. 3520-3534

Skrifvars, B-J., Backman, R., Hupa, M., Salmenoja, K., and Vakkilainen, E. (2008), "Corrosion of Superheated Steel Materials under Alkali Salt Deposits Part 1: The Effect of Salt Deposit Composition and Temperature", *Corrosion Science*, Vol. 50, Is. 5, pp. 1274-1282.

Sloan, E. D. (2003), "Fundamental Principles and Applications of Natural Gas Hydrates", *Nature*, Vol. 426, Iss. 6964, pp. 353-363.

Sloan, E. D. (2005), "A Changing Hydrate Paradigm - from Apprehension to Avoidance to Risk Management", *Fluid Phase Equilibria*, Vol. 228-229, pp. 67-74.

Sloan, E. D. and Koh, C.A. (2007), "Clathrate Hydrates of Natural Gases", 3rd Edition, CRC Press, USA.

Smith, J.M., Van Ness, H.C. and Abbott, M.M. (2008), "Introduction to Chemical Engineering Thermodynamics", 7th Edition, McGraw-Hills, New York.

Snell, E., Otto, F.D. and Robinson, D.B. (1961), "Hydrates in Systems Containing Methane, Ethylene, Propylene and Water", *AIChE Journal*, Vol. 7, Iss. 3, pp. 482–485

Soares, C.G and Garbatov, Y. (1999), "Reliability of Maintained, Corrosion Protected Plate Subjected to Non-linear Corrosion and Compressive Loads", *Marine Structures*, Vol. 12, Iss. 6, 425-446

Soares, C.G, Garbatov, Y, Zayed, A. and Wang, G (2005), "Non-linear Corrosion Model for Immersed Steel Plates Accounting for Environmental Factors", *Marine Technology Conference & Expo.*, Society of Naval Architects and Engineers, New Jersey, pp 193-211

Soares, G. C., Garbatov, Y., Zayed, A. and Wang, G. (2009), "Influence of Environmental Factors on Corrosion of Ship Structures in Marine Atmosphere", *Corrosion Science*, vol. 51, pp. 2014-2026

Song, F.M. (2009), "Predicting the Mechanisms and Crack Growth Rates of Pipelines Undergoing Stress Corrosion Cracking at High pH", *Corrosion Science*, Vol. 51, Is. 11, pp. 2657-2674.

Song, H.W., Kim, H.J., Saraswathy, V. and Kim, T.W. (2007), "A Micro-mechanics Based Corrosion Model for Predicting the Service Life of Reinforced Concrete Structures", *Int. J. Electrochem. Sci.*, Vol. 2, pp. 341-354

Sonibare, J.A., Obanijesu, E.O., Adebiyi, F.M. and Akeredolu, F.A. (2005)," Potential Contribution of Volatile Organic Compounds (VOCs) to Nigeria's Airshed by Petroleum Refineries", *NAFTA Journal*, Year 56, No 6, pp 231-242

Sonibare, J.A. and Akeredolu, F.A. (2006), "Natural Gas Domestic Market Development for Total Elimination of Routine Flares in Nigeria's Upstream Petroleum Operations", *Energy Policy*, Vol. 34, Iss. 6, pp. 743 – 753

Sonibare, J.A, Adebiyi, F.M, Obanijesu, E.O and Okelana, O.A. (2010), "Air Quality Index Pattern around Petroleum Production Facilities", *Management of Environmental Quality: An Internal Journal*, Vol. 21, Iss. 3, pp. 379-392.

Southwell, C., Bultman, J. and Hummer, C. (1979), "Estimating of Service Life of Steel in Seawater", *Seawater Corrosion Handbook*, pp. 374-387

Sovago, M., Campen, R.K., Wurpel, G.W.H, Muller, M., Bakker, H.J., and Bonn, M (2008), "Vibrational Response of Hydrogen-bonded Interface Water is Dominated by Intramolecular Coupling", *Phys Rev Lett.* , Vol. 100, Iss. 17, pp. 173901-1 - 173901-4

Stack, M.M. and Abd El-Badia, T.M. (2008), "Some Comments on Mapping the Combined Effects of Slurry Concentration, Impact Velocity and Electrochemical Potential on the Erosion-Corrosion of WC/Co-Cr Coating", *Wear*, Vol. 264, Is. 9-10, pp 826-837.

Stack, M.M., Corlett, N. and Turgoose, S. (2003), "Some Thoughts on Modelling the Effects of Oxygen and Particle Concentration on the Erosion-Corrosion of Steels in Aqueous Slurries", *Wear*, Vol. 255, Is. 1-6, pp. 225-236

Stern, J. (2001), "Traditionalists Versus the New Economy: Competing Agendas for European Gas Markets to 2020", Briefing Paper-Draft, The Royal Institute of International Affairs – Energy and Environment Programme, London, New Series, No. 26, pp 1-7

Steven, E. (2000) "Plan for Degassing Lakes Nyos and Monoun", www.lake nyos\Lake Nyos plan for degassing lakes Nyos and Monoun, Cameroon_ Gas disaster at Nyos mitigation of a natural hazard at Nyos.htm

Stevens P., (2003), "Cross-Border Oil and Gas Pipelines: Problems and Prospects". Joint UNDP/World Bank Energy Sector Management Assistance Program (ESMAP). pp. 130

Stockert, L. and Bohni, H. (1989), "The Pitting Potential of Aluminum in Halide Solution", *Corrosion Engineering and Sciences*, Vol 42, Iss. 4, pp 158-168

Stress (2003), "Pipeline Corrosion", Stress Engineering Services, Inc., USA.

Sun, H. H., Yong, B., Bea, R. and Cui, W.C. (2001), "Time-Variant Reliability of FPSO Hulls", *Transaction – Society of Naval Architects and Marine Engineers*, Vol. 109, pp. 341-366

Sun, H.H. and Yong, B. (2003), "Time-variant Reliability Assessment of FPSO Hull Girders", *Marine Structures*, Vol. 16, pp. 219–253

Sun, Z., Wang, R., Ma, R., Guo, K. and Fan, S. (2003b), "Natural Gas Storage in Hydrates with the Presence of Promoters", *Energy Conversion and Management*, Vol. 44, Iss. 17, pp. 2733-2742

Sun, Y., George, K. and Nesic, S. (2003a), "The Effect of Cl^- and Acetic Acid on Localized CO_2 Corrosion in Wet Gas Flow", *CORROSION*, Paper No 3327, Houston, Texas, NACE International.

Sun, Z.G., Jiang, C.M. and Xie, N.L. (2008), "Hydrate Equilibrium Conditions for Tetra-n-butyl Ammonium Bromide", *J. Chem. Eng. Data,* Vol. 53, Iss. 10, pp. 2375–2377.

Surovetseva, D., Barifcani, A. and Amin, R. (2009), "Cryogenic Condensation Capture of Cr_2 from IGCC flue gases", *CO2CRC Research Symposium*, Coolum, Queensland, Australia, December, 1-5.

Tada, E., Sugawara, K. and Kaneko, H. (2004), "Distribution of pH During Galvanic Corrosion of a Zn/Steel Couple", *Electrochimica Acta*, Vol. 49, Is. 7, pp 1019-1026.

Takeya, S., Hori, A., Uchida, T. and Ohmura, R. (2006), "Crystal Lattice Size and Stability of Type H Clathrate Hydrates with Various Large-Molecule Guest Substances", *J. Phys. Chem. B*, Vol. 110, pp. 12943-12947

Talaghat, M.R., Esmaeilzadeh, F. and Fathikaljahi, J. (2009), "Experimental and Theoretical Investigation of Simple Gas Hydrate Formation with or without Presence of Kinetic Inhibitors in A Flow Mini-Loop Apparatus", *Fluid Phase Equilibria*, Vol. 279, Is. 1, pp 28-40

Teryusheva, S.A., Beloglazov, G.S. and Beloglazov, S.M. (2012), "Experimental and Quantum Chemical Study of Quinone Derivatives as Inhibitors of Corrosion and Hydrogen Absorption by Steel", *Solid State Phenomena*, Vol. 183, pp. 249-255

TET (2011a), "Gases-Densities: Densities and molecular weights of some common gases - acetylene, air, methane, nitrogen, oxygen and many others", The Engineering Toolbox, Access on 20/12/2011 at http://www.engineeringtoolbox.com/gas-density-d_158.html

TET (2011b), "Gases-Specific Gravities: "Specific gravity of air, ammonia, butadiene, carbon dioxide, carbon monoxide and some other Common Gases", The Engineering Toolbox, Access on 20/12/2011 at http://www.engineeringtoolbox.com/specific-gravities-gases-d_334.html

Theobald, N. (2006) "The World's Most Significant Gas Field: Gorgon Project.", http://www.igu.org/html/wgc2006pres/data/wgcppt/pdf/WOC%20Working%20Comm itteeWOC%201/The%20worlds%20most%20significant%20gas%20fields/1.1CS.07.p df Accessed on 19th January, 2012 from

Thompson, N.G. and Vieth, P.H. (2003), "Corrosion Costs U.S. Transmission Pipelines as much as \$8.6 billion/year", *Pipeline & Gas Journal*, March Edition, pp. 21-23

Tourkolias, C., S. Mirasgedis, S., Damigos, D., and Diakoulaki, D. (2009), "Employment Benefits of Electricity Generation: A Comparative Assessment of Lignite and Natural Gas Power Plants in Greece", *Energy Policy*, Vol. 37, Iss. 10, pp. 4155–4166

Ueber, E and McCall, A (1982), "The Rise and Fall of the Calfornia Sardine Empire", In: Climate Variability, Climate Change and Fisheries, Edited by Glantz, M.H, Cambridge University Press, UK, 31-48

UNCTAD (2009), "Info Comm Market Information in the Commodity Areas", United Nations Conference on Trade and Development, Palais des Nations, Geneva, Switzerland.

Uno, B., Okumura,N., Goto, M. and Kano, K. (2000), "n-ó Charge-Transfer Interaction and Molecular and Electronic Structural Properties in the Hydrogen-Bonding Systems Consisting of p-Quinone Dianions and Methyl Alcohol", *J. Org. Chem.*, Vol, 65, pp. 1448-1455

US DOE (Department of Energy) (1985), "Characterization of Infornation Requirements for Studies of CO_2 Effects: Water Resources, Agriculture, Fisheries, Forests and Human Health", DOE/ER-0236, Washington DC,: Carbon Dioxide Research Division, US DOE

Van Hunnik, E.W.J., Pot, B.F.M. and Hendrisken, E.L.J.A. (1996), "The Formation of Protective $FeCO_3$ Corrosion Product Layers in CO_2 Corrosion", *CORROSION*, Paper 6, NACE, Houston Texas.

Vashi, R.T. and Naik, D. (2010), "Hexamine as Corrosion Inhibitors for Zinc in Phosphoric Acid", *E-Journal of Chemistry*, Vol. 7, Iss. S1, pp. S1-S6

Valais, M. (1983), "Analyse des Chaines Gas. Etudes, Ressources et Valorisation du Gas. Les Reserves et la Production de Gaz Naturel dans le Monde: Situation et Perspectives", *Intern. Rep. Inst. Fr. Petr.*, No. 31092, p. 31 (fr).

Veawab, A and Aroonwilas, A. (2002), "Indentification of Oxidizing Agents in Aqueous Amine-CO_2 Systems using a Mechanistic Corrosion Model", *Corrosion Science*, Vol. 44, Is. 5, pp. 967-987.

Videla, H.A. (1996), "Manual of Biocorrosion", CRC Press, Boca-Raton, Florida, U.S.A.

Villano, L.D., Kommedal, R. and Kelland, M.A. (2008), "Class of Kinetic Hydrate Inhibitors with Good Biodegradability", *Energy & Fuels*, Vol. 22, pp. 3143–3149

Vlachos, N.A., Paras, S.V. and Karabelas, A.J. (1997), "Liquid-to-wall shear stress distribution in stratified/atomization flow", *International Journal of Multiphase Flow*, Vol. 23, Iss. 5, pp. 845-863

Vongbupnimit, K., Noguchi, K. and Okuyama, K. (1995), "1-Dodecylpyridinium Chloride Monohydrate", *Acta Crystallographica Section C, Crystal Structure Communications*, Vol. 51, Part 9, pp. 1940-1941

Vysniauskas, A. and Bishnoi, P.R. (1983), "A Kinetic Study of Methane Hydrate Formation", *Chemical Engineering Science*, Vol. 38, pp. 1061- 1072.

Wang, W. and Free, M.L. (2003), "Prediction and Measurement of Mild Steel Corrosion Inhibition by Alkyl Pyridinium Chloride and Alkyl Trimethyl Ammonium Bromide Surfactants in Acidic Chloride Media", *Anti-Corrosion Methods and Materials,* Vol. 50, Is. 3, pp. 186-192.

Wang, G., Spencer, J. and Elsayed, T. (2003), "Estimation of Corrosion Rates of Oil Tankers", *Proceedings of 22nd International Conference on Offshore Mechanics and Arctic Engineering*, ASME, Paper OMAE2003-37361

Wang, W., Fan, S., Liang, D., and Li, Y. (2010), "Experimental Study on Flow Characteristics of Tetrahydrofuran Hydrate Slurry in Pipelines", *Journal of Natural Gas Chemistry*, Vol. 19, Iss. 3, pp. 318-322.

Wenji, S., Rui, X., Chong, H., Shihui, H., Kaijun, D.,and Ziping, F. (2009), "Experimental investigation on TBAB Clathrate Hydrate Slurry Flows in a Horizontal Tube: Forced Convective Heat Transfer Behaviors", *International Journal of Refrigeration*, Vol. 32, Iss. 7, pp. 1801-1807.

Wharton, J.A. and Wood, R.J.K. (2004), "Influence of Flow Conditions on the Corrosion of AISI 304L Stainless Steel', *Wear*, Vol. 256, Iss. 5, pp. 525–536

Whited, T. (2003), "Use of Corrosion Inhibitors for Control of Corrosion in Double Bottom AST's", Praxair Services, Inc. (PSI), Broomfield, CO, USA, pp 1-5. Accessed on 3rd November, 2011 from http://www.cortecvci.com/Publications/Papers/AST%20Corrosion%20Inhibitor%20Process%20v2.pdf

Williams, D.E, Westcott, C and Fleischmann, M (1985), "Stochastic Models of Pitting Corrosion of Stainless Steels", *J. Electrochem, Soc.*, Vol. 132, 1796-1804

Wooster, W.S (1982), "King Crab Dethroned", In: Climate Variability, Climate Change and Fisheries, Edited by Glantz, M.H, Cambridge University Press, UK, pp 15-30

Wu, B., Scully, J.R, MiKhailov, A.S and Hudson, J.L., (1997), "Cooperative Stochastic Behaviour in Localized Corrosion: Model I", *J. Electrochem. Soc.*, Vol. 144, 1614-1620

Wu, Q., Gao, X. and Zhang, B.Y. (2011), "SDS Effect on $CH_4/N_2/O_2$ Hydrate Formation Rate for CMM Separation and Storage", *Advanced Materials Research*, Vol. 201-203, pp. 471-475.
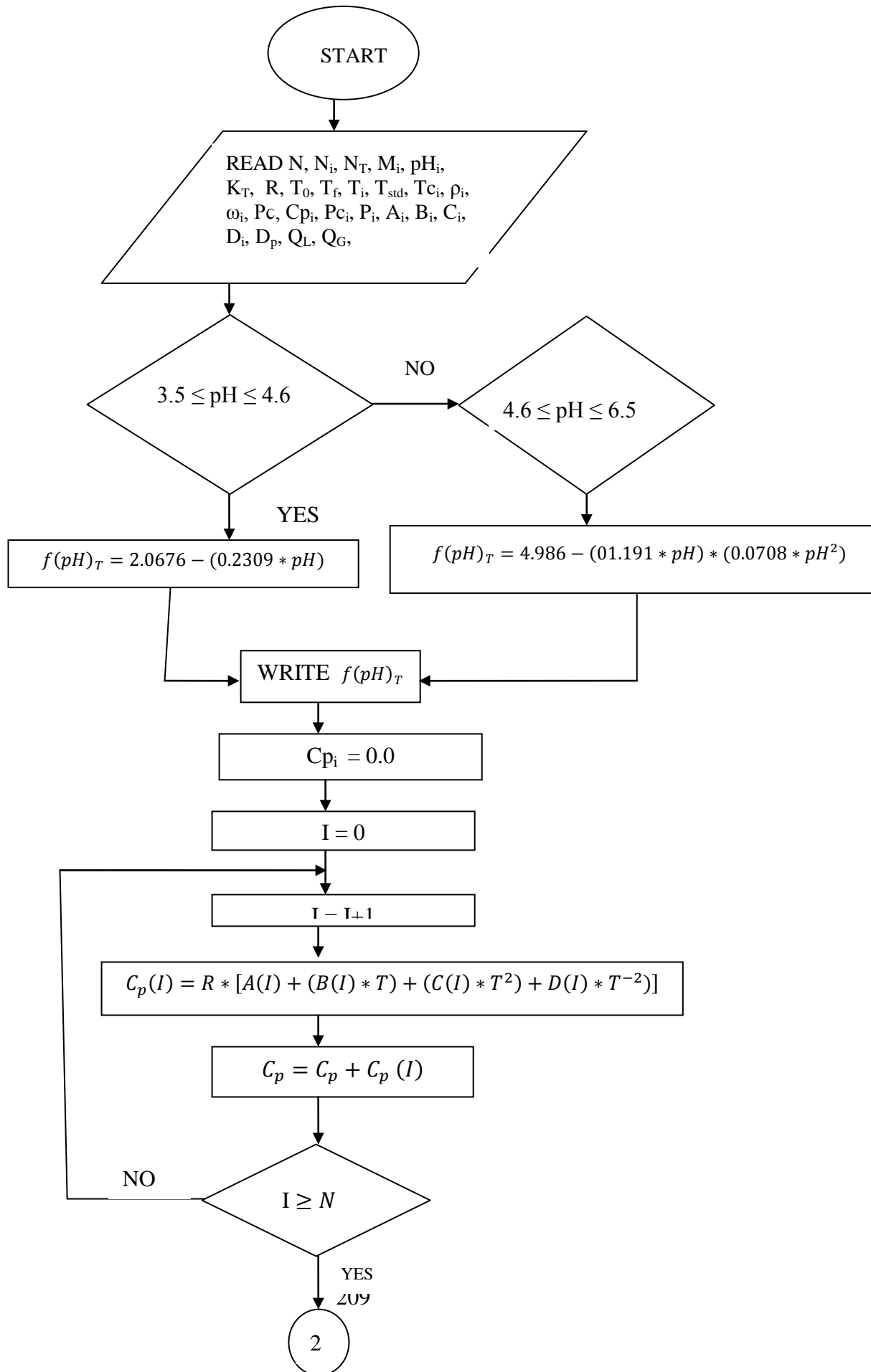
Xiao, Y. and Nesic, S. (2005), "A Stochastic Prediction Model of Localized CO_2 Corrosion", *CORROSION*, Paper # 05057, NACE, Houston, Texas, pp. 1-12.

Xu, W., Daub, K, Zhang, X., Noel, J.J., Shoesmith, D.W. and Wren, J.C. (2009a), "Oxide Formation and Conversion on Carbon Steel in Mildly Basic Solutions", *Electrochimica Acta*, Vol. 54, Is. 24, pp. 5727-5738.

Xu, J., Zhuo, C., Han, D., Tao, J., Liu, L. and Jiang, S. (2009b), "Erosion-Corrosion Behaviour of Nano-Particle-Reinforced Ni Matrix Composite Alloying Layer by Duplex Surface Treatment in Aqueous Slurry Environment", *Corrosion Science*, Vol. 51, Is. 5, pp. 1055-1068.

Yamamoto, N. and Ikegami, K (1998), "A Study on the Degradation of Coating and Corrosion of Ship's Hull Based on the Probabilistic Approach", *Journal of Offshore Mechanics and Arctic Engineering*, Vol. 120, Iss. 3, pp. 121-128

Yang, C.Y., Chu, H.F., Tsai, S.S., Chng, C.C., and Chuang, H.Y. (2002) "Increased Risk of Preterm Delivery in Areas with Cancer Mortality Problems from Petrochemical Complexes", *Environmental Research*, Vol. 89, Iss. 3, pp. 195 – 2000.

Yapa P.D. and Zheng, L (1998), "Simulations of Oil Spills from Under Accidents I: Model Development, *Journal of Hydraulic Research*, Vol. 35, No 5, pp 673-687.

Zcan, M.O. and Dehri, I. (2004), "Electrochemical and Quantum Chemical Studies of Some Sulphur-Containing Organic Compounds as Inhibitors for the Acid Corrosion of Mild Steel", *Progress in Organic Coatings*, Vol. 51, Iss. 3, pp. 181–187

Zhang, L. Burgass, R., Chapoy, A. and Bahman, B. (2011), "Measurement and Modeling of Water Content in Low Temperature Hydrate–Methane and Hydrate–Natural Gas Systems", *J. Chem. Eng. Data*, Vol. 56, Iss. 6, pp. 2932–2935

Zhang, Z.X and Wu, D. (2012), "Reliability Analysis of Factors Affecting Gas Pipeline Operational Conditions", *Applied Mechanics and Materials*, Vol. 135-136, pp. 720-724

Zhao, M., Liu, M., Song, G. and Atrens, A. (2008), "Influence of pH and Chloride ion Concentration on the Corrosion of Mg alloy ZE41", *Corrosion Science*, Vol. 50, Is. 11, pp 3168-3178

Zheng, L and Yapa P.D (1998), "Simulations of Oil Spills from Under Accidents II: Model Verification", *Journal of Hydraulic Research*, Volume 36, No 1, pp 117-134.

Zhong, Y. and Rogers, R.E. (2000), "Surfactant Effects on Gas Hydrate Formation", *Chemical Engineering Science*, Vol.55, Iss. 19, pp. 4175-4187.

Zhongha, L., Dong, W., and Sheng, Z.Y. (2003), "DNA Damage and Changes of Antioxidative Enzymes in Chronic Benzene Poisoning Mice", *Bing Za Zhi*, Vol 21, Iss. 6, pp. 423 – 425.

APPENDIX A

START

READ N, N_i, N_T, M_i, pH_i, K_T, R, T_0, T_f, T_i, T_{std}, Tc_i, ρ_i, ω_i, Pc, Cp_i, Pc_i, P_i, A_i, B_i, C_i, D_i, D_p, Q_L, Q_G,

$3.5 \leq pH \leq 4.6$

NO

$4.6 \leq pH \leq 6.5$

YES

$$f(pH)_T = 2.0676 - (0.2309 * pH)$$

$$f(pH)_T = 4.986 - (01.191 * pH) * (0.0708 * pH^2)$$

WRITE $f(pH)_T$

$Cp_i = 0.0$

$I = 0$

$I = I+1$

$$C_p(I) = R * [A(I) + (B(I) * T) + (C(I) * T^2) + D(I) * T^{-2})]$$

$$C_p = C_p + C_p\,(I)$$

NO

$I \geq N$

YES

209

2

$$\boxed{2}$$

$$\tau = \frac{T}{T_0}$$

$$I =$$

$$I = I +$$

$$P_i(I) = \frac{(n_i(I)*P}{n_T}$$

$$\Delta H(I) = R * \left[A(I)T_0(\tau - 1) + \frac{B(I)}{2}T_0{}^2(\tau^2 - 1) + \frac{C(I)}{3}T_0{}^3(\tau^3 - 1) \right.$$

$$\Delta S(I) = R * \left[\left[A(I)ln\tau + \left\{ B(I)T_0 + \left((C(I)T_0{}^2 + \frac{D(I)}{\tau^2 T_0{}^2}) \right) \right\} \right] \left(\frac{(\tau + 1)}{2} \right) \right] \{\tau - 1\} - ln\frac{Pi\,(I)}{P_0}$$

$$\Delta G(I) = \Delta H(I) - T * \Delta S(I)$$

$$f_i(I) = P_i(I) * e^{\frac{\Delta G(I)}{RT}}$$

$$f_i = f_i + f_i(I)$$

NO

$$I \geq N$$

YES

$$\text{WRITE } f_i$$

$$\boxed{3}$$

$$I = 0$$

$$I = I + 1$$

$$P_r(I) = \frac{P_i(I)}{P_{Ci}(I)}$$

$$T_r(I) = \frac{T}{T_{Ci}(I)}$$

$$Z(I) = 1 + \left(0.083 - \frac{0.422}{T_r(I)^{1.6}}\right)\frac{P_r(I)}{T_r(I)} + w(I)\left(0.139 - \frac{0.172}{T_r(I)^{4.2}}\right)\frac{P_r(I)}{T_r(I)}$$

$$Z = Z + Z(I)$$

$$\rho_g(I) = \frac{P_i M_i}{RT}$$

$$\rho_g = \rho_g + \rho_g(I)$$

$$I \geq N$$

NO

YES

$$\rho_G = \frac{627.1047 * \rho_g * P}{Z * (460 + T_f)}$$

$$\lambda = \frac{Q_L}{Q_L + Q_G}$$

4

$$\text{4}$$

$$\emptyset = \frac{f_i}{P}$$

$$\rho_L = (\emptyset * \rho_w) + \rho_G * (1 - \lambda)$$

$$\rho_m = (\rho_L * \lambda) + \rho_G * (1 - \lambda)$$

$$\mu_w = 10^{\left(\frac{1301}{(998.333 + 8.1855(T-20) + 0.00585(T-20)^2)}\right) - 1.30233} * 10^{-3}$$

$$I =$$

$$I = I +$$

$$\mu_G = \mu_G + \mu_G(I) * \left[\left(\frac{T}{T_o}\right)^{\frac{3}{2}} \frac{T_o + S}{T + S}\right]$$

NO — $I \geq N\text{-1}$

YES

$$\mu_L = \mu_W$$

$$\mu_m = (\mu_L * \lambda) + \mu_G * (1 - \lambda)$$

$$\text{5}$$

212

$$A = \frac{\pi D_p^2}{4}$$

$$U_L^s = \frac{Q_L}{A}$$

$$U_G^s = \left(\frac{Q_G}{A}\right) * Z * \left(\frac{T}{T_{std}}\right)$$

$$U_m = U_L^s + U_G^s$$

$$f_T = 0.001375 \left[1 + \left(20000\frac{k}{D_p} + 10^6\frac{\mu_m}{\rho_m U_m D_p}\right)^{0.33}\right]$$

$$S = 0.5 * \rho_m * f_T * U_m$$

$$C_{rt=} K_T * f_T^{0.36} * \left(\frac{S}{19}\right)^{0.146+0.0324(logf_T)} * f(pH)_T$$

WRIT $C_{rt}, T, S, U_m, f_i, f_T, f(pH)_T, \Delta H, \Delta S, \Delta G, P$
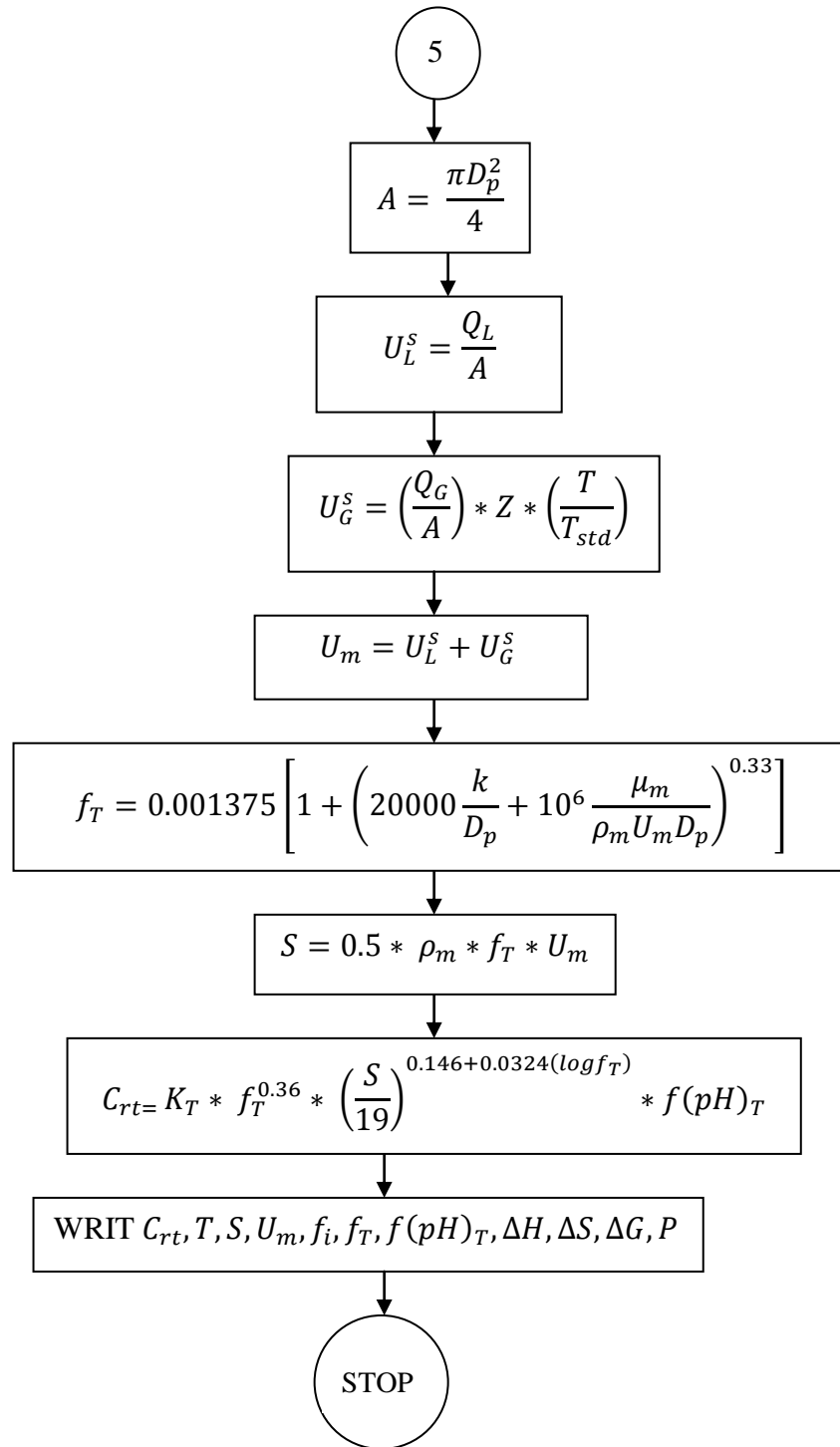
STOP

Figure A1: The solution flowchart for the newly developed corrosion model